SYNTHESIS, CHARACTERIZATION, BIOLOGICAL SCREENING, AND CORROSION INHIBITION STUDIES OF N, S, O-DONOR HETEROCYCLES AND SOME OF THEIR TRANSITION METAL COMPLEXES

Thesis Submitted to
the University of Calicut for the award
of the degree of

DOCTOR OF PHILOSOPHY IN CHEMISTRY

RUGMINI AMMAL P

DEPARTMENT OF CHEMISTRY
UNIVERSITY OF CALICUT
KERALA – 673635
INDIA

MARCH - 2018

CERTIFICATE

This is to certify that the thesis entitled ***"Synthesis, characterization, biological screening, and corrosion inhibition studies of N,S,O-donor heterocycles and some of their transition metal complexes"*** *submitted by* ***Rugmini Ammal P****, to the University of Calicut for the award of the degree of Doctor of Philosophy in Chemistry, is the result of bona fide research work carried out in the Department of Chemistry, University of Calicut under my supervision and guidance. The contents in the thesis have been checked for plagiarism using the software "Urkund" and the similarity index falls under permissible limit. I further certify that the thesis or part therefore has not previously formed the thesis for the award of any degree, diploma or associateship of any other university or institute*.

Dr.Abraham Joseph

Calicut University
March 2018

DECLARATION

I hereby declare that the matter embodied in the thesis is the result of studies carried out by me in the Department of Chemistry, University of Calicut, under the supervision of **Dr.Abraham Joseph,** Professor, Department of chemistry, University of Calicut and the same has not previously formed the basis for the award of any degree or diploma from any university/institute. Whenever the work described or cited is based on the findings of other researchers, due acknowledgement is made in keeping with the general practice of reporting scientific observations. However, errors and unintentional over-sights if any are regretted.

Rugmini Ammal P

ACKNOWLEDGEMENTS

By the blessings of Almighty, I wish to express my heartfelt gratitude to all my well wishers who supported me in this endeavor.

At this moment of accomplishment, first and foremost, I most sincerely and respectfully, express my gratitude towards my guide ***Dr.Abraham Joseph*** *for giving me the opportunity to work in his group. Sir, I consider myself fortunate enough to have you as my supervisor. I am greatly indebted to your unwavering support, scholarly inputs, valuable guidance, and consistent encouragement which made this thesis come true. Thank you sir, for all your help, advice and support.*

I am empty of syllables when it comes to the expression of gratitude towards my appa, amma, valiyachan and valiyamma for their affection, love, prayer, blessings and sacrifices throughout my life. I owe a lot to them for their mental strength without which this dream wouldn't accomplish. I also like to express my token of love and affection for my father-in-law and mother-in-law for their prayer and blessings.

I also acknowledge the Head of the department Dr.P.Raveendran and former heads of the Department, Dr.K.Muraleedharan, Dr.V.M.Abdul Mujeeb and Dr.Ganga Devi for providing all the facilities to do my research work. My sincere thanks also go to all other faculty members and non-teaching staff of Department of chemistry of Calicut University for their timely advice and help.

With immense pleasure and respect, at this moment, with gratitude, I remember all teachers in my life who inspired and lit the lamp of knowledge in me and showed the path for all my achievements in my life.

I am grateful to Dr.T.Ramachandran, Principal of Zamorin's Guruvayurappan college and the former principals, Ms. M.Madhavikutty and Dr.P.C.Rethi Thampatty and the Manager, for their support. In this occasion, I wish to express my sincere gratitude to all my colleagues in the Department of chemistry, Zamorin's Guruvayurappan College for their constant encouragement, and all other teaching and non-teaching staff for their gentle concern.

I am blessed to have a cheerful, helping and affectionate group of fellow research mates. With immense pleasure I would like to mention the sisterly affection I experienced from Shamsheera K O and Anupama R Prasad. I also express my sincere gratitude to all my friends, Dr.Anupama K K, Dr.Prajila M, Dr.Ramya K, Dr.Shainy K M, Julia Garvasis, Sumitha Tom, Jaseela P K, Sr.Asha Thomas, Dr.Revathy Mohan, Dr.Sam John, Dr.Bincy Joseph, Dr.Mathew Kuruvila and Dr.Sabeel.M.Basheer, for their encouragement and support throughout my research period. I am also expressing my sincere thanks to all my fellow lab mates of inorganic chemistry lab and all other researchers of department of chemistry for their support.

I am grateful to UGC for sanctioning the FDP programme for completing my research work.

I am thankful to the staff of BINA Photostat for the neat presentation of my thesis.

Dedicated to

To My husband who shares my joys, sorrows and responsibilities

To my sons who strengthen me with their enchanting smiles, love and affection

To my Anna and sister-in-law for their unconditional love, support and blessings

PREFACE

Coordination chemistry, one of the fascinating fields of inorganic chemistry with its myriads of developments, has become a central trunk which helps to flourish various fruitful branches. It has attracted a great deal of attention owing to its promising properties with miscellaneous application in various fields like bioinorganic chemistry, medicinal chemistry, metallurgy, industry, analytical chemistry, etc. Metals and their compounds have been used for therapeutic applications since ancient times. But it was the success story of serendipitous discovery of platinum complex, cisplatin, for its anticancer activity, which triggered the inorganic chemist to a search for potential biological activities that was expected to be exhibited by various ligands and metal complexes. After an extensive research for decades, a structure activity relationship was established for these compounds. This paved the way for the importance of ligand designing in the practical applications of coordination chemistry especially in bio inorganic and medicinal fields. N,S,O donor heterocycles with diverse applications as chelating agents, pharmaceuticals, agrochemicals, corrosion inhibitors, dye stuffs, fluorescent sensors, brightening agents, analytical reagents etc. became a hot spot in the research arena. The Schiff bases derived from N,S,O-donor heterocycles like 1,2,4-triazines and 1,2,4-triazoles have got considerable attention in coordination chemistry due to excellent complex formation ability and versatile biological activities exhibited by ligands as well as their metal complexes. Many of them are used as potent pesticides, herbicides, fungicides etc. The Schiff bases along with their transition metal complexes were reported to exhibit range of biological properties like antibacterial, antifungal, anticancer, antitumor, anticonvulsant, anti-inflammatory,

analgesic, antidiabetic etc. The growing resistance of microbes towards already existing antibiotics, increasing growth of life threatening diseases like cancer, diabetes mellitus etc. urged the development of new compounds with potent biological activities.

The past few years have witnessed a revolution in the field of pharmaceuticals by the incorporation of *in silico* methods for studying their pharmacokinetics via modelling and docking studies which saved money and time as well as increased their efficacy. In vitro and in vivo analysis is done to authenticate the results of *in silico* analysis.

The increasing use of metals for engineering applications and their susceptibility towards various corrosive attacks has recognized corrosion as one of the major area of interest to both academia and industrial world. It has constrained various challenges in the form of huge loss of finance, wastage of natural resources, man power, and great deal of human suffering and has to be inhibited. So it is the responsibility of the science community to meet these challenges with their expertise and to patch up the blight of corrosion by newer, greener and efficient methods. Among various methods resorted to counteract the corrosion problem, the use of corrosion inhibitors is the widely accepted one. They are the substances or formulations consisting of organic compounds with hetero atoms and π electron clouds, inorganic salts or plant extracts which when added in low quantity with corrosive environment either decrease or forestall the corrosion progress between metal and environment by getting adsorbed on metal surface. Recently many researchers diverted their interest to

develop and investigate various heterocyclic compounds as corrosion inhibitors.

The work embodied in this thesis is an attempt to synthesize, characterize and screen the biological activity and corrosion inhibition properties of N,S,O donor heterocycles and some of their transition metal complexes .

This thesis is divided into eight chapters

Chapter I is an introductory chapter which is divided into two parts. Part A presents a brief introduction on coordination chemistry, N,S,O donor heterocycles and their metal complexes. Various methods of web based *in silico* studies of pharmacokinetics of drug molecules and *in vitro* biological screening studies were also discussed. Various aspects of corrosion, its control using corrosion inhibitors, and theory behind various corrosion monitoring techniques adopted in the present thesis are included in Part B. This part also deals with an introduction to the relevance of theoretical calculations in predicting the corrosion inhibition behaviour of organic molecules. A detailed literature review was also given at the end of each part.

Chapter II describes the experimental details involved in the whole work. It includes preparation and characterization of ligands for both complex formation and corrosion inhibition studies. The instrumental details of various characterization techniques, the procedure of corrosion monitoring methods like gravimetric measurements and electroanalytical techniques, details of *in silico*, *in vitro* biological screening and molecular docking studies, and theoretical calculations performed are also discussed.

Chapter III contains the synthesis, characterization, biological screening and molecular docking studies of metal complexes of Fe(III), Co(II), Ni(II), Cu(II) and Zn(II) with two 4-amino-3-mercapto-6-methyl-5-oxo-[1,2,4]triazine based Schiff bases; 4-[(4-hydroxy-3-methoxybenzylidene)amino]-6-methyl-3-thioxo-3,4-dihydro-1,2,4-triazin-5(2*H*)-one(MHMMT)and 4-{[(1*E*)-(2,4-dihydroxyphenyl)methylene]amino}-3-mercapto-6-methyl-1,2,4-triazin-5(4*H*)-one (DMSTT) and **Chapter IV** deals with the synthesis, characterization, biological screening, and molecular docking studies of Co(II), Ni(II), Cu(II) and Zn(II) complexes of two 4-amino-4-H-1,2,4-triazole-3,5-dimethanol based Schiff bases: 4-[(*E*)-{[3,5-bis(hydroxymethyl)-4*H*-1,2,4-triazol-4-yl]imino}methyl]benzene-1,3-diol (DHATD) and 4-[(*E*)-{[3,5-bis(hydroxymethyl)-4*H*-1,2,4-triazol-4-yl]imino}methyl]-2 methoxyphenol (HMATD). These chapters illustrate the antimicrobial, antidiabetic activities of ligands as well as complexes, anticancer studies of Fe-MHMMT complex and the corresponding molecular docking studies.

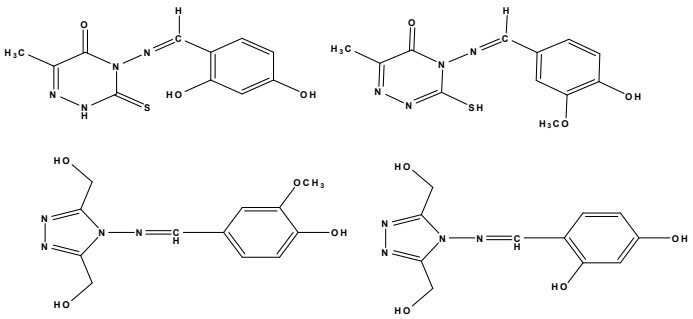

Structure of ligands (A) DMSTT (B) MHMMT (C) HMATD (D) DHATD

Chapter V discusses the corrosion inhibition behaviour of three different benzimidazole motifs; 2-(2-methyl-1H-benzimidazol-1-yl)acetahydrazide (EMBAH), and 2-(2-ethyl-1H-benzimidazol-1-yl)acetahydrazide (EEBAH),

and 2-(2-propyl-1H-benzimidazol-1-yl)acetahydrazide (EPBAH) for mild steel in HCl. The corrosion inhibition was investigated by weight loss measurements, electrochemical impedance spectroscopy (EIS) and potentiodynamic polarization studies (PDP). The temperature dependence of inhibition was explained by considering thermodynamic and kinetic parameters. All the three inhibitors showed good inhibition efficiency at lower as well as higher temperatures. Inhibition efficiency of EMBAH, EEBAH and EPBAH for mild steel in HCl at 303 K

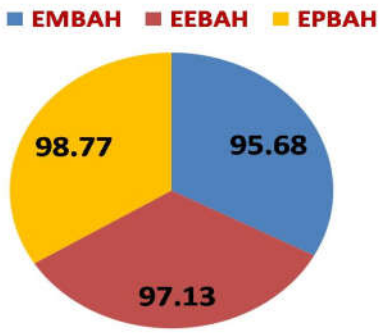

Chapter VI encompasses inhibition effect of three 1,3,4-oxadiazole derivatives 5-((2-methyl-1H-benzo[d]imidazol-1-yl)methyl)-1,3,4-oxadiazole-2-thiol (MBIMOT), 5-((2-ethyl-1H benzo[d]imidazol-1-yl)methyl)-1,3,4-oxadiazole-2-thiol (EBIMOT), and 5-((2-propyl-1H-benzo[d]imidazol-1-yl)methyl)-1,3,4-oxadiazole-2-thiol (PBIMOT) towards the corrosion of mild steel in HCl and H_2SO_4. Various techniques like gravimetric, EIS, PDP, and surface morphological studies were used for monitoring corrosion inhibition mechanism. The influence of immersion time, inhibitor concentration, temperature, and concentration of acid on

inhibition was investigated. Adsorption and kinetic studies also were carried out. EBIMOT was found to be the best among the three studied inhibitors. The effect of MBIMOT, EBIMOT and PBIMOT on the corrosion of mild steel in 0.25 M HNO_3 is illustrated in **Chapter VII.** The investigation was done using electro analytical techniques like EIS and PDP. The effect of temperature on corrosion inhibition was analysed for five different temperatures. The inhibitive mechanism, kinetics and adsorption properties of mild steel in 0.25 M HNO_3 have also been discussed. In these acid solutions at 303 K, the inhibitors follow the order of efficiency as EBIMOT > PBIMOT > MBIMOT.

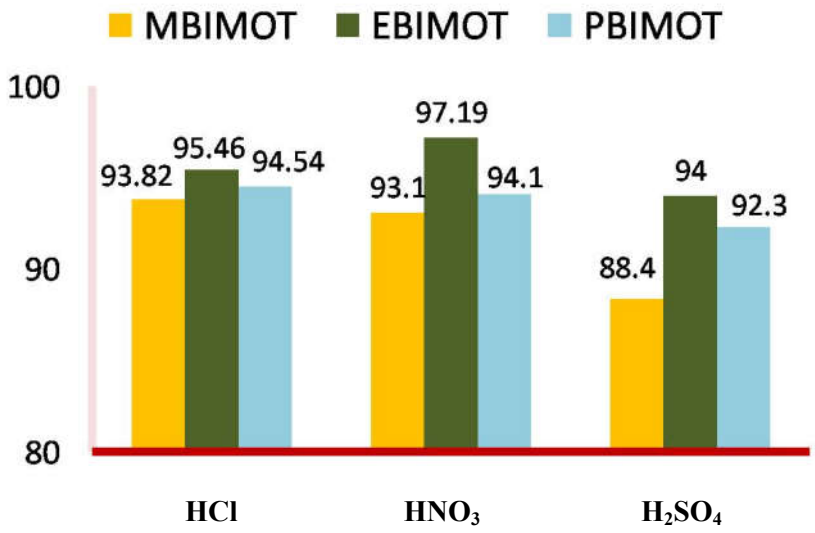

Chapter VIII presents the anti-corrosion behaviour of 1,2,4-triazole based Schiff base, HMATD, towards Pmild steel in HCl. Various techniques like weight loss measurements, EIS, PDP, Scanning electron microscopy (SEM) were used for elucidating the variation of inhibition efficiency with

temperature and acid concentration. The inhibition mechanism was ascertained using adsorption and kinetic studies.

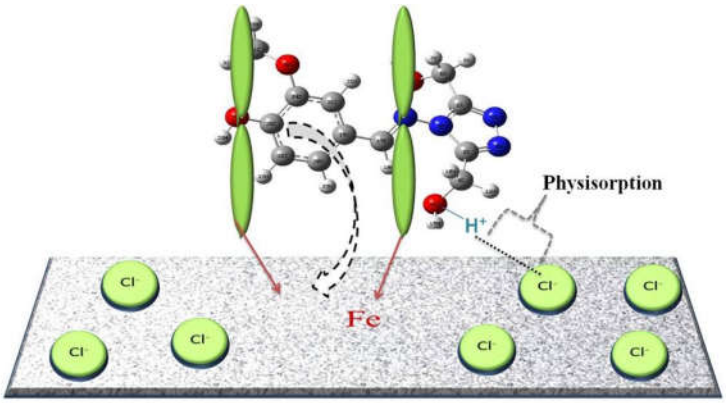

The summary and future prospective of the whole work is included towards the end of the thesis. The studied ligands MHMMT, DMSTT, HMATD and DHATD were found to be ligands with moderately good biological properties like antimicrobial, antidiabetic activities as evidenced from in vitro studies. With regard to the corrosion inhibition studies, all the studied inhibitors showed comparatively good anti-corrosion behaviour for mild steel in various acid media. The future scope of this present study is in the in vivo analysis and cytotoxic studies for developing the biologically active compounds as potential drugs. The benzimidazole based corrosion inhibitors gave a scope for the development of newer one on this scaffold.

CONTENTS

1 GENERAL INTRODUCTION

Chapter I is an introductory chapter which is divided into two parts. Part A presents a brief introduction on coordination chemistry, N,S,O donor heterocycles and their metal complexes. Various methods of web based in silico studies of pharmacokinetics of drug molecules and in vitro biological screening studies were also discussed. Various aspects of corrosion, its control using corrosion inhibitors, and theory behind various corrosion monitoring techniques adopted in the present thesis are included in Part B. This part also deals with an introduction to the relevance of theoretical calculations in predicting the corrosion inhibition behaviour of organic molecules. A detailed literature review was also given at the end of each part.

PART A

INTRODUCTION TO COORDINATION CHEMISTRY

I.A.1 Introduction

Coordination chemistry is one of the rapidly advancing fields of inorganic chemistry which has fostered myriads of developments and comprises a major part of current inorganic research. Coordination compounds, since their identification, have posed a challenge for inorganic chemists due to their defence against usual valence rules. So they were labelled as 'complexes'. It was the two great chemists Alfred Werner and Sophus Mads Jorgenson who put forward a tremendous revolution in this field and made it as one of the most intellectual and experimentally demanding branches with its influence in diverse areas of our life. The most striking features of coordination chemistry are the plethora of compounds and the variety in their colour. The studies on the structure of various naturally existing bio molecules like haemoglobin, chlorophyll, vitamin B_{12} etc. revealed the importance of coordination compounds in biomedical fields. The practice of chemotherapy is one of the excellent applications of coordination compounds in medical fields. In industry, applications in metal purification, ion exchange chromatography, catalysis etc. are astounding. The idea of interdisciplinary research led various scientists to apply the concepts of modern coordination chemistry to areas like biochemistry, catalysis, energy conversion, solar cells, optical storage devices etc. [1-3] and it is at a propitious stage of development.

The modern scientific world is indebted to various pioneers whose fruitful findings made this field an astonishing one. The restless nights spent by Alfred Werner gifted him with the prestigious position of first inorganic

chemistry Nobel laureate in the year1913, for developing coordination theory, is really the greatest contribution in this area [4]. His coordination theory became one of the greatest landmarks in chemistry and triggered the imagination of other chemists to divert coordination chemistry into diverse areas. The benefaction of other pioneers like Lewis, Sidgwick, Linus Pauling, Bethe, Orgel, Jorgenson, Ballhausen, Pearson etc. in the structure and bonding are milestones in the history of coordination compounds. The grandeur and the diversity of coordination compounds, enthralling range of concepts in demand for their interpretation and the wide range of applicability in various fields has invited the quest of researchers towards the synthesis and characterization of new coordination compounds.

I.A.1.1 Nature of metal ions and ligands

The combination of metal ions especially transition metals with other ions and molecules called ligands yield coordination compounds whose enormous number and diversity provide the wealth to co-ordination chemistry. The beauty of coordination compounds lies in the changes in its properties and stability depending on the nature of metal ion, oxidation state of metal ion, structure of ligands, nature of the donor atoms, steric factors, metal-ligand orbital interaction etc. The stability and specificity of metal complexes depends on properties of both the metal atom and the ligands. There are various explanations proposed for the nature of chemical bond in complexes; the well-known being the Lewis acid base concept in which the central metal ions are considered as Lewis acids or electron pair acceptors and they are surrounded by Lewis bases or electron pair donors referred to as ligands. Metal ions and ligands were classified as class (a) or class (b) according to their preferential bonding by Ahrland et al [5]. Alkali metals and alkaline earth metals, lighter transition metals in higher oxidation state are grouped as class (a) whereas heavier transition metals in lower oxidation state were labelled as class (b) metals. According to preferences towards

either class (a) or class (b) metal ions, ligands were also classified as class (a) or class (b). Class (a) metal forms strongest complexes with light donor atoms whereas class (b) with heavier donor ligands. Later in 1963, Pearson followed the various criteria introduced by Irving, Williams, Ahrland etc. and put forward his HSAB principle. He introduced the terms 'hard' and 'soft'. According to him, 'hard' species are small, slightly polarisable, highly electronegative, having empty'd' orbitals of high energy and difficult to oxidize ones whereas 'soft' species encompasses large and more polarisable ones. He equated class (a) metals as hard acids and class (b) as soft acids and ligands having N, O, F as donor atoms as hard bases and P, S, I as soft bases. He proposed the well accepted HSAB principle for predicting the stability of complexes as "hard acids prefer to bind hard bases and soft acids prefer to bind soft bases" [6-8]. The acids and bases of intermediate character were grouped as "border line". This classification serves as an initial tool in the prediction of preference of metal ions for ligands. In coordination complexes hard-hard and soft-soft interactions exist between donor atoms of ligands and metal centres.

I.A.2 The coordination chemistry of N, S, O donor ligands

The ligand selection is one of the important considerations in the practical applications of coordination chemistry especially in bio inorganic, medicinal, and catalysis fields. Generally the binding atoms of the ligands comprise of elements of group V to VII with high electro negativities. The most common donor atoms are N, P, As, Sb, O, S, Se, Te, F, Cl, Br, and I. The N and S atoms act a major role in binding metals to active sites of metallo biomolecules [9]. The ligands with N and S as donor atoms were found to possess a wide spectrum of physicochemical, biological, electroanalytical and catalytic activities [10-15]. The occurrence of a large number of metal sulphide minerals in nature explains the high affinity of metals towards sulphur. The high polarizability of electrons on sulphur atoms facilitates variety of structures and reactivity for metal complexes with

sulphur containing ligands and makes the M─S bonds more covalent than M─N and M─O bonds. Several bioactive molecules were found to contain donor environment of N, S chelating ligand, so the study of coordination chemistry of N, S, and O donor ligands are significant [16-19]. The complexation of ligands leads to the enhancement of bio activity in most of the cases [20-22]. The electron deficient heterocyclic N donor and sp^2 hybrid N donor ligands with their σ donor and π acceptor properties [23] constitutes a promising area of current research due to their facile coordinating ability, easy synthetic strategy and wide spectrum of properties. So it became a challenge to inorganic chemists to synthesize N, S and O donor ligands with desired properties.

I.A.2.1 Importance of thioamide group in N, S, O donor ligands

The major class of N, S, O donor ligands or their derivatives comprises of thioamide groups (rarely also known as thionamide) ranging from thiourea to thioamido proteins and amino acids [24]. These thioamide groups play a vital role in deciding the linkage of donor atoms with the acceptor metal ions in complexes. A promising contribution to the IR spectra of thioamide group has been done by Rao et al. in 1963 [25]. After the detailed study of thioamide bands in various compounds, it has been found that this group forms complex vibrational spectra with four prominent bands in the IR region and was grouped as thioamide bands I-IV and their assignments are as given below.

Region	Band	Assignment
1550-1600	I	$\delta(N\text{-}H)_{major} + \nu\ (C{=}N)_{minor} + \nu(C\text{-}H)_{minor}$
1250-1300	II	$\nu(C{=}N)_{major} + \delta(N\text{-}H)_{minor} + \nu(C{=}S)$minor
500-1000	III	$\nu(C{=}N)_{major} + \nu(C{=}S)$minor
750-850	IV	Predominantly $\nu(C{=}S)$

The reports revealed the existence of thiol-thione tautomerism in thioamide group as represented below [26, 27]

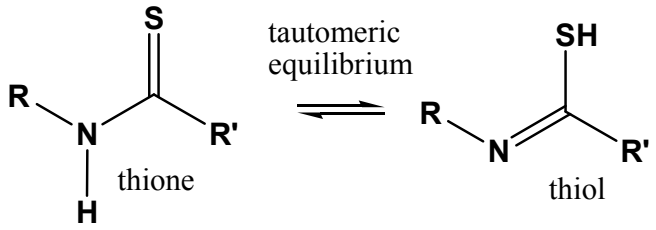

The complexation occurs either by deprotonation and subsequent coordination to metal as a monodentate ligand via the sulphur atom of thiol form or by forming a chelate structure by coordinating through sulphur and nitrogen. The coordination sites of the ligand are distinguished by analyzing the thioamide bands. The complexation of thioamide moiety with a metal atom involves significant perturbation of various thioamide bands. There are ample evidences available in the literature for the following shifts in the thioamide bands due to complexation [28]. According to some researchers, the alteration in the position of thioamide band IV alone acts as an effective diagnostic tool for determining metal-ligand coordination [29-31]. But some others proposed that a clear picture of bonding between metal and ligand can be derived from the changes in the positions and intensities of all the four thioamide bands [32, 33]. The generally observed alterations in the thioamide bands on complexation can be outlined as follows: metal – sulphur bonding alters the position of thioamide band IV by a blue shift of about 50 cm^{-1}. But the coordination through thioamide N generally does not alters this band or only causes a very low red shift. A strong blue shift of about 70-100 cm^{-1} in the position of thioamide band IV is a clear support for metal-sulphur bonding [34]. The thioamide band II experiences a red shift of about 30 cm^{-1} and the thioamide band I undergoes either a blue or red shift depending on the nature of the ligand.

A confirmation to nitrogen and sulphur coordination to metal can be obtained from low frequency spectral absorptions. The metal-sulphur stretching frequency is very much dependent on the nature of ligands as well as the central metal ions [35-39]. Usually in the sulphur bonded metal complexes, the M-S stretching frequency lies in the range of 480-210 cm^{-1}. There are complications in the assignment of metal-sulphur stretching frequency of chelated ligands due to coupling between the frequencies corresponding to ν(M-S) and ring deformation [40]. There are various reports available which reveals that the M-S stretching frequency can occur in the wide range 160-400 cm^{-1} [41]. M-N stretching can be seen over a broad range of 600-200 cm^{-1}.

I.A.2.2 N, S, O donor heterocycles – substituted 1,2,4-triazines and 1,2,4-triazoles

The vivid spectrum of pronounced biological and physicochemical properties displayed by N, S donor ligands and their transition metal complexes has created extra academic interest in the research field of these compounds. There are various well known N, S donor ligands such as semicarbazides, thiosemicarbazides, thiocarbohydrazides and their derivatives, 1,2,4-triazine, 1,2,4-triazoles and their derivatives, etc. [42-47] with very interesting bonding, biological, and physico chemical properties.

1,2,4-triazines are heterocyclic compounds analogous to benzene with a replacement of carbon at the three positions by nitrogens. 1,2,4-triazines otherwise known as asymmetrical triazine (as-triazine) or α-triazine or isotriazine forms a part of variety of well- known natural and synthetic biologically and pharmacologically active compounds [48, 49]. 1,2,4-triazines with their derivatives are well noticed for their anti AIDS [50, 51], anticancer [52, 53], antiviral [54], antitumour [55], antimicrobial [56-60] activities. Many of the triazine derivatives were tested for their function as

colouring agents for metal determination [61]. The introduction of thiol group into the 3rd position of 1, 2, 4-triazines can enhance the coordination ability as well as physico chemical properties of the system.

1,2,4-triazoles, ($C_2H_3N_3$), are another important class of N donor ligands. 1,2,4-triazoles and their derivatives were first discovered by Bladin in 1885. The inherent biological properties of 1,2,4-triazoles and their derivatives has grown the interest in their studies in an exponential manner. They formulate an excellent class of heterocyles with various medicinal properties [62-67]. Variety of 1,2,4-triazole bearing compounds like Fluconazole, Itraconazole etc. have been widely utilized as antifungal agents since a long time [68].

I.A.3 Schiff bases

Schiff bases, named after Hugo Schiff, are one of the most widely utilized classes of organic compounds with variety of applications [69-72]. They have got considerable attention in coordination chemistry due to their excellent complex formation ability and the versatile biological activities shown by the ligands as well as their complexes due to the presence of azomethine C=N linkage [73, 74]. Chiral Schiff bases play an important role in asymmetric catalysis. The development of a copper Schiff base complex for asymmetric synthesis bagged the Nobel Prize for chemistry in 2001 [75]. Since the first synthesis of Schiff base in 1864, various synthetic strategies including solvent free/clay/microwave irradiation, solid state synthesis, K-10, ultrasound irradiation etc. with shorter time period, high efficiency and greener approach have been developed till date [76-82].

I.A.4 Virtual screening of pharmacological behaviour

Virtual screening of pharmacological behaviour of compounds is suggested by global pharmacological scenario due to the inter relationship of

chemical structure and biological properties. The past few years have perceived through a revolution in the drug discovery and the related developmental process due to the introduction of new fundamental knowledge, technology, techniques and strategy. Medicinal chemistry and in vitro screening studies in the development of novel pharmaceuticals have greatly influenced by the incorporation of many modelling and docking studies. Combinatorial chemistry has played a significant role in the drug discovery. Cheminformatics as defined by Greg Paris "is a generic term which encompasses the design, creation, organization, management, retrieval, analysis, dissemination, visualization and use of chemical information" [83].

I.A.4.1 Drug likeness and bioavailability

Various descriptors and drug likeliness parameters were analyzed for discriminating drug like molecule from non-drug compounds. According to Chris Lipinski "Drug-like is defined as those compounds that have acceptable ADME/tox properties to survive through the completion of human phase I trials" and according to Ronald.T.Borchardt "drug like responses are intrinsic properties of the molecules, and it is the responsibility of medicinal chemists to optimize not only the pharmacological properties, but also the drug-like properties of the molecules". There are various drug likeness rules which act as guidelines for structural properties of compounds and help in the fast calculation of drug like properties.

I.A.4.1.1 Lipinski's rule*:*

The pioneer in the field of drug discovery is Chris Lipinski, who put forward the famous "Rule of Five" or better known as "Lipinski's Rule" [84]. These rules are a set of property values which were derived from the classification of key physico chemical properties of drug like compounds. According to Lipinski, the drugs like molecules are those in which

- No. of hydrogen bond donors ≤ 5 (The sum of OH's and NH's)
- No. of hydrogen bond acceptors ≤ 10 (The sum of O's and N's)
- Molecular weight ≤ 500
- logP≤ 5

The impact of this rule in the field of drug discovery has made it as a benchmark due to its speed, ease, and no cost implementation. These rules have strong physico chemical support. Hydrogen bonds increase the solubility of the compound and they have to be broken in order to permeate a compound through membrane, so the increase in number of hydrogen bonds decreases the drug likeliness. Molecular weight is related to the size of the molecule, so high molecular size impedes the diffusion through membrane ie why molecular weight should be ≤ 500. Increasing logP, decreases aqueous solubility and reduces absorption.

Apart from Lipinski's rule, there are some other rules which incorporate other parameters like number of rotatable bonds, polar surface area etc. These are Veber Rules [85], Lead like rule [86], CMC like Rule [87], MDDR like Rule etc.

The strict dependence on Rule of five (Ro5) has led to a loss in opportunities, especially in difficult targets and with various natural products. So the recent developments in drug discovery have increased the chemical space for oral druggable candidates beyond Lipinski's Rule of 5 (bRo5) by considering target interaction and to incorporate various natural products rich in activities [94]

I.A.4.2 Pharmacokinetic analysis of drug molecule –ADMET analysis – Important models of ADMET analysis

Drug likeness expresses a complex balance of various molecular properties as described above and pharmacological features like bio availability, transport properties, affinity towards proteins, toxicity etc. When a drug is introduced into the body, the activity of various native proteins, enzymes etc. in the body (drug targets or biological targets) gets modified leading to a desirable therapeutic effect. The most common drug targets are proteins like enzymes, ion channels and receptors (Eg: GPCR) and inhibitors (Protease inhibitor, kinase inhibitor etc.). The interaction of drug molecules with these drug targets are expressed by bioactivity scores.

Absorption, distribution, metabolism, excretion and toxicity (ADMET) are important parameters for predicting the success of an orally introduced drug candidate's journey through the body towards the site of action. In the earlier period of drug discovery almost half of the potential therapeutic compounds failed in the clinical trial due to unavoidable side effects and poor pharmacokinetic (ADMET) properties [89]. ADMET property measurement gives a pharmacokinetic profile of a therapeutic candidate [90]. So the evaluation of ADMET should be done at the early stages of discovery and is very essential [91]. The orally given drug has to encounter various barriers from the point of application to its target site which reduces the amount of dosage that reaches the target [92].

I.A.4.3 Toxicity estimation

The toxicity considerations put forward an attrition in the potential use of many designed compounds as drugs. The toxicity of a therapeutic can be like carcinogenity, mutagenicity, cytotoxicity etc. Various toxicity tests like Ames test, Rodent carcinogenity etc. are effective in toxicity estimation [93]. The early screening of toxicity can control the attenuation in the pre clinical and clinical stages and can boost the efficacy in drug discovery.

I.A.4.4 In vitro biological studies

The in silico analysis is followed by in vitro and in vivo analysis to authenticate the results. In vitro analysis is dealt with studies of biological properties done in a controlled environment, outside of a biological organism. These studies are conducted using components of an organism isolated from their original biological environment. So the studies cannot be relied for the whole organism analysis in a biological environment [94, 95].

I.A.4.5 Molecular docking:

Molecular docking is a powerful tool of bioinformatics modelling in computer aided structure based drug designing. Docking mainly involves the

computational simulation of a drug molecule (known as ligand or guest) with receptor molecules (like proteins or enzymes) which are the target sites of drug molecules. The main objective of docking is to predict the binding modes of ligand with a target site of known three dimensional structures. It mainly involves the evaluation of non covalent interaction such as hydrogen bonding, Van der Waals's interaction between drug molecules and target [96,97].

I.A.5 Complexing ability and biological screening of Schiff bases derived from substituted 1,2,4-triazole and 1,2,4-triazines – a review

The Schiff bases of 1,2,4-triazoles and 1,2,4-triazines and their derivatives are widely studied for their excellent complex formation ability and biological activities. The coordination ability of these ligands depends upon the nature of metal ion, nature of substituents on the ligand and pH of the medium. The metal complexes are found to possess a wide spectrum of properties and applications. A review of literature was conducted with a view to extract the knowledge in this field and to synthesize new Schiff bases of same class with excellent pharmacological properties. Singh et al studied the coordination behaviour of 1,2,4-triazine derivative, 4-[{3-(4-bromophenyl)-1-phenyl-1Hpyrazol-4-ylmethylene -amino]-3-mercapto-6-methyl-5-oxo-1,2,4-triazine with transition metals like Co, Ni, Cu and Zn via N,S,O as donor sites and screened their in vitro antimicrobial activity [98]. Taha and co-workers synthesized a novel Schiff base, 2-benzylidene-3-hydroxy -1-(5,6-diphenyl-1,2,4-triazine-3-yl)hydrazine (HBDHT) and its complexing ability towards Ni and Cu, optoelectronic properties and computational studies were reported [99]. Transition metal complexes of 5-bromosalicylidene-4-amino-3-mercapto-1,2,4-triazine-5-one were synthesized, characterized and tested for catalytic as well as biological activity by Ramasubramanian et al and found to possess appreciable

bactericidal properties [100]. The same authors reported the anti-bacterial activity of 5- nitro salicylidene 4-amino-3-mercapto-1,2,4 triazine-5-one and its various transition metal complexes [101]. Research group of Kiran Singh reported the studies on the coordination behavior of Schiff base 4-(4-cyanobenzylideneamino)-3-mercapto-5-oxo-1,2,4-triazine with transition metal complexes and reported significant anti-microbial activities of ligand as well as complexes [102]. A bidentate Schiff base ligand, 4-(4-hydroxy-3,5-dimethoxy benzilideneamino)-3-mercapto-6-methyl-5-oxo-1,2,4-triazine, coordinate through azomethine nitrogen and sulphur to the metals, was studied for its antimicrobial properties by Singh et al [103]. Ghassemzadeh and co-workers developed single crystals of some mono- and bis-Schiff base compounds based on1, 2, 4-triazine by the condensation reaction of 4-amino-3-hydrazinyl-6-methyl-1,2,4-triazin-5(4H)-one with o-, m- and p-methoxybenzaldehyde and their complexation behavior with Ag(I) ion was studied in 2012 [104]. A new series of cobalt, nickel, copper, and zinc complexes of bidentate Schiff bases derived from the condensation of 5-bromothiophene-2-carboxaldehyde with 4-amino-3-mercapto-6-methyl-5-oxo-[1,2,4] triazine were synthesized and screened for anti-bacterial and antifungal properties by Singh et.al and observed the partial quenching of fluorescence of Schiff base on metal coordination [105]. The research group also reported the Co(II), Ni(II), Cu(II) and Zn(II) complexes of 4-(4-fluorobenzalideamino)-3-mercapto-6-methyl-5-oxo-1,2,4-triazine(fbmmot) and 4-(2-acetylfuranlideamino)-3-mercapto-6-methyl-5-oxo-1,2,4-triazine) with a detailed thermal and spectral studies in 2010 [106]. Hammam et al synthesized a new series of transition metal complexes of 1,2,4-triazole based Schiff base with an enhanced anti microbial activities for the complexes compared to that for ligand [107]. Patel and others described the synthesis and characterization, of Co(II), Ni(II) and Cu(II) complexes of Schiff bases derived from 3-substituted-4-amino-5-mercapto-1,2,4-triazole and 8-formyl-7

hydroxy-4-methylcoumarin. They have also evaluated in vitro anti-bacterial and anti-fungal activities and the brine shrimp bioassay was also carried out to understand in vitro cytotoxic properties [108]. In 2016, Singh and others reported the synthesis of two novel Schiff bases by the condensation of 4-amino 1, 2, 4-triazoles with 5-bromothiophene-2-carboxyaldehyde and examined their coordination behaviour with Co, Ni, Cu and Zn and screened the anti-microbial activity against various pathogens [109]. Jha et al reported the synthesis, characterization and bioactivity of transition metal complexes of new 3-methyl-5-mercapto-4-triazole Schiff bases and indicated a better biological activity for complexes compared to free ligands, giving a new thrust that metallization increases the activity [110]. Zahid H. Chohan designed a new class of triazole Schiff bases derived from the reaction of 3,5-diamino-1,2,4-triazole with 2-hydroxy-1-naphthaldehyde, pyrrole-2-carboxaldehyde, pyridine-2-carboxaldehyde and acetyl pyridine-2-carboxaldehyde and their oxovanadium(IV) complexes and the ligands as well as complexes were screened for their in vitro antibacterial activity [111]. Chandra and co-workers reported the synthesis, characterization, DFT studies and anti cancer cell line activities of some novel 1, 2, 4-triazole based Schiff bases and their metal complexes with an elaborate discussion [112]. Chohan and team synthesized and characterized 1,2,4-triazole based Schiff bases by condensing 3-amino-1H-1,2,4-triazole with pyrrol-2-carboxaldehyde, 4-bromo-thiophene-2-carboxaldehyde, and 5-iodo-2-hydroxy benzaldehyde and examined their spectral and biological characteristics [113]. Spectral, antitumor and antimicrobial studies on Cu(II) complexes of purine and triazole Schiff base derivatives were reported by Wakiel et al [114]. Singh et al have reported the synthesis of new Zn(II) complexes of Schiff bases derived from 3-substituted phenyl-4-amino-5-hydrazino-1,2,4-triazole and benzaldehyde, 2- hydroxyacetophenone or indoline-2,3-dione and screened their anti-bacterial activity by petriplates methods [115]. The recently

published work of Chandra and coworkers described the coordination behavior, anticancer activity and protein binding studies of (E)-5-(pyridin-4-yl)-4-((thiophen-2-ylmethylene)amino)-4H-1,2,4-triazole-3-thiol and E)-5-(pyridin-3-yl)-4-((thiophen-2-ylmethylene)amino)-4H-1,2,4-triazole-3-thiol and has been concluded that the Schiff base derived from nicotinic acid hydrazide display better activity in comparison to Schiff base derived from isonicotinichydrazide [116]. Nassar et al described the synthesis and biological activity of new 3-substitued-4-amino-5-hydrazino-1,2,4-triazole Schiff bases and their Cu(II), Co(II) and Ni(II)complexes along with the photocatalytic activity of these metal oxide nano particles [117,118]. A work on antimicrobial studies of transition metal complexes with bidentate Schiff bases derived from the condensation of 4-amino-5-mercapto-3-methyl/ethyl-1,2,4-triazole with 5-nitrofurfuraldehyde were reported by Singh et al in 2017 [119].

The present investigation

After conducting a detailed literature survey, it has been convinced that no work has been done on coordination compounds of Schiff bases derived from 4-amino-3-mercapto-6-methyl-5-oxo-[1,2,4]triazine with 2,4-dihydroxy benzaldehyde and vanilline. So after the perusal of literature and noticing the versatile biological properties of 1,2,4-triazine and triazole based Schiff bases and their transition metal complexes, we aimed at the synthesis, characterization and biological screening studies of some N,S, O donor ligands for the present investigation.

PART B

INTRODUCTION TO CORROSION INHIBITION STUDIES

I.B.1 Corrosion – the phenomenon

The pure metals extracted from ores possess more bound energy and are in a meta stable state. As per the general rule of universe, the pure metals are also strived to return to their lowest energy state of chemically bound form. The common route for this reversion is the process of corrosion. So corrosion can be considered as metals'endeavour to return to their mineral state, i.e., corrosion can be considered as the reversal of extractive metallurgy [120-123]. The undesirable corrosion can be viewed as a universal, omnipresent and omnipotent phenomenon. So everyone who utilizes materials of any sort must be aware of the basics of corrosion, its prevention and remediation methods.

I.B.2 Electrochemical aspects of corrosion

The involvement of electrochemical reactions in all forms of aqueous corrosion was established in the early period of 19th century and Whitney proposed the well-known electrochemical theory of corrosion [124-126]. The basic reactions in aqueous corrosion can be considered as the occurrence of anodic oxidation of metal surface and counter reaction of reduction in the environment. Coupling of these two inter-related half-cell reactions form a complete corrosion reaction [127]. The generalized representation of corrosion of a metal M can be given by the following equations

At the anode: Oxidation of metal $M \rightarrow M^{+n} + ne^{-}$ (1.1)

The cathodic reaction encountered in metal corrosion differ depends on the pH of the aggressive medium

Hydrogen evolution $2H^+ + 2e^- \rightarrow H_2 \uparrow (p^H < 7)$ (1.2)

Oxygen reduction $O_2 + 4H^+ + 4e^- \rightarrow 2H_2O \ (p^H \geq 7)$ (1.3)

Metal ion reduction

$$M^{x+} + e^- \rightarrow M^{(x-1)+} \quad (1.4)$$

Metal deposition

$$M^+ + e^- \rightarrow M \quad (1.5)$$

(1.2) and (1.3) are the most common ones compared to reactions (1.4) and (1.5) [120]. There is a possibility for the oxidized metal to react with oxygen to form a protective passive coating [128] which help the metals to escape from further corrosion. These electrochemical reactions accompany current flow and this current is termed as corrosion current i_{corr} which is a measure of corrosion rate [129].

I.B.3 Thermodynamics of corrosion:

Electrochemistry and thermodynamics play a critical role in understanding corrosion, its mechanism and control [120, 130]. In an electrochemical reaction, there is equilibrium between the electrode and its environment and the feasibility of reactions in such systems can be monitored with the help of thermodynamic principles. They can explain the corrosion behaviour of a metal in a corrosive environment. For a reaction to be feasible the change in free energy ΔG should be negative

$$\Delta G = -nF\Delta E \quad (1.6)$$

where 'n' is the number of electrons transferred, ΔE, the potential difference between two half cells, and F, is Faraday constant. So the thermodynamic tendency for corrosion can be studied from electrode potential E. At room temperature most of the metal compounds are at a lower energy than that of the pure metal. So ΔG will be negative for the corrosion (oxidation) process

and as per the thermodynamic principles most of the metals have an inherent tendency to undergo (oxidation) corrosion. For some noble metals like gold, platinum etc. have positive ΔG of oxidation (corrosion) reactions and they will not corrode [131]. M.Pourbiax summarized the thermodynamic data in a potential-pH diagrammatic form to relate the electrochemical and corrosion behaviour of any metal in water [132]. These E-pH diagrams help us to adjust the pH and potential of a metal in order to prevent it from corrosion as applied in cathodic protection. Thermodynamics is an excellent initiator for corrosion studies with Pourbiax diagrams as the essential tool [133].

I.B.4 Corrosion mitigation methods:

Corrosion is ubiquitous and is a silent destructor operating in all establishments. Corrosion control is a process which is aiming at the reduction of the corrosion rate to a permissible limit. There are various methods available to combat corrosion which mainly involves either a separation between the corrosive environment and metal or removal of any one of the components of electrochemical cells which accelerates deterioration.

I.B.4.1 Use of inhibitors in corrosion mitigation and mechanism of inhibition

The alteration in the environment is counted as one of the efficient methods for corrosion mitigation and the most accepted mode of alteration is by adding substances called inhibitors [134-136]. Corrosion inhibitors (CI) are chemicals which when added in very small concentrations into the corrosive environment can effectively reduce the corrosion rate to a large extent [137]. They can slow down the corrosion by

- inhibiting anodic or cathodic corrosion reaction
- controlling the movement or diffusion of ions from the solution to the metallic surface

► increasing the resistance of the metallic surface

The action of CIs depends on the type of metal to be protected and the nature of corrosive environment. A large volume of research is being dedicated to this field nowadays.

I.B.4.1.1 Classification of corrosion inhibitors:

Jones et al. preferred the chemical functionality for classifying the inhibitors [138] and grouped CIs as inorganic and organic. Various inorganic substances containing anions like chromates, phosphates etc.were discarded due to their harmful effects. Organic compounds containing hetero atoms like N, S, O, P and/or multiple bonds and conjugate systems are found to possess the ability to get adsorbed on the metal surface thus preventing corrosion. The most widely accepted grouping is on the basis of their inhibition functionality [139]. On the basis of functioning, CIs can be qualitatively classified as follows (Fig 1.1)

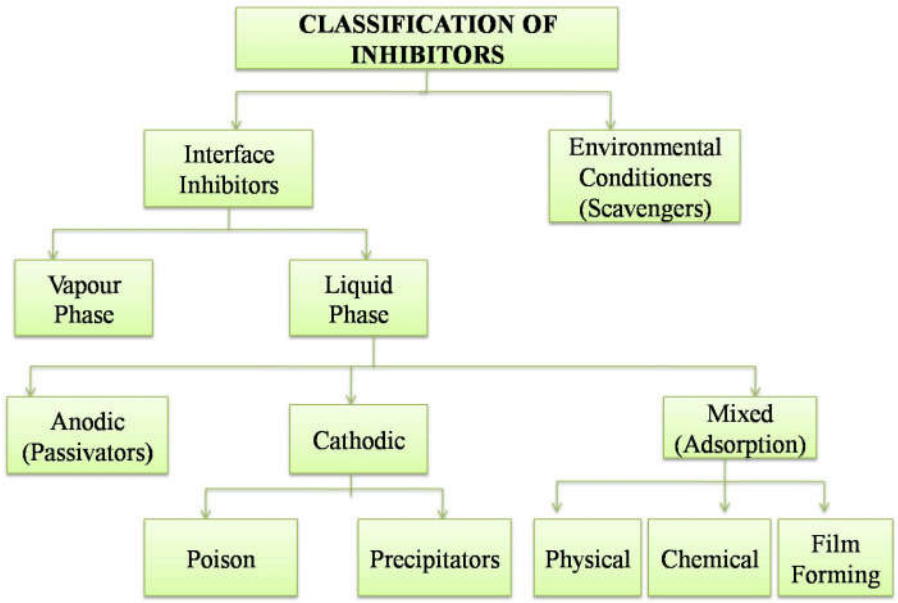

Fig 1.1

Corrosion inhibitors protect the metal by getting adsorbed on its surface thus blocking active sites and substituting for water molecules in order to form a compact barrier film and reduce the corrosion rate [140]. The adsorption can be represented as

$$Org_{soln} + XH_2O(ads) \rightarrow Org_{ads} + XH_2O(soln) \qquad (1.7)$$

Adsorption of the organic compound depends upon the charge and the nature of the metal surface, temperature of the corrosion reaction and the electrochemical potential at the metal solution interface [141].

The exact nature of adsorption can be studied from adsorption isotherms which describe the surface coverage (θ) by the inhibitor on the metal surface and the concentration of the inhibitor. Various adsorption isotherms are drawn for correlating the adsorption phenomenon and they include Langmuir, Temkin, Frumkin, Flory-Huggins, Bockris-Swinkels and thermodynamic/kinetic model of El-Awady etc. [142-146]. The basic representation to denote adsorption phenomenon is

$$f(\theta, x)e^{-\alpha\theta} = kC \qquad (1.8)$$

where f(θ, x) is the configuration factor representing the physical model and assumptions made in deriving the isotherm. The quantity x is the size ratio which represents the number of water molecules replaced by inhibitor, α is the molecular interaction parameter depicting the lateral interaction between the adsorbed species, C concentration of the inhibitor and k equilibrium constant. Some of the frequently used adsorption isotherms are [147]

(a) ***Langmuir adsorption isotherm***: This isotherm representing uniform mono layer adsorption without any lateral interaction between the adsorbates is given by the equation

$$\frac{C}{\theta} = \frac{1}{k} + C \qquad (1.9)$$

The verification plot for testing and fitting of this isotherm is drawn as a plot of $\frac{C}{\theta}$ Vs C.

(b) ***Temkin isotherm:*** This isotherm demonstrates the adsorption on heterogeneous surfaces with adsorbent-adsorbate interaction and is represented by the equation

$$lnkC = a\theta \qquad (1.10)$$

A plot of θ Vs lnC agrees well with Temkin adsorption.

(c) ***Frumkin isotherm:*** This isotherm is represented by the equation

$$\frac{\theta}{1-\theta} e^{-2a\theta} = kC \qquad (1.11)$$

The applicability of this isotherm can be checked from the plot of

log C($\frac{\theta}{1-\theta}$) Vs θ

(d) ***Flory Huggins isotherm:*** The characteristic equation for this isotherm can be written as

$$log\frac{\theta}{C} = logk + xlog(1-\theta) \qquad (1.12)$$

The utility of this isotherm can be verified by drawing plots of log(θ/C) Vs log(1-θ)

The interpretation of adsorption of inhibitors, various adsorption parameters and performance of inhibitors can be obtained from best fitted verification plot with regression coefficient R^2 =1.

I.B.5 Corrosion Monitoring Systems:

The non-destructive inspection and monitoring can play a major role in the struggle against corrosion which can imply enormous savings, improved safety, quality control and preservation [148]. An approximate and trustworthy tool for the monitoring of corrosion is inevitable to guarantee the balance between corrosion and mitigation methods [149]. The process of corrosion usually incorporates weight loss together with mechanical, structural or physicochemical changes in the specimen [150] which can be diverted for ascertaining the corrosion process. The experimental methods employed for corrosion monitoring ranges from classical weight loss method, electro chemical methods to modern spectroscopic methods like FTIR, Raman, Mossbauer spectroscopy etc.

I.B.5.1 Weight loss measurements

The weight loss method is a simple, accurate and reliable one and is considered as "gold standard" in corrosion testing. A cleaned, pre-weighed specimen of the material (coupon) is allowed to expose in the corrosive environment for a given duration, and is removed for analysis. The basic parameter determined in this technique is weight loss, from which the corrosion rate can be validated using the following relations

$$Corrosion\ rate\ (CR) in\ mgcm^{-2}hr^{-1} = \frac{weight\ loss\ in\ mg}{Area\ in\ cm^2 \times time\ in\ hours} \quad (1.13)$$

$$CR\ in\ mpy = \frac{weight\ loss\ in\ g\ \times 5.34\ \times 10^5}{Density\ in\ g/cm^3 \times Area\ in\ inches^2 \times time\ in\ hours} \quad (1.14)$$

$$CR\ in\ mmy = \frac{weight\ loss\ in\ g\ \times 8.76\ \times 10^4}{Density\ in\ g/cm^3 \times Area\ in\ cm^2 \times time\ in\ hours} \quad (1.15)$$

The simplicity, versatility and the possibility of physical inspection of corrosion mechanism makes the method as the base line method for other

means of corrosion monitoring programme and accounted for its attractive sustained popularity.

I.B.5.2 Electrochemical techniques:

These techniques of corrosion monitoring are nowadays increasingly popular primarily due to its rapidity in the measurement and well established theoretical understanding. The electrochemical excitation to an electrode makes the electrode polarized and measuring the response of the electrode to the excitation can be applied to elucidate the corrosion rates [151].

Polarization: When a metal is placed in contact with a solution and kept in equilibrium, depending on the nature of the metal and solution, a potential will be assumed, referred to as corrosion potential, E_{corr}, at which rate of anodic metal dissolution is equal to that of cathodic hydrogen/oxygen reduction. If current is supplied to such a metal by means of an external inert auxiliary electrode, deviations from equilibrium is induced which changes the potential of the metal without causing any change in current. This process of potential shift away from E_{corr} is termed as polarization. It can be anodic, if the potential drift is above E_{corr} or cathodic, if it is below $E_{corr.}$ The potential difference between the polarized and unpolarized electrode potential is referred as over voltage (η) [120]. During polarization, there will be a net flow of current through the solution compared to zero current flow at equilibrium.

The polarization can occur either due to the development of a concentration gradient around the metal/solution interface by the diffusion of ions (concentration polarization) or by the involvement of a slow step in the electrode reaction (activation polarization). The potential drop due to high resistance around electrode surface also causes resistance polarization or iR drop polarization. The formation of an insulation film around the electrode surface formed from the reaction products can also lead to the potential drop [152]

Thus the overall polarization $\eta_{Total} = \eta_{Act} + \eta_{Conc} + \eta_{Resis}$

The common procedure for all the polarization methods involve electrochemical excitation (altering the potential) of the working electrode and measuring the response (current) which has a potential or time domain.

I.B.5.3 Electrochemical reaction kinetics:

The corrosion rate of a metal immersed in an electrolyte can be better explained by electrochemical reaction kinetics which depends on the electrode potential and can be characterized from parameters like corrosion current density i_{corr}, corrosion potential E_{corr} and Tafel slopes β_a and /or β_c. The value of i_{corr} can be considered as a parameter governing corrosion rate. A higher value of i_{corr} suggests a higher corrosion rate.

The classical Faraday's laws are utilized for computing the corrosion rate from corrosion current as per the given equation

$$CR\ (mpy) = \frac{0.13 I_{corr}(EW)}{d} \qquad (1.16)$$

where I_{corr} is the corrosion current density in $\mu A/cm^2$, EW = equivalent weight of the electro active species and d the density of the corroding species[153].

The data obtained from polarization were diagrammatically represented as polarization curve (potential vs I_{corr} or log I_{corr}). The polarization curve of a corroded material shows three distinct types of behaviour. The current density (current per unit area) has a linear relation with the potential up to an over voltage of 10 mV. At higher polarizing voltages, the linearity between current and voltage is lost and above some particular higher voltage, a linear relationship between E and log i occurs. This region is known as Tafel region. The frequently used representations of

polarization curves are Evans diagrams which represent the linear polarization for reversible electrodes and Stern diagrams representing nonlinear polarization for irreversible electrodes [152].

I.B.6 Techniques for corrosion rate measurements

Based on mixed potential theory, two approaches are used for determining the polarization resistance and corrosion current density from polarization curves; the Tafel extrapolation method and Linear polarization method.

A. Tafel extrapolation method (Potentiodynamic Polarization):

This method was primarily used by Wagner and Traud for verifying the mixed potential theory [154] and can be used for determining polarization parameters from a single nonlinear polarization curve polarized by a sufficiently high over voltage. For most of the metals and alloys, the polarization curves at sufficiently high overvoltage (Tafel region) will be linear to log I as represented by Stern diagram (Fig 1.2). In such cases in order to obtain the value of E_{corr} and I_{corr}, the Tafel regions of Stern diagram are extrapolated until they meet at a single point taken as E_{corr}, open circuit potential, and the corresponding exchange current density, I_{corr}.

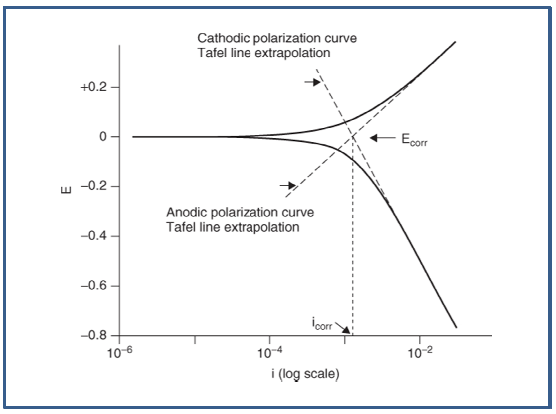

Fig 1.2

The Tafel equations representing the linear behaviour of potential and logi in the Tafel region was extracted from Butler-Volmer equation and is as follows [152]

$$log\ I = log I_{corr} + \frac{\alpha ZF}{2.303\ RT}\ \eta \tag{1.17}$$

where α is the symmetry coefficient, Z is the oxidation state of metal ion, F the Faraday constant.

For anodic and cathodic Tafel plots, Tafel equations can be written as

$$\eta_a = \frac{2.303RT}{\alpha ZF} log \frac{I_a}{I_{corr}} \tag{1.18}$$

$$\eta_c = \frac{-2.303RT}{(1-\alpha)ZF} log \frac{I_c}{I_{corr}} \tag{1.19}$$

$$\beta_a = \frac{2.303RT}{\alpha ZF}\ and\ \beta_c = \frac{-2.303RT}{(1-\alpha)ZF} \tag{1.20}$$

β_a and β_c are termed as anodic and cathodic slopes of Tafel plots.

Potentiodynamic polarization study is an application of Tafel extrapolation method to find the polarization parameters. This involves the excitation of a working electrode to a wider range of over voltage ≥ 150 mV with respect to E_{corr} both in anodic and cathodic directions so that both corrosion processes can be monitored in a single experiment. Since the over voltage applied is high there will be a Tafel region in both the curves which can be used for evaluating various polarization parameters by extrapolation method. The potential is first swept in the negative direction up to a preset value and then potential is reversed to more positive value to undergo anodic polarization.

B. Linear polarization method (LPR):

The Tafel extrapolation method which uses high over voltage causes enough disturbances in the system so that further measurements using the same specimen will be difficult. Sometimes the extrapolation will not give exact $E_{corr\ and}$ I_{corr} values also. So in order to overcome the difficulties, Linear Polarization method was developed [155] where the polarization was done using a very small over voltage such that a linear relationship exists between the potential and current density. The slope of this linear portion is termed as polarization resistance (R_P).

$$R_P = \frac{\Delta E}{\Delta i} = \frac{\eta}{\Delta i} \tag{1.21}$$

The corrosion current density I_{corr} can be defined by the equation

$$I_{corr} = \frac{\beta}{R_P} \tag{1.22}$$

The constant β, known as Stern-Geary constant, is a function of Tafel anodic and cathodic slopes (β_a and β_c) which is given by the equation

$$\beta = \frac{\beta_a \beta_c}{2.303(\beta_a + \beta_c)} \tag{1.23}$$

It can be seen that this method also requires the determination of Tafel slopes from a Tafel plot. Thus using the slope of Linear Polarization plot and Tafel slopes I_{corr} can be determined which can be converted to corrosion rate in mm/yr using the equation (1.16) [156].

C. Electrochemical impedance spectroscopy (EIS)

Electrochemical impedance spectroscopy is a non-destructive method for characterizing corrosion behaviour of metals and protective coatings

[157]. The method involves the measurement of response of a working electrode to a potential modulation at different frequencies and can be modelled using a mathematical approach similar to that of Ohm's law. The non-linearity of current and voltage in the electrochemical systems are overcome by using a small range of potential perturbation where the current-voltage linearity is maintained [158]. The technique utilizes a continuous AC sine wave perturbation of small amplitude (5-10 mV) centered on the corrosion potential to a corroding system. This method uses an equivalent circuit to model the corrosion process which gives a transient response to the AC sine wave. The equivalent circuit models consist of a solution resistance (R_s), charge transfer resistance (R_{ct}) and a double layer capacitance (C_{dl}) for a charge transfer controlled system and a diffusion impedance (Z_D) is incorporated for a diffusion controlled one. The most widely used equivalent circuit models for charge transfer controlled system is the Randles circuit which is schematically given in Fig (1.3). The discrete frequencies of AC sine wave cause a phase shift (θ) between applied potential wave form and current response. The mathematical expression for impedance can be given as a complex number

$$Z(\omega) = \frac{E(\omega t)}{I(\omega t)} = \frac{E_0 \sin(\omega t)}{I_0 \sin(\omega t + \theta)} = Z_0 \frac{\sin(\omega t)}{\sin(\omega t + \theta)} = Z'(\omega) + Z''(\omega) \quad (1.24)$$

where $\omega = 2\pi f$ = angular frequency (Hz)

f = signal frequency (Hz)

$Z'(\omega)$ = real part of impedance

$Z''(\omega)$= imaginary part of impedance

The phase shift θ can be represented as

$$\theta = tan^{-1}\left[\frac{Z^{'}(\omega)}{Z^{''}(\omega)}\right] \tag{1.25}$$

In a charge transfer controlled electrochemical system, the impedance can be described by the form (1.25)

$$Z(\omega) = \left[R_s + \frac{R_{ct}}{1-\omega^2 C_{dl}^2 R_{ct}^2}\right] - j\left[\frac{\omega C_{dl} R_{ct}^2}{1-\omega^2 C_{dl}^2 R_{ct}^2}\right] \tag{1.26}$$

The impedance value at each frequency can be calculated and two extreme situations can be given as

$$Z(\omega)_0 = R_s + R_{ct} \ @\ \omega = 0 \ and \ \ Z(\omega)_\infty = R_s \ @\ \omega = \infty$$

So charge transfer resistance can be obtained as the difference between the impedance at zero frequency and that at infinite frequency.

The corrosion current density (i_{corr}) and corrosion rate (CR) can be obtained from impedance measurements using the equations [152]

$$I_{corr} = \frac{\beta}{R_{ct}} \quad and\ C_R = \frac{\beta EW}{R_{ct} ZFd} \tag{1.27}$$

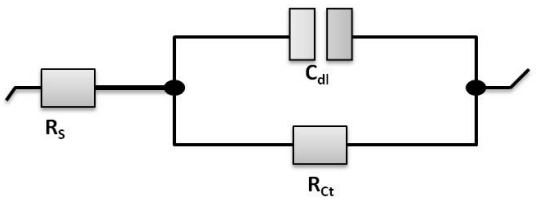

Fig 1.3

The data obtained from impedance spectroscopy can be represented in three different ways – Nyquist plot, Bode phase angle plot and Bode magnitude plot.

A. ***Nyquist plot:*** This is a type of complex plane plot also known as Argand representation or Cole-Cole representation is a plot of series of points representing the real and imaginary component of the complex impedance at a particular frequency (Z" vs Z'). Usually the shape of the plot will be semicircular one for charge transfer process with diameter equivalent to R_{ct} and straight line below the imaginary axis for capacitive responses. The value of frequency will be decreasing from left to right. The impedance data at a particular point can be represented as a vector of length equivalent to the magnitude of impedance. The angle between this vector and real axis is the phase angle (Fig.1.4). The existence of an electrical double layer at the metal solution interface creates a double layer capacitance C_{dl} which can be correlated with frequency by the equation

$$C_{dl} = \frac{1}{2\pi f_{max} R_{ct}} \tag{1.28}$$

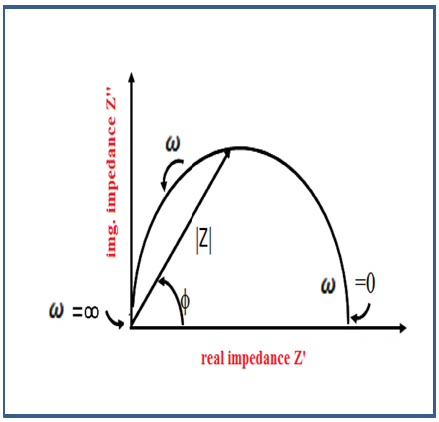

Fig 1.4

B. ***Bode plot:*** The information pertaining to frequencies can be obtained from another type of plot called "Bode plot" named after Henrik Wade Bode. There are two kinds of Bode plot viz., Bode magnitude plot and Bode phase angle plot which shows the effect of angular frequency on the impedance and

phase shift angle. Both the quantities are represented in the abscissa against the logarithmic frequency (Fig. 1.5). Both the plots can be represented in a single Bode plot with two ordinates one representing log (magnitude of impedance) and the other phase shift. These plots can be used for characterizing various processes from the slope and phase angle values. For capacitive processes, the Bode magnitude plot will be linear with a slope of −1 and Bode phase angle plot with a phase angle approximately 90^{o} [159]. The charge transfer processes result in sigmoidal shaped magnitude plots. The impedance at highest and lowest frequencies is mainly resistive in nature. So at these points the plot will be flat with phase angle 0^{o} and at intermediate frequencies the phase angle will be nearly 90^{o}.

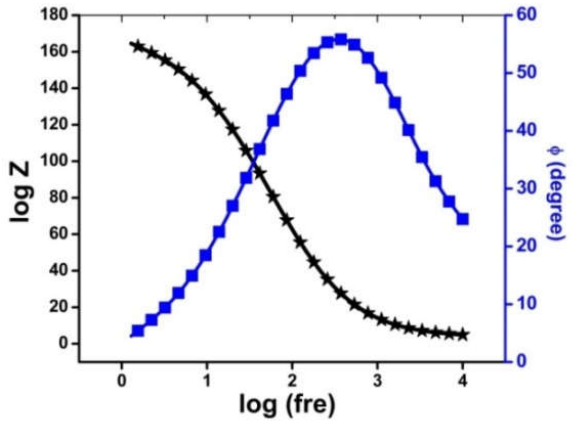

Fig 1.5

I.B.7. Theoretical calculations

The computer revolution has marked its influence in almost all the fields. The essence of this field is the incorporation of computer models and theoretical chemistry principles for solving chemical phenomenon associated with molecular energies, structures, geometry optimization, spectroscopic parameters, excited states, reaction pathways etc. Depending on the initial

assumption used for modelling, the Computational methods can be grouped into (a) classical methods and (b) quantum chemical methods. The classical methods include Molecular mechanics and Molecular dynamics and quantum chemical methods include *Ab initio*, semi empirical and density functional theory [160].

Ab initio methods, as the name implies "from the first principles" [161, 162], are distinguishable from other methods by the non involvement of experimental data except fundamental physical constants and mathematical approximations such as the use of functional form for a function or finding an approximate solution to a differential equation. These methods helped in the development of modelling tools capable of accurate prediction of structure, energetic, reactivity and other properties. The low speed and accuracy of *Ab initio* methods are overcome in Semi empirical methods (SE) by incorporating some experimental data to Hartree-Fock formalism and are parameterized to reproduce the results. These quantum chemical methods are characterized by the use of many approximations in order to improve the performance both in speed and accuracy [163]. The most frequently employed semi empirical methods include MNDO, AM1, PM3 etc. These methods are very useful for the description of medium sized organic compounds and can be used for the studies related to solids, nano structures and inorganic compounds by applying different parameterization [164]. Density functional methods (DFT) are rapidly developing cost effective procedure for studying the physical properties of molecules [165,166]. The basic goals of quantum chemistry like prediction of molecular structure and energy, explanation of nature of bonding etc. are best satisfied by these methods. These methods incorporate functional of electron density for the calculation of various properties of many electron systems.

Two important approximation methods are molecular mechanics and molecular dynamics. These techniques are empirical in nature since they depend on experimental data to obtain various parameters. The greater speed of these tools allows them to use in procedures in conformational analysis, docking etc. which require lot of energy calculations.

I.B.7.1 Geometry optimization and quantum chemical descriptors

One of the important computations performed in quantum chemical calculations is the geometry optimization of a molecule to a minimum energy configuration with most stable atomic arrangement at a stationary point in the potential energy surface where the net inter atomic force on each atom is almost equals to zero [167]. The geometry optimization enabled to extract a large number of molecular and local quantum chemical descriptors like energy, dipole moment, polarizability, Mulliken charges etc. that characterize reactivity, shape, binding capacity etc. of a molecule, its fragments and substituent. Thus Quantitative Structure Activity Relationship (QSAR) studies using quantum chemical methods that inter-relate molecular as well as electronic structures and reactivity was verified as an efficient tool in foreseeing various chemical and biological activities exhibited by the compounds [168,169]. The quantum chemical parameters are useful in predicting the activities of a compound merely on the basis of molecular structure and it also provide a confirmation test for the proposed mechanism for a particular activity [162].

I.B.7.2 Relevance of theoretical studies of corrosion inhibitors

Corrosion inhibitors are substances with lone pair of electrons and/or π electrons and multiple bonds, which can prevent corrosion by adsorbing on the metal surface forming a protective layer. So the main concern for a compound to show inhibition activity is the availability of electrons for

adsorption. So the corrosion inhibition activity of a molecule is closely related to its electronic properties [170] which can be extracted from the quantum chemical descriptors like energies of frontier orbitals (highest occupied molecular orbital, E_{HOMO} and lowest unoccupied molecular orbital, E_{LUMO}), the energy gap ($\Delta E = E_{LUMO} - E_{HOMO}$), global hardness and softness etc. [171,172]. So the theoretical studies are very important for screening and comparing the inhibition efficiency of already synthesized compounds and to predict the efficiency of compounds yet to be synthesized.

The energies of frontier molecular orbitals, E_{HOMO} and $E_{LUMO,}$ are closely associated with electron donation and electron acceptance of inhibitor molecules. E_{HOMO} is associated with electron donating ability of a molecule. The higher the value of E_{HOMO}, the greater will be the tendency of the molecule to donate electrons to metal orbitals and higher will be inhibition efficiency. E_{LUMO} is associated with the electron accepting ability of a molecule. Lower the value of E_{LUMO}, greater the tendency to accept the electrons from the metal by back donation. So a compound to behave as an efficient inhibitor should not only be a good donor of electrons to the empty d orbitals of metal but also be a good acceptor to receive electrons from metal. Thus an efficient inhibitor should have lower values of ΔE [173]

The global reactivity parameters are used to describe the inter dependence of structure, stability and global chemical reactivity [174]. They are mainly calculated from the two quantities, ionization potential (IE) and electron affinity (EA) ,which are represented by Koopman's theorem as [175]

$$IE = -E_{HOMO} \tag{1.29}$$

$$EA = -E_{LUMO} \tag{1.30}$$

Pearson introduced the terms chemical hardness (η) and its

multiplicative inverse chemical softness (σ) and electronegativity (χ) are defined as

$$\eta = \frac{E_{LUMO} - E_{HOMO}}{2} \tag{1.31}$$

$$\sigma = {}^{1}/_{\eta} \tag{1.32}$$

$$\chi = \left(\frac{IE + EA}{2}\right) \tag{1.33}$$

As introduced by Parr et al., electrophilicity index (ω) measures the propensity of chemical entity to accept electrons, is defined as [176]

$$\omega = \frac{(I + A)^2}{8(I + A)} \tag{1.34}$$

The anti corrosion behaviour of various molecules can be correlated to these global parameters. According to HSAB principle, the bulk metals are considered as softest one, so the higher value of global softness (σ) will enhance better metal-inhibitor interaction, thus pronounced inhibition efficiency [177]. The chemical hardness (η) describes the resistance towards polarization of electron cloud and a harder molecule thus will have a large ΔE value and less inhibition efficiency [178]. The higher value of electrophilicity index (ω) proposes stronger feedback bond and thus a higher anti corrosion behaviour. Another important parameter obtained from quantum chemical studies is the number of electrons transferred between the inhibitor molecules and the metal (ΔN).

$$\Delta N = \frac{\chi_{Fe} - \chi_{inh}}{2(\eta_{Fe} + \eta_{inh})} \tag{1.35}$$

The theoretical value of electro negativity of iron (χ_{Fe}) and hardness of iron (η_{Fe}) are 7 and 0 eV/mol respectively as obtained from Pearson's electro

negativity scale [179] and the assumption of equality between the ionization enthalpy and electron affinity for a metallic bulk [180]. According to Lukovits, if ΔN is less than 3.6, the inhibition efficiency supposed to increase with increase in electron donating ability at the metal surface [181].

1.B.8 Surface morphological studies

The surface morphological study of metal specimens is an important step in understanding corrosion inhibition. One of the prominent methods for surface imaging and analysis of bulk specimens is Scanning Electron Microscopy (SEM). It produces the surface image by scanning the surface using a focused electron beam [182]. A primary electron beam from a source is accelerated through a potential difference ranging from 0.1 keV-50 keV and is focused through a narrow probe which will scan the surface of the specimen. The interaction of primary electron beam and atomic electrons of surface can produce two types of signals. The inelastic collision between these two electrons will produce a beam of secondary electron and elastic collision will generate back scattered electrons. These signals are fed into the detectors to produce the image. Out of the various signals given to the detector, X-ray signals allow the determination of elemental composition by EDAX (energy dispersive X-ray spectroscopy). Nowadays the advancement of electronics has introduced new techniques for surface studies with better resolution.

1.B.9 Use of benzimidazole and 1,3,4-oxadiazole derivative as corrosion inhibitors – A review

Benzimidazoles and 1,3,4-oxadiazoles were reported as best scaffolds which possess all the desired properties for corrosion inhibitors (CI). They are planar compounds with a five membered ring containing hetero atoms, aromatic ring system which can form a uniform film on

transition metal surfaces thereby prevent the corrosive attack [140]. They are also considered as promising class of bio active compounds exhibiting a range of biological activities and they possess a significant place in organocatalysis, organometallics and material chemistry [183,184]. In recent years benzimidazoles with their derivatives and 1,3,4-oxadiazole based compounds have received considerable attention as excellent corrosion inhibitors for metals and alloys in acidic solution. A review of the same is presented below:

Abboud et.al synthesized a novel compound 2,2'-bis (benzimidazole) and investigated its anti corrosion capacity on mild steel in 1 M HCl employing monitoring techniques like weight loss and PDP studies [185]. Sayed H. El Ashry conducted some QSAR calculations on benzimidazole and 2-substituted derivatives as corrosion inhibitors by some quantum chemical parameters and proposed some linear equations to predict the inhibition efficiency [186].

Elmsellm et.al investigated some novel benzimidazole derivatives 1-allyl/1,3-diallyl-5-nitro-1H-benzo[d]imidazol-2(3H)-one as CIs for mild steel corrosion in 1 M HCl at 308 K by weight loss techniques and adsorption studies [187]. Mohana et.al synthesized novel compounds abbreviated as BDB, BPMP, BFB and examined their influence on the corrosion of mild steel in 0.5 M HCl using mass loss and electrochemical techniques [188]. The benzimidazole derivatives viz., 4-(phenyl)-5-[(2-methyl-1Hbenzimidazol-1-yl)methyl] -4H-1,2,4-triazole-3-thiol,4-(4-methylphenyl)-5-[(2-methyl-1H benzimidazol-1-yl)methyl]-4H-1,2,4triazole-3-thiol, and 4-(4-methoxyphenyl)-5-[(2-methyl-1H-benzimidazol-1-yl)methyl]-4H-1,2,4-triazole-3-thiol were tested for their anti corrosion behaviour towards mild steel in 15 % HCl by weight loss and electro analytical studies by Yadav and his crew [189]. The corrosion prevention ability of 1,4-bis (benzimidazolyl)

benzene on the corrosion of mild steel in acid solutions were investigated by Wang and co-workers through weight loss and electro analytical methods [190]. Three novel benzimidazole derivatives, 2-aminomethyl benzimidazole (ABI), bis (2-benzimidazolylmethyl) amine (BBIA) and tri (2-benzimidazolylmethyl) amine (TBIA), were studied for their inhibition ability for mild steel in 1.0 M HCl by forming a insoluble complex on ferrous surface by Tang and his group [191]. Al-Amiery et.al reported a quantum chemical assessment of three benzimidazole derivatives and gave a detailed explanation on the effect of substituents on corrosion inhibition [192]. An ionic molecule containing benzimidazole moiety1-butyl-3-methyl-1*H*-benzimidazolium iodide was investigated as a mixed type inhibitor for mild steel corrosion in H_2SO_4 by Zheng et.al [193]. Tang and his co-workers investigated the Inhibition performance of long-chain alkyl-substituted benzimidazole compounds and explained the effect of benzimidazole segment and alkyl part in efficiency [194]. An assessment on effect of nature of substituent as well as its position on corrosion inhibition ability of benzimidazole derivatives for mild steel corrosion in 1 M HCl was carried out by Dutta et.al and structure-activity relationship on corrosion inhibition was established [195]. Bentiss et.al studied the corrosion inhibition efficacy of a substituted 1,3,4 - oxadiazole compound by weight loss, polarization and impedance techniques and XPS , SEM characterizations were also done to confirm the results [196]. Ouici et.al investigated the corrosion inhibition of 5-(2-hydroxyphenyl)-1,3,4-oxadiazole-2-thiol (5-HOT) as corrosion inhibitor using weight loss, different electrochemical techniques and X-ray photoelectron spectroscopy (XPS) [197]. Mohana and co-worker synthesized three new pyridine based 1,3,4-oxadiazole derivative and their efficiency for corrosion inhibition of mild steel in 0.5 M HCl was tested by weight loss, electro analytical, surface studies and quantum chemical calculations. A remarkable correlation was obtained between theoretical and experimental

results [198]. Thiazole based 1,3,4-oxadiazoles were synthesized, characterized and studied their anti oxidant and corrosion inhibition ability for mild steel in HCl and thermodynamic and kinetic aspects of corrosion were discussed by Mohana et.al in 2013 [199]. A detailed experimental and quantum chemical study on corrosion inhibition of some substituted 1,3,4-oxadiazoles on mild steel corrosion was conducted by Udhayakala et.al and a very good correlation was obtained between theoretical and experimental results [200]. Hammouti et.al extended their research towards the mode of inhibition of 2,5-bis(4-methoxyphenyl)-1,3,4-oxadiazole for mild steel corrosion in H_3PO_4 by weight loss techniques and explained the role of adsorption in corrosion inhibition [201]. The research team of Bentiss studied some pyridyl based 1,3,4-oxadiazoles as corrosion inhibitors for mild steel in 1 M $HClO_4$ by weight loss, impedance and polarization studies and established them as very good inhibitors [202]. An interesting work on fatty acid based 1,3,4-oxadiazoles as anti corrosion agents for mild steel corrosion in 15% HCl was done by M.A.Quriaschi and team and a mixed type adsorption was found which is responsible for corrosion [203].

After a thorough survey of literature and considering the excellent pharmacological properties of benzimidazoles as well as 1,3,4-oxadiazoles, the present investigation aims to check the corrosion inhibition capacity of benzimidazole derivatives alone and by an incorporation of these two classes of compounds for designing the structure and its corrosion inhibition capacity for mild steel in various acidic environments.

References

1. A.P. Mishra, M.Khare, Indian J Chem. Soc., 77 (2000) 367

2. R.S.Siddiqui, N.Nishat, Synth React Inorg Met-Org Chem., 30 (2000) 1005

3. M.R.Maurya, N.Bharatia, Transition Met Chem., 23 (1993) 5

4. N. Hall, "The New Chemistry", Cambridge University Press, (2000).

5. S.Ahrland, J.Chatt, D.R.Davies, Quart.Rev., 12 (1958) 265

6. R.G.pearson, J.Am.Chem.Soc., 85 (1963) 3533

7. R.G.Pearson, Chem.Eng.News, 43 (1965) 90

8. R.G.Pearson, Chem.Brit.3 (1967) 103

9. Richard H. Holm, Pierre Kennepoh, Edward I. Solomon, Chem. Rev., 96 (1996) 2239

10. S.M. Saadeh, Arab. J. Chem., 6 (2013) 191

11. M.Kalita, P.Gogoi, P.Barman, B.Sarma, A.K.Buragohain, R.D. Kalita, Polyhedron, 74 (2014) 93

12. Sujit Baran Kumar, Ankita Solanki, Suman Kundu, J.of Mol.str., 1143, (2017) 163

13. Debanjana Biswal , Nikhil Ranjan Pramanik , Syamal Chakrabarti ,G.B. MichaelDrew, Bithika Sarkar , Mannar R. Maurya , Sanjib K. Mukherjee and Pramit Chowdhury,

    New J. Chem., 41 (2017) 4116

14. Puspendu Roy, Apurba Sau Mondal, Ajoy Kumar Pramanik, Tapan Kumar Mondal, J.Organomet.Chem 828 (2017) 1

15. Sethuraman Kannan, Rengan Ramesh, polyhedron, 25 (2006) 3095

16. R.H. Holm, E.I. Solomon, Chem. Rev., 104 (2004) 347

17. P.V. Rao, R.H. Holm, Chem. Rev., 104 (2004) 527

18. R. Panda, Y.G. Zhang, C.C. McLauchlan, P.V. Rao, F.A.T. deOliveira, E. Munck, R.H. Holm, J. Am. Chem. Soc., 126 (2004) 6448

19. J.F. Jiang, R.H. Holm, Inorg. Chem., 43 (2004) 1302

20. Chung-Hang Leung, Sheng Lin,b Hai-Jing Zhonga and Dik-Lung Ma, Chem. Sci., 6 (2015) 87

21. Tahmeena Khan, Shalini Dixit, Rumana Ahmad, Saman Raza Iqbal Azad, Seema Joshi, Abdul Rahman Khan J Chem Biol., (2017) 1091

22. Khushbu Gumber Anjali Sidhu Robin preet Kaur, Appl Nanosci., 7 (2017) 95

23. M.Wang, X. Hu, P. Liu, W. Li, X. Gong, F. Huang, Y.Cao, J. Am. Chem. Soc.133 (2011) 9638

24. Wiberg,B.Kenneth, Rablen,R. Paul, . *J*. Am. Chem.Soc*.,* 117 (8) (1995) 2201

25. C. N. R. Rao, R. Venkataraghavan, T. R. Kasturi, Can. J. Chem., 42(1) (1964) 36

26. Text Book of Heterocyclic Chemistry by Raj.K Bansal, New age international publishing limited page No.223, (2005), Third edition, ISBN No.81-224-1212-2

27. C. N. R. Rao, R. Venkataraghavan, Spectrochem. Acta., 18 (1962) 541

28. C.S.G Prasad , S K Banerjee, J.of Inorg.Nucl.Chem.37 (1975) 1989

29. G.Contreras, R.Schmidt, J.of Inorg.Nucl.Chem.32 (1970) 1295

30. Mohamed M. Ibrahim, Abd El-Motaleb M. Ramadan Shaban Y. Shaban Gaber A. M. Mersal1,Mohamed M. Soliman Salih Al-Juaid, J Inorg Organomet Polym.,27 (2017) 1252

31. Pecile C, Inorg.Chem.5 (1966) 210

32. A.Norman,Bell,N.Timothy,Branston,WilliamClegg Lynn Parker, Eric. S. Raper Chris Sammon Christopher P. Constable, Inorganica Chim. Acta., 319 (2001) 130

33. B.Singh and R.D.Singh, J.Inorg.Nucl.Chem. 39 (1977) 25

34. D.C.Jicha, D.H.Busch J.Inorg.Chem., (1962) 878

35. D.M.Adams, P.J.chadler, J.Chem.Soc., (1969) 558

36. D.M.Adams, "Metal ligand and Related vibrations", Arnold Publishing company, London, 269 (1967) 316

37. R.Ferraro, Low Frequency Vibrations of Inorganic and Coordination Compounds, Plenum Press, New York (1971)

38. S.Chandra, D.Jain, A.K.Sharma, Spectrochim. Acta A., 71 (2009) 1712

39. Kazuo Nakamoto, Text book of Infrared and Raman Spectra of Inorganic and Coordination Compounds, Wiley Interscience Publication, (1997)

40. A.Tramer, J.Chem.Phy., 59 (1962) 232

41. Tarlok S. Lobana, , Poonam Kumari, , Geeta Hundal, , Ray J. Butcher, , A. Castineiras Takash, Inorg.Chim.Acta., 394 (2013) 605

42. Kiran Singh, Ritu Thakur, Vikas Kumar, beni-suef university journal of basic and applied sciences 5 (2016) 21

43. Kiran Singh Sunita Raparia Parveen Surain, Med Chem Res., 24 (2015) 2336

44. Sangamesh A. Patil, M. Manjunatha, Ajaykumar D. Kulkarni & Prema S. Badami, Complex Metals., 1:1 (2014) 128

45. Prateek Tyagi , Monika Tyagi, Swati Agrawal , Sulekh Chandra , Himanshu Ojha , Mallika Pathak, Spectrochimica Acta Part A: Molecular and Biomolecular Spectroscopy 171 (2017) 246

46. R. Ragab Amin, A.Ahmed , M. El-Reedy, Y.Tajedin Alansi,Yamany B. Yamany, Open Journal of Inorganic Chemistry, 6 (2016)) 89

47. Lj. S. Vojinović-Ješić, V. M. Leovac, M. M. Lalović, V. I. Češljević, Lj. S. Jovanović, M. V. Rodić and V. Divjaković:, J. Serb. Chem. Soc., 76 (6) (2011) 865

48. M.Reda. Abdel-Rahman, S.T.Mohamed.Makki, E.Tarik. Ali, Magdy A. Ibrahimb, J. Heterocyclic Chem., 5(52) (2015) 1595

49. Abdel-Rahman, R. M. Farmaco 1991, 46, 379-384. PMid:1859590

50. M. Abdel-Rahman Pharmazie, 56 (2001) 18

51. Hosam A. Saad , Mohamed M. Youssef ,Mosselhi A. Mosselhi, , Molecules 16 (2011) 4937

52. Z.El-Gendy, J.M.Morsy, H.A.Allimony, W.R.Abdel-Monem, R.M. Abdel-Rahman Phosphorus, Sulfur Silicon Relat. Elem., 178 (2003) 2055

53. Krzysztof Sztanke , Jolanta, Rzymowska , Maciej Niemczyk , Izabela Dybała, Anna E. Kozioł, Eur. J. Med. Chem., 41 (2006) 539

54. L M Mironovich, M A Ivanov Chem Heterocycl Compd., 39 (2003) 1207

55. Pascal Dao, Daniel Lietha, Mélanie Etheve-Quelquejeu, Christiane Garbay, Huixiong Chen, Bioorganic Med. Chem. Lett. 27 (2017) 1727

56. Mardia Telep El Sayed, Hoda Abdel Rauof Hussein, Dalia Ahmed Osman, J of Chinese chemical society., 64(1), (2017) 36

57. N. Parmar, S.Teraiya, R.Patel, H.Barad, H.Jajda, V.Thakkar, J Saudi Chem Soc., 19:36 (2015) 36

58. J.N. Sangshetti, D.B. Shinde Bioorg. Med. Chem. Lett., 20 (2010) 742

59. P.D. Bremner, and J.J. Meyer. Planta Med., 64 (8) (1998) 777.

60. S.F. Nielsen, T. Boesen, M. Larsen, K. Schonning, and H. Kromann. Bioorg. Med. Chem., 12 (11) (2004) 3047

61. K.Singh etal., Eur. J.l of Med. Chem.., 42 (2007) 394

62. MM. Meenaxi, R. Ainapure, PB. Patil, & AR. Bhat, Asian J. Res. Chem., 4 (7) (2011) 1050

63. YP. Hou, J. Sun, ZH. Pang, PC. Lv, DD. Li, L. Yan, HJ. Zhang, EX. Zheng, J. Zhao, & HL. Zhu, Bioorg. Med. Chem., 19 (2011) 5948

64. K. Arul, & AA. Smith, " The Experiment, 21 (1) (2014) 1439

65. MN. Mousa, & SAN. Al-jadaan, Bas. J. Vet. Res., 11 (1) (2012) 122

66. S. Nachiket. Dighe et al Annals of Biological Research., 1 (2010) 82

67. Birsen Tozkoparana, Nesrin Gökhana, Göknur Aktayb, Erdem Yes¸iladac, Mevlüt Ertan, Eur. J. Med. Chem,. 35 (2000) 743

68. D. N. Dhar and C. L. Taploo, J. of Sci. and Ind.Res., 41(8) (1982) 501

69. Rayati, Saeed, et al. J. of.Coord.Chem.,70:.8 (2017) 1424

70. M Prajila., Abraham Joseph, J. of Mol. Liq. 241 (2017) 1

71. *D. H. Busch, Rec. Chem. Prog*. *25* (1964) *107*

72. TechniquesKarema MasoudeAbuamer, Abdussalam Ali Maihub, Marei Miloud El-Ajaily, Abdunnaser MohamedEtorki, Mortaja MohamedAbou-Krisha, Majda AlbashirAlmagani, International Journal of Organic Chemistry, 4(1) (2014) 4362

73. G. Bringmann, M. Dreyer, J.H. Faber, P.W. Dalsgaard, D. Staerk, sJ.W. Jaroszewski, *J*. Nat. Prod., 67 (2004) 743

74. A.O. De Souza, F.C.S. Galetti, C.L. Silva, B. Bicalho, M.M. Parma, S.F. Fonseca, Quim. Nova., 30 (2007) 1563

75. *H. Nozaki; H. Takaya; S. Moriuti; R. Noyori,* Tetrahedron.. *24 (9) (1968) 365*

76. R.S. Varma, R. Dahiya, S. Kumar, Tetrahedron Lett., 38 (12) (1997),2039

77. J. Schmeyers, F. Toda, J. Boy, G. Kaupp, Chem Soc Perkin Trans., 2 (4) (1998) 989

78. A. Vass, J. Dudás, R.S. Varma, Tetrahedron Lett., 40 (27) (1999) 4951

79. K. Tanaka, R. Shiraishi, Green Chem, 2 (6) (2000) 272

80. C.K.Z. Andrade, S.C.S. Takada, L.M. Alves, J.P. Rodrigues, P.A.Z. Suarez, R.F. Brandão, *et al,* Syn let., 12 (2004) 2135

81. MÁ Vázquez, M. Landa, L. Reyes, R. Miranda, J. Tamariz, F. Delgado, Synth Commun., 34 (15) (2004) 2705

82. M. Gopalakrishnan, P. Sureshkumar, V. Kanagarajan, J. Thanusu, R. Govindaraju, J.Chem Res, 5 (2005) 299

83. Karthikeyan, Muthukumarasamy, Vyas, Renu, Text book of Practical Chemoinformatics, Springer India, 2014

84. C.A.Lipinski,, F.Lombardo,, B.W.Donimy,., & P.J.Feeny, Advanced Drug Delivery Reviews, 23 (1997) 3

85. D.F.Veber, S.R.Johnson, H.Cheng, B.R.Smith, K.W.Ward, & K.D.Kopple, J. of Med. Chem., 45 (2002) 2615

86. M.Congreve, R.Carr, C.Murray, H.Jhoti, Drug Discov. Today. 8 (19): (2003) 876

87. Ghose,A.K. et al. J. Comb. Chem. 1 (1999) 55

88. C.Bradley, Doak & Jan Kihlberg, Expert Opinion on Drug Discovery, 12:2 (2017) 115

89. I.Kola,; J.Landis, Nat. Rev. Drug. Discovery,3 (2004) 711

90. Feixiong Cheng, Weihua Li, Yadi Zhou, Jie Shen, Zengrui Wu, Guixia Liu, Philip W. Lee, and Yun Tang, J. Chem. Inf. Model., 52 (2012) 3099

91. T.Hou,; J.Wang,. Expert. Opin. Drug Metab. Toxicol. 4 (2008) 759

92. Text book Drug like properties, concepts structure design and methods from ADME to Toxicity optimization – Edward H Kerns & Li Di – Elsevier , 2008

93. Ames B.N.,Proc,Nat.Acad.Sci., 69(1972) 3128

94. N Quignot; J Hamon.; F Bois, Extrapolating in vitro results to predict human toxicity, in In Vitro Toxicology Systems, Bal-Price A., Jennings P., Eds, Methods in Pharmacology and Toxicology series. New York, USA: Springer Science (2014) 531

95. J H Sung, M B Esch, , M L Shuler, Expert Opinions in Drug Metabolism and Toxicology., 6 (2010) 1063

96. B J McConkey, V Sobolev, M Edelman, Current Science. 83 (2002) 845

97. Nahid Shahabadi, SomayehBagheri, Spectrochimica Acta Part A: Molecular and Biomolecular Spectroscopy, 136 (C5) (2015) 1454

98. Kiran Singh , Ritu Thakur , Vikas Kumar**,** b e n i - s u e f u n i v e r s i t y journal of b a s i c and a p p l i e d s c i e n c e s, 5 (2 0 1 6) 21

99. A. Taha , A.A.M. Farag , O.M.I. Adly , N. Roushdy , Magdy Shebl, H.M. Ahmed, J. of Mol. Str., 1139 (2017) 31

100. A. S, Ramasubramanian, B.Ramachandra Bhat, R. Dileep, Sandya Rani, J. Serb. Chem. Soc., 76 (1) (2011) 75

101. A.S. Ramasubramanian, B. Ramachandra Bhat and R. Dileep,

Rasayan J of Chemistry.,.3(1) (2010) 1496

102. Singh, Kiran., Sunita Raparia, and Parveen Surain, Med.Chem.Res., 24.6 (2015): 2336

103. Kiran Singh, YogenderKumar,ParveshPuri ,Chetan Sharma,K. R.Aneja, Med Chem Res., 21 (2012) 1708

104. Ghassemzadeh, Mitra, et al., Journal of the Iranian Chemical Society 9.3 (2012) 285

105. Kiran Singh, Yogender Kumar, Parvesh Puri, Chetan Sharma,and Kamal Rai Aneja., ' International Journal of Inorganic Chemistry., 2012 (2012), Article ID 873232

106. K. Singh, Y. Kumar and M.S. Barwa, 168 S. Afr. J. Chem.,63 (2010) 169

107. A. M. Hammam , M. A. EL-Gahami, Z. A. Khafagi, M. S. AL-Salimi and S. A. Ibrahim, *J. Mater. Environ. Sci. 6 (6) (2015) 1596*

108. Gangadhar B. Bagihalli, Prakash Gouda Avaji ,Sangamesh A. Patil , Prema S. Badami, Eur. J. of Med.l Chem., 43(12) (2008) 2639

109. Kiran Singh, Manish Kumar and Vikas Kumar, Int. J of chemical science and Technology.,

110. Anjali Jha, Y L N Murthyb ,and G Durga,m RJPBCS 6(1) 1306

111. Zahid H. Chohan , Sajjad H. Sumrra , Moulay H. Youssoufi , Taibi B. Hadda, Eur. J.of Med. Chem., 45 (2010) 2739

112. Prateek Tyagi, Sulekh Chandra, B.S. Saraswat, Deepak Yadav Spectrochimica Acta Part A: Molecular and Biomolecular Spectroscopy 145 (2015) 155

113. Muhammad Hanif, Zahid H. Chohan Spectrochimica Acta Part A: Molecular and Biomolecular Spectroscopy 104 (2013) 468

114. Said Amer, Nadia El-Wakiel Hoda El-Ghamry, J. of Mol. Str., 1049 (2013) 326

115. A. K. Singh, O. P. Pandey and S. K.Sengupta, Spectrochimica Acta Part A: Molecular and Biomolecular Spectroscopy, 85(1) (2012) 1

116. Prateek Tyagi Monika Tyagi Swati Agrawal Sulekh Chandra Himanshu Ojha Mallika Pathak, Spectrochimica Acta Part A: Molecular and Biomolecular Spectroscopy 171 (2017) 246

117. Mostafa Y. Nassar · Hisham M. Aly · Moustafa E. Moustafa1 · Ehab A. Abdelrahman, J Inorg Organomet Polym., DOI 10.1007/s10904-017-0569-x

118. Mostafa Y. Nassar, Hisham M. Aly, Ehab A. Abdelrahman, Moustafa E. Moustafa, J. of Mol. Str. 1143 (2017) 462

119. Kiran Singh , Yogender Kumar , Parvesh Puri , Chetan Sharma , Kamal Rai Aneja, Arab.J. of Chem., 10 (2017) S978

120. M.G. Fontana, Corrosion Engineering, 3rd edn. New York: McGraw-Hill Book Company (1986)

121. Zaki Ahmad , Text Book of Corrosion Engineering and Corrosion Control, Elsevier, ISBN -13: 978-0-7506-5924-6

122. Prayer, J.H., et al. Material Performance, (1980). May-Nov.

123. Branko.N.Popov., corrosion Engineering – Principles and solved problems, Elsevier (2015)

124. H. Hadert, Industrie Lackierbetrieb, 36 (1968) 184.

125. Oliver P Watts, J. Electrochem. Soc., 64(1) (1933) 125

126. W. R. Whitney, Corrosion. ,3(7) (1947) 331

127. Robert Heider S Bach, Metallurgy and Corrosion control in oil and gas Product, Wiley, (2011)

128. D. F. Bahr, A. L. Olson, K. R. Morasch, M. S. Kennedy, D. R. Marek, and A. Alamr, Materials Research Society Symposium Proceedings, 795 (2004) 55

129. Fundamentals of Electrochemical corrosion 2000 ASM International, www.asminternational.org

130. R.Narayan, An introduction to metallic corrosion and its prevention, Oxford Publishing Company, New Delhi (1990).

131. Corrosion Understanding the Basics, edited by J.R Davis, Davis and Associates, ASM International, (2000) ISBN No.0-87170-641-5

132. Varma Marimuthu, Isabelle Dula. Krishnan Kannoorpatti , J Bio Tribo Corros , 2:17 (2016)

133. M.J.Mimoz, Portero, J.Garcia Anton, J.L.Guinon, V.Peres, Herranz, Corrosion, 63(7) (2007) 625

134. M. S. Al-Otaibi, A. M. Al-Mayouf,. M. Khan, A. A. Mousa, S. A. Al-Mazroa e H. Z. Alkhathlan, Arab. J. of Chem., 7(3) (2014) 340

135. A.L.d.Q. Baddini, S.P. Cardoso, E. Hollauer, J.A.d.C.P. Electrochim. Acta, 53 (2007). 434

136. V. Gentil, Corrosão, 4 ed., Rio de Janeiro: LTC, 2003

137. I.B. Obot, N.O. Obi-Egbedi, S.A. Umoren, Corros Sci., 51(8), (2009) 1868.

138. Jones, L. W., Corrosion and Water Technology for Petroleum Producers, Tulsa, Okla, Oil and Gas Consultants International, (1988).

139. N. Hackerman, , E.S. Snaveley, Inhibitors, in Brasunas, A. de S. (ed.), Corrosion Basics, Houston, Tex., NACE International, (1984), 127

140. Evelin Gutierrez, Jose A.Ratriguez, Julian Cruz Borbolla, Pandiyan Thangarasu, Corros. Sci., 108 (2016) 23

141. R. F. V. Villamil, P. Corio, S. M. L. Agostinho, J. C. Rubin, J. Electroanal. Chem. 472 (1999) 112

142. E.McCafferty, Leidheiser Jr. H (Ed.), Corrosion control by coating, Science Press, Princeton, (1979)

143. E. Khamis, Corrosion 46 (1990) 476

144. S. S. Abd El-Rehim, A. Magdy, A.M. Ibrahim, K.F. Khaled, J. Appl. Electrochem. 29 (1999) 593

145. H. Ashassi-Sorkhabi, D. Seifzadeh, M.G. Hosseini, Corros.Sci., 50 (2008) 3363

146. S Martinez, Mat. Chem. and Phy., 77(1) (2003).97

147. S.Shibli, V.Saji,Corros. 47(.9) (2005).2213.

148. Techniques for corrosion monitoring, 1st edn., Woodhead Publishing ISBN : 9781845694050.

149. M.Winkelmans, M.Wevers, J.Accoustic emission, 20 (2002) 206

150. Neagoe, C. (2001) Ph.D Thesis, University of Bucharest, Bucharest

151. Electrochemical Polarization techniques for corrosion monitoring, Sankara papavinasam, Canmet, Canada, chapter 3

152. Nestor Perez, Electrochemistry and Corrosion Science, SpringerInternational Edn., (2010)

153. Benedetti M. D., Loreto G., Matta F. and Nanni A., Material In Civil Engineering Journal © ASCE, (2013) 1022

154. C. Wagner and W. Traud, Z. Elektrochem. 44 (1938) 391

155. S Evans and EL Koehler, etectrochem. Sot:, 108 (1961) 509

156. M Stern and A Geary ElectrtK'hem. Soc 104 (1957) 56

157. U.Rammett & G.Reinhard, Prog. in Org. coat. 21(2-3) (1992) 205

158. H. Cesiulis, N. Tsyntsaru, A. Ramanavicius, G.Ragoisha, The Study of Thin Films by Electrochemical Impedance Spectroscopy, Nanostructures and Thin Films for Multifunctional Applications pp 3-42

159. Robert G Kelly, John R Scully david, W.Shoesmith, Rudolph G.Buchheit, Marcel Dekker Inc, Electrochemical Techniques in corrosion science and Engineering

160. Computational Chemistry: A Practical Guide for Applying Techniques to Real-World Problems. David C. Young Copyright (2001) John Wiley & Sons, Inc.ISBNs: 0-471-33368-9 (Hardback); 0-471-22065-5

161. J. P. Lowe, "Quantum Chemistry," 2nd edn, Academic Press, New York, (1993)

162. I. N. Levine,"Quantum Chemistry," 4th edn, Prentice Hall, Engelwood Clif

163. K I Ramachandran et al., Computational chemistry and molecular modeling, Springer (2008), chapter 7, New Jersey, 200

164. Mudar A. Abdulsattar and Khalil H. Al-Bayati, Phys. Rev. B 75, 245201 (2007)

165. P. Hohenberg and W. Kohn, Phys. Rev. B 136 (1964) 864

166. W. Kohn and L. J. Sham, Phys. Rev. A 140 (1965) 1133

167. David Lai Gwai Cheung, Structures and properties of Liquid crystals and Related Molecules from Computer Simulation, Doctoral thesis, Durham University.

168. Gökhan Gece , Corros. Sci. 50 (2008) 2981

169. E. Kraka, D. Cremer, J. Am. Chem. Soc. 122 (2000) 8245

170. G.T. Xavier, B Thirumalairaj,. , M Jaganathan,. International Journal of Corrosion, (2015) 1-15

171. I B Obot, E E Ebenso., A S Afolabi, E E Oguzie, Res.on Chem.l Intermed. 39(5) (2013) 1927

172. S. Junaedi, A A Al-amiery, ., A Kadihum, A. and Kadhum,A. A. H.. Int. J. of Mol. Sci., 14 (2013) 11915-11928

173. Obi-Egbedi, N. O. 1andOjo, J.of Sci.Res. 14 (2015) 50

174. H J Chermette, Comput. Chem., 20 (1999) 129

175. R.G Pearson., Inorg. Chem. 27 (1988) 734

176. R G Parr, P K Chattaraj. Principle. J Am Chem Soc., 113 (1991) 1854

177. Edward Ghali, V. S. Sastri, M. Elboujdaini, Corrosion prevention and protection Practical solutions, John.Wiley and Sons, Ltd., (2007)

178. C. Verma, M.A. Quraishi, A. Singh, J. Taiwan Inst. Chem. Eng. 58 (2016) 127

179. H.Ju.Z.Kai, Y.Li, Corros. Sci, 50 (2008) 865

180. Sam John and Abraham Joseph, RSC Advances, 2, 9944 (2012)

181. I.Lukovits, Zucchi F, E.Kalmann,, Corrosion, 57 (2001) 3

182. Compilation of ASTM Standard Definitions, 3rd ed., American Society for Testing and Materials, Philadelphia, Pa. 19103 (1976).

183. Benavent, Llorenç, et al. Molecules 22.8 (2017): 1333.

184. Apohan, Elif, et al. *Journal of* Org.omet. Chem. 828 (2017) 52

185. Y. Abboud , A. Abourriche , T. Saffaj , M. Berrada , M. Charrouf ,A. Bennamara , A. Cherqaoui , D. Takky App. Sur. Sci.252 (2006) 8178

186. H El Sayed, et al. Prog. in Org. Coat.61.1 (2008): 11

187. K. Bouayad, Y. Kandri Rodi, E. H. El Ghadraoui, H. Elmsellem, Y. Ouzidan, B. El Mahi, E. M. Essassi, I. Abdel-Rahman, A. Chetouani, B. Hammouti Mor. J. Chem. 5N°2 (2017) 285

188. oddahosuru M. Gurudatt and Kikkeri N. Mohana, J of Applicable Chem. 2 (5) (2013) 1296

189. Yadav, D. Behera, S. Kumar and R. R. Sinha. Ind. Eng. Chem. Res., 52 (2013) 6318

190. X. Wang, Y. Wan, Q. Wang and Y. Ma, *Int. J. Electrochem. Sci.,*8 (2013) 806

191. Tang, Yongming, et al. . Corros. Sci.74 (2013): 271

192. Hasan R Obayes, Ghadah H Alwan, Abdul Hameed MJ Alobaidy,Ahmed A Al-Amiery, Abdul Amir H Kadhum, Abu Bakar Mohamad Chemistry Central Journal , 8 (2014) 21

193. X. Zheng, et al. Corros. Sci., 80 (2014): 383

194. Zhang, Dongqin, et al. Corrosion Science 102 (2016) 517

195. *A.K.*Dutta, et al. Corros. Sci. 123 (2017) 256

196. F. Bentiss, M. Traisnel, M. Lagrenee. Corros. Sci. 42.1 (2000) 127

197. H. Ouici , M. Tourabi , O. Benali , C. Selles , M. Traisnel , C. Jama , F. Bentiss , R. Salghif, J. Mater. Environ. Sci. 7 (8) (2016) 2971

198. Doddahosuru M. Gurudatt and Kikkeri N. Mohana, Ind. Eng. Chem. Res. 53 (2014) 2092

199. C. B. Pradeep Kumar and K. N. Mohana, Journal of Chemical and Pharmaceutical Research, 5(10) (2013) 28999.

200. P. Udhayakala, A. Maxwell Samuel, T. V. Rajendiran, S. Gunasekaran., Der Pharmacia Letters, 5 (2) (2013) 272

201. M. Benabdellah, B. Hammouti, A. Warthan, S.S. Al-Deyab, C. Jama, M. Lagrenée, F. Bentiss Int. J. Electrochem. Sci., 7 (2012) 3489

202. M. Lebrini et al. App. Sur. Sci. 252 (2005) 950

203. A.Quraishi, D. Jamal Mat. Chem. and Phy. 71 (2001) 202

2 MATERIALS AND METHODS

Chapter II describes the experimental details involved in the whole work. It includes preparation and characterization of ligands for both complex formation and corrosion inhibition studies. The instrumental details of various characterization techniques, the procedure of corrosion monitoring methods like gravimetric measurements and electroanalytical techniques, details of in silico, in vitro biological screening and molecular docking studies, and theoretical calculations performed are also discussed.

This chapter describes the details regarding the reagents, preparation and characterization of ligands for complex formation and corrosion inhibition studies, electroanalytical techniques employed and details of biological and computational studies.

II.1. Reagents used

The metal salts for the synthesis of coordination compounds are ferric nitrate (Merck), cobalt acetate (Merck), nickel acetate (Sisco-Chem industries), copper acetate (SRL chemicals) and zinc acetate (SRL chemicals). Various reagents used in the synthesis of ligands include hydrazine monohydrate (E.Merck), glycolic acid (E.Merck), carbon disulphide, pyruvic acid, o-phenylene diamine (Lobachemie), acetic acid, propionic acid, n-butyric acid, ethyl chloroacetate, potassium carbonate, potassium hydroxide, vanillin, and 2,4-dihydroxy benzaldehyde .

II.2 Ligands for complex formation studies

The complex formation of Schiff bases of 1,2,4-triazole and 1,2,4-triazine derivatives were studied. The synthetic strategies of ligands are discussed below.

II.2.1. *Synthesis of 4-amino-4-H-1,2,4-triazole-3,5-dimethanol (ATD) and Schiff bases DHATD and HMATD*

1,2,4-triazole precursor, 4-amino-4-H-1,2,4-triazole-3,5-dimethanol (ATD) was prepared by the condensation of hydrazine monohydrate with glycolic acid. 0.75 mol of hydrazine monohydrate was added drop wise to 0.50 mol of 70% glycolic acid at 0°C. The resulting solution was refluxed at 120°C for 6 h. Then the reflux condenser was replaced with a downward condenser and the reaction mixture was heated at 160 °C for a further 18 h allowing excess hydrazine and water to distil off. After cooling, the yellowish

crystalline solid obtained and was recrystallized from water to give analytically pure ATD [1]. M.P. of the compound is 206°C. The Schiff bases, 4-{[3,5-bis(hydroxymethyl)-4*H*-1,2,4-triazol-4-l]imino}methyl]-2 methoxyphenol (HMATD) and 4-{[3,5-bis(hydroxymethyl)-4*H*-1,2,4-triazol-4-yl]imino}methyl]benzene-1,3-diol (DHATD) were synthesized by the condensation of ATD with vanillin and 2,4-dihydroxybenzaldehyde respectively using ethanol as solvent. The schematic representation of synthetic strategy is given in Fig 2.1

II.2.2. Synthesis of 4-amino-3-mercapto-6-methyl-1,2,4-triazine-4H-5-one (AMMT) and Schiff bases MHMMT and DMSTT

1,2,4-triazine derivative 4-amino-3-mercapto-6-methyl-1,2,4-triazine-4H-5-one (AMMT) was synthesized in two steps. In the first step, to a mixture of 50 mL of hydrazine hydrate and 150 mL of water, about 0.2 mol of carbon disulphide (CS_2) were added drop wise over about an hour maintaining the temperature below 15°C with constant and vigorous stirring. After the completion of addition, the reaction mixture was refluxed for an hour at 90°C, and then cooled. White crystals of thiocarbohydrazide (TCH) separated out, recrystallized from hot water and dried (M.P - 170°C). In the later stage, about 23 g of TCH was added to 170 mL of boiling water in a beaker and 14 g of pyruvic acid was added to it slowly with constant stirring. Light yellow crystals of AMMT were separates out and the same is recrystallized from ethanol (M.P - 80°C). The refluxing of AMMT with vanillin and 2,4-dihydroxybenzaldehyde in ethanolic medium yields yellow crystalline Schiff bases 4-[(4-hydroxy-3-methoxybenzylidene)amino]-6-methyl-3-thioxo-3,4-dihydro-1,2,4-triazin-5(2*H*)-one (MHMMT) and 4-{[(1*E*)-(2,4-dihydroxyphenyl)methylene]amino}-3-mercapto-6-methyl-1,2,4-triazin-5(4*H*)-one (DMSTT). The scheme of synthesis is given as Fig 2.2 [2].

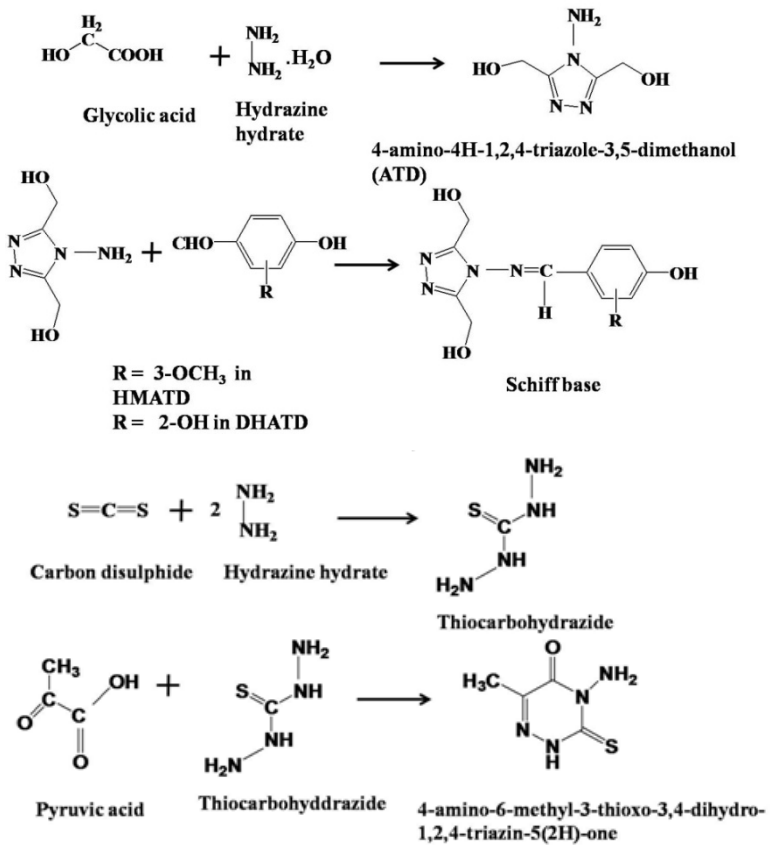
Glycolic acid
Hydrazine hydrate
4-amino-4H-1,2,4-triazole-3,5-dimethanol (ATD)
R = 3-OCH3 in HMATD
R = 2-OH in DHATD
Schiff base
Carbon disulphide
Hydrazine hydrate
Thiocarbohydrazide
Pyruvic acid
Thiocarbohyddrazide
4-amino-6-methyl-3-thioxo-3,4-dihydro-1,2,4-triazin-5(2H)-one

Fig 2.1

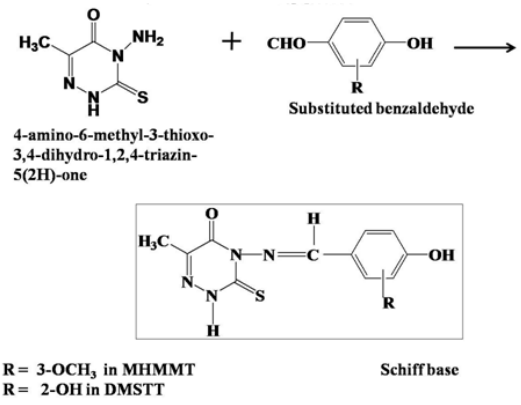
4-amino-6-methyl-3-thioxo-3,4-dihydro-1,2,4-triazin-5(2H)-one
Substituted benzaldehyde
R = 3-OCH3 in MHMMT
R = 2-OH in DMSTT
Schiff base

Fig 2.2

II.3 Synthesis of compounds for corrosion inhibition studies

Two classes of 2-substituted benzimidazole bearing compounds viz., acetahydrazides and 1,3,4-oxadiazoles were tested for their corrosion inhibition ability. The synthesis of inhibitors was done as reported in literature [3,4].

II.3.1 *Synthesis of 2-(2-methyl/ethyl/propyl)-1H-benzimidazol-1-yl)acetohydrazide (EMBAH, EEBAH, EPBAH) (A)*

The synthesis consists of three steps. A mixture of o-phenylenediamine and aliphatic acid (1:1) was dissolved in 4 N HCl and refluxed at 100°C for 12 h. Afterwards the contents were cooled and neutralized with saturated solution of $NaHCO_3$. The solid separated out was 2-alkyl substituted benzimidazole. In the II stage, a solution of 2-alkyl substituted benzimidazole in acetone was refluxed with equal molar concentration of ethyl chloroacetate and potassium carbonate for 6 h. Excess acetone was distilled off, the solid product separated was recrystallized from ethyl acetate to give Ethyl (2-alkylbenzimidazolyl) acetate. In the last step, ethanol solution of the above compound refluxed with equal molar concentration of hydrazine hydrate for 4 h. The excess solvent was distilled off and the contents were added to excess of water, solid separated out which is recrystallized from ethanol to yield 2-(2-alkyl-1H-benzimidazol-1-yl)acetohydrazides. The scheme of synthesis is represented as Fig 2.3 [3].

II.3.2 *Synthesis of 1,3,4-oxadiazole bearing 2-alkyl benzimidazole Moiety: 5-((2-methyl/ethyl/propyl)-1H-benzo[d]imidazol-1-yl)methyl)-1,3,4-oxadiazole-2-thiol (MBIMOT,EBIMOT, PBIMOT) (B)*

A reaction mixture of ethanolic solution of potassium hydroxide (1.7 g in 25 mL), 0.02 mole of 2-(2-alkyl-1H-benzimidazol-1-yl)acetohydrazide (A) and 0.04 mole of carbon disulphide was refluxed for 6h. Then the

reaction mixture was allowed to cool to room temperature, concentrated, diluted with minimum amount of water and acidified with 1 N HCl. The solid thus separated was recrystallized using ethanol-DMF mixture. The scheme showing the steps involved are given in Fig (2.3) [4]

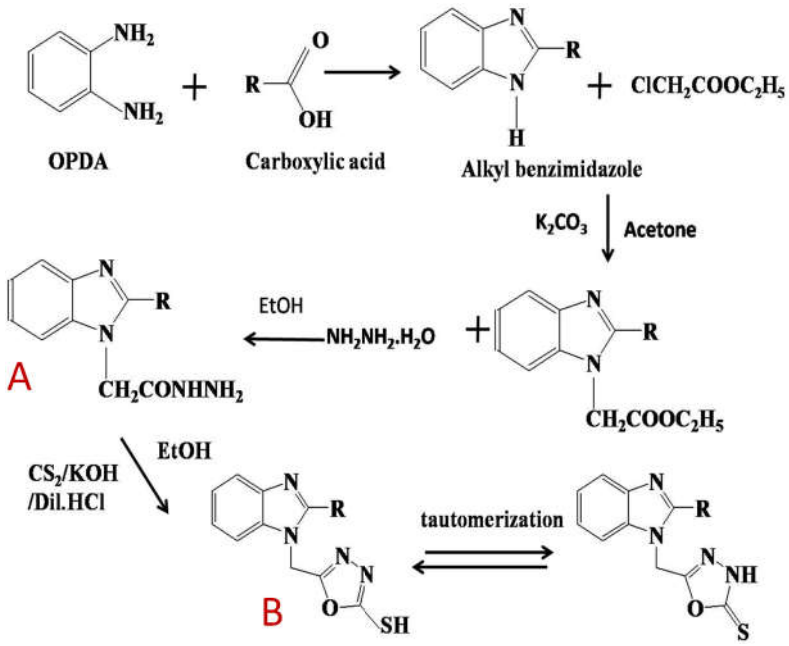

Fig 2.3

II.4 Characterization techniques

Various physico-chemical techniques including elemental, magnetic, IR, NMR, ESR and UV-VIS spectral techniques are employed for the characterization of ligands and their complexes as well as for the elucidation of their molecular structure.

II.4.1 Elemental analysis

Percentage of carbon, hydrogen, nitrogen and sulphur in the ligands as well as complexes were determined using a CHNS analyzer (Elementar Vario

EL III Model) at STIC, SAIF, Kochi. The instrument works on the principle of conversion of elements into their corresponding oxides by combustion and subsequent quantitative determination yields the percentage of elements. The percentage of metal in the complexes was determined by standard procedures [5].

II.4.2 Magnetic Susceptibility measurements

The magnetic susceptibility measurements of paramagnetic complexes are one of the most trusted methods to ascertain the molecular geometry of metal complexes. The studies were carried out in a Gouy balance (Sherwood Scientific Cambridge, UK) at room temperature using $Hg[Co(SCN)_4]$ as calibrant. The magnetic moment (μ_{eff}) was calculated form susceptibility values using the relation

$$\mu_{eff} = 2.828\sqrt{\chi_M^{corr}T}\ BM \qquad (2.1)$$

where χ_M^{corr} is the molar susceptibility corrected for diamagnetic moment, T the absolute temperature in K. The magnetic moment measurement gives valuable insight into the oxidation state of metal ion as well as geometry of complexes.

II.4.3 Infrared Spectroscopy

IR spectroscopy is a valuable tool for the characterization of ligands as well as complexes. The variation in the various stretching frequencies of ligand after complex formation can be effectively utilized for predicting the coordination site in the complex which can be subsequently confirmed by metal-donor atom vibrations. The IR spectra of ligands as well as complexes were taken by KBr pellet method on a JASCO FTIR-4100 instrument.

II.4.4 Proton Nuclear Magnetic Resonance Spectroscopy (^{1}H NMR)

The proton NMR spectra of ligands as well as diamagnetic zinc complexes were taken in solution front using DMSO as the solvent in Bruker Avance III 400 MHz NMR instrument at STIC, SAIF, Kochi. Tetramethylsilane (TMS) was used as the internal reference. The NMR spectrum helps to detect the protons at different chemical environments as well as the coordination site in complexes.

II.4.5 Electron Paramagnetic Resonance Spectroscopy (EPR)

EPR spectroscopy is one of the important techniques for the structure elucidation of paramagnetic metal complexes. The 'g' values, $g_{\parallel}$ and $g_{\perp}$, are helpful for illustrating the stereochemistry of Cu(II) complexes. They are mainly used for studying the coordination environment around copper complexes. The EPR spectra of copper complexes were taken in JES-FA200 ESR spectrometer at, SAIF, IIT Chennai using DMF as solvent.

II.4.6 Electronic Spectroscopy (UV-VIS)

Electronic spectroscopy is an important tool in the characterization of metal complexes. The spectrum is usually taken in the range of 200-900 nm. The ligands usually absorb in the lower wavelength region due to $\pi - \pi^*$ and $n - \pi^*$ transitions. On complex formation with metal ions, the wavelength as well as intensity of absorption alters and at the same time some new charge transfer bands and d-d- transitions may appear. These bands act as a valuable guide in the structure elucidation. The electronic spectra of ligands as well as paramagnetic metal complexes were recorded using JASCO-V-550 spectrophotometer both in Diffused Reflectance mode and in solution form.

II.5 Electroanalytical measurements

The electroanalytical measurements were employed mainly for the corrosion inhibition studies of mild steel in various acid media. A brief discussion of materials and techniques used for these studies are given below

II.*5.1 Material and medium*

The material used for corrosion studies was mild steel having the composition (wt. %): C (0.20%), Mn (1%), P (0.03%), S (0.02%) and Fe (98.75%), which was mechanically press cut into specimens of dimension 2 x 1.8 cm^2 and was used for the weight loss measurements. The electrochemical studies were conducted using the above said metal coupons as working electrode with an exposed area of 1 cm^2. The specimens were polished using various grades of emery paper, washed with distilled water, degreased in acetone, ethanol and dried at room temperature as per ASTM standard G-1-72. The corrosive medium for the studies were obtained by the dilution of reagent grade HCl, H_2SO_4 and HNO_3 (Merck) using distilled water. All the studies were conducted in aerated medium under standard conditions and at different temperatures using test solutions consisting of corrosive medium containing various concentrations of inhibitors.

II.5.2 Techniques

II.5.2.1 Gravimetric measurements

Gravimetric measurements were performed on mild steel coupons pre-treated as per ASTM standard and is immersed in aggressive corrosion solution with and without inhibitors for specific immersion time. The coupons were weighed before and after immersion in an analytical balance. From the weight loss, inhibition efficiency (IE) can be calculated using the following equation [6]

$$IE = \frac{W_0 - W_i}{W_0} \times 100 \qquad (2.2)$$

where W_0 and W_i represent weight loss in the absence and presence of inhibitor respectively.

II.5.2.2 Electroanalytical techniques

Two types of electroanalytical measurements - electrochemical impedance spectroscopy (EIS) and potentiodynamic polarization (PDP), incorporated in the present work were done in a conventional three electrode corrosion measurement system, Gill AC computer controlled electrochemical workstation (ACM instrument, model No: 1475) (Fig 2.4). The metal under investigation, a platinum foil and saturated calomel electrode with a Luggin capillary to minimize the IR drop function as working electrode, counter electrode and reference electrode respectively. Prior to each measurement, the working electrode is cleaned as per ASTM –G-1-72 standard procedure [7] and immersed in the electrolyte for a stabilization period for attaining a stable quasi steady state potential, which is represented as corrosion potential E_{corr}. All the experiments were triplicated. The data processing was done using ACM analysis software by non linear least square fitting procedure [8].

Fig 2.4

II.5.2.2.1 Electrochemical impedance spectroscopy (EIS)

The electrochemical impedance studies were done by perturbing the electrochemical system with an overvoltage of 10 mV with respect to E_{corr} at a frequency range of 0.1 Hz to 10 KHz. The response of the system was analyzed by the non-linear fitting of data to an equivalent circuit mainly Randles circuit shown in (Fig 1.4). The parameters like double layer capacitance C_{dl}, corrosion rate CR, charge transfer resistance R_{ct} were extracted by circle fitting methods. From the charge transfer resistance, the inhibition efficiency can be evaluated using the relation

$$IE = \frac{R_{ct} - R^{*}_{ct}}{R_{ct}} \times 100 \qquad (2.3)$$

where R_{ct} and R^{*}_{ct} represents the charge transfer resistance in the inhibited and uninhibited solutions respectively [9].

II.5.2.2.2 Potentiodynamic polarization studies (PDP)

In PDP measurements, the working electrode is polarized by an overvoltage of 250 mV with respect to E_{corr} first cathodically and then anodically using a potential with scan rate of 1mV/s. The Tafel plots obtained from this polarization help to explore the electrochemical parameters like the corrosion current density I_{corr}, corrosion potential E_{corr} , anodic and cathodic Tafel slopes β_a and β_c. by Tafel extrapolation method. The inhibition efficiency can be calculated from I_{corr} as

$$IE = \frac{I_{corr} - I^{*}_{corr}}{I_{corr}} \times 100 \qquad (2.4)$$

where I_{corr} and I^{*}_{corr}represents the corrosion current density in the absence and presence of inhibitors [10].

II.5.2.3 Surface Studies – Scanning Electron Microscopy (SEM)

The alteration in the morphology of mild steel surface in the absence and presence of inhibitor was analyzed also by surface morphological studies carried out using scanning electron microscopy (JEOL JSM 6380 LA Scanning Electron Microscope) at NITK, Surathkal. Prior to the analysis, the mild steel samples were thoroughly cleaned as per ASTM standard and immersed in corrosive solution with and without the inhibitors for 7 h. After the stipulated time, the samples were taken out, washed under running water and dried. The micrographs were taken at an accelerating voltage of 20 kV at different magnifications of x 500, x 1000 etc.

II.6 In silico biological screening studies

The literature revealed that 1,2,4-triazole and 1,2,4-triazine based Schiff bases and their metal complexes are potential candidates, considering their diverse applications in biological fields. The process of drug discovery requires a pre clinical test for oral bioavailability, drug likeness, toxicity etc. These pre-requisite tests were done by *in silico* methods using the following web based programmes.

II.6.1 Drug likeness and bioactivity score – Molinspiration software

The drug likeness and bioactivity scores of ligands and metal complexes were determined online using *www.molinspiration.com* website [11]. It has a wide range of cheminformatics tools which help in property calculations as well as Lipinski rule validation. Chemical structures and SMILES notations for the molecules were obtained using Chemdraw ultra software. These SMILES were then uploaded to the molinspiration software 2011.06 version to calculate various molecular properties like logP, topological surface area (TPSA), number of hydrogen bond donors and

acceptors, etc. and to predict bioactivity scores towards various drug targets like enzymes, nuclear receptors, kinase inhibitors, GPCR ligands, and ion channel modulators etc. [12].

II.6.2 ADME and Toxicity determination – ADMETSAR software

Pharmacokinetic studies of drug molecule mainly refer to the ADMET (absorption, distribution, metabolism, excretion and toxicity) properties evaluation which plays an important role in the early phases of drug discovery process. The online application on the website *http://www.lmmd.org/database/cheminformatics* has implemented various models which can predict ADMET properties. The SMILES notations obtained for chemical structure from ACD lab Chemsketch is fed into the ADMETSAR software to obtain bioavailability information [13, 14].

II.6.3 Prediction of Probable Activity Spectra of Substances – PASS online software

The biological activity of various chemical compounds that reflects the interaction of the compound with various biological entities can be obtained from PASS online software *www.pharmaexpert.ru/passonline*. It predicts the biological property of a compound as an intrinsic property which mainly depends on the structure and physicochemical behavior of the compound. This software gives two values for a particular activity p_a and p_i which represents the probability for a compound to be active (p_a) and probability to be inactive (p_i). For a compound considered for a particular activity, $p_a > p_i$ and if $p_a > 0.7$, the chances of finding the activity by experiment is high [14, 15].

*II.*7 In vitro studies*:*

II.7.1 In vitro antimicrobial studies:

In vitro anti bacterial and anti fungal studies were conducted by disc diffusion method and the procedure is as follows: Initially the bacterial and fungal stock cultures were inoculated in broth media followed by incubation at 37^{o}C. The standardized inoculums is inoculated in the aseptically prepared plates and allowed to dry at room temperature. Each plate was divided into 4 parts and in each part sample discs and standard discs were placed and refrigerated at 4^{o}C for diffusion of drug. Incubated at 37^{o}C for 24 h for bacterial study and 28^{o}C for 48 h for fungal studies and the diameter of the zone of inhibition was measured [16]

II.7.2 In vitro anticancer studies:

In vitro anticancer studies were conducted by MTT assay. It is one of the most frequently used assays for evaluating metabolic activity of cells which measures the cell viability and proliferation. The reduction of yellow tetrazolium salt 3-(4,5-dimethylthiazolyl-2)-2,5-diphenyl tetrazolium bromide (MTT) occurs in metabolic active cells by the action of NADH and NADPH dependent dehydrogenase enzyme to produce purple colored formazon and is solubilized in DMSO and quantitatively determined by spectrophotometric methods. MCF-7 cell lines purchased from National centre for Cell science, Pune, were kept as per the standard conditions [17]. The cell lines in the log phase were seeded into 96-well plates having a concentration 1 x 10^4 cells/well, were incubated overnight at 37^{o}C. The cells were then treated with different concentration of drug candidate. The control was also cultivated in the same condition without complex. The cells were incubated for 48 h and MTT assay was carried out. A stock solution of 5 mg/mL of MTT was prepared; 100 µL was added to each drug candidate treated wells

and incubated for 4 h. The purple colored formazon crystals obtained were dissolved in 100 µL of DMSO and spectrophotometrically determined at 620 nm in a multi well ELISA plate reader (Thermo, Multiskan).

II.7.3 Antidiabetic studies – α-amylase inhibition studies

α-amylase activity was carried out by starch-iodine method which works on the principle of hydrolysis of starch by α-amylase [18]. The starch solution without α-amylase shows a highly intense blue color (blank) B. But the solution with α-amylase, without any metal complexes, will be almost colorless (control) C and the introduction of metal complexes will retain some blue color for starch with iodine indicating the inhibition of α-amylase activity (A). 20 µl of α-amylase solution (1mg/mL) was mixed with 390 µL of phosphate buffer (0.02M phosphate buffer pH 7.0 containing 0.006 M NaCl, pH 7.0) containing different concentration of extracts. After incubation at 37°C for 10 min, 100 µL of starch solution (1%) was added, and the mixture was re-incubated for 1h. Next, 0.1 mL of 1% iodine solution was added, and after adding 5 mL distilled water, the absorbance was taken at 565 nm. Sample, substrate and α-amylase blank determinations were carried out under the same reaction conditions. Inhibition of enzyme activity was calculated as (%) = (A-C) X100/ (B-C), where, A= absorbance of the sample, B= absorbance of blank (without α-amylase), and C=absorbance of control (without starch).

II.8 Molecular docking studies

Molecular docking is an increasingly efficient tool of drug discovery which aims at modeling the interaction between drug molecules and proteins at atomic levels. It helps to characterize the interaction of drug molecule with the binding sites of target proteins and thus to illustrate fundamental biochemical process [19]. *In silico* docking studies were carried out using

Autodock 4.2 version and the images are rendered using Accelry's Discovery Studio Visualizer v 4.0 interface [20]. The crystal structure of the target enzyme/protein was obtained from RCSB protein data bank. The missing atoms in the crystal structure were repaired using repair command module of Autodock. Prior to docking, the enzyme/protein structure was modified by deleting the water molecules and by adding hydrogen atoms for exact ionization and tautomeric states of amino acid residues, and was used for semi flexible docking. The ligand molecules were drawn using ACD Chemsketch software. The energy minimization of ligand and target entity was done in Steepest Descent and Conjugate Gradient methods using Accelrys Discovery Studio (Version 4.0, Accelrys Software Inc.) [21]. The minimization was carried out with biomolecular simulation programme CHARMM (Chemistry at Harvard Macromolecular Mechanics) force field [22].

Autodock is helpful in predicting the binding site with associated binding energy and IC_{50} value of the compounds with target domain using the protocols followed elsewhere [23,24]. Lamarckian genetic Algorithms (LGA) were used as docking engine and all the docking parameters were set to default [25]. After each run, Autodock gives the report of best docking solution with IC_{50} values, and the results are obtained on the basis of cluster analysis. Binding energy is the sum of energies like dispersion/repulsion, electrostatic interactions, hydrogen bonding, and deviations from covalent geometry, desolvation effects and internal ligand torsional constraints. After 10 docking modes of LGA cluster analysis, the lowest energy docking mode with IC_{50} values were selected for simulation. Every compound was allowed to have active rotatable bonds to make them flexible.

II.9 Theoretical calculations

The geometry optimization of ligand molecules were done using DFT with Beck's three parameter exchange functional and the Lee-Yang-Parr non local correlation functional (B3LYP) with a 6-31G* basis set of atomic orbitals as implemented in Gaussian 09 programme package [26,27]. B3LYP is a hybrid version of DFT and HF methods which is one of the most accurate methods for energy calculations. The quantum chemical indices like E_{HOMO}, E_{LUMO}, ΔE, dipole moment, electro negativity, ionization potential, chemical softness and hardness etc. were taken into account.

II.10 Characterization of ligands

The synthesized ligands were characterized by elemental analyses, FT-IR, ^{1}H NMR, electronic spectra and computational studies.

II.10.1 Elemental analysis

The elemental analysis data of ligand molecules are recorded in Table 2.1 and it can be seen that there is a close agreement between the experimental values and theoretical values from the expected structure.

Table 2.1: Analytical data of synthesized ligands

Ligands	MF	C % Exp (cal)	H % Exp (cal)	N % Exp (cal)	S % Exp (cal)
MHMMT	$C_{12}H_{12}O_3N_4S$	48 (49.3)	4.1 (4.1)	20.7 (19.1)	12.2 (10.93)
DMSTT	$C_{11}H_{10}O_3N_4S$	45.55 (47.4)	4.58 (3.59)	19.81 (20.1)	10.29 (11.5)
HMATD	$C_{12}H_{14}O_4N_4$	51.02 (51.75)	5.70 (5.03)	19.46 (20.13)	--
DHATD	$C_{11}H_{12}O_4N_4$	50.12 (50)	4.32 (4.54)	20.12 (21.20)	--
EMBAH	$C_{10}H_{12}ON_4$	58.13 (58.82)	5.25 (5.88)	26.92 (27.45)	--
EEBAH	$C_{11}H_{14}ON_4$	59.52 (60.50)	6.14 (6.42)	24.12 (25.69)	--
EPBAH	$C_{12}H_{16}ON_4$	61.52 (62.07)	6.55 (6.90)	24.01 (24.14)	--
MBIMOT	$C_{11}H_{10}ON_4S$	53.41 (53.65)	4.01 (4.07)	21.56 (22.76)	13.42 (13.00)
EBIMOT	$C_{12}H_{12}ON_4S$	55.01 (55.38)	4.16 (4.61)	20.87 (21.54)	11.97 (12.31)
PBIMOT	$C_{13}H_{14}ON_4S$	56.77 (56.93)	5.02 (5.11)	20.08 (20.44)	11.23 (11.68)

II.10.2 ^{1}H NMR spectra

The ^{1}H NMR spectra of synthesized compounds (some representative one) are given as Fig 2.5 and the chemical shift values are listed in Table 2.2. From the close examination of Table 2.2, we can confirm the formation of Schiff bases by the presence of peak due to azomethine protons which appear at 8.4 (in MHMMT), 8.66 (in DMSTT), 8.8 (in HMATD) and 8.22 (in DHATD). The ligands MHMMT and DMSTT shows predominant peaks at 13.6 and 13.7 ppm respectively which suggest the existence of thiol form of ligands in solution condition [28, 29]. Multiplet peaks were obtained for

aromatic protons within a range of 6.3-7.9. The structure of the synthesized ligands is in good agreement with their NMR spectra.

Table 2.2: Chemical shift values of ligand with probable assignments

Ligands	Chemical shift (ppm) in d6-DMSO
MHMMT	2.1 (s, 3H, CH_3), 3.8(s, 3H, OCH_3), 6.8 (s, 1H,OH), 7.2-7.4(m, aromatic hydrogen), 8.4 (s, 1H, CH=N) , 13.7 (s, 1H, SH)
DMSTT	2.17 (s, 3H, CH_3), 6.3-6.4(s, 2H, phenolic OH), 7.4-7.6(m, aromatic hydrogen) 8.66 (s,1H, CH=N), 13.6 (s, 1H, SH)
HMATD	3.861 (3 H, s, OCH_3), 4.6 (4H, s, $C\underline{H_2}OH$), 5.6 (2H, s, $CH_2\underline{OH}$), 6.9-7.5 (4H, m, aromatic protons), 8.806 (1H, s, CH=N), 10.035 (1 H, s, phenolic OH)
DHATD	4.59 (4H, CH_2), 5.616 (2H, CH_2OH) 6.3-7.3(m, aromatic hydrogen), 8.220 (s, 1H, CH=N), 10,.64 and 12.24 ((2H, phenolic 4-OH, 2-OH)
EMBAH	2.1-2.3 (combined peaks of CH_3 and NH_2), 4.8(2H, NCH_2), 7.5-7.1(m, aromatic hydrogen), 9.5 (s, NH)
EEBAH	1.3 (t, 3H, CH_3)2.2 (2H, NH_2),2.9 (q, 2H, CH_2) 5.7(2H, NCH_2), 7.5-7.1(m, aromatic hydrogen), 9.5 (s, NH)
EPBAH	1.2(t, 3H, C H_3)2.1 (m 2H, CH_2), 2.2 (2H, NH_2),2.9 (t, 2H, CH_2) 5.7(s,2H, NCH_2), 7.5-7.1(m, aromatic hydrogen), 9.5 (s, NH)
MBIMOT	2.1(s, 3H, CH_3), 5.2 (s, 2H, NCH_2), 8.1(s,1H, NH), 7.1-7.7(m, 4H, aromatic hydrogens)
EBIMOT	1.35 (t, 3H, CH_3), 2.67(q, 2H, CH_2), 4.25(s, 2H, NCH_2), 7.2-7.7(m, aromatic hydrogen), 8.2 (s, 1H, NH)
PBIMOT	0.98(t, 3H, CH_3), 1.8 (m, 2H, CH_2), 2.8 (t, 2H, CH_2), 5.5 (s, 2H, NCH_2), 7.1-7.5 (m, aromatic hydrogens), 8.291 (s, 1H, NH)

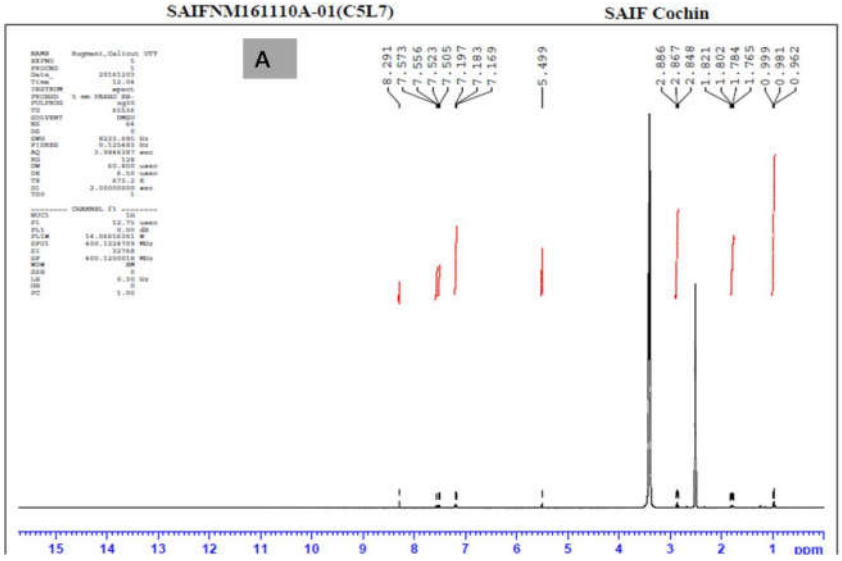
SAIFNM161110A-01(C5L7)
SAIF Cochin
A
8.291
7.573
7.556
7.523
7.505
7.197
7.183
7.169
5.499
2.886
2.867
2.848
1.821
1.802
1.784
1.765
0.999
0.981
0.962
15 14 13 12 11 10 9 8 7 6 5 4 3 2 1 ppm

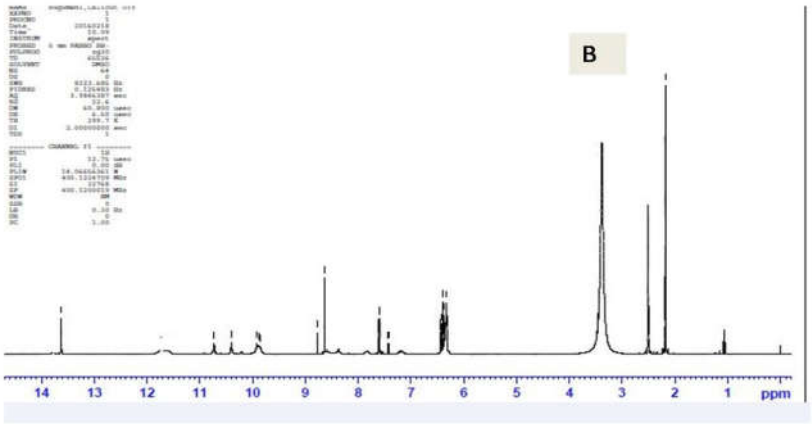
B
14 13 12 11 10 9 8 7 6 5 4 3 2 1 ppm

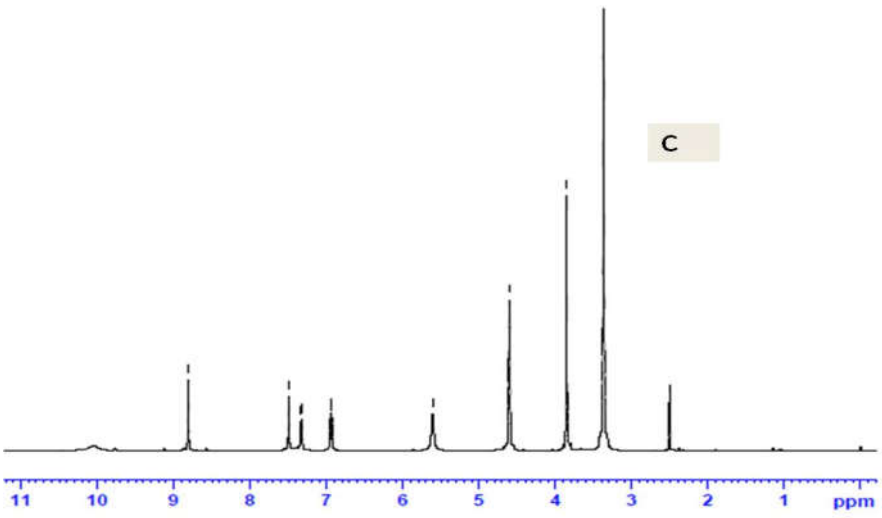
C
11
10
9
8
7
6
5
4
3
2
1
ppm

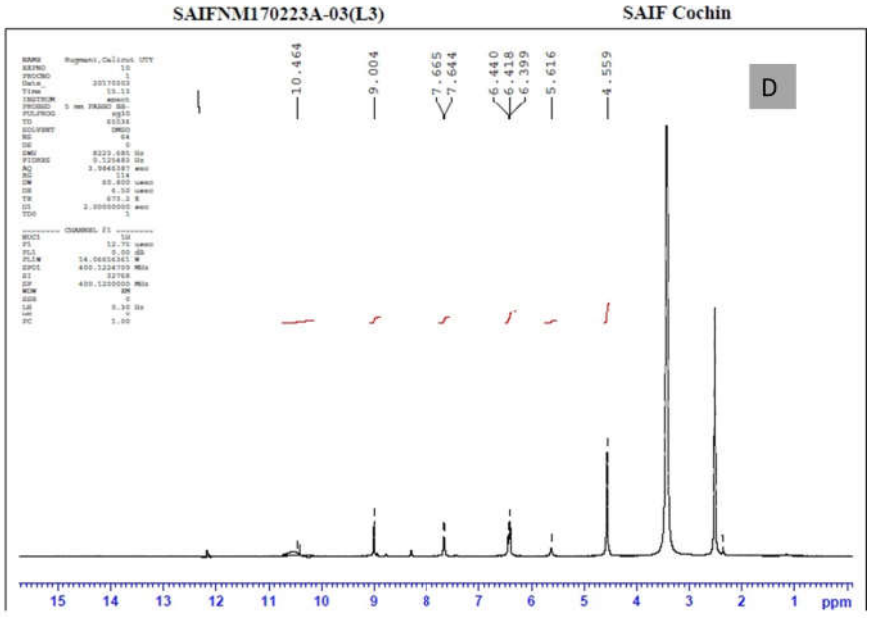
SAIFNM170223A-03(L3)
SAIF Cochin
10.464
9.004
7.665
7.644
6.440
6.418
6.399
5.616
4.559
D
15
14
13
12
11
10
9
8
7
6
5
4
3
2
1
ppm

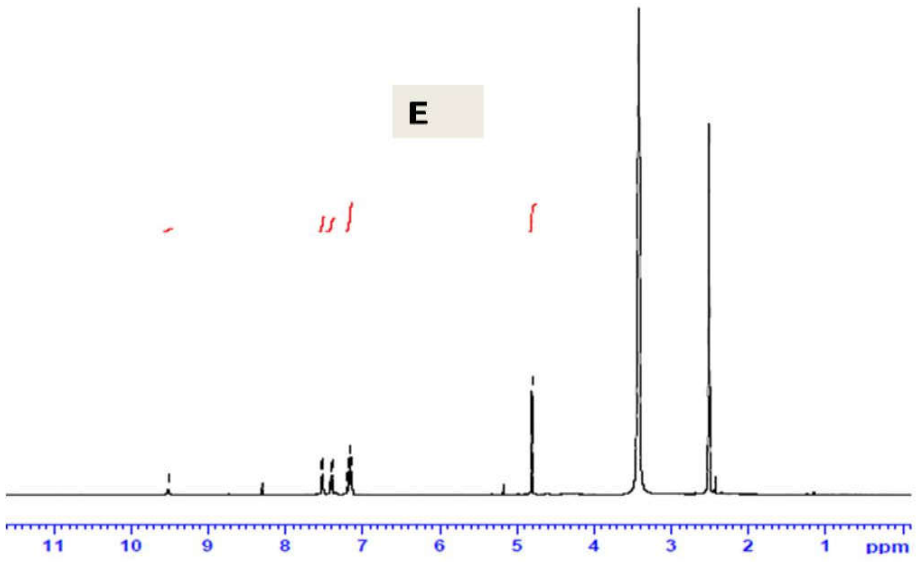

Fig 2.5 NMR spectra of (A) PBIMOT (B)DMSTT (C) HMATD (D) DHATD (E) EMBAH

II.10.3 Infrared spectra

IR spectra of ligands help to identify the functional groups present in the compounds. The IR frequencies with their probable assignments are presented in Table 2.3. The peaks in the region 3300-3000 cm^{-1} can be ascribed due to the presence of NH, OH and CH stretching vibrations. The existence of peaks due to NH and C=S vibrations in the ligands MHMMT and DMSTT indicates the existence of thiol-thione tautomerism in the compound and there is no peak in the SH stretching region of 2500 cm^{-1}. Similar results of existence of preferable thione form in the solid state of thioamide groups are reported earlier also[30,31].The spectra of MHMMT, DMSTT, HMATD and DHATD show characteristic peaks due to the stretching of azomethine (HC=N) group in the region 1575-1627 cm^{-1} which confirms the formation of Schiff base [29,32,33]. The peaks appear in the

range 1600-1700 cm^{-1} can be due to the stretching vibrations of carbonyl (C=O) groups in the ligands [34] (Fig 2.6).

Table 2.3: FTIR (KBr) frequencies of ligands and their assignments

Ligands	IR frequencies (cm^{-1}) (KBr Pellet method)
MHMMT	3413 (O─H), 3169 (N─H), 1691 (C=O), 1598 (C=N), 1199 (C=S)
DMSTT	3450 (O─H), 3216 (N─H), 1694 (C=O), 1627 (C=N), 1173 (C=S)
HMATD	3413 (O─H),
DHATD	3345 (O─H), 1626 (azomethine C=N), 1330, 1354 (δ (phenolic O-H), 1252, 1172(phenolic C-O)
EMBAH	3300 (N─H), 2917 (C-H), 1527 (ring C=N), 1661 (C=O)
EEBAH	3256 (N─H), 2969 (C-H), 1534 (ring C=N), 1670 (C=O)
EPBAH	3293 (N─H), 3054 (C-H), 1540 (ring C=N), 1663 (C=O)
MBIMOT	3440 (N─H), 2988 (C-H), 1568 (C=N), 1485 (C-O-C), 1150 (C=S), 2612 (S-H)
EBIMOT	3406 (N-H, 2983 (C- H), 1609 (C=N), 1462 (C-O-C), 1122 (C=S), 2456 (S-H)
PBIMOT	3414 (N-H), 2965(C- H), 1629 (C=N), 1418 (C-O-C), 1112 (C=S), 2678 (S-H)

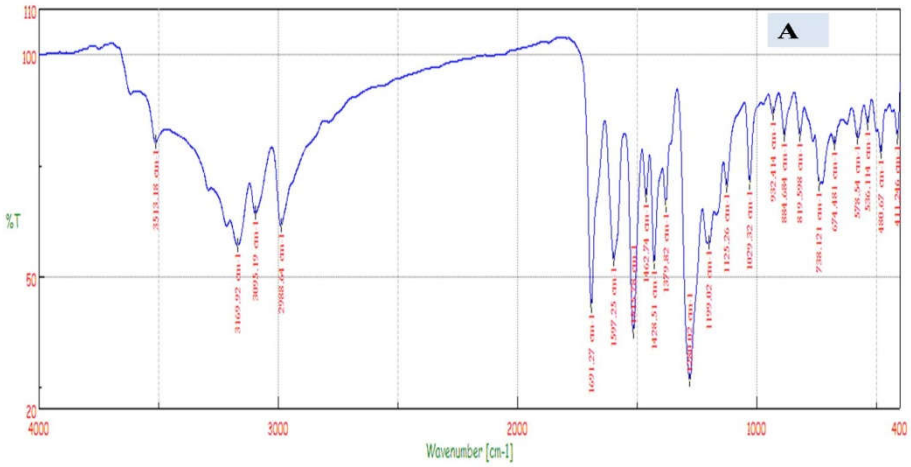

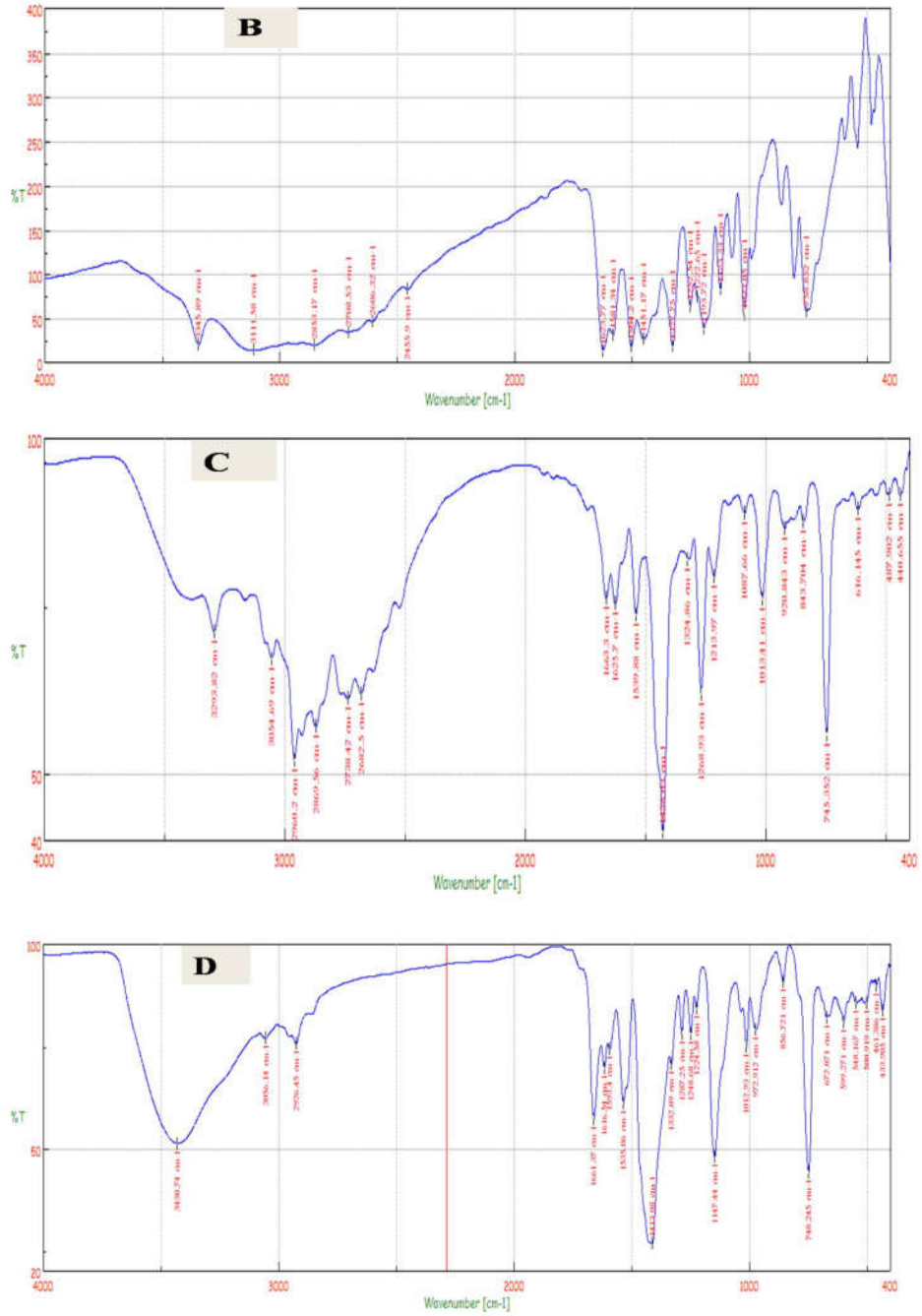

Fig 2.6 IR spectrum of (A) MHMMT (B) DHATD (C) EPBAH (D) MBIMOT

II.10.4 Quantum chemical studies

The quantum chemical studies were done and various quantum chemical parameters were obtained which helped in determining the possible binding sites in the ligands as well as for the comparison of corrosion inhibition efficiencies. The parameters such as energies of the highest occupied molecular orbital (E_{HOMO}), lowest unoccupied molecular orbital (E_{LUMO}), HOMO-LUMO energy gap (ΔE), total energy of the molecule (TE), dipole moment (μ), electro negativity (χ), hardness (η) and fraction of electrons transferred (ΔN) along with the figures of optimized geometry, HOMO and LUMO of the ligands are presented in Fig 2.7 (A-J).

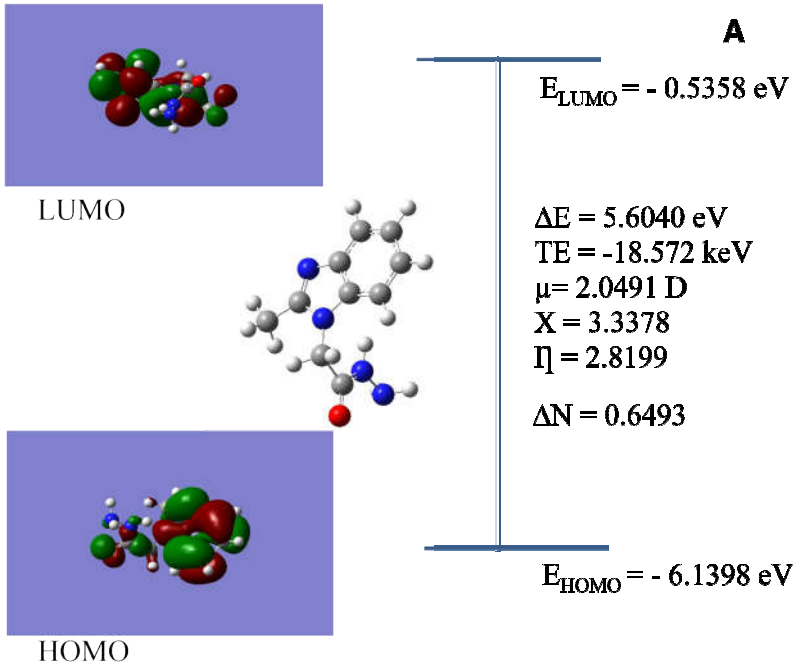
A
LUMO
E_{LUMO} = - 0.5358 eV
ΔE = 5.6040 eV
TE = -18.572 keV
μ= 2.0491 D
X = 3.3378
Ƞ = 2.8199
ΔN = 0.6493
HOMO
E_{HOMO} = - 6.1398 eV

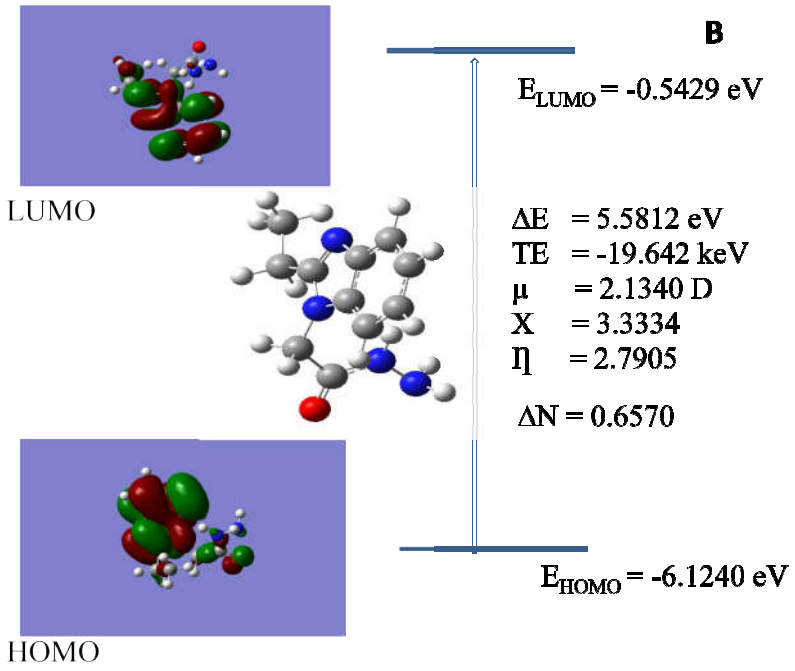
B
LUMO
E_{LUMO} = -0.5429 eV
ΔE = 5.5812 eV
TE = -19.642 keV
μ = 2.1340 D
X = 3.3334
Ƞ = 2.7905
ΔN = 0.6570
HOMO
E_{HOMO} = -6.1240 eV

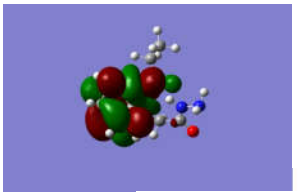

LUMO

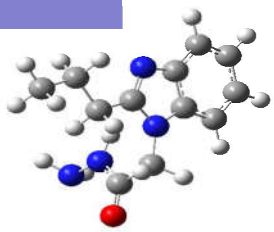

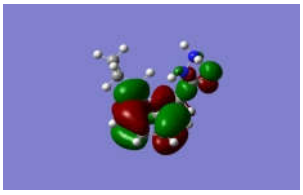

HOMO

C

E_{LUMO} = -0.5309eV

ΔE = 5.5787 eV
TE = -20.712 keV
μ = 2.1636 D
X = 3.3202
Ƞ = 2.7894

ΔN = 0.6596

E_{HOMO} = -6.1096 eV

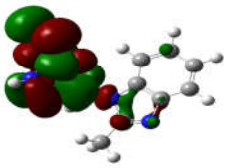

LUMO

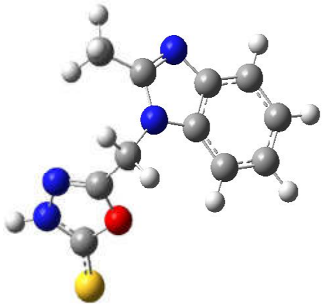

HOMO

D

E_{LUMO} = −1.0746 eV

ΔE = 5.1571 eV
TE = - 30.41 keV
μ= 6.957 D
X = 3.6532
Ƞ = 2.5785

ΔN = 0.6490

E_{HOMO} = −6.2317 eV

E

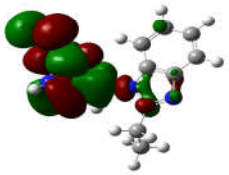

LUMO

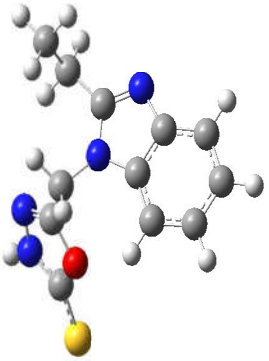

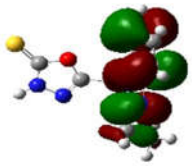

HOMO

$E_{LUMO} = -1.0802$ eV

$\Delta E = 5.1451$ eV
TE = -31.52 keV
$\mu = 7.1941$ D
X = 3.6528
$\eta = 2.5726$
$\Delta N = 0.6505$

$E_{HOMO} = -6.2254$ eV

F

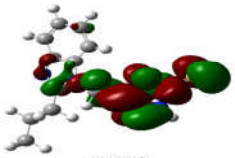

LUMO

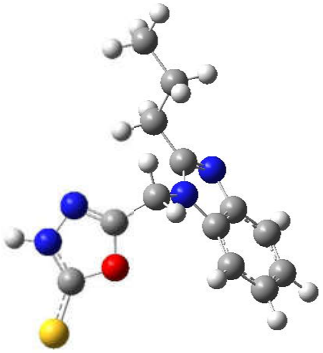

HOMO

$E_{LUMO} = -1.0691$eV

$\Delta E = 5.1351$ eV
TE = −32.55 keV
$\mu = 7.4650$ D
X = 3.6367
$\eta = 2.5676$
$\Delta N = 0.6550$

$E_{HOMO} = -6.2042$ eV

G

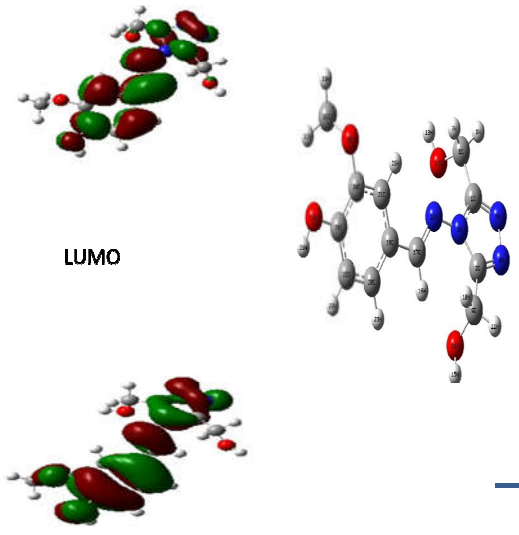

LUMO

HOMO

$E_{LUMO} = -1.592$ eV

$\Delta E = 4.285$ eV
TE = - 26.82 keV
$\mu = 8.1393$ D
X = 3.7345
$\eta = 2.1425$

$E_{HOMO} = -5.877$ eV

H

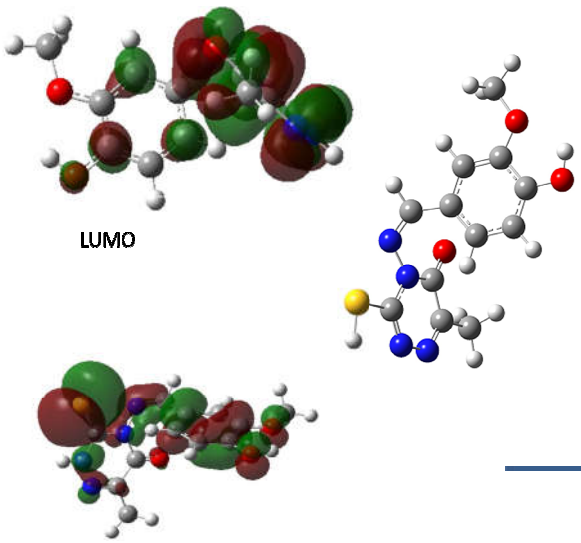

LUMO

HOMO

$E_{LUMO} = -1.870$ eV

$\Delta E = 4.050$ eV
TE = −35.375 keV
$\mu = 5.100$ D
X = 3.8900
$\eta = 2.0400$

$E_{HOMO} = -5.920$ eV

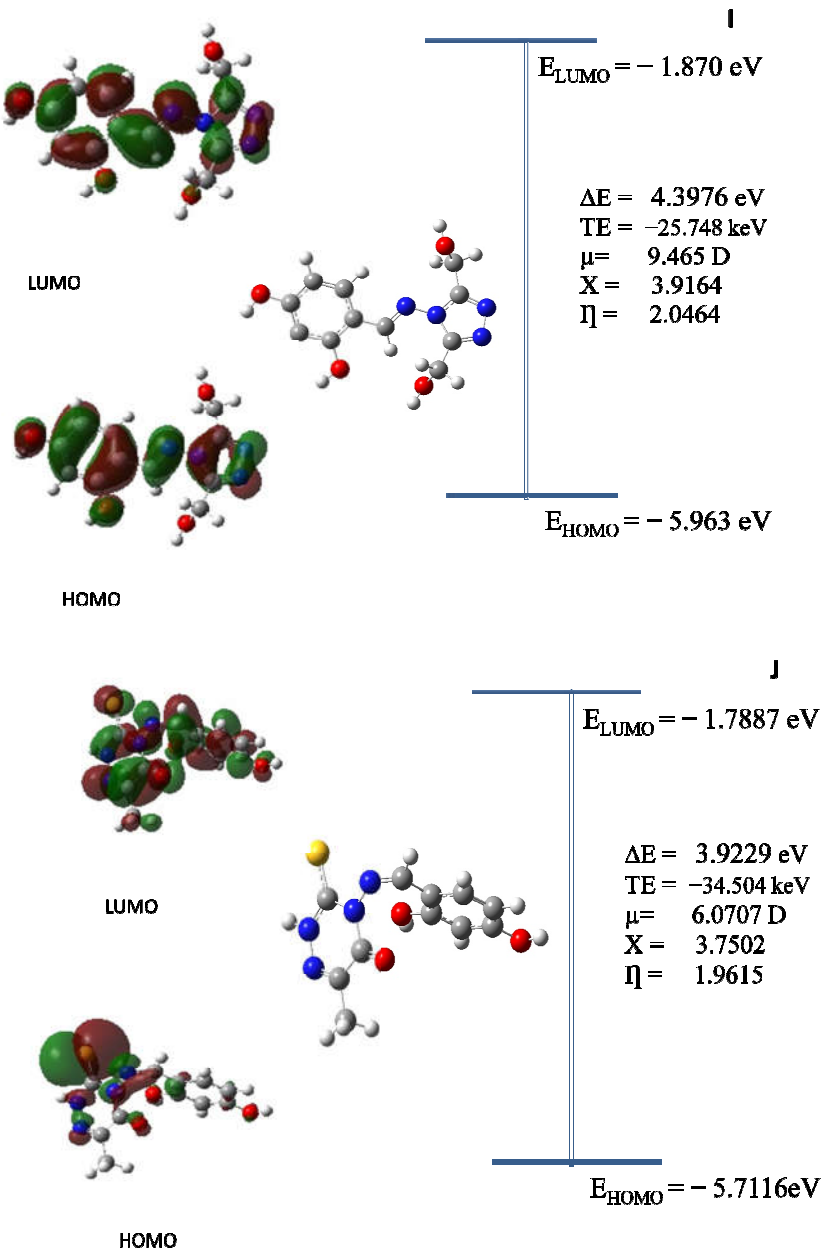

Fig 2.7 Optimized geometry, HOMO and LUMO and calculated quantum chemical parameters of (A) EMBAH (B) EEBAH (C) EPBAH (D) MBIMOT (E) EBIMOT (F) PBIMOT (G) HMATD (H) MHMMT (I) DHATD (J) DMSTT

References

1. Bincy Joseph and Abraham Joseph, Portugaliae Electrochimica Acta., 29(4) (2011) 253

2. A. Dornow, H. Mengel, P. Marx, "Uber Chemische Berichte, 97(1964). 2173

3. J.Gowda, A.M.Khader, B.Kalluraya, N.S.Kumari, Ind.J.Chem.B, 49 (2010) 1130

4. Shabbir A Kazi, chem. Sci. Trans, 3(2) (2014) 796

5. A.I.Vogel "A text Book of Quantitative Inorganic Analysis", Longmann, Londom, (1975)

6. I.B. Obot1, E.E. Ebenso, Zuhair M. Gasem, Int. J. Electrochem. Sci., *7* (2012) 1997

7. F. Bentiss, M. Lagrenee, M. Traisnel, and J.C. Hornez, Corros. Sci., 41 (1999) 789

8. M.G. Hosseini, H. Tavakoli, and T. Shahrabi, J. Appl. Electrochem., 38 (2008) 1629

9. I. Ahamad, R. Prasad, and M.A. Quraishi, Corros. Sci., 52 (2010) 3033

10. F. Bentiss, M. Traisnel, and M. Lagrenee, Corros. Sci., 42 (2000) 127

11. Asif Husain , Aftab Ahmad , Shah Alam Khan, Mohd Asif Rubina Bhutani , Fahad A. Al-Abbasi, Saudi Pharmaceutical Journal 24 (2016) 104

12. T. Ozen, M. Taş, J. of Enz.Inh. and Med. Chem. 24 (2009) 1141

13. Chellaian Justin Dhanaraj, Jijo Johnson, J. of Photochem. & Photobio., B: Biology 161 (2016) 108

14. Khaled Lotfy, J. of Biophysical Chem., 6 (2015) 91

15. Rajesh Kumar Goel Damanpreet Singh Alexey Lagunin Vladimir Poroikov, Med Chem Res 20 (2011) 1509

16. A. L. Barry,The Antimicrobial Susceptibility Test, Principles and Practices, E.L.B.S, 4th edition, 1976

17. J Carmichael, W G DeGraff, A F Gazdar, J D Minna, J B Mitchell , Cancer Res.;47 (1987)936

18. J H Sheikh, Iyo, M T Tsujiyama, I MdAshabul,S B Rajat and A Hitoshi Food Sci Technol Res.14 (2008)261

19. B J McConkey , V Sobolev,M Edelman, .Current Science., 83 (2002) 845

20. G M Morris,., R Huey, ,W Lindstrom,., M F Sanner, R Belew,. K., Goodsell, D. S. and A J Olson, *J. Co*mputational Chemistry 16 (2009)2785

21. http://accelrys.com/products/discovery-studio/visualization-download.php

22. K Vanommeslaeghe et al. J Comput Chem. 31 (2010) 671

23. S V Reddy et al. J Biomol Struct Dyn. 11 (2015) 1 [PMID: 25671592]

24. SH Basha et al. European J, of Biotechnology and Bioscience. 2 (2014) 30

25. G M Morris et al. J. of Computl. Chem.19 (1998) 1639

26. A.O.Yule, B.D.Mert, G.Kardas, B.Yazici, Corro.Sci.83(2014)

27. Zhe Zhang, NingchanTian, Lingzhi Zhang, Ling Wu, Corros. Sci., 98 (2015) 438

28. K, Raparia S, Surain P., Med Chem Res., 24 (2015) 2336

29. Kiran Singh Ritu Thakur , Vikas Kumar, b e n i - s u e f u n i v e r s i t y journal of b a s i c and a p p l i e d s c i e n c e s 5 (2 0 1 6) 21

30. CNR Rao., Canadian J of chemistry, 42 (1964)

31. Carlop Reti, Giuseppteo, Can. J. Chem. *54,* (1976)1558

32. Kiran Singh , Yogender Kumar, Parvesh Puri, Chetan Sharma, K. R. Aneja. , Med Chem Res 21 (2012) 1708

33. A Sangamesh Patil, M. Manjunatha, D Ajaykumar Kulkarni and S Prema. Badami, Complex Met. 1 (2014) 28–137

34. R.M. Silverstein, F.X. Webster, D.J. Kiemle, Spectrometric Identification of Organic Compounds, 7th edition, John Wiley & Sons, Inc. New York, (2005).

3 SYNTHESIS, CHARACTERIZATION AND BIOLOGICAL SCREENING OF 1,2,4-TRIAZINE BASED SCHIFF BASES AND THEIR TRANSITION METAL COMPLEXES

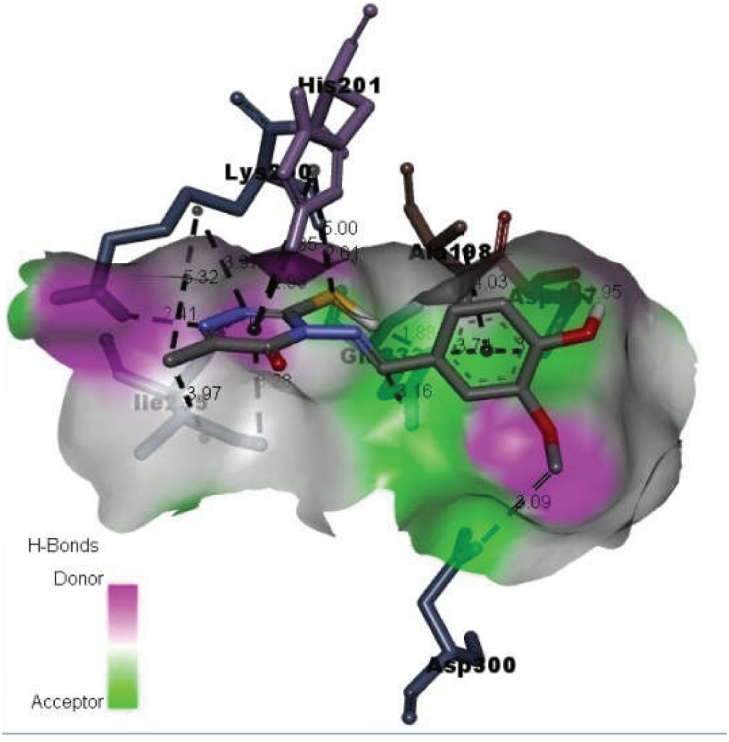

Chapter III *contains the synthesis, characterization, biological screening and molecular docking studies of metal complexes of Fe(III), Co(II), Ni(II), Cu(II) and Zn(II) with two 4-amino-3-mercapto-6-methyl-5-oxo-[1,2,4]triazine based Schiff bases; 4-[(4-hydroxy-3-methoxybenzylidene)amino]-6-methyl-3-thioxo-3,4-dihydro-1,2,4-triazin-5(2H)-one(MHMMT) and 4-{[(1E)-(2,4-dihydroxyphenyl)methylene] amino}-3-mercapto-6-methyl-1,2,4-triazin-5(4H)-one (DMSTT)*

III.1. Introduction

The literature review has revealed an umpteen number of investigations on complex formation and biological studies on various 1,2,4-triazine based ligands. It was proposed that metal complexes will be more biologically active than the bare ligands and many synthetic metal complexes mimicking the biomolecules are also known [1-4]. So we aimed at the study of complex formation and biological screening of 4-amino-3-mercapto-6-methyl-5-oxo-[1,2,4]triazine based Schiff bases; - 4-[(4-hydroxy-3-methoxybenzylidene)amino]-6-methyl-3-thioxo-3,4-dihydro-1,2,4-triazin-5(2*H*)-one(MHMMT)and 4-{[(1*E*)-(2,4-dihydroxyphenyl)methylene]amino}-3-mercapto-6-methyl-1,2,4-triazin-5(4*H*)-one (DMSTT) and their transition metal complexes. The chosen ligands contain hard N, O and soft S as donor atoms and are polydentate in nature. The potential coordination sites are (1) S of mercapto group without or with deprotonation (2) the N atoms on the triazine ring (3) the N atom of azomethine group and (4) the O atoms in the aldehyde part. In silico biological screening studies were done to predict the drug likeness, bioavailability, ADME properties and probable activity spectrum (PASS) of ligands as well as complexes. In vitro antibacterial, antifungal, anticancer and antidiabetic and the respective molecular modeling studies were also conducted.

III.2 Experimental

The description of various materials and methods used for the synthesis as well as characterization of ligands are given in chapter II (sec. II.2 and II.10).

III.2.1 Preparation of metal complexes of MHMMT and DMSTT

The solid complexes of Fe(III), Co(II), Ni(II), Cu(II) and Zn(II) were prepared as per the following procedure. To a hot aqueous/ethanolic solution

of metal salt (1mmol), hot ethanolic solution of ligand (2mmol) was added drop wise with stirring. The resulting mixture was then refluxed for 4 h. Then the solution was cooled, the complex separated was filtered, washed with water, ethanol and dried (Fig 3.1).

III.3. Results and discussion

The metal complexes were found to be stable, non hygroscopic solids, insoluble in water and ethanol but soluble in DMF, DMSO etc. The ligands exist as an equilibrium mixture of thiol and thione forms which is evident from the IR and NMR analysis. The ligands exist preferably in thione form in solid state (as evident from IR) and in thiol form in liquid state [5]. The analytical data presented in Table 3.1 revealed the close agreement between the theoretical and experimental values of the CHNS percentage. Except Co(II), all other synthesized metal complexes form in the mole ratio 1:2 (M:L) whereas Co forms a 1:1 complex.

III.3.1 ^{1}H NMR spectra of Zn complexes

The ^{1}H NMR spectra of ligands as well as the diamagnetic Zn complexes were recorded in DMSO-d6 at room temperature and the corresponding chemical shift values, δ (ppm), and the corresponding spectra are presented in Fig 3.2 respectively. As explained in chapter II section II.10.2 (Table 2.2), the ligands exhibit peaks due to azomethine protons at 8.4 and 8.66 ppm respectively in MHMMT and DMSTT which has undergone a shift on complexation with Zn(II) ions. The Zn-MHMMT complex has shown a slight up field shift and appears at (δ = 8.289 ppm) pointing out the involvement of N in coordination [6, 7]. In Zn-DMSTT complex, the azomethine proton exhibited a downfield shift and appears at δ= 9.908 ppm which indicates the deshielding of this proton due to the drift of electrons towards metal ion and the coordination of ligand through azomethine N [8,

9]. The peaks due to SH group (δ = 13.7 and 13.6 ppm) in the ligands indicating a thiol-thione tautomerism are found to be absent in the spectra of Zn complexes indicating the coordination of ligands through S atom of SH group via deprotonation [10]. The peaks due to methoxy protons, phenolic OH groups, and aromatic hydrogens remain almost same in the ligands as well as complexes indicating the non-involvement of these groups in coordination. The Zn-DMSTT complex exhibits a singlet peak at 1.891due to the presence of coordinated water molecules.

III.3.2 Magnetic moment measurements

Among the various methods to ascertain the stereochemistry of metal complexes, the measurement of magnetic moment plays an important role. The arrangement of electrons in the d-orbitals of metal ion gets changed by the attachment of ligands around it. So the magnetic moment studies are very useful for predicting the type of bonds, oxidation state of metal ions and the stereochemistry of metal complexes. The magnetic moment of paramagnetic complexes determined using Gouy's method is listed in Table 3.1.

III.3.2.1 Fe(III) complexes

Fe(III) complexes can exist either as spin paired (low spin) or spin free (high spin) complexes with an octahedral stereochemistry as the commonest one. Fe(III) is a d^5 system with a stable half filled arrangement. The magnetic moment of high spin Fe(III) octahedral complexes with a $t_{2g}^3 e_g^2$ arrangement amounts to be 5.92 BM whereas the low spin complexes with $t_{2g}^5 e_g^0$ arrangement has a magnetic moment of 2.3 BM. The calculated values of magnetic moment for Fe-MHMMT complex is found to be 4.82 BM which is lower than that of high spin octahedral and is much higher than that of low spin octahedral complex. It has been suggested that in an octahedral field for a d^5 system with ^6A_1g configuration like Fe^{3+}, a spin state equilibrium as well

as anti ferromagnetic exchange is possible, which results in a subnormal magnetic moment values [11, 12]. This tentative explanation tends us to expect an octahedral structure for Fe-MHMMT complex. In the case of Fe-DMSTT complex a magnetic moment of 5.73 was obtained which implied a high spin octahedral nature of the complex [13].

III.3.2.2 Co(II) complexes

The Co(II) complexes with d^7configuration can have octahedral, tetrahedral and/or square planar stereochemistry. The high spin octahedral Co(II) complexes with a $^4T_{1g}$ ground term can have a orbital contribution towards the magnetic moment and magnetic moment will be in the range 4.8-5.2 BM, higher than the spin only value of 3.87 BM. But for a low spin octahedral complex, the magnetic moment will be in the range 1.7-1.85 BM. The magnetic moment values of Co-MHMMT and Co-DMSTT complexes at room temperature are 4.65 and 2.50 BM respectively. For a tetrahedral Co complex, no orbital contribution can be expected and the complexes will have the spin only magnetic moment of 3.87 BM. Here the higher value of 4.65 BM for Co-MHMMT can be explained as follows:- The excited state $^4T_2$ ($e^3t_2^4$) carries orbital magnetic moment, so a spin-orbit coupling brings out some mixing between ground state and excited state, thus some orbital contribution [13]. So Co-MHMMT complex, which has a magnetic moment of 4.65 BM, is in agreement with the reported values of tetrahedral complexes [14]. The tetragonal elongation of octahedral geometry can result into a square planar geometry and such a cobalt complex with one unpaired electron registers a magnetic moment in the range 2.2-2.9 BM. So the Co-DMSTT complex with 2.50 BM can be expected to have a square planar geometry [13].

III.3.2.3 Ni(II) complexes

On the basis of magnetic moment values, Ni(II) complexes with a d^8 system can be divided as

(a) Octahedral complexes with a magnetic moment of 2.9-3.3 BM due to spin only contribution

(b) Tetrahedral complexes with $^3T_1$ ground state and magnetic moment 3.2-4.0 BM due to orbital and spin contribution

(c) Square planar diamagnetic complexes

In the present investigation, the Ni-MHMMT and Ni-DMSTT complexes have magnetic moment values of 3.2 and 2.8 BM which suggested an octahedral structure for the complexes [15].

III.3.2.4 Cu(II) complexes

The interpretation of geometry of Cu(II) complexes from magnetic studies is a complicated one. The Cu(II) complexes with a d^9 systems can show either the normal magnetic moments equivalent to one unpaired electron (1.73 BM) or sometimes as high as 2.2 BM due to orbital contribution. The magnetic moment values of Cu-MHMMT and Cu-DMSTT complexes are 1.73 and 1.40 BM respectively which is quite close to the spin only values of one unpaired electron [16].

III.3.3 Electronic spectra

Electronic spectroscopy in combination with magnetic moment studies is an important tool in the structure elucidation of transition metal complexes. The λ_{max}, their possible assignments and calculated ligand field parameters for the complexes depicted in Table 3.2 and the representative

spectra in Fig 3.3 helps to predict the extent of covalent bonding and geometry of the complexes.

III.3.3.1 Fe(III) complexes

Fe(III), a d^5 system with lowest energy term ^6S splits in an octahedral field to $^6A_{1g}$ ground state. The higher levels ^4G, ^4P etc. are of multiplicity 4, so all transitions of Fe(III) systems are double forbidden (spin as well as Laporte forbidden), so the electronic spectral bands will be extremely weak. In this case Fe complexes register three absorption maxima and they can be assigned to various transitions as given in Table 3.2 [17, 18].

III.3.3.2 Co(II) complexes

Co-MHMMT exhibits absorption maxima at 1091 (ca), 606 and 459 nm due to various transitions described in Table 3.2 and are characteristic of tetrahedral geometry of complexes. By using band fitting equations of Lever et al. [16], the ligand field parameters can be calculated using the equations υ_1 = 10 Dq, υ_2 = 18 Dq and υ_3 = 12 Dq + 15 B. The Racah parameter (B) values of 719 cm^{-1} which is less than B_0 value for free Co(II) ion (971 cm^{-1}) suggests overlapping of orbitals as well as electron delocalization in the metal ion [10]. β value of 0.74 pointed out a covalency of 26 % in the complex. The electronic spectra supports the structure obtained from magnetic studies. In the case of Co-DMSTT complex only one peak at 505 nm characteristic of transition of square planar geometry supports the value of magnetic moment obtained and hence a square planar geometry was suggested for Co-DMSTT complex [13].

III.3.3.3 Ni(II) complexes

The electronic absorption peaks with the corresponding transitions as given in Table 3.2 suggested octahedral geometry for Ni(II) complexes of

both MHMMT and DMSTT. The band fitting calculations provide B values (898, 854 cm^{-1}) which are less than that of free Ni(II) ion (1030cm^{-1}). The ligand field parameters are in concordance with magnetic moment values and suggest an octahedral geometry.

III.3.3.4 Cu(II) complexes

The peaks in the electronic spectra of Cu(II) complexes are very much useful in the structure elucidation. As presented in Table 3.2, Cu-MHMMT gave three bands at 362 nm, 433 nm and a broad band at 606 nm. The first two bands can be due to charge transfer and the broad band at 606 nm can be ascribed to a combination of $^2B_{1g} \rightarrow {}^2E_g$ and $^2B_{1g} \rightarrow {}^2A_{1g}$ transitions [19]. These transitions along with magnetic moment value of 1.73 BM imply a square planar structure for the complex [16, 20]. In the case of Cu-DMSTT complex low intensity broad band at 700 nm and 370 nm can be assigned to charge transfer and $^2E_g \rightarrow {}^2T_{2g}$ transition which supports an octahedral structure for Cu(II) complex. An octahedral d^9 system with ^2E_g ground state is very sensitive to Jahn-Teller distortion, and hence the existence of regular Cu(II) complex is very rare. So Cu-DMSTT complex can be considered to be a distorted octahedral geometry.

III.3.4 Infrared spectra

The binding sites of ligands to the metal ions can be best studied by comparing the IR spectra of ligand and complexes. On comparing IR spectrum of complexes and ligands (Table 3.3, Fig 3.4), it can be seen that complexation alters the stretching frequency of C=N bond suggesting the coordination of ligands to metal ions through azomethine nitrogen atom [21]. The disappearance of peaks due to υ(N-H) at 3169 $cm^{-1}$and υ(C=S) at 1199 $cm^{-1}$and the appearance due to υ(C-S) around 600-700 cm^{-1}suggested the existence of thiol-thione tautomerism which is also confirmed by NMR

studies. On complexation, deprotonation of thiol group takes place followed by coordination via sulphur atom [10]. This was further supported by the appearance of new bands of υ(M-S) and υ(M-N) around 350-550 cm^{-1} [6]. In the spectra of Fe(III), Co(II) and Ni(II) complexes of MHMMT and Fe(III), Co(II), Ni(II), Cu(II) and Zn(II) complexes of DMSTT, peaks in the region 3300-3500 cm^{-1} and 750-850 cm^{-1} indicate the presence of coordinated water molecules [22]. Strong peaks at 1740 cm^{-1} in Co(II) complexes were assigned to acetate group in the complexes. The presence of nitrate groups were confirmed by the peaks at (1460 and 1304 cm^{-1}) in Fe-MHMMT complex and at (1180 and 1322 cm^{-1}) in Fe-DMSTT complex. The lower value of separation between the two peaks denotes the monodentate nature of nitrate groups [23]. The thioamide band I remains unaltered in the complexes, so a non involvement of N of thioamide group is expected in complexation. The shift of about 50-100 cm^{-1} towards lower wave number side for the thioamide band IV on complexation supports a bonding between metal ions and S [24].

III.3.5 Thermogravimetric studies (TG)

TG analysis is useful for gathering information on thermal stability, nature of bound water molecules as well as decomposition products of metal complexes. The TG analysis of metal complexes of MHMMT and DMSTT within a temperature range of 40-800℃ was done and the representative thermo grams are given in Fig 3.5. In most cases the decomposition found to occur in two or three stages. It is visible from the thermo grams that up to 200^{o}C, various phenomenon can be assigned like elimination of some gases adsorbed or some volatile substances produced by the evaporation during complex synthesis, removal of adsorbed and coordinated water molecules etc. The final stage in the decomposition of complexes is the oxide formation [9, 25]. The thermograms of Fe(III), Co(II) and Ni(II) complexes of MHMMT

and all the synthesized metal complexes of DMSTT shows the presence of coordinated water molecules. In the thermogram of Fe(III) complexes of MHMMT and DMSTT, the mass loss in the region 80-150^{o}C corresponds to the loss of water molecules with an observed mass loss of 3.0 and 2.8 % respectively which is in good agreement with the calculated value of 2.5 and 2.6 %. The mass loss of 43.2 and 41.5 % (calculated value 40.6 and 40.2 %) in the temperature range 440-570^{o}C corresponds to loss of ligand moiety. After 600^{o}C, only metal oxide remains with a residue percentage of 10.9 and 10.7 % in Fe-MHMMT and Fe-DMSTT complexes (calculated value: 9.9 and 10.3 %).

The thermogram of cobalt complexes of MHMMT and DMSTT decomposes in three stages. In the first stage around 50-140^{o}C with a loss of 5.51 % and 5.43 % occurs which agrees well with the theoretical water loss percentage of 4.21 and 5.11 %. These anhydrous complexes decomposed into metal oxide via two intervening stages where loss of organic part in the temperature range 250-400^{o}C and 400-700 ^{o}C leaving behind CoO as the residue. The thermo gram of Ni-MHMMT and Ni-DMSTT shows the mass loss (found 4.7 and 6 and calculated 5.3 and 5.5 % respectively) corresponding to loss of two water molecules in the range 50-170^{o}C. In the second stage of decomposition of 250-500^{o}C, loss of organic matter occurs and finally the residue percentage is that of NiO (calculated 11, 11.5% and found 14.2, 11.2% respectively).

Copper complex of MHMMT is stable up to 200^{o}C indicating the absence of coordinated water molecules in the complex. The complex decomposed in two stages which involve the partial loss of organic matter and finally the complete loss of ligand to give CuO as residue. But the Cu-DMSTT complex shows a weight loss of 5.2 % in the temperature range 85-180^{o}C due to the loss of coordinated water molecules which are in well

agreement with the theoretical value of 5.5 %. Similar results are obtained for Zn-DMSTT complex also.

III.3.6 ESR spectra

The basic idea of ESR studies of transition metal complexes is to gather as much as information related to metal ion environment which helps in the structure elucidation. The X band EPR spectra of copper complexes were recorded in DMSO at liquid nitrogen temperature (Fig 3.6). The observed g values for Cu-MHMMT complex is $g_{\parallel}$ = 2.24,$g_{\perp}$= 2.05 ie., $g_{\parallel} > g_{\perp} > 2.0023$ indicate that the unpaired electron of Cu is localized in $d_{x^2-y^2}$ orbital. The exchange interaction term G, calculated (G= 5)>4, suggests that the local axes are aligned parallel or only slightly misaligned and magnetic interaction between Cu(II) ions in its complex in solid state is negligible [26]. The EPR spectrum of Cu-DMSTT shows four well resolved peaks in low field region and one intense peak in the high field region. The observed g values is $g_{\parallel}$ = 2.11,> $g_{\perp}$= 2.06 >2.0023 suggest that the complex has an octahedral geometry with $^2B_{1g}$ as its ground state. Calculated G value for the complex (G= 2.01) suggested a considerable exchange interaction in the solid complex [13].

III.3.7 Virtual screening of pharmacological behavior

The virtual screening of some pharmacological behavior like drug likeness, bioactivity score, ADME tox studies, PASS spectrum etc. of ligands as well as metal complexes were done in an *in-silico* manner using various online software like *www.molinspiration.com, http://www.lmmd.org/database/cheminformatics,www.pharmaexpert.ru/passonline,* and the results obtained are discussed below.

III.3.7.1 Druglikeness, bioactivity and bioavailability prediction

In order to predict the drug likeness, bioavailability and bioactivity of ligands as well as complexes, they were subjected to Molinspiration calculations [27]. The obtained results are presented in Table 3.4. The validation of Lipinski's rule of five is an important step in drug designing and development. The molecular descriptors obtained from molinspiration cheminformatics software helped in validating Lipinski's rule. The ligands MHMMT, DMSTT and their cobalt complexes did not violate any of the Lipinski's rules. The molecular weight of these entities were also found to be less than 500 and the topological surface area (TPSA) of it is less than 160Å, thus they are expected to be easily transported, diffused and absorbed compared to other complexes and have good oral bioavailability [28].

The molecular hydrophobicity or lipophilicity expressed by $m_i$logP values of ligands as well as all the complexes (0.29 to −6.09) are well within the accepted Lipinski range of <5 indicates good permeability of compounds through cell membrane. Thus the ligands and metal complexes were supposed to have good bioavailability.

A drug molecule was expected to bind with biological targets like enzymes, ion channels, receptors etc. to have a beneficial pharmacological activity. The bioactivity scores like binding to g-protein coupled receptor ligand (GPCRL), nuclear receptor ligand (NRL), ion channel modulator (ICM), kinase inhibition (KI) protease inhibition (PI), enzyme inhibition (EI) etc. calculated using molinspiration software was displayed in Table 3.4. It has been suggested that metal complexes with bioactivity score >0 are highly bioactive in nature whereas those with scores between −5.0 to 0 have moderate activity and if the score is less than −5.0, then they are inactive [29]. It can be read from Table 3.4 that ligands as well as metal complexes have values within −1.42 to −0.01, so they are expected to have moderate

activity [30]. The recent developments in drug discovery have increased the chemical space for oral druggable candidates beyond Lipinski's Rule of 5 (bRo5) by considering target interaction and to incorporate various natural products rich in activities [31]. So the studied complexes also can be included into the chemical space of bRo5 with some modifications.

III.3.7.2 ADMETox prediction

ADMETox prediction involves the study of absorption, distribution, metabolism, excretion and toxicity of drug molecules from the site of administration, absorption into systemic circulation, and movement in the blood and excretion is a major component of pharmacokinetic studies. The online software ADMETSAR methodology [32] utilizes various absorption and excretion models like Caco-2 cell, BBB etc. and various ADME parameters like Blood Brain Barrier (BBB) penetration, Human Intestinal absorption (HIA), in vitro Caco-2 cell permeability and toxicity parameters like carcinogenity, LD_{50} dosage etc. for the ligands as well as metal complexes were determined and are summarized in Table 3.5. The ADMET properties revealed that metal complexes are having high absorption, distribution properties indicated by high HIA, BBB, Caco2 permeability values in comparison with ligands and it implies the more favorable pharmacokinetic properties for metal complexes compared to ligands. The important information gathered from Admetsar is the computed median lethal dose (LD_{50}) dosage in rat model which helps in deciding the lethalness of a compound. Compounds with lower dose of LD_{50} are more lethal compared to those with higher LD_{50} values. The LD_{50} values of studied complexes are more than that of commonly used drug streptomycin (LD_{50}= 1.8409 mol/kg).

III.3.7.3 Probable activity spectrum of substances (PASS)

As a preliminary to *in vitro* biological screening studies, the ligands as well as complexes were screened *in silico* with the help of a robust analysis based on structure activity relationship using an online software PASS (*www.pharmaexpert.ru/passonline)* which helps to predict the probable biological activity spectrum of compounds. The probability of compound to be active (P_a) or inactive (P_i) for a particular biological activity are obtained. It has been proposed that structures with P_a greater than Pi were the only compounds considered for a particular pharmacological activity [33, 34]. If the P_a value for a particular activity is greater than 0.5, it is probable that the compound will show that biological activity on *in vitro* analysis. It has been found that depending on the nature of metal ion and ligand, the probability of showing a particular activity differs. The most probable activities shown by ligands and complexes are tabulated in Table 3.6. MHMMT and DMSTT and all their studied complexes except Fe(III) complex shows insulysin inhibitor activity with P_a values greater than 0.5 which suggested an *in vitro* antidiabetic activity for these compounds. The Fe(III) complex of MHMMT has a comparatively high Pa value for antineoplastic activity against breast cancer and melanoma cancer which indicated an anticancer activity for this compound. The Cu(II) and Zn(II) complexes of MHMMT and DMSTT and its Ni(II), Cu(II) and Zn(II) complexes possess P_a values greater than 0.5 for anti tuberculosis activity which is consistent for showing in vitro antituberculosis activity.

III.3.8 In vitro antimicrobial activity

In vitro antimicrobial screening of ligands as well as complexes were tested against the bacterial species like *Escherichia coli*(gram negative) and *Bacillus subtilis* and *Micrococcus luteus* (gram positive) and fungal species like *Candida albicans* and *Aspergillus niger* by disc diffusion method (Fig

3.7) (Section II.7.1) [35]. From the results of antimicrobial studies displayed in Fig 3.8 and 3.9, it is obvious that ligands and metal complexes show moderate inhibition efficiency against both gram negative and gram positive bacterial as well as fungal strains used in this study. In most cases the ligands exhibit higher microbial activity than its respective metal complexes. This can be due to the presence of azomethine groups and hydroxyl groups and thiol groups which are capable of developing hydrogen bonding interactions with cellular compartment [28]. The lesser activity of complexes may also be due to their inability to diffuse through cell wall of the microbes thus obstructing their biological action or because of some unknown cellular mechanism by microbial enzymes after diffusion [36].

III.3.9 *In vitro anticancer studies*

The PASS analysis has shown a comparatively higher P_a value (0.799) for antineoplastic (breast cancer) activity for Fe-MHMMT complex. So *in vitro* cytotoxic activity and anticancer studies were carried out for Fe-MHMMT complex against human breast cancer cell line (MCF-7) using the colorimetric method of MTT assay as per the procedure given in section II.7.2 [37]. The dose dependent cytotoxic effect was observed (Fig 3.10) for Fe-complex treated MCF-7 cell lines. The concentration of complex which produces 50 % cell death and 25 % cell death gives the IC_{50} and IC_{25} values of Fe-MHMMT complex against MCF-7 cells and this value was found to be 24 μM and 13 μM respectively. The changes in the morphology of MCF-7 cell lines in presence of Fe complex was analyzed using a Nikon (Japan) bright field inverted light microscope at 40x magnification. The presence of strong blue fluorescence in the DAPI images and the cellular uptakes shown in the images (Fig 3.11) and (3.12) revealed the anticancer activity of Fe-MHMMT complex against human breast cancer cell lines MCF-7.

III.3.10 *In vitro antidiabetic studies*

The Pass analysis gave comparatively high probability for insulysin inhibitor activity for ligands and some of their metal complexes as listed in Table 3.6. Insulysin is otherwise known as insulin degrading enzyme (IDE), so the inhibition of insulysin will improve the insulin signaling which is beneficial to diabetic patients. So insulysin inhibitors are promising antidiabetic drugs to treat diabetes. Type II diabetes occurs mainly because of carbohydrate and lipid metabolism disorders. So along with insulysin inhibitors, present oral therapeutic for the treatment includes use of α-amylase inhibitor. α-amylase is a protein enzyme which hydrolyses α-bonds of polysaccharides like starch to provide glucose and maltose. Micro organisms, some plants and animals produce a large number of protein inhibitors which control the activity of α-amylase. These inhibitors work in an effective strategy by shutting down the post prandial rise of glucose level and are very important for diabetic patients for whom low insulin level prevent the flow of extra cellular glucose from blood. So diabetic patients should have low α-amylase level and α-amylase inhibitors are potential source of antidiabetic drugs (anti hyperglycemic agents).

In view of the above knowledge, we conducted the antidiabetic studies of our ligands as well as some complexes by α-amylase inhibitory method depicted in section II.7.3 [38]. The results obtained are tabulated in Table 3.7 and the pictorial representation of the experimental set up is given in Fig 3.13

The α-amylase inhibition activity of MHMMT and their complexes follow the order MHMMT<Ni-MHMMT<Co-MHMMT<Zn-MHMMT<Cu-MHMMT and that of DMSTT in the order DMSTT<Co-DMSTT<Zn-DMSTT<Ni-DMSTT<Cu-DMSTT. In the case of both ligands, the

complexes exhibit better inhibition activity which may be due to the incorporation of metal [39].

III.3.11 *Molecular docking studies*

Molecular docking studies were carried out using Autodock 4.2 software to model the interaction between drug molecules and proteins at atomic levels and to illustrate fundamental biochemical process [40, 41,42]. The detailed procedures of the studies are given section II.8. Autodock is helpful in predicting the binding site with associated binding energy and IC_{50} value of the compounds with target domain using the protocols followed elsewhere [44,45,46].

III.3.11.1 Docking studies with α-amylase enzyme and VEGFR 2 as active sites

After analyzing the results of in vitro antidiabetic and anticancer studies, we have interested to do the *in silico* molecular docking to elucidate the interaction between the enzyme and some selected ligands and complexes. The docking studies of MHMMT and its Co(II), Ni(II), Cu(II), and Zn(II) complexes with α-amylase enzyme (1SMD) (human salivary amylase) and Fe-MHMMT complex with VEGFR-2-kinase enzyme were done. The commercially available drug molecules which are used as α-amylase inhibitors (acarbose) and VEGFR-2-kinase inhibitors (Lenvatinib) were also subjected to docking studies for comparison. The crystal structures of the target enzymes were obtained from RCSB protein data bank. The docking parameters and corresponding binding pockets give the docking poses which help to evaluate the inhibitory activities of the studied compounds on the enzymatic action. Various docking parameters, detailed interactions between the target enzyme and ligands along with computed IC_{50} values are tabulated in Table 3.8. The compounds were shown to be

successfully docked inside the enzyme as evident from the values of binding energies. On the basis of binding energies, it can be inferred that the α-amylase inhibition is in the order Zn-MHMMT>Cu-MHMMT>MHMMT>Ni-MHMMT>Co-MHMMT. The IC_{50} values are in the range of 2.76 μM - 29 μM for α-amylase inhibition and 36μM for VEGFR inhibition. It is also evident from table that all the studied compounds have a higher binding energy and lower IC_{50} in comparison with commercial amylase inhibiting drug acarabose (binding energy = ─0.04 and IC_{50} = 8.61 mM).

The docking snapshots of studied compounds at the active binding site of enzyme are represented in Fig 3.14. From the figures it is clear that that the studied compounds have excellent binding sites to interact with enzyme, and there are various kinds of interactions between the ligand and receptor which stabilizes the ligand-receptor complexes and inhibit the action of enzymes. The major interactions involved are hydrogen bonding, Van der Waal's and other types of interactions like π-cation, π-anion, π-alkyl, π-π stacked etc. with various amino acid residues in the enzyme. Further in vivo and cytotoxic studies are required for developing them as potential drugs.

Conclusions

On the basis of physico chemical, magnetic, thermal, and spectroscopic analysis, it has been found that both the ligands are bidentate and coordinating through N of azomethine group and S atom of thiol group after deprotonation. An octahedral geometry was proposed for Fe(III) and Ni(II) complexes of both the ligands. Zn-DMSTT was also supposed to possess an octahedral structure. A square planar structure for Cu-MHMMT and Co-DMSTT complex and distorted octahedral structure for Cu-DMSTT, and tetrahedral structures for Co(II) and Zn(II) complexes of MHMMT were also proposed (Fig 3.15). *In silico* biological screening indicated drug like

properties for both the ligands as well as their Co(II) complexes and a moderate bioactivity for ligands as well as complexes. The ADMETox studies shows more preferred pharmacokinetic ADME properties for complexes compared to ligands with all studied compounds possessing non carcinogenic nature with comparatively high LD_{50} values. In vitro antimicrobial studies revealed that the ligands exhibit a higher activity compared to their complexes against the microbial strains used in this study. *In vitro* anticancer studies by MTT assay of Fe-MHMMT complex revealed a comparatively good anticancer activity with an IC_{50} value of 24 μM against breast cancer cells MCF7 and *in vitro* antidiabetic studies by α-amylase inhibitory method revealed a reasonable antidiabetic activity for metal complexes. The molecular docking studies also support the antidiabetic and anticancer activities of investigated compounds.

Table 3.1 (A) Physical and Analytical data of transition metal complexes of MHMMT

compounds	Magnetic moment μ_{eff} BM	Analysis percentage exptl (theoretical)				
		C	H	N	S	M
$Fe(L-H)_2(NO_3)(H_2O)$ (735) (Oh) $C_{24}H_{24}O_{10}N_9S_2Fe$	4.82	39.65(39.18)	4.07(3.26)	17.93(17.14)	9.15(8.70)	7.01(7.59)
$Co(L-H)OAc.H_2O$ (427) (Td) $C_{14}H_{16}O_9N_4SCo$	4.65	35.6(39.34)	3.75(3.74)	14.35 (13.11)	8.95(7.49)	14.02(13.81)
$Ni((L-H)_2.2\ H_2O$ (676) (Oh) $C_{24}H_{26}O_8N_8S_2Ni$	3.20	41.8(42.60)	3.62(3.84)	16.34(16.56)	9.21(9.46)	8.39(8.57)
$Cu((L-H)_2$ (645) (SP) $C_{24}H_{22}O_8N_8S_2Cu$	1.73	43.78(44.65)	3.19(3.41)	17.05(17.36)	9.73(9.92)	9.52(9.71
$Zn((L-H)_2$ (647.35) Td $C_{24}H_{22}O_8N_8S_2Zn$	--	43.12(44.5)	4.1(3.39)	18.1(17.30)	9.95(9.89)	9.10(10.04)

Table 3.1 (B) Physical and Analytical data of transition metal complexes of DMSTT

compounds	Magnetic moment μ_{eff} BM	Analysis percentage exptl (theoretical)				
		C	H	N	S	M
$Fe(L-H)_2(NO_3)(H_2O)$ 689.8) Oh $C_{22}H_{20}O_{10}N_9S_2Fe$	5.73	38.65(38.38)	3.07(2.90)	17.73(18.32)	9.18(9.31)	7.00(8.11)
$Co(L-H)OAc.H_2O$ (413) SP $C_{13}H_{14}O_6N_4SCo$	2.50	36.82(37.77)	3.25(3.38)	12.43(13.55)	6.67(7.74)	13.90(14.28)
$Ni((L-H)_2.2\ H_2O$ (648) Oh $C_{24}H_{22}O_8N_8S_2Ni$	2.79	40.14(40.74)	3.15(3.39)	17.03(17.28)	9.68(9.87)	8.70(8.95)
$Cu((L-H)_2.2H_2O$ (653)Oh $C_{22}H_{22}O_8N_8S_2Cu$	1.40	38.62(40.4)	3.12(3.36)	16.16(17.15)	9.3(9.8)	9.83(9.64)
$Zn((L-H)_2.2\ H_2O$ (655) Oh $C_{22}H_{22}O_8N_8S_2Zn$	--	39.14(40.30)	3.79(3.36)	16.48(17.09)	8.43(9.77)	11.00(9.92)

Table 3.2: Electronic spectral bands with probable assignments

compound	Band position nm	Assignment	Dq cm^{-1}	B	$\beta = B/B_0$
MHMMT	267	$\pi - \pi^*$	--	--	--
	333	$n - \pi^*$			
Fe-MHMMT	344	$T_{2g} - \pi^*$	898.7	817	0.81
	510	$^6A_{1g} \rightarrow {}^4T_{1g}$			
	277	$^6A_{1g} \rightarrow {}^4T_{2g}$			
Co-MHMMT	1091(ca)	$^4A_2 \rightarrow {}^4T_2$	916.7	719	0.74
	606	$^4A_2 \rightarrow {}^4T_1(F)$			
	459	$^4A_2 \rightarrow {}^4T_1(P)$			
Ni-MHMMT	820(ca)	$^3A_{2g} \rightarrow {}^3T_{2g}(F)$	1218	898	0.87
	454	$^3A_{2g}(F) \rightarrow {}^3T_{1g}(F)$			
	356	$^3A_{2g}(F) \rightarrow {}^3T_{1g}(P)$			
Cu-MHMMT	362	CT			
	433	CT			
	606 (b)	$^2B_{1g} \rightarrow {}^2E_g$			
DMSTT	278	$\pi - \pi^*$			
	332	$n - \pi^*$			
Fe-DMSTT	530	$^6A_{1g} \rightarrow {}^4T_{1g}$	864.6	786	0.77
	360	$T_{2g} - \pi^*$			
	290	$^6A_{1g} \rightarrow {}^4T_{2g}$			
Co-DMSTT	505	$^2B_{1g} \rightarrow {}^2A_{1g}$			
Ni-DMSTT	350	$^3A_{2g}(F) \rightarrow {}^3T_{1g}(P)$	1313	854	0.83
	425	$^3A_{2g}(F) \rightarrow {}^3T_{1g}(F)$			
	761(ca)	$^3A_{2g} \rightarrow {}^3T_{2g}(F$			
Cu-DMSTT	370	CT			
	700	$^2E_g \rightarrow {}^2T_{2g}$			

Table 3.3 (A) Important infrared spectral bands (cm^{-1}) and their tentative assignments for MHMMT and its complexes

compound	υ (O-H)/N-H /H_2O	υ (C=N)	thioamide I & II	υ (C-O)	thioamide III & IV	δ (phenolic O-H)	υ (C-S)	υ (M-N)	υ (M-S)	Coordinated water/ Nitrate/ OAc
MHMMT	3413, 3169	1598	1515 1428	1280	1125 884	1380	--	--	--	--
$Fe(L-H)_2$ $.NO_3.H_2O$	3432, 3377	1591	1512 1460	1281	1120 862	1384	616	463	418	782, 1460, 1304
Co(L−H) OAc. H_2O	3431, 3396	1590	1509 1458	1285	1121 864	1376	628	464	428	734, 1730
$Ni((L-H)_2.$ $2H_2O$	3414, 3216	1591	1513 1450	1282	1128 822	1389	614	501	408	730
$Cu((L-H)_2$	3409	1604	1510 1433	1276	1118 706	1378	604	482	453	--
$Zn((L-H)_2$	3425	1590	1512 1450	1282	1128 790	1388	614	501	408	--

Table 3.3 (B) Important infrared spectral bands (cm^{-1}) and their tentative assignments for DMSTT and its complexes

compound	υ (O-H)/ (H_2O)	υ (C=N)	thioamide I & II	υ (C-O)	thioamide III & IV	δ (phenolic O-H)	υ (C-S)	υ (M-N)	υ (M-S)	Coordinated water/ Nitrate/ OAc
DMSTT	3450 3095	1629	1513 1461	1235	1048 799	1381	--	--	--	--
$Fe(L-H)_2$ $.NO_3.H_2O$	3463 3221	1618	1514 1452	1220	1043 738	1380	646	527	463	843. 1180, 1322
Co(L−H) OAc. H_2O	3431,32 95	1611	1521 1440	1222	1050 741	1380	636	458	422	848
$Ni((L-H)_2.$ $2H_2O$	3415 3215	1610	1517 1441	1220	1039 723	1383	634	512	460	846
$Cu((L-H)_2.$ $2H_2O$	3401 3222	1614	1537 1450	1212	1052 718	1380	667	500	445	800
$Zn((L-H)_2$ $2H_2O$	3429 3215	1614	1501 1442	1222	1045 743	1379	631	506	437	848

Table 3.4: Validation of Lipinski's rule and bio activity scores as obtained from Molinspiration software

compound	Druglikeness			Bioactivity scores					
	milogP	TPSA	Nviolations	GPCRL	ICM	KI	NRL	PI	EI
MHMMT	0.19	93	0	−1.33	−1.17	−1.16	−1.28	−1.47	−0.91
Fe-MHMMT	-6.00	239	2	−0.39	−1.05	−0.73	−0.80	−0.38	−0.47
Co-MHMMT	−5.41	130	0	−0.29	−0.29	−0.36	−0.30	−0.34	−0.06
Ni-MHMMT	−5.97	190	3	−0.29	−0.70	−0.46	−0.49	−0.31	−0.28
Cu-MHMMT	−5.53	158	2	−0.20	−0.51	−0.36	−0.42	−0.20	−0.22
Zn-MHMMT	−5.36	158	2	−0.20	−0.51	−0.36	−0.42	−0.20	−0.15
DMSTT	0.29	104	0	−1.37	−1.25	−1.21	−1.24	−1.45	−0.92
Fe-DMSTT	−5.98	261	3	−0.23	−0.78	−0.52	−0.52	−0.27	−0.26
Co-DMSTT	−5.39	140	0	−0.26	−0.25	−0.32	−0.18	−0.27	−0.01
Ni-DMSTT	−6.07	207	3	−0.26	−0.65	−0.40	−0.45	−0.23	−0.28
Cu-DMSTT	−6.09	229	3	−0.18	−0.45	−0.25	−0.25	−0.18	−0.13
Zn-DMSTT	−6.00	229	3	−0.18	−0.45	−0.25	−0.25	−0.18	−0.10

Table 3.5 ADMETOX properties of ligands and complexes studied using ADMETSAR software

compounds	**BBB**	**HIA**	**Caco-2 Permeability**	**Renal Organic cation transporter**	**carcinogenity**	**LD_{50} mol/kg**
MHMMT	0.5250	0.7201	0.5201	Non-inhibitor	Non-carcinogen	2.2793
Co-MHMMT	0.8444	0.9666	0..5937	Non-inhibitor	Non-carcinogen	2.6370
Ni-MHMMT	0.8333	0.9394	0.5702	Non-inhibitor	Non-carcinogen	2.6627
Cu-MHMMT	0.8117	0.8511	0.5679	Non-inhibitor	Non-carcinogen	2.6016
Fe-MHMMT	0.7552	0.9345	0.5781	Non-inhibitor	Non-carcinogen	2.5513
DMSTT	0.5157	0.7876	0.5401	Non-inhibitor	Non-carcinogen	2.2396
Co-MHMMT	0.7739	0.8830	0.5874	Non-inhibitor	Non-carcinogen	2.4484
Ni-MHMMT	0.7734	0.9151	0.5671	Non-inhibitor	Non-carcinogen	2.5259
Cu-MHMMT	0.7734	0.9151	0.5671	Non-inhibitor	Non-carcinogen	2.5259

Table 3.6: Probable Activity Spectrum of ligands and complexes as obtained from online software PASS online

Activities	P_a values											
	MHMMT (L1)	**FeL1**	**CoL1**	**NiL1**	**CuL1**	**ZnL1**	**DMSTT (L2)**	**FeL2**	**CoL2**	**NiL2**	**CuL2**	**ZnL2**
Insulysin inhibitor	0.794	0.383	0.703	0.618	0.748	0.726	0.665	--	0.687	0.735	0.732	0.712
Mcl-1 antagonist	0.717	--	0.510	0.243	0.618	0.584	0.864	0.118	0.606	0.722	0.728	0.686
Maillard reaction inhibitor	0.597	--	0.611	0.384	0.632	0.620	0.651	0.322	0.667	0.692	0.692	0.680
Anti tuberculosis	0.470	--	0.449	0.497	0.597	0.735	0.595	--	0.201	0.589	0.592	0.729
Anti neoplastic		0.799										

Table 3.7 Antidiabetic studies of MHMMT, DMSTT and their complexes
Optical density of blank (without α-amylase*)* (B) = 0.620
Optical density for control (with α-amylase*)* (C) = 0.006

Compound	**Optical density at 565 nm for (A)**			**% of inhibition (A─C/B─C) x 100**		
	50 µg	**100 µg**	**300 µg**	**50 µg**	**100 µg**	**300µg**
MHMMT (L1)	0.018	0.138	0.188	2	22	30
Co-L1	0.009	0.092	0.415	0.5	14	67
Ni-L1	0.021	0.033	0.283	3	5	45
Cu-L1	0.025	0.282	0.551	3	45	89
Zn-L1	0.036	0.308	0.531	5	49	86
DMSTT (L2)	0.008	0.020	0.084	0.3	3	13
Co-L2	0.012	0.035	0.095	1	5	15
Ni-L2	0.026	0.104	0.158	3	16	25
Cu-L2	0.032	0.312	0.518	4	50	83
Zn-L2	0.030	0.226	0.386	4	36	62

Table 3.8 Docking results of selected compounds targeting α-amylase enzyme (PDB ID: 1SMD) and VEGFR 2 (PDB ID: 3VHE)

Drug target	compound	Binding Energy in Kcal/mol	Predicted IC_{50} value	Active sites with mode of interaction	
				Van der Waals	Hydrogen bonding
Alpha-amylase enzyme (PDB ID: 1SMD)	MHMMT	-6.84	9.76 uM	VAL98 LEU 162 HIS101 TYR62 HIS 299 TRP 58 ARG 195 SER 199 VAL 234	ASP 197 GLU233 LYS 200 ILE 235
	Co-MHMMT	-6.19	29.10 uM	ASP 356 HIS 305 TRP59 TYR 62	LYS 352 HIS 299 ASP 197
	Ni-MHMMT	-6.54	16.10 uM	LYS 352 ILE 51 HIS 101 GLY 304 VAL 234 TRP 58 GLU 233	GLN 63 TRP 59
	Cu-MHMMT	-7.06	6.63 uM	ALA 198 GLU 233 LEU 162 GLN 63 GLY 104 PRO 54 LYS 352 VAL 354 ASP 356	HIS 299 ASR 197 HIS 305
	Zn-MHMMT	-7.58	2.76 uM	LEU 162 GLY 306 HIS 305 GLY 309 ALA 310 VAL 234 GLU 233 ASP 236 ALA 198	GLY 308 GLY 238 LYS 200 ILE 235 HIS 201
	acarbose	-0.04	8.61 mM	ASP 236 PRO 241 SER 163 LEU 162 HIS 201 ALA 307	GLY 239 GLU 238 LEU 237 GLU 240 ILE 235 GLY 306 ASN 152
VEGFR-2-kinase	Fe-MHMMT	-5.80	36.02 uM	LEU 840 PHE 1047 GLY841 ALA 1050 LYS 871 ASP 1052 GLY 843 ALA 844 ARG 842	ARG 1051
	Lenvatinib	-8.05	1.27 Um	HIS 894 GLU 828 PHE 829 GLY 903 ILE 856 ASP 857 ASN 900 LEU 901 HIS 891	ILE 890 LEU 889 LYS 826 LEU 902

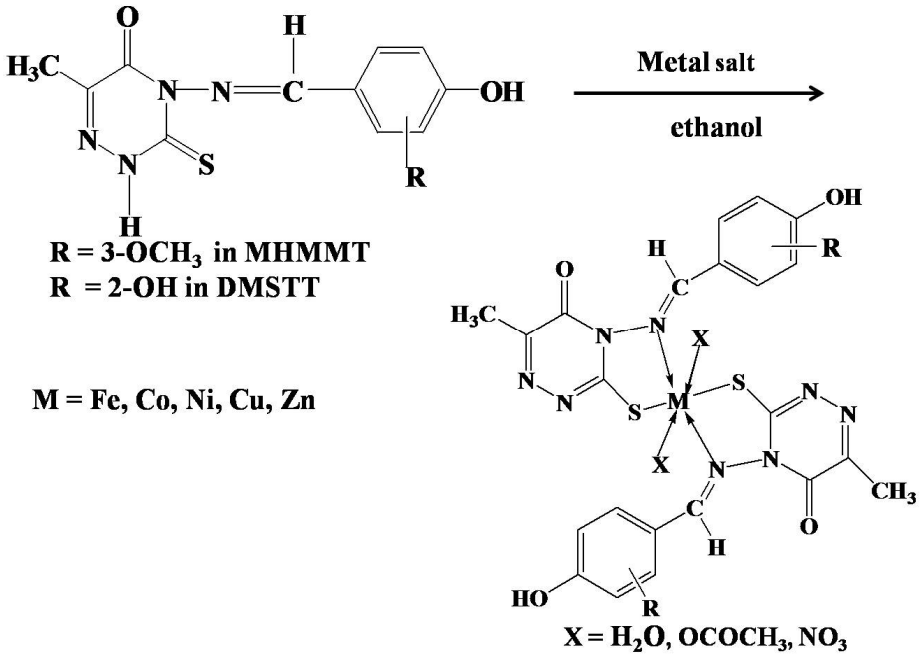

Fig 3.1 Scheme of preparation of metal complexes

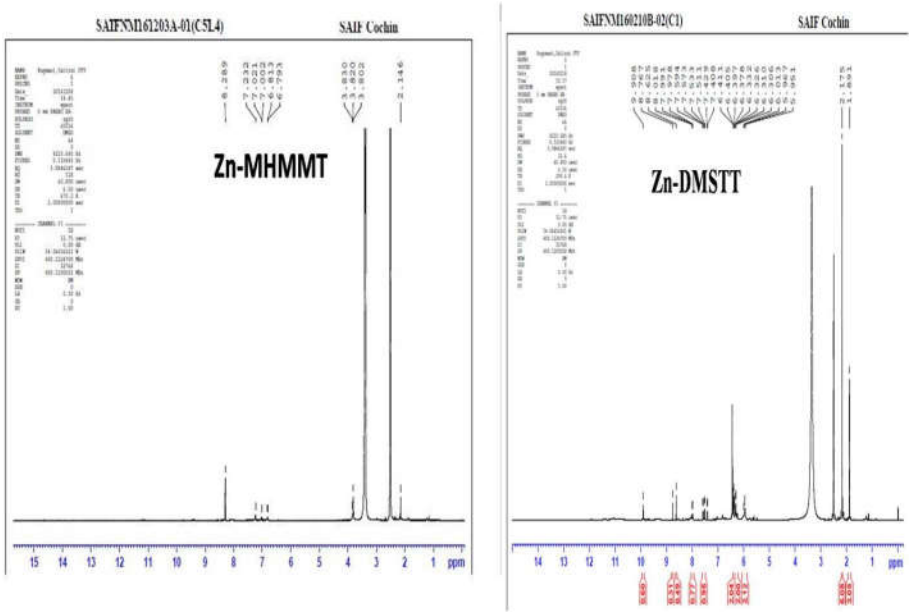

Fig 3.2 ^{1}H NMR spectra of Zn complexes

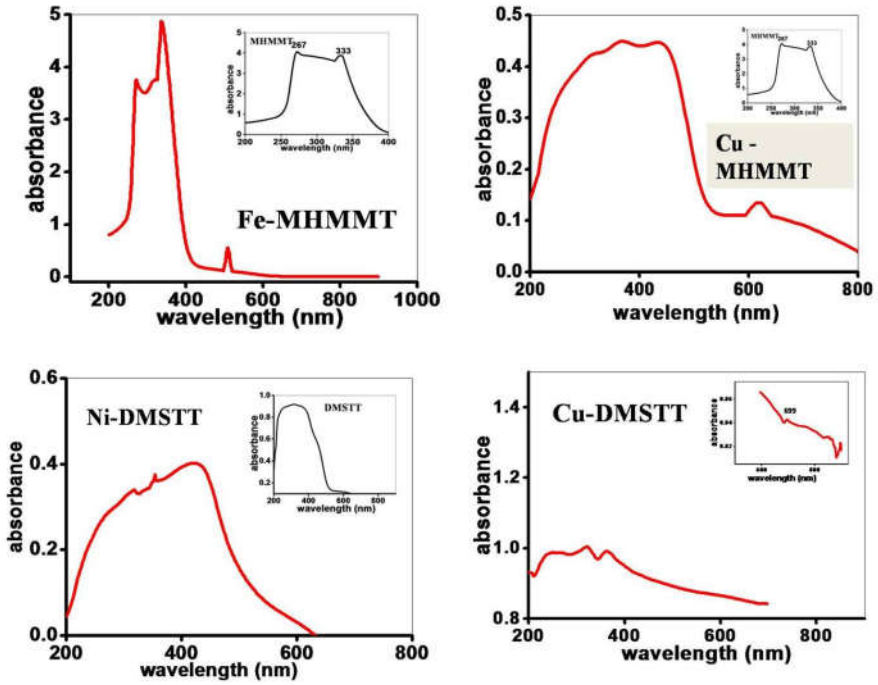

Fig 3.3 Electronic spectrum of metal complexes of MHMMT and DMSTT

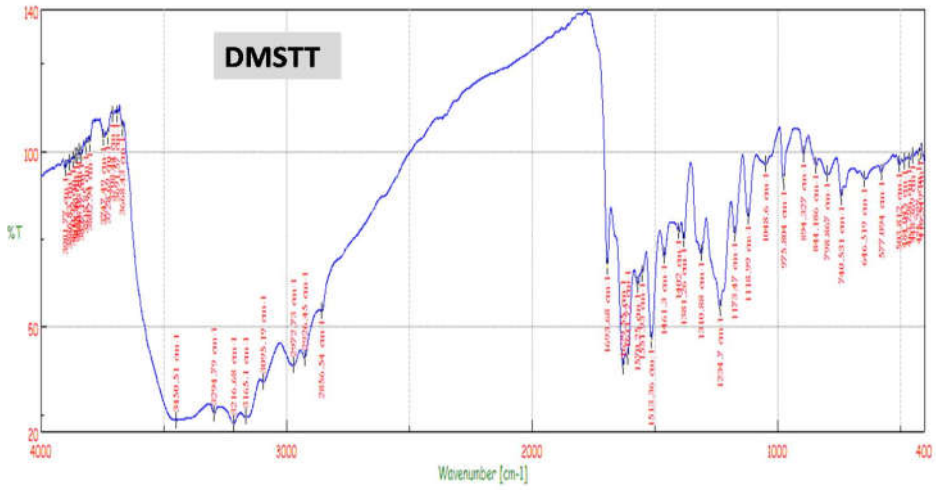

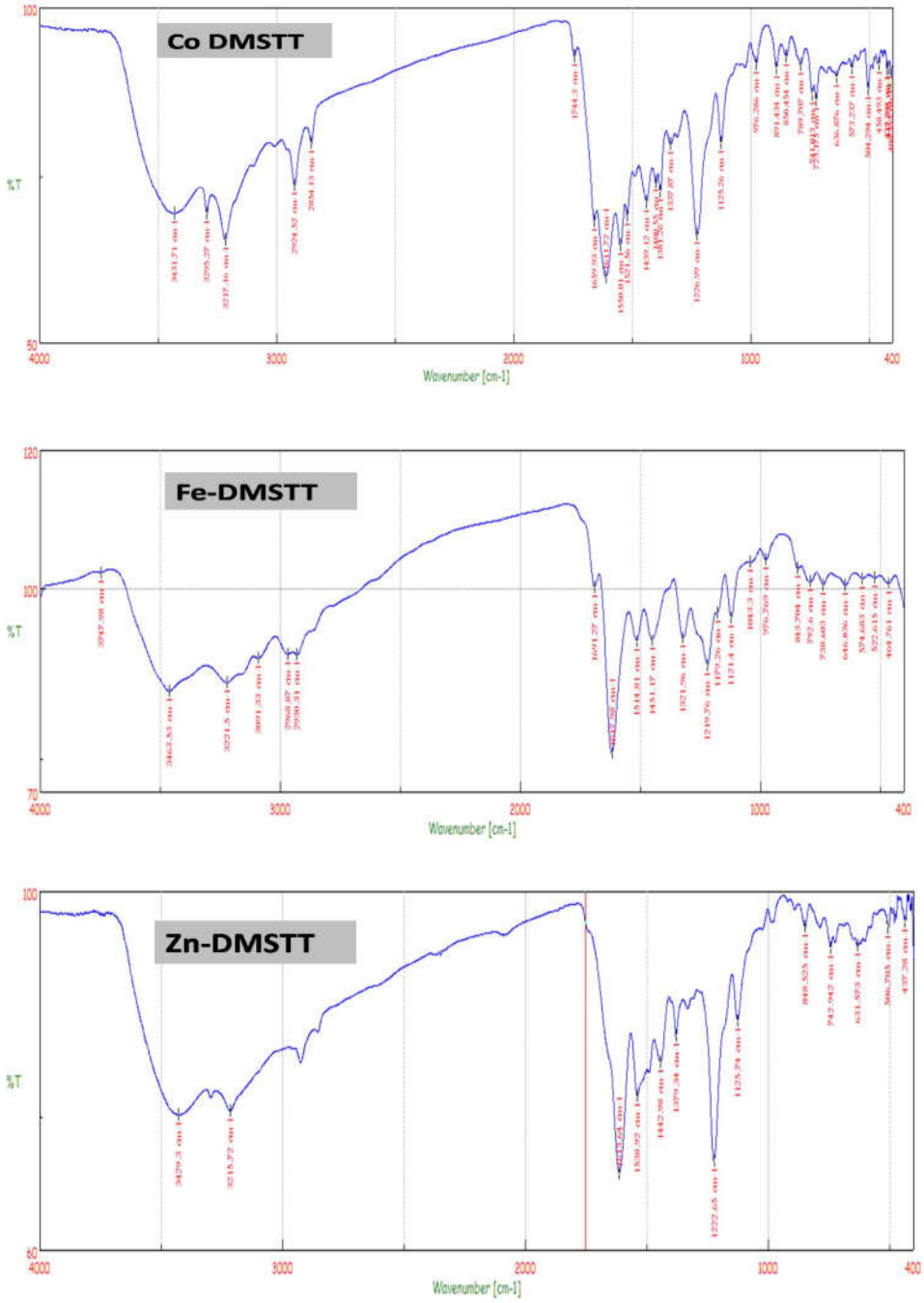

Fig 3.4 (A) IR spectrum of DMSTT and some of its complexes

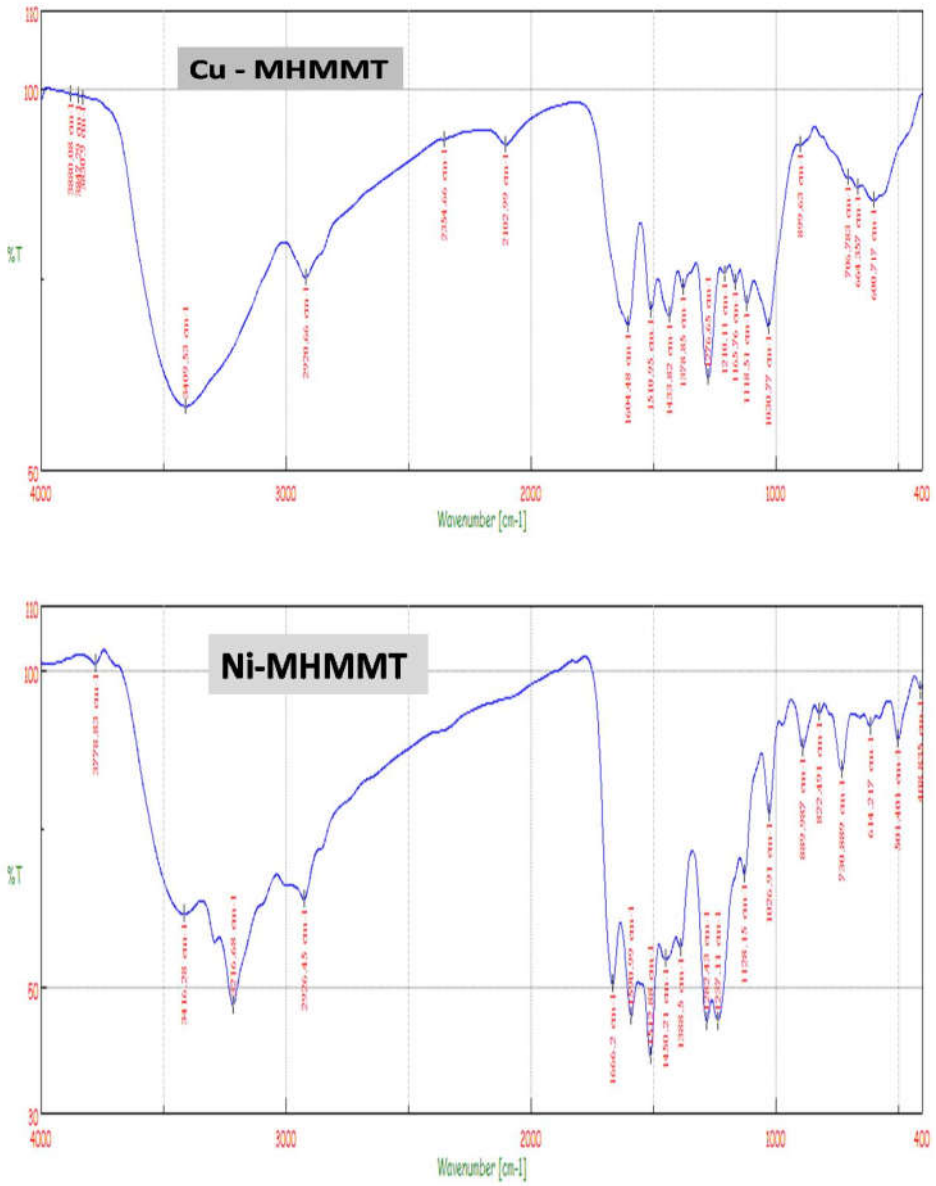

Fig 3.4 (B) IR spectrum of MHMMT and some of its complexes

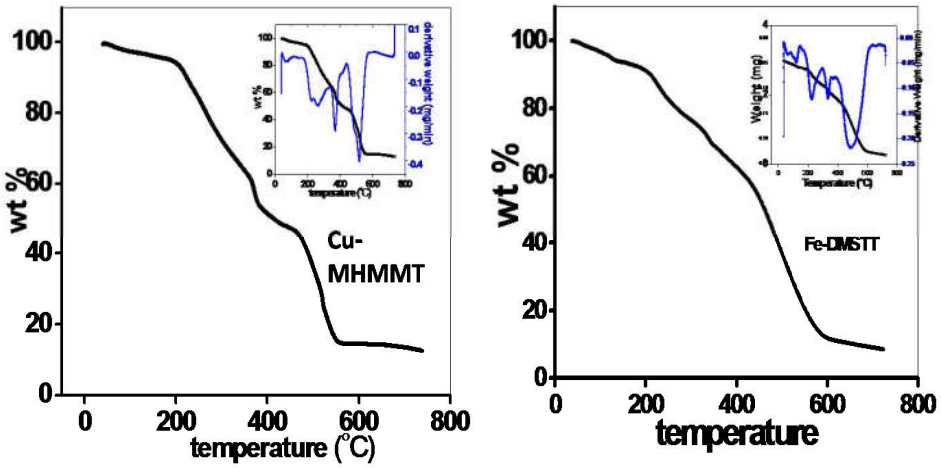

Fig 3.5 Thermogram of Cu-MHMMT and Fe-DMSTT complexes

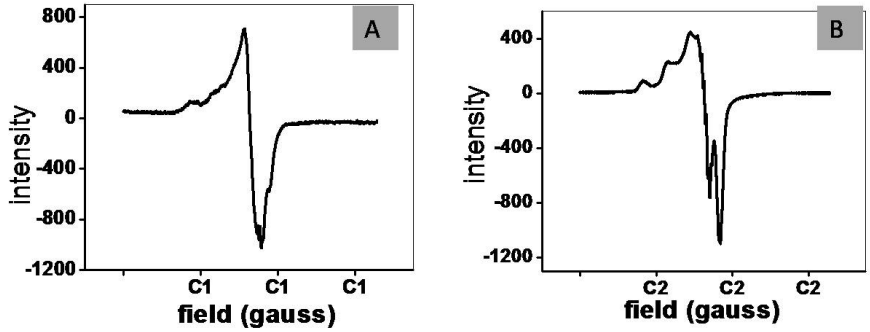

Fig 3.6 ESR spectrum of (A) Cu-MHMMT and (B) Cu-DMSTT complexes

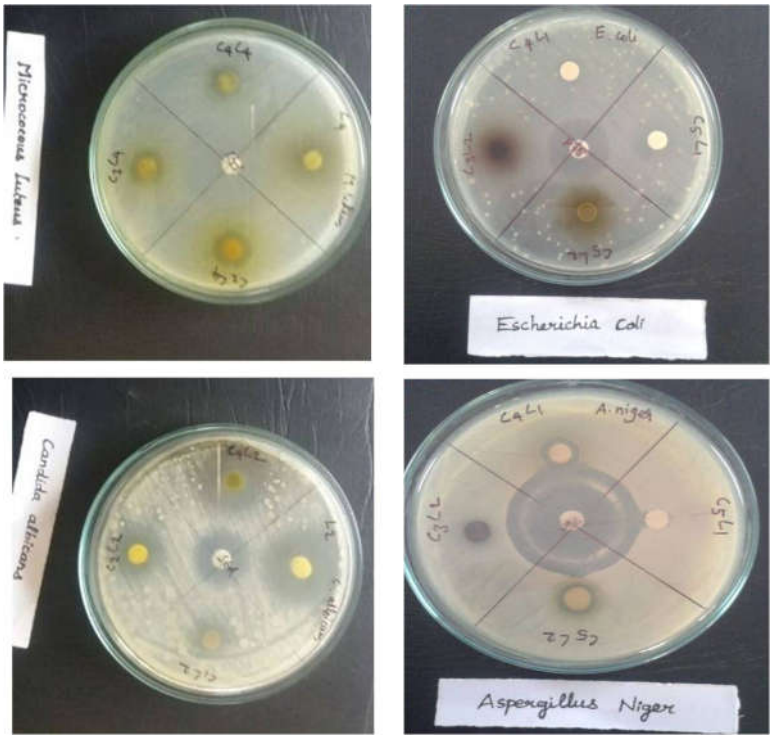

Fig 3.7 Pictorial representation of anti microbial studies

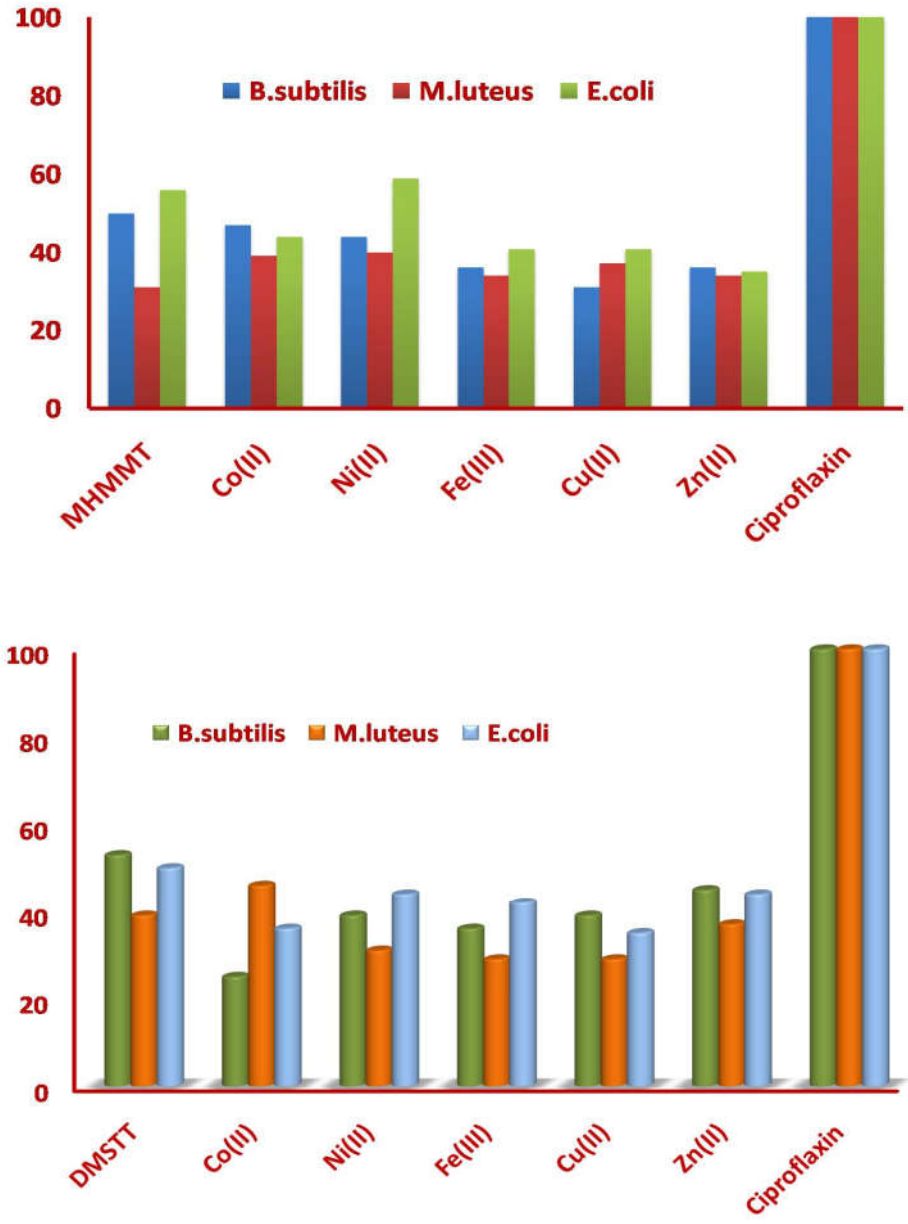

Fig 3.8 Antibacterial inhibition efficiency (%) of ligands and complexes

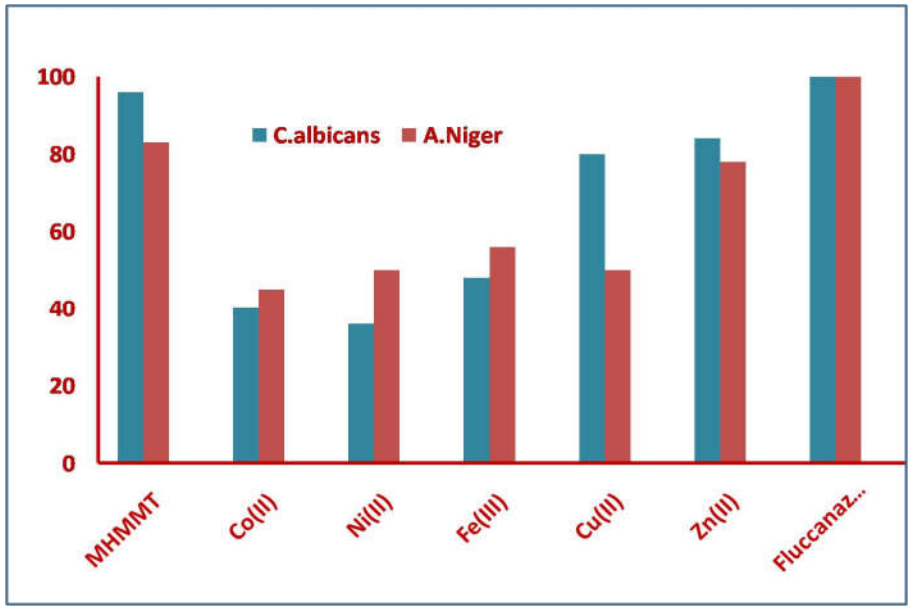

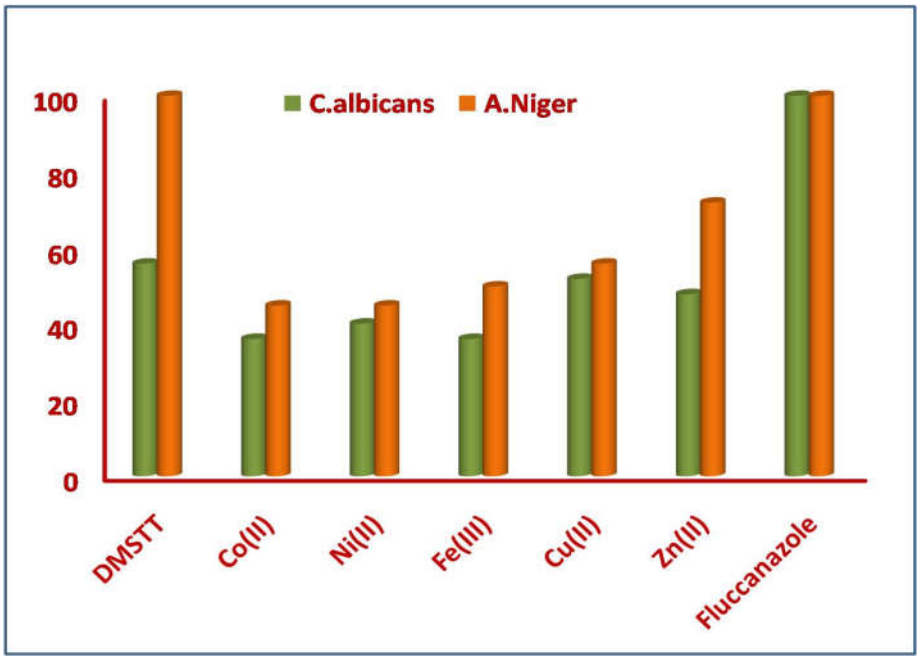

Fig.3.9 Antifungal inhibition efficiency (%) of ligands and complexes

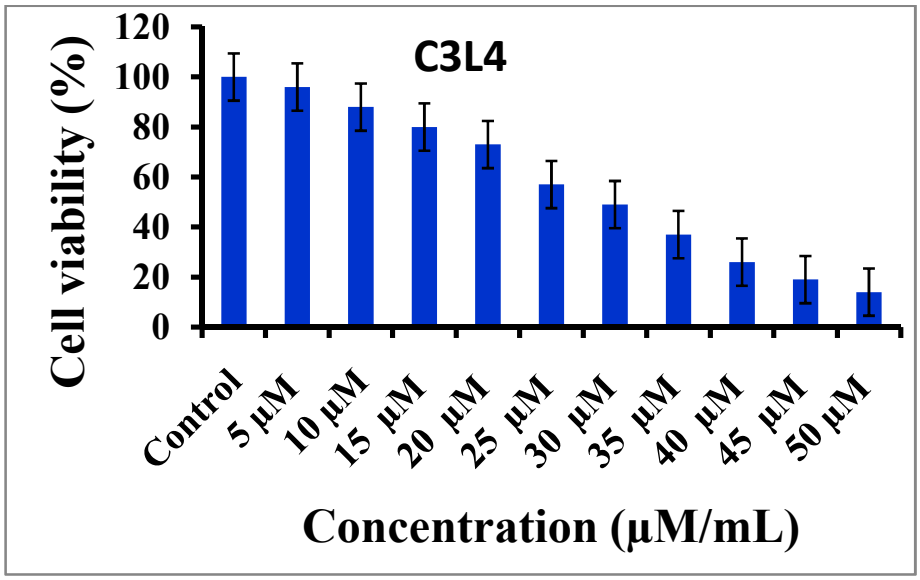

Fig 3.10 Dose dependent cyto toxic activity of Fe-MHMT complex against MCF-7 cell lines

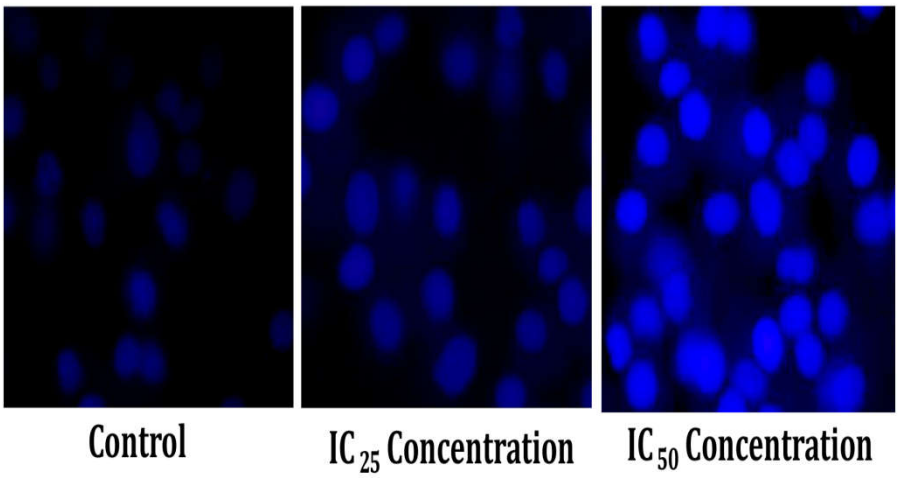

Fig. 3.11. Bright field inverted light microscopy images (DAPI) of control cells, IC_{25} and IC_{50} of Fe-MHMMT treated MCF-7 cells.

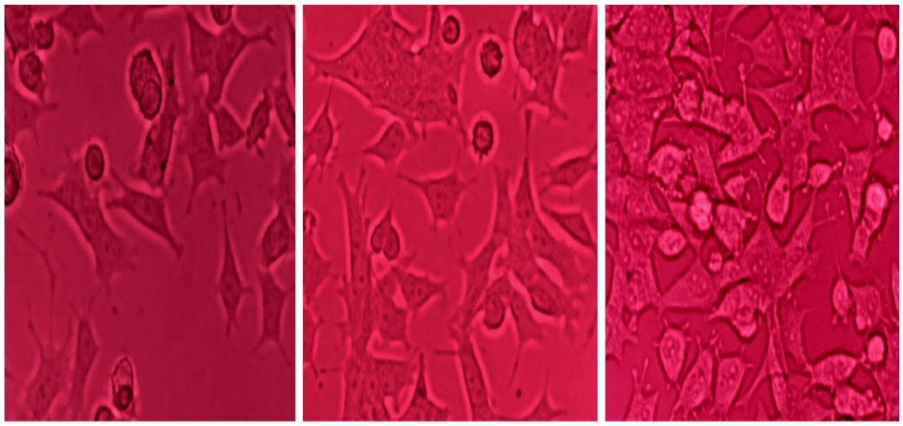

.Fig 3.12 : Fluorescence microscopic images of control cells, IC_{25} and IC_{50} of Fe-MHMMT treated MCF-7 cells.

Fig 3.13 Experimental set up for antidiabetic activity studies

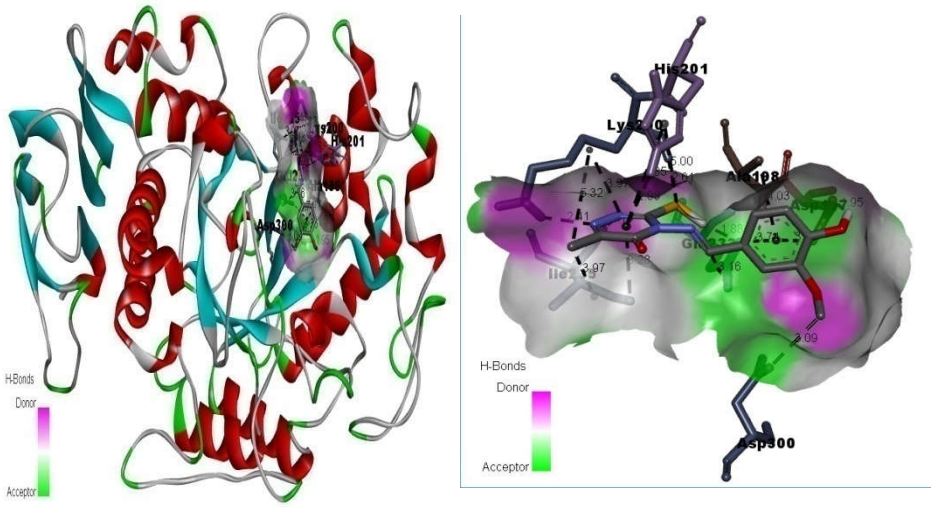
H-Bonds
Donor
Acceptor
His201
Asp300
H-Bonds
Donor
Acceptor

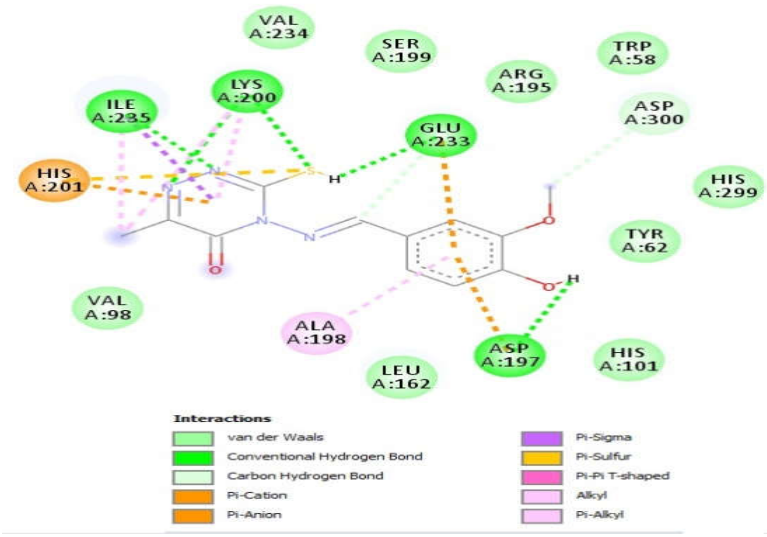
VAL A:234
SER A:199
TRP A:58
ARG A:195
LYS A:200
ILE A:235
ASP A:300
GLU A:233
HIS A:201
HIS A:299
TYR A:62
VAL A:98
ALA A:198
ASP A:197
HIS A:101
LEU A:162
Interactions
van der Waals
Conventional Hydrogen Bond
Carbon Hydrogen Bond
Pi-Cation
Pi-Anion
Pi-Sigma
Pi-Sulfur
Pi-Pi T-shaped
Alkyl
Pi-Alkyl

A

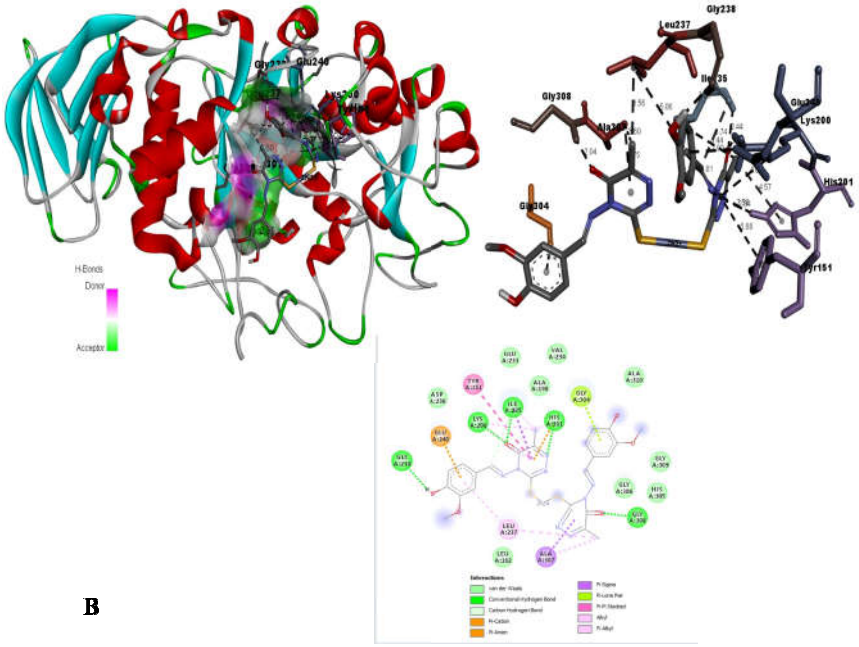
Gly238
Leu237
Gly308
Lys200
His201
Gln304
Tyr151
H-Bonds
Donor
Acceptor

B

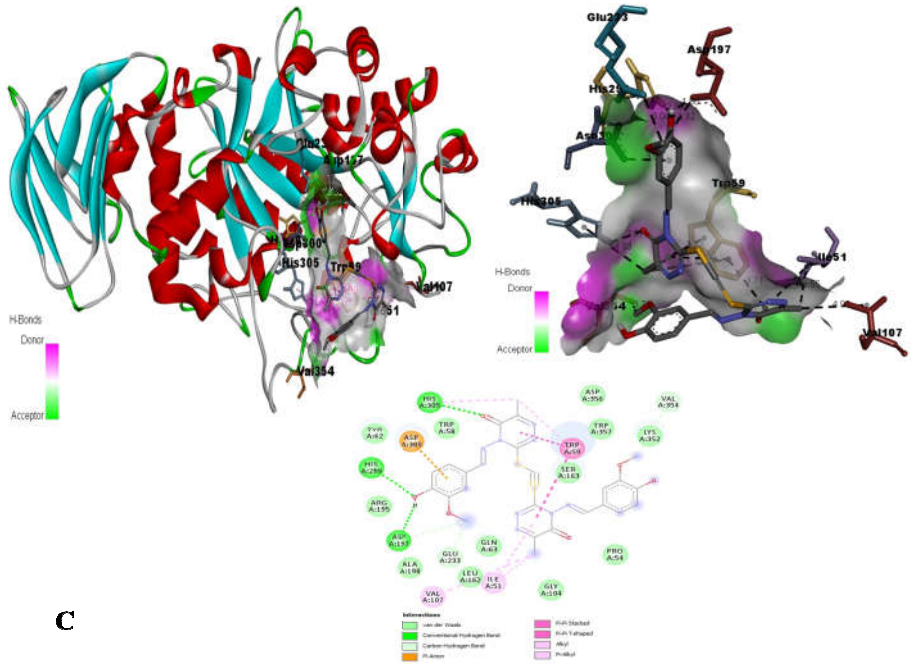
Asp197
Trp59
His51
Val107
Val354
H-Bonds
Donor
Acceptor

C

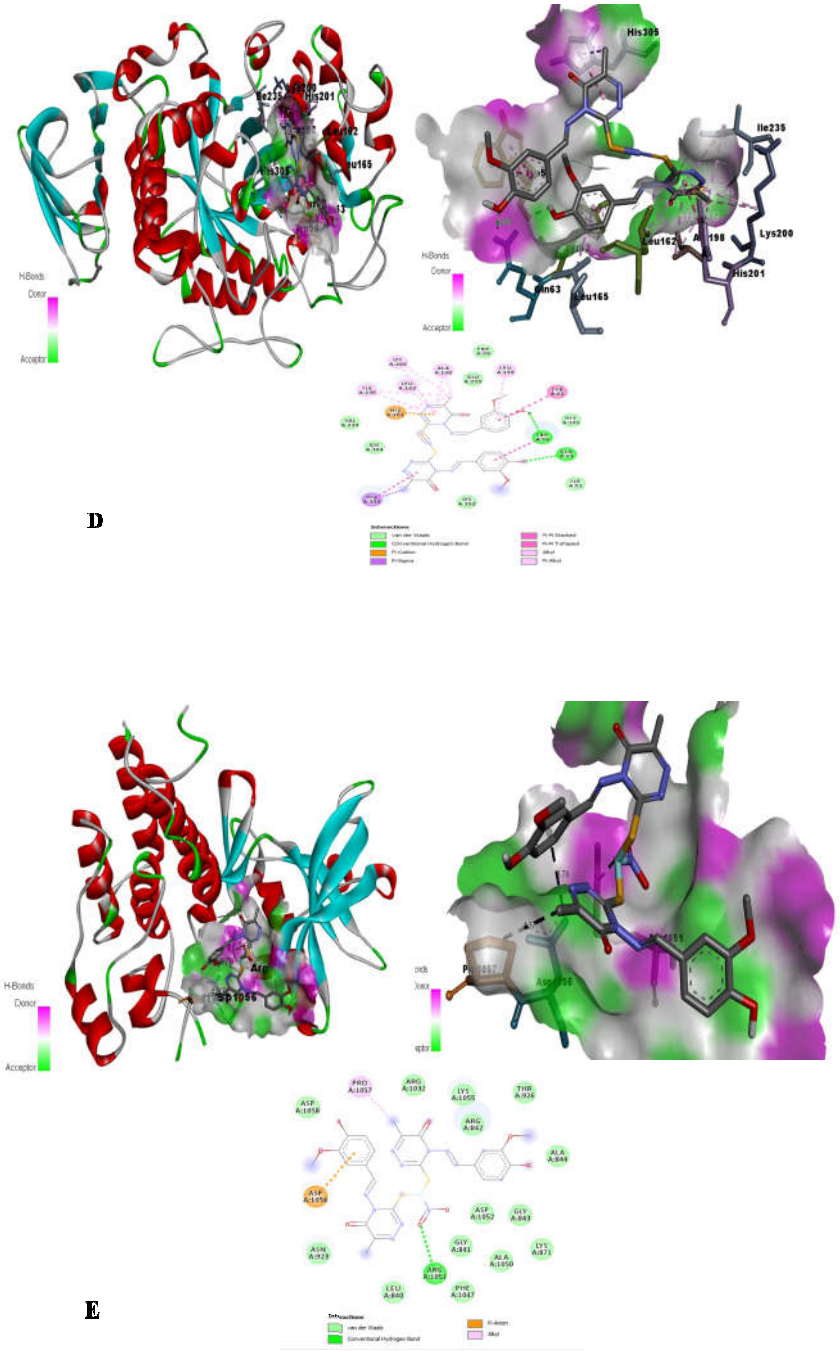

Fig 3.14 Snapshots of molecular docking studies of (A) MHMMT (B) Zn-MHMMT (C) Cu-MHMMT (D) Ni-MHMMT with α-amylase and E) Fe-MHMMT with VEGFR -2-kinase

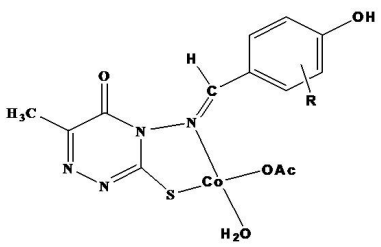

Cobalt complexes

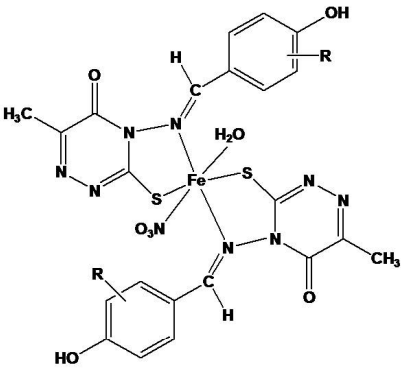

Iron complexes

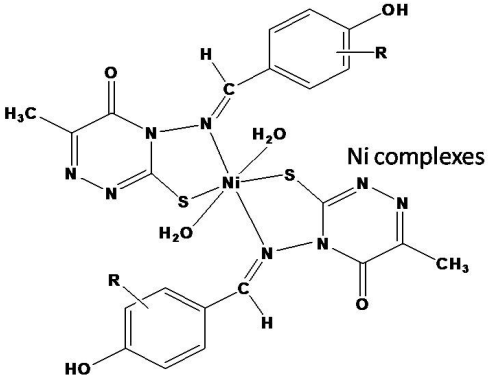

Ni complexes

R= 3-OCH_3 in MHMMT
R=2-OH in DMSTT

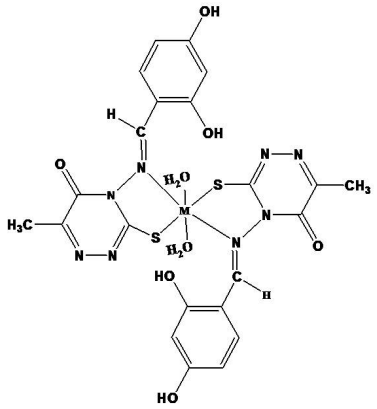

Complexes of DMSTT

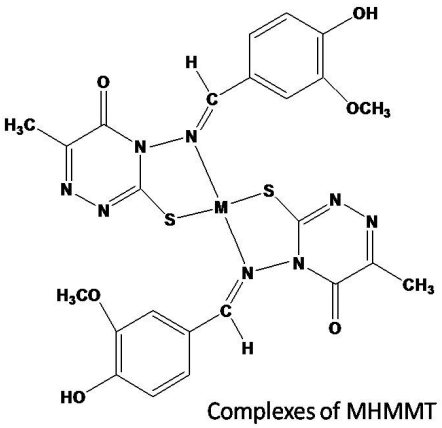

Complexes of MHMMT

M = Cu^{2+} , Zn^{2+}

Fig 3.15 structure of metal complexes

References

1. M. Yildiz, B. Dulger, S.Y. Koyuncu, B.M. Yapici, J. Indian Chem. Soc. 81 (2004)7

2. N.K. Singh, P. Tripathi, M.K. Bharty, A.K. Srivastava, S. Singh, R.J. Butcher, Polyhedron., 29 (2010)1939

3. K.S. Siddiqi, S. Khan, S.A.A. Nami, M.M. El-Ajaily, Spectrochim. Acta., Part A 67 (2007) 995

4. M. Akbar Ali, A.H. Mirza, R.J. Butcher, M.T.H. Tarafder, T.B. Keat, A.M. Ali, J. Inorg. Biochem. 92 (2002) 141

5. Carlo Preti and Gluseppe Tosi., Can. J. Chem., 54 (1976) 1558

6. Kiran Singh,, Ritu Thakur, Vikas Kumar, Beni - suef University journal of basic and applied sciences,5 (2 0 1 6) 21

7. P Gurmit Singh,. Ashutosh Singh, K Ashok Sen, Kiran Singh, Surendra N. Dubey,{ Ram N. Handa, and Junghoon Choi , Synth.React.Inorg.Met-Org Chem., 32(1) (2002) 171

8. Kiran Singh, Yogender Kumar , Parvesh Puri , Chetan Sharma K. R. Aneja, Med Chem Res 21 (2012)1708

9. Singh K, Singh DP, Barwa MS, Tyagi P, Mirza Y, J Enz Inhib Med Chem 21(2006) 749

10. Singh K, Raparia S, Surain P, Med Chem Res 24 (2015) 2336.

11. Sangamesh A Patil, M.Manjunatha, Ajayakumar, D.Kulkarni etal. Complex Metals , 1l (2014) 128

12. B.S.Garg, M.R.P.Kurup, S.K.Jain, Y.K.Bhoon, Syn.React.Inorg.Met.Org.Chem., 28 (1998) 1415

13. Text book of Elements of Magnetochemistry, R.L.Dutta and Syamal, East West Press Pvt.Ltd., New Delhi

14. L. Calu, M. Badea, M.C. Chifiriuc, C. Bleotu, G. David, G. Ionit, L. Ma˘rut¸escu, V. Laza˘r, N. Stanica˘, I. Soponaru, D. Marinescu, R. Olar, J. Therm. Anal.Calorim. 120 (2015) 375.

15. Lever, A.B.P., Inorg.Chem.4(1965) 763

16. A.B.P Lever, Inorganic Electronic Spectroscopy, 2nd edition, Elsiever, Amsterdam (1984)

17. R.L.Carlin., J.Amer.Chem.Soc., 83 (1961) 3773

18. K.Nakamoto, J.Phys.Chem. 64 (1960) 1420

19. P Bindu P., M R P Kurup., Trans.Met.Chem 22 (1999) 578

20. L.Larabi, Y.Hared, A.Reguig, M.Mostafa,J.Serb.Chem.Soc. 68 (2003) 85

21. A.S. Ramasubramanian, B.R. Bhat, R. Dileep, S. J Serb Chem Soc, 76 (2011) 7522.

22. Infrared and Raman Spectra of Inorganic and Coordination Compounds , Kazuo Nakamoto, Wiley Interscience Publication, 1997

23. A. B. P. Lever, Mantovanain, D.B.S.Ramaswamy, Can. J. of Chem., 49 (1971) 1957

24. D.C.Jicha and D.H.Busch, Inorg.Chem., 1 (1962) 878

25. K.Singh, Y.Kumar, M.S.Barwa, S.Afr.J.Chem., 63 (2010) 169 (2010)

26. N Raman Raja, S.J, Joseph.J, etal., J.Chil.Chem.soci., 52(2) (2007) 1138

27. T. Ozen, M. Taş, J. of Enz. Inh. and Med. Chem. 24 (2009) 1141

28. Chellaian Justin Dhanaraj, Jijo Johnson, J. of Photochemistry & Photobiology, B: Biology 161 (2016) 108

29. Khan T, Dixit S, Ahmad R, Raza S, Azad I, Joshi S, Khan AR.J Chem Biol. 10(3) (2017) 91

30. Dar A M, Khan M A, Mir.S.Gatoo MA Pharm. Anal. Acta. 7(2016) 464

31. Bradley C. Doak & Jan Kihlberg, Expert Opinion on Drug Discovery, 12:2(2017) 115

32. Feixiong Cheng, Weihua Li, Yadi Zhou, Jie Shen, Zengrui Wu, Guixia Liu, Philip W. Lee, and Yun Tang J. Chem. Inf. Model., 52 (2012)3099

33. B. Mathew, J. Suresh, S. Anbazhagan, J. Pharm. Bioallied Sci. 5 (2013)39

34. R.K. Goel, D. Singh, A. Lagunin, et al, Med. Chem. Res. 20 (2011) 1509

35. A.L.Barry,The Antimicrobial Susceptibility Test, Principles and Practices, E.L.B.S, 4th edition, 1976.

36. M. Salehi, A. Amoozadeh, A. Salamatmanesh,M. Kubicki, G. Dutkiewicz, S. Samiee, A. Khaleghian, J. Mol. Str., 1091 (2015) 81

37. J Carmichael, W G DeGraff, A F Gazdar, J D Minna, J B Mitchell , Cancer Res.;47 (1987) 936

38. J H Sheikh JH, Iyo, M T Tsujiyama, MdAshabul I, S B Rajat and A Hitoshi. Food Sci Technol Res. 14 (2008)261

39. S R Pattan,., S B Pawar,., S S Vetal,., U D Gharate, & S B Bhawar , 2012. The scope of metal complexes in drug design - a review, Indian Drugs, 49(11):5-12

40. B J McConkey, V Sobolev, M Edelman..Current Science. 83 (2002) 845

41. G M Morris,., R Huey, W Lindstrom, M F Sanner,., R K Belew,, D S Goodsell,.and A J Olson,. *J. Co*mputational *Chemistry* 16 (2009) 2785

42 .http://accelrys.com/products/discovery-studio/visualization-download.php

43. Vanommeslaeghe K et al. J Comput Chem. 31 (2010) 671 [PMID: 19575467

44. S V Reddy et al. J Biomol Struct Dyn. 11 (2015) 1 [PMID: 25671592]

45. SH Basha et al. Eur. J. of Biotech. and Biosci..2(2014) 30

46. G M Morris et al. J. of Comp. Chem.19 (1998) 1639

4 SYNTHESIS, CHARACTERIZATION AND BIOLOGICAL SCREENING OF 1,2,4-TRIAZOLE BASED SCHIFF BASES AND THEIR TRANSITION METAL COMPLEXES

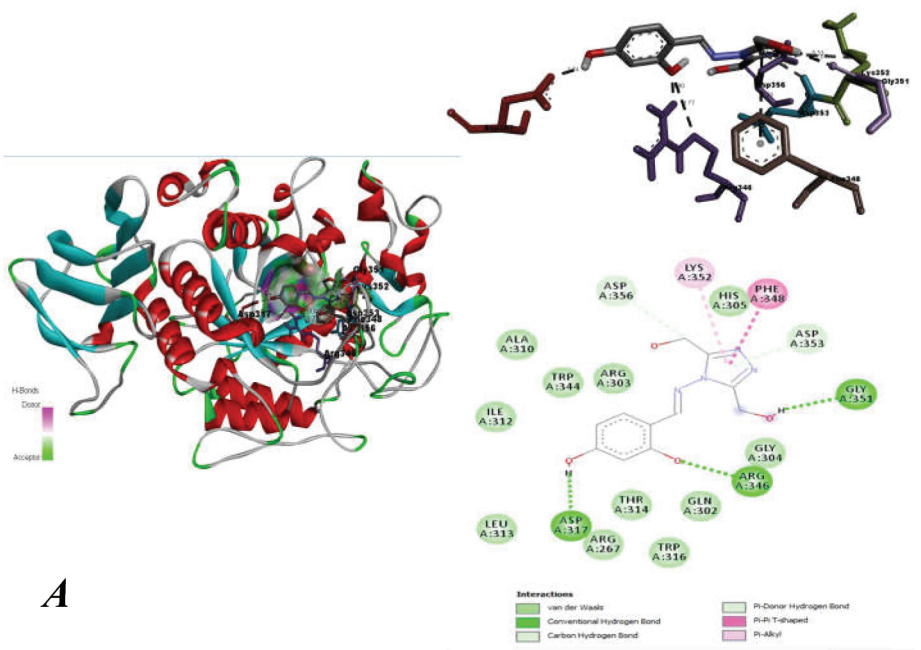

A

Chapter IV deals with the synthesis, characterization, biological screening, and molecular docking studies of Co(II), Ni(II), Cu(II) and Zn(II) complexes of two 4-amino-4-H-1,2,4-triazole-3,5-dimethanol based Schiff bases: 4-[(E)-{[3,5-bis(hydroxymethyl)-4H-1,2,4-triazol-4-yl]imino}methyl]benzene-1,3-diol (DHATD) and 4-[(E)-{[3,5-bis(hydroxymethyl)-4H-1,2,4-triazol-4-yl]imino} methyl]-2 methoxyphenol (HMATD).

IV.1 Introduction

The five member heterocyclic systems consisting of two or three nitrogen atoms (azoles) are biologically important, such as the imidazole group of histidine, acting as a potential ligand using the N-atoms, in most of the hemeproteins [1]. The vivid biological activities like antimicrobial, anticonvulsant, antiviral etc. shown by coordination compounds of 1,2,4-triazole systems made them part of many recent researches [2, 3]. From that intuition, the present chapter describes the synthesis, characterization and biological screening studies of two Schiff bases; 4-[(*E*)-{[3,5-bis(hydroxymethyl)-4*H*-1,2,4-triazol-4-yl]imino}methyl]benzene-1,3-diol (DHATD) and 4-[(*E*)-{[3,5-bis(hydroxymethyl)-4*H*-1,2,4-triazol-4-yl]imino}methyl]-2 methoxyphenol (HMATD). These ligands are synthesized by the condensation of substituted 1,2,4-triazole; 4-amino-4-H-1,2,4-triazole-3,5-dimethanol (ATD) with 2,4-dihydroxybenzaldehyde and 3-methoxy-4-hydroxybenzalehyde respectively (Section II.2.1). The compounds contain potential coordinating sites like N atom of azomethine group, O atom of hydroxyl group with or without deprotonation and O atom of methoxy group. So the chelating power of these ligands were examined with transition metal ions like Co(II), Ni(II), Cu(II) and Zn(II) and characterized by various spectroscopic and analytical techniques and biological screening studies were carried out via *in silico* methods using various online software and also by *in vitro* methods.

IV.2 Experimental

1,2,4-triazole based Schiff bases DHATD and HMATD were synthesized as per the procedure given in chapter II (Section II.2.1) and re-crystallized from ethanol. The metal complexes were synthesized by mixing

hot ethanolic solution of ligands and hot aqueous/ethanolic solution of metal salts in the ratio (M:L 1:2) drop by drop with stirring and refluxing the resulting mixture for about 3 h. The complexes separated out on cooling were filtered and washed with ethanol, distilled water and ether. The complexes were dried in a hot air oven.

IV.3 Results and discussion

The ligands and metal complexes were characterized by various physical property measurements and spectroscopic analysis. The metal complexes are colored, non hygroscopic, stable in air at room temperature, insoluble in water but soluble in non polar solvents and undergo decomposition at higher temperature. The analytical data produced in Table 4.1 (A and B) revealed a close agreement between theoretical and experimental CHN percentage. The elemental analysis proposed a 1:2 (M:L) ratio for both DHATD and HMATD complexes.

IV.3.1 ^{1}H NMR spectra

The prominent signals exhibited by ^{1}H NMR spectrum of DHATD and its Zn (II) complex in DMSO-d6 are tentatively assigned as follows: δ 4.59 (4H, s, C$\underline{H_2}$O$\underline{H}$), 5.616 (2H, s, $CH_2\underline{OH}$), 6.3-7.3(4H, m, aromatic protons), 8.220 (1H, s, CH=N), broad peak at 10.464 and 12.24 (2H, phenolic 4-OH, 2-OH). The NMR spectrum of Zn-DHATD complex was devoid of peak at 12.24 indicating the deprotonation of 2-OH groups. The signal of azomethine proton has undergone a downfield shift and appears at 9.004 ppm indicating the deshielding of azomethine proton due to drift of electrons of azomethine nitrogen towards Zn(II) ions and coordination of ligand through azomethine nitrogen (Fig 4.1) [4].

The ^{1}H NMR spectrum of HMATD showed the following peaks at δ 3.861 (3 H, s, OCH_3), 4.6 (4H, s, $C\underline{H_2}OH$), 5.6 (2H, s, $CH_2\underline{OH}$), 6.9-7.5 (4H, m, aromatic protons), 8.806 (1H, s, CH=N), 10.035 (1 H, s, phenolic OH). The peak due to azomethine proton at 8.806 has undergone a downward shift and appeared at 8.9 in the Zn complex suggests the coordination of HMATD to Zn(II) ion through azomethine nitrogen [4].

IV.3.2 Magnetic moment measurements

The magnetic moment measurements are very useful for ascertaining the stereochemistry of transition metal complexes. The magnetic moment of Co(II) complex of DHATD and HMATD at room temperature was found to be 5.23 and 4.56 BM respectively. The high spin octahedral Co(II) complexes possess a $^{4}T_{1g}$ ground term with an orbital contribution towards magnetic moment, so μ_{eff} will be higher than the spin only value for 3 electrons i.e., 3.87 BM [5]. But for a tetrahedral cobalt complex, no orbital contribution can be expected and the complexes will have the spin only magnetic moment of 3.87 BM. So the magnetic moment value of Co-DHATD complex is suggestive of an octahedral geometry. A μ_{eff} value of 4.56 BM for Co-HMATD is higher than that expected for a tetrahedral complex which can be explained as follows:- The excited state $^{4}T_2$ ($e^3t_2^4$) carries orbital magnetic moment, so a spin-orbit coupling brings out some mixing between ground state and excited state, thus some orbital contribution [5]. Thus Co-HMATD complex can be considered to have a tetrahedral structure.

Ni (II) complexes of DHATD and HMATD gave μ_{eff} values of 2.78 and 2.84 BM respectively indicating the presence of two unpaired electrons with an octahedral environment around the metal ion [6]. In an octahedral field around Ni(II) with $^{3}A_{2g}$ as ground state, no orbital contribution was

expected towards magnetic moment, so spin only value gave μ_{eff} in the range 2.9-3.4 BM.

Considering Cu(II) complexes, it was very difficult to elucidate the stereochemistry using magnetic moment values. The Cu(II) complexes of DHATD gave a high value of magnetic moment 2.16 BM due to the spin of one unpaired electron with some orbital contribution. This high value gave a suggestion of an octahedral stereochemistry for Cu-DHATD complex [5]. Cu-HMATD complexes were found to be diamagnetic in nature which suggests the possibility of dimerization with a Cu-Cu bond. The single electron in each Cu(II) ion became spin paired due to strong Cu-Cu interaction leading to diamagnetic nature [7].

IV.3.3 Infrared spectral measurements

The coordination sites of ligands were elucidated by comparing the IR spectra of ligand with those of metal complexes. Tentative assignments of selected IR bands are summarized in Table 4.2 (A) and. (B). The IR spectrum of DHATD exhibited a strong peak at 1626 cm^{-1} is a characteristic stretching frequency of azomethine group. In complexes there is a reduction in this frequency to 1581-1618 cm^{-1} due to the coordination of azomethine nitrogen to metal ions which causes a flow of electrons from N to metal and a subsequent reduction in electron density on C=N bond as well as the IR frequency [8]. The ligand has two phenolic OH groups at C*4* and C*2* positions. The broad bands in the ligand spectrum in the region 3345 cm^{-1} (C4 OH) and 3111 (C2 OH) groups are due to these groups. The OH group at ortho position resonates at a lower frequency due to considerable amount of hydrogen bonding with adjacent C=N group [9]. This peak disappeared in the spectrum of complexes indicating a deprotonation of this OH group. This deprotonation was further supported by the following observations. The spectra of ligand displayed two bands at 1330, 1354 cm^{-1}corresponding to δ

(O-H) and two bands at 1245 and 1172 cm^{-1}due to υ(C-O). This is due to OH groups at ortho and para positions. On complexation, the band at 1354 $cm^{-1}$is still present which indicates the deprotonation at only one OH group (ortho OH). One of the υ (C-O) frequencies at (1245 cm^{-1}) appears nearly in its position in the complexes whereas the other one at 1172 cm^{-1}shifts to higher frequency by a range of 30 cm^{-1}[10]. These observations suggest a monobasic bidentate behavior for DHATD with a free para OH group. This was again confirmed by M-O stretching in the region 405-455 cm^{-1} and M-N stretching in 520-540 cm^{-1}[11] which are absent in the ligand spectrum. The presence of coordinated water molecules were reflected by the peaks at around 3400-3200 and 750-850 cm^{-1} [12].

In the case of HMATD, the ligand exhibits peaks at 3411, 3059,1597, 1301, 1240 and 1030 cm^{-1}which are ascribed to υ(O-H), υ(C=N), δ phenolic (O-H), υ phenolic (C-O) and υ methoxy (C-O)vibrations. The peak due to azomethine (C=N) group has undergone a downward shift in metal complexes because of its coordination to metal ions via nitrogen atom [8]. It has been found that the peaks due to δ(O-H), υ phenolic (C-O) and υ methoxy (C-O) remain unchanged in the metal complexes indicating non deprotonation of OH and non involvement of oxygen atoms on coordination.The presence of acetate anions in the complexes were indicated by $\upsilon_{asy}(COO^{-})$ around 1660 cm^{-1} and $\upsilon_{sy}(COO^{-})$ around 1430 cm^{-1} with a difference in the range 225-232 suggesting unidentate nature of its coordination [13]. Thus IR analysis pinpoints unidentate nature for HMATD. The representative IR spectra of complexes are given in Fig 4.2.

IV.3.4 Electronic spectra

Electronic spectra and measurement of magnetic moment are important tools in the structure elucidation of metal complexes. The λ_{max}, their possible assignments and calculated ligand field parameters for the

complexes depicted in Table 4.3 helps to predict the extent of covalent bonding and the geometry of the complexes. The representative electronic spectra of complexes are given in Fig 4.3

IV.3.4.1 Cobalt complexes

The high spin octahedral Co(II) complexes are expected to exhibit three transitions in the increasing order of energy as ^4T_1g (F) $\rightarrow$ ^4T_2g (F), ^4T_1g (F) $\rightarrow$ ^4A_2g (F) and ^4T_1g (F) $\rightarrow$ ^4T_1g (P). The first transition was not recorded since it is beyond the range of the instrument used. But its position can be obtained from the second transition. The Co-DHATD complex exhibits peaks at 1110 (ca), 495, 475 nm and with the help of band fitting equations as $\upsilon_1 = 8$ Dq, $\upsilon_2 = 18$ Dq and $\upsilon_3 = 6$ Dq + 15 B, the ligand field parameters were calculated. A high CFSE of 1122.0 and B value 954 (< 971 cm^{-1}) suggested an overlapping of ligand and metal orbitals. The value of nephelauxetic ratio (β) <1 suggested partial covalency in M-L bond. These ligand field parameters support an octahedral structure for Co-DHATD complex.

Co-HMATD exhibits absorption maxima at 1040 (ca), 578 and 475 nm due to various transitions described in Table 4.3 and are characteristic of tetrahedral geometry of complexes. The ligand field parameters were calculated using band fitting equations as explained in chapter III (3.3.2). The Racah parameter (B) value of 635 cm^{-1} is less than B_0 value for free Co(II) ion (971 cm^{-1}) suggests overlapping of orbitals as well as electron delocalization in the metal ion [14]. β value of 0.65 pointed out a covalency of 35% in the complex. The electronic spectra supports the structure obtained from magnetic studies.

IV.3.4.2 Nickel complexes

The electronic absorptions and the corresponding transitions given in Table 4.3 suggested octahedral geometry for Ni-DHATD and Ni-HMATD complexes. The band fitting calculations were done on the basis of the equations: $^3A_{2g} \rightarrow {}^3T_{2g}(F)$ (υ_1) = 10 Dq, $^3A_{2g}(F) \rightarrow {}^3T_{1g}(F)$ (υ_2) = 18 Dq and $^3A_{2g}(F) \rightarrow {}^3T_{1g}(P)$ (υ_3) = 12 Dq +15 B and it provides B values of 773 and 745 cm^{-1} and β values of 0.74 and 0.72 respectively for Ni-DHATD and Ni-HMATD complexes. The ligand field parameters are in concordance with magnetic moment values and hence suggested octahedral geometry for these nickel complexes.

IV.3.5 Thermo *gravimetric analysis*

The Thermal analysis of complexes revealed the presence of coordinated water molecules in Co(II), Ni(II), Cu(II) and Zn(II) complexes of DHATD and Ni(II) complex of HMATD. The mass loss of these complexes in the temperature range 100-240^oC indicated the loss of coordinated water molecules. In most cases the mass loss occurred in two or more stages. Co(II) complexes of DHATD exhibited an initial mass loss at 140-240^oC region with a mass loss percentage of 5.2, which is in good agreement with the theoretical mass corresponding to two water molecules (5.7%). The thermogram of Ni(II) complex of DHATD showed an initial mass loss at 140^oC which can be ascribed to the loss of coordinated water molecule. An exothermic peak is appeared in the DTA spectrum at 123^oC and the experimental mass loss was found to be 6.3 % which is almost consistent with the theoretical mass loss of two water molecules (5.8%). The mass loss at 250-360^oC will be the result of decomposition of organic matter. The major mass loss occurs at 400-800^oC and there after the mass remains almost constant indicating the formation of metal oxide. Similar results are shown by other metal complexes of DHATD.

The analysis of thermograms of complexes of HMATD revealed the presence of water molecules in Ni(II) and Cu(II) complexes. The other complexes are stable up to 180^{o}C indicating the absence of coordinated water molecules. Then mass loss occurs in two regions around 200-350^{o}C and 350-550^{o}C which are due to the decomposition of organic part and acetate moiety in the complexes and thereafter the mass remains the same indicating the formation of metal oxide as the final product. Thermograms of complexes are shown in Fig 4.4.

IV.3.6 Biological screening studies

The virtual screening of pharmacological behavior like drug likeness and bioactivity score of ligands as well as metal complexes were done using the online software *www.molinspiration.com.*

IV.3.6.1 Validation of Lipinski's rule of 5 and bioactivity prediction

In order to predict the drug likeness, bioavailability and bioactivity of ligands as well as complexes, they were subjected to molinspiration calculations [15]. The results are presented in Table 4.4. The molecular hydrophobicity or lipophilicity expressed by $m_i$logP values of ligands as well as complexes (-0.78 to ─6.48) are well within the accepted Lipinski range (<5) for a drug candidate to possess good permeation through bio membranes and to display good bioavailability [16, 17].

The bioactivity scores for binding sites like g-protein coupled receptor ligand (GPCRL), nuclear receptor ligand (NRL), ion channel modulator (ICM), kinase inhibition (KI), protease inhibition (PI), enzyme inhibition (EI) etc. calculated using molinspiration software was given in Table 4.4. It has been suggested that metal complexes with bioactivity score >0 are highly bioactive in nature whereas those with scores between ─5.0 to

0 have moderate activity and if the score is less than −5.0, then they are inactive [18]. Table 4.4 shows that ligands as well as metal complexes have values within −1.45 to 0.02, so they are expected to have moderate bioactivity [19]. The studied complexes also can be included into the chemical space of bRo5 of drug likeness with some modifications.

IV.3.6.2 In vitro antimicrobial activity

In vitro antimicrobial screening of ligands as well as complexes were tested against the bacterial species like *Escherichia coli*(gram negative) and *Micrococcus luteus* (gram positive) and fungal species like *Candida albicans* and *Aspergillus niger* by disc diffusion method as described in chapter II (Section II.7.1) (Fig 4.5). The results of antimicrobial screening represented in Fig 4.6 revealed that HMATD is active against the positive bacterial strain *M.Luteus* but inactive against gram negative *E.coli* whereas DHATD is active against both bacterial strains. All the metal complexes are active against both gram positive and gram negative bacterial strains. Zn-DHATD is found to be almost as active as standard drug ciproflaxin against the studied bacterial strains. Most of the metal complexes are found to be more active than the corresponding ligands and the antibacterial effect follows the order Zn (II)>Co (II)>Cu (II)>Ni (II).

From Fig 4.7, it is clear that ligands as well as metal complexes are active against fungal strains *C.albicans* and *A.niger*. Metal complexes inhibit the fungal action effectively compared to ligands. Cu(II) complexes of HMATD shows higher efficiency against *C.albicans* and Zn(II) complex of HMATD offer higher inhibition efficiency against *A.niger*. The antifungal activities follow the order Zn (II)>Cu (II)>Co (II)>Ni (II).

The enhanced antimicrobial behavior of the metal complexes can be explained by (1) Overtone's theory [20] and Tweedy's chelation theory [21]

which deals with the reduction in polarity of metal ions on chelation due to sharing of positive charges on metal ions with donor atom of ligands. This in turn increases their lipophilic nature. The enhanced lipophilicity promotes the diffusion of metal complexes through biomembrane of micro organisms and inhibits their action.

IV.3.6.3 In vitro antidiabetic studies

In vitro antidiabetic studies of ligands and some of their complexes were carried out by α-amylase inhibition method. The procedural details are given in chapter II (Section II.7.3). The results revealed (Table 4.5) that the HMATD and its complexes shows comparatively higher α-amylase inhibition efficiency compared to that of DHATD. The order of inhibition activity for HMATD and its complexes is in the order Zn-HMATD > Cu-HMATD> Ni-HMATD> HMATD>Co-HMATD and that for DHATD and its complexes is Zn-DHATD>Cu-DHATD>Ni-DHATD>DHATD>Co-DHATD. The cobalt complexes exhibit lesser activity than ligands.

IV.3.6.4 Molecular docking Studies

The molecular docking studies for HMATD, DHATD and some of their complexes were done using Autodock 4.2 software. Various docking parameters, detailed interactions between the target enzyme and ligands along with computed IC_{50} values are tabulated in Table 4.6. The selected compounds were shown to be successfully docked inside the enzyme as evident from the values of binding energies. The docking results also showed a lesser inhibition by cobalt complexes compared to ligands and a higher inhibition for Zn complexes. The docking snapshots of studied compounds at the active binding site of enzyme are represented in Fig 4.9. The figures demonstrated that these compounds have excellent binding sites to interact with enzyme, and there are various kinds of interactions between the ligand

and receptor which stabilizes the ligand-receptor complexes and inhibit the action of enzymes. The major interactions involved are hydrogen bonding, Van der Waal's and other types of interactions like π-cation, π-anion, π-alkyl, π-π stacked etc. with various amino acid residues in the enzyme. Further in vivo and cytotoxic studies are required for developing them as potential drugs.

Conclusions

In this chapter, the chelating ability of 1,2,4-triazole based Schiff bases DHATD and HMATD were studied and the ligands as well as their metal complexes were characterized by various physic-chemical methods. Schiff base DHATD was found to be bidentate, monobasic in nature and all of its complexes have octahedral geometry. The Schiff base HMATD has a monodentate nature and its Co(II) and Zn(II) complexes possess tetrahedral geometry. The Ni(II) and Cu(II) complexes of HMATD have octahedral and square planar geometries respectively (Fig 4.8). *In vitro* antimicrobial studies revealed a moderate activity for ligands as well as metal complexes against the bacterial and fungal strains employed in the study. The ligands as well as selected complexes possess comparatively good α-amylase inhibition activity also.

Table 4.1 (A) Physical and Analytical data of transition metal complexes of DHATD

Compounds/ Mol.wt	μ_{eff} BM	Analysis percentage exptl (theoretical) C	H	N	M
DHATD (L) $C_{11}H_{12}O_4N_4$ (264)	--	48.5 (50)	4.43 (4.54)	20.82 (21.20)	--
$Co(L\text{-}H)_2.\ 2H_2O$ $CoC_{22}H_{26}O_{10}N_8$ (621) (Oh)	5.23	42.51 (42.51)	4.46 (4.18)	17.07 (18.03)	9.84 (9.50)
$Ni(L\text{-}H)_2.\ 2H_2O$ $NiC_{22}H_{26}O_{10}N_8$ (620.6) (Oh)	2.78	42.76 (42.53)	4.96 (4.51)	19.44 (18.04)	8.86 (9.44)
$Cu(L\text{-}H)_2.\ 2H_2O$ $CuC_{22}H_{26}O_{10}N_8$ (625) (Oh)	2.16	41.84 (42.24)	4.34 (4.16)	17.09 (17.92)	9.54 (10.08)
$Zn(L\text{-}H)_2.\ 2H_2O$ $ZnC_{22}H_{26}O_{10}N_8$ (627) (Oh)	dia	41.90 (42.10)	4.18 (4.15)	16.43 (17.86)	9.74 (10.36)

Table 4.1 (B) Physical and Analytical data of transition metal complexes of HMATD

Compounds/ Mol.wt	μ_{eff} BM	Analysis percentage exptl (theoretical) C	H	N	M
HMATD (L) $C_{12}H_{14}O_4N_4$ (278)	--	48.67 (51.75)	5.97 (5.03)	19.81 (20.13)	--
$CoL_2.\ (OAc)_2$ $CoC_{28}H_{34}O_{12}N_8$ (733) (Td)	4.56	45.43 (45.84)	4.84 (4.64)	14.00 (15.28)	9.06 (8.04)
$NiL_2.(OAc)_2\ .2H_2O$ $NiC_{28}H_{38}O_{14}N_8$ (768.6) (Oh)	2.84	43.26 (43.71)	4.38 (4.94)	13.44 (14.57)	6.96 (7.62)
$(CuLOAc.H_2O)_2$ $Cu_2C_{28}H_{38}O_{14}N_8$ (836) (SP)	dia	39.21 (40.19)	4.13 (4.54)	13.39 (14.00)	13.84 (15.07)
$ZnL_2.(OAc)_2$	dia	47.72	5.02	16.30	7.74

$ZnC_{28}H_{34}O_{12}N_8$ (739) (Td)	(45.46)	(4.60)	(15.15)	(8.79)

Table 4.2 A Important infrared spectral bands (cm^{-1}) and their tentative assignments for DHATD and its complexes

Ligand	**Complexes**				**Assignments**
	Co(II)	**Ni(II)**	**Cu(II)**	**Zn(II)**	
3345,3130	3424	3208	3384	3384	υ (OH)/water
1626	1619	1605	1617	1581	υ(C=N)
1354	1364	1365	1356	1363	δ (phenolic C_4(O-H)
1252	1249	1247	1256	1246	υ phenolic(C_4-O)
1172	1195	1203	1196	1203	υ phenolic(C_2-O)
--	532	524	536	523	υ(M-N)
--	435	404	455	405	υ(M-O)
--	720	788	853	799	Coordinated water

Table 4.2 B Important infrared spectral bands (cm^{-1}) and their tentative assignments for HMATD and its complexes

Ligand	**Complexes**				**Assignments**
	Co(II)	**Ni(II)**	**Cu(II)**	**Zn(II)**	
3228	3322	3130	3410	3415	υ (OH)/water
1604	1583	1581	1587	1570	υ(C=N)
1301	1291	1283	1292	1300	δ (phenolic C_4(O-H)
1240	1234	1246	1240	1240	υ phenolic(C-O)
1030	1028	1031	1032	1037	υ methoxy(C-O)
--	456	523	580	556	υ(M-N)
	412	459	430	417	υ(M-O)
--	1661, 1430	1620, 1400	1665, 1441	1650, 1418	$\upsilon(asy)_{COO-}$, $\upsilon(sy)_{COO-}$,

Table 4.3: Electronic spectral bands with probable assignments

compound	Band position nm	Assignment	Dq cm^{-1}	B	β
DHATD		$\pi - \pi^*$ $n - \pi^*$	--	--	--
Co-DHATD	1110(ca) 495 475	$^4T_1g\ (F) \rightarrow {}^4T_2g\ (F)$ $^4T_1g\ (F) \rightarrow {}^4A_2g\ (F)$ $^4T_1g\ (F) \rightarrow {}^4T_1g\ (P)$.	1122	954	0.98
Ni-DHATD	777 (ca) 432 370	$^3A_{2g} \rightarrow {}^3T_{2g}(F)$ $^3A_{2g}(F) \rightarrow {}^3T_{1g}(F)$ $^3A_{2g}(F) \rightarrow {}^3T_{1g}(P)$	1286	773	0.74
HMATD	350, 417	$\pi - \pi^*$ $n - \pi^*$	--	--	--
Co-HMATD	1040(ca) 578 475	$^4A_2 \rightarrow {}^4T_2$ $^4A_2 \rightarrow {}^4T_1(F)$ $^4A_2 \rightarrow {}^4T_1(P)$	961	635	0.65
Ni-HMATD	729(ca) 440 380	$^3A_{2g} \rightarrow {}^3T_{2g}(F)$ $^3A_{2g}(F) \rightarrow {}^3T_{1g}(F)$ $^3A_{2g}(F) \rightarrow {}^3T_{1g}(P)$	1262	744	0.72

Table 4.4: Validation of Lipinski's rule and bio activity scores as obtained from Molinspiration software

compound	Druglikeness			Bioactivity scores					
	milogP	**TPSA**	**Nviolations**	**GPCRL**	**ICM**	**KI**	**NRL**	**PI**	**EI**
DHATD	−0.78	124	0	−0.89	−0.94	−0.84	−0.85	−0.98	−0.57
Co-DHATD	−6.45	254	3	0.01	−0.32	−0.13	−0.10	−0.01	−0.01
Ni-DHATD	−6.45	254	3	0.01	−0.32	−0.13	−0.10	−0.01	−0.01
Cu-DHATD	−6.48	254	3	0.01	−0.32	−0.13	−0.10	−0.01	−0.01
Zn-DHATD	−6.42	254	3	0.01	−0.32	−0.13	−0.10	−0.01	0.02
HMATD	−0.88	113	0	−0.89	−0.89	−0.81	−0.92	−1.04	−0.58
Co-HMATD	−6.04	260	3	−0.55	−1.34	−0.97	−0.96	−0.34	−0.77
Ni-HMATD	−6.44	306	3	−0.79	−1.69	−1.29	−1.30	−0.51	−1.06
Cu-HMATD	−6.24	260	3	−0.66	−1.51	−1.12	−1.12	−0.42	−0.91
Zn-HMATD	−6.00	260	3	−0.55	−1.34	−0.97	−0.96	−0.34	−0.74

Table 4.5Antidiabetic studies of DHATD, HMATD, and some of their complexes

Optical density of blank (without α-amylase*)* (B) = 0.620
Optical density for control (with α-amylase*)* (C) = 0.006

Compound	**Optical density at 565 nm for (A)**			**% of inhibition**		
	50 µg	**100 µg**	**300 µg**	**50 µg**	**100 µg**	**300µg**
DHATD (L1)	0.007	0.011	0.186	0.2	0.8	29
Co-L1	0.004	0.008	0.018	─0.3	0.3	2
Ni-L1	0.012	0.028	0.183	0.9	4	28
Cu-L1	0.018	0.058	0.201	2	8	32
Zn-L1	0.046	0.178	0.431	7	28	69
HMATD (L2)	0.010	0.062	0.253	0.6	9	40
Co-L2	0.005	0.034	0.085	─0.2	5	13
Ni-L2	0.014	0.074	0.268	1	11	43
Cu-L2	0.016	0.082	0.284	2	12	45
Zn-L2	0.028	0.132	0.316	4	21	50

Table 4.6 Docking results of selected compounds targeting α-amylase enzyme(PDB ID: 1SMD)

Drug target	compound	Binding Energy in Kcal/ mol	Predicted IC_{50} value (µM)	Active sites with mode of interaction	
				Van der Waals	Hydrogen bonding
Alpha-amylase enzyme (PDB ID: 1SMD)	DHATD	-5.70	65.81	LEU313 ARG267 TRP316 THR314 GLN302 GLY304 ALA310 TRP344 ARG303 ILE 312 HIS 305	ASP317 ARG346 GLY351
	Co-DHATD	-4.26	753.68	TYR2 ASN5 ARG421 SER4 PRO332	ASP402 THR336 ARG398 GLY 334 SER 3 ARG291 ASP 290
	Zn-DHATD	-5.94	44.13	PHE315 TRP316 ARG319 THR377 CYS378	LYS322 ARG343 TRP382 GLU484
	HMATD	-5.50	93.12	VAL383 ARG387 THR377 ARG343 ALA318	TRP382 CYS378 ARG389 LYS322
	Co-HMATD		378.29	GLU233 HIS101 ALA198 LEU165 LEU162 TRP58	HIS201
	Zn-HMATD		81.05	GLY309 GLU240 LYS200 ILE235 TYR151 LEU162 HIS201 ALA307 LYS261	GLY306 ALA310

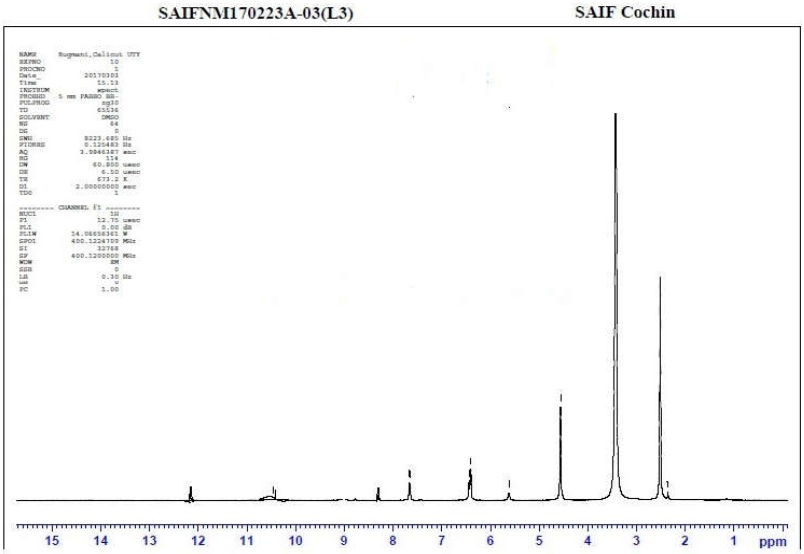

(A)

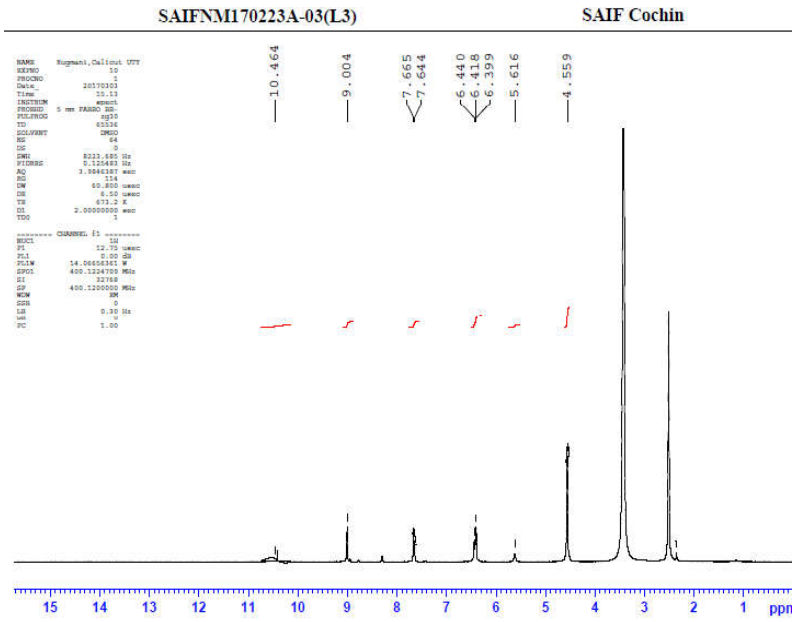

(B)

Fig 4.1 NMR spectrum of (A) DHATD and (B) Zn-DHATD complex

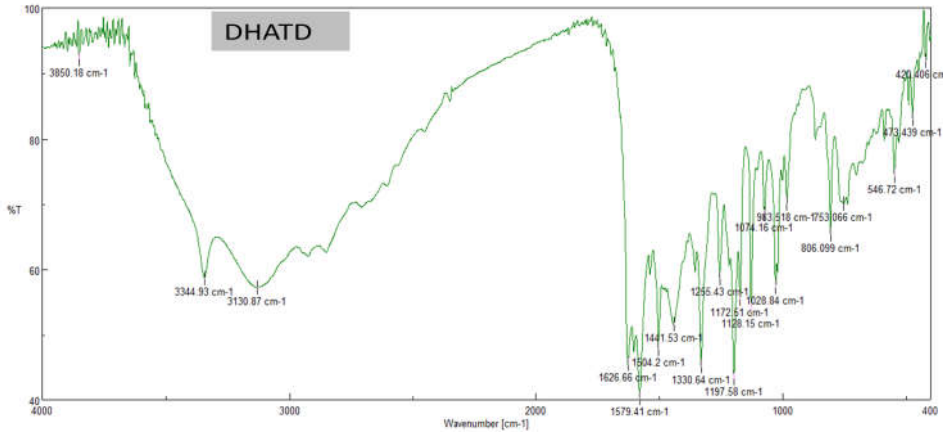
DHATD
%T
Wavenumber [cm-1]
3850.18 cm-1
3344.93 cm-1
3130.87 cm-1
1626.66 cm-1
1579.41 cm-1
1504.2 cm-1
1441.53 cm-1
1330.64 cm-1
1255.43 cm-1
1197.58 cm-1
1172.51 cm-1
1128.15 cm-1
1074.16 cm-1
1028.84 cm-1
983.518 cm-1
873.439 cm-1
806.099 cm-1
753.066 cm-1
546.72 cm-1

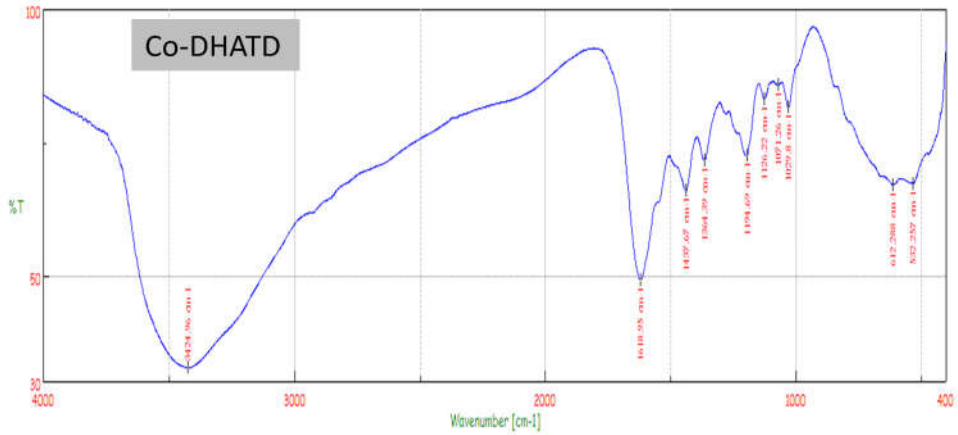
Co-DHATD
%T
Wavenumber [cm-1]

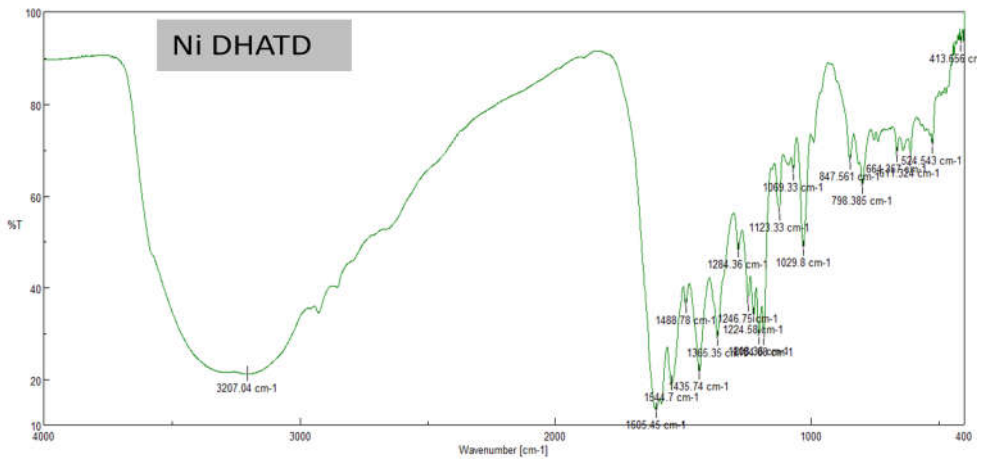
Ni DHATD
%T
Wavenumber [cm-1]
3207.04 cm-1
1605.45 cm-1
1544.7 cm-1
1435.74 cm-1
1488.78 cm-1
1365.35 cm-1
1284.36 cm-1
1246.75 cm-1
1224.58 cm-1
1123.33 cm-1
1069.33 cm-1
1029.8 cm-1
847.561 cm-1
798.385 cm-1
524.543 cm-1

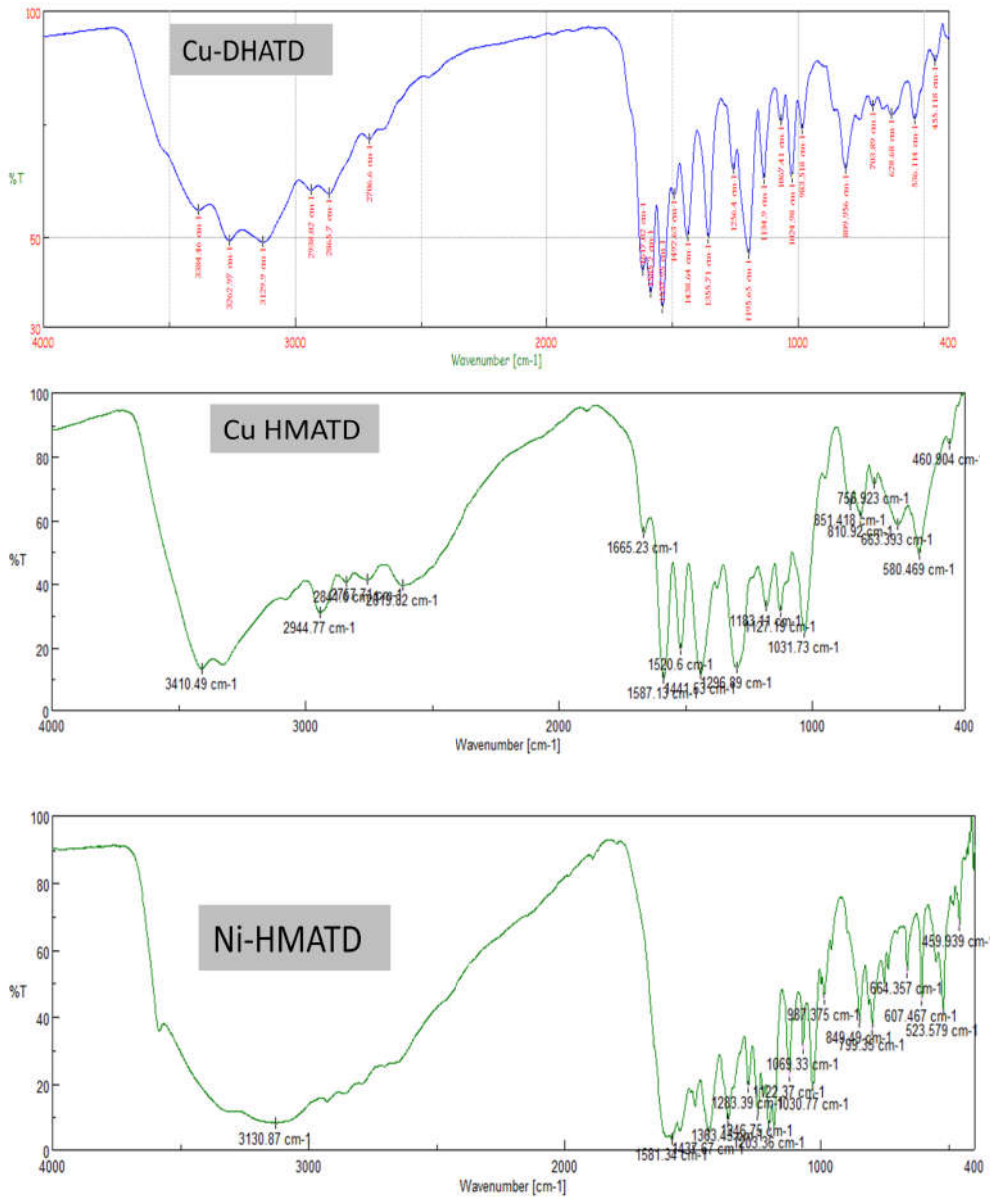

Fig 4.2: IR spectrum of complexes of DHATD and HMATD

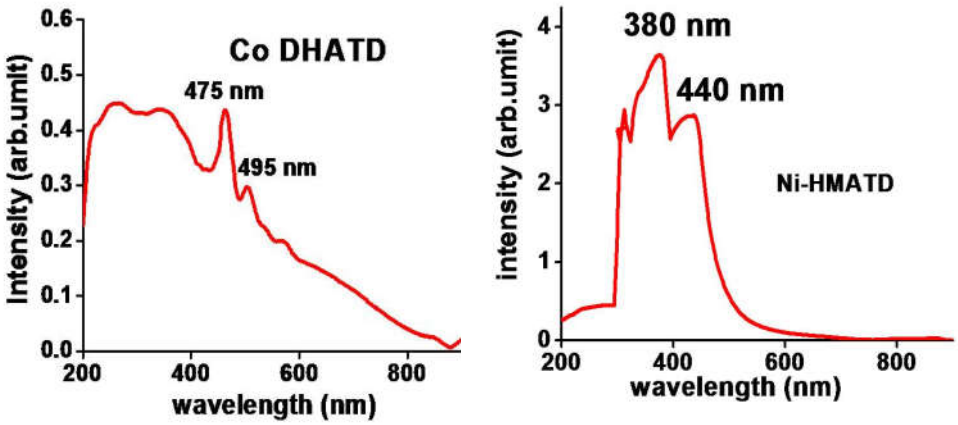

Fig 4.3: Electronic spectra of complexes

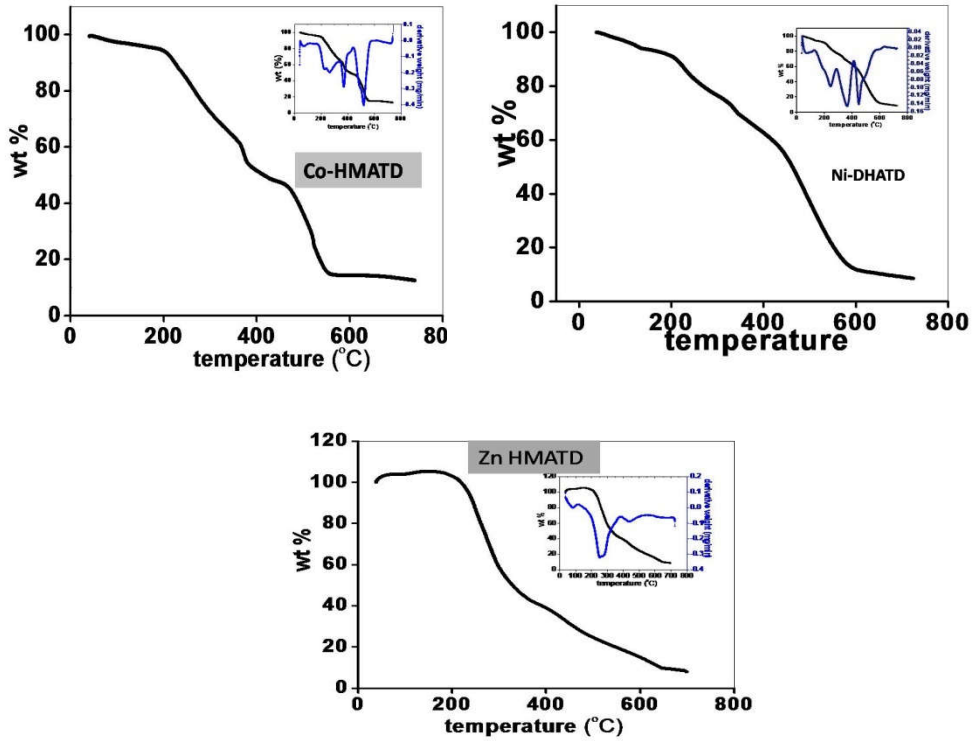

Fig 4.4: Thermograms of complexes of DHATD and HMATD

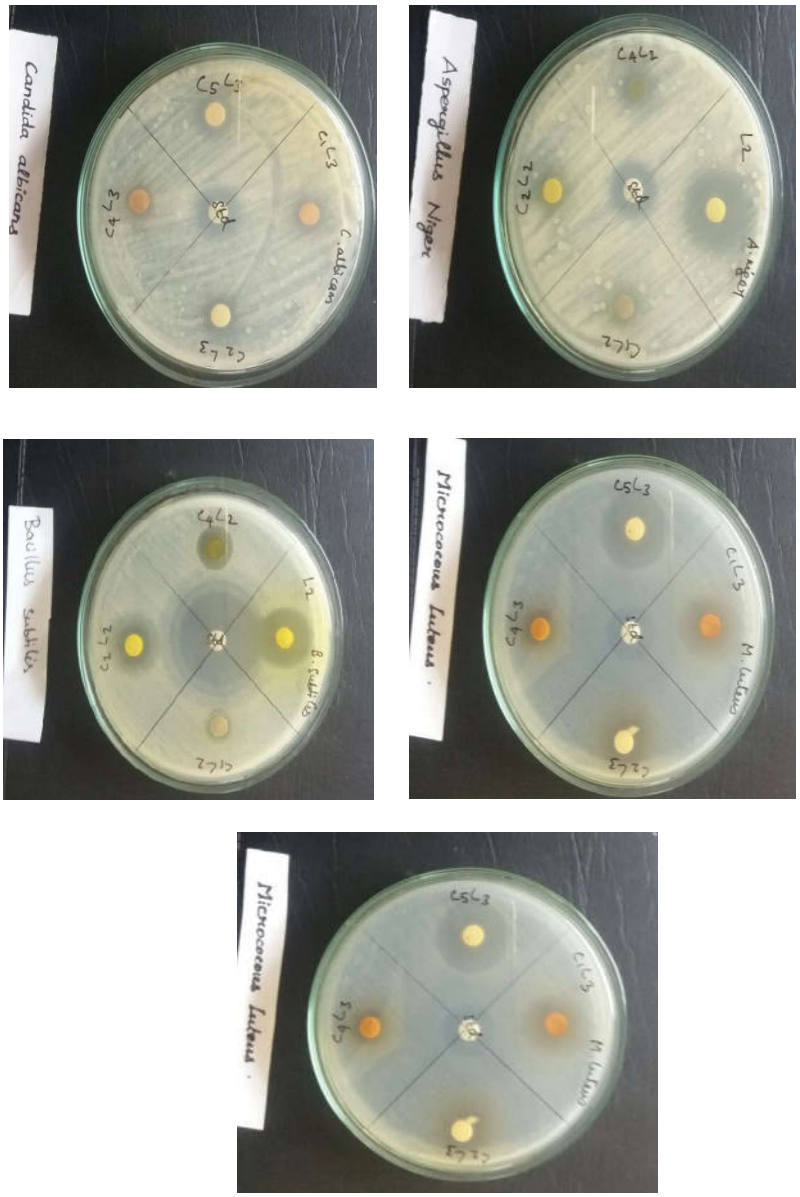

Fig 4.5 Pictorial representation of anti microbial studies

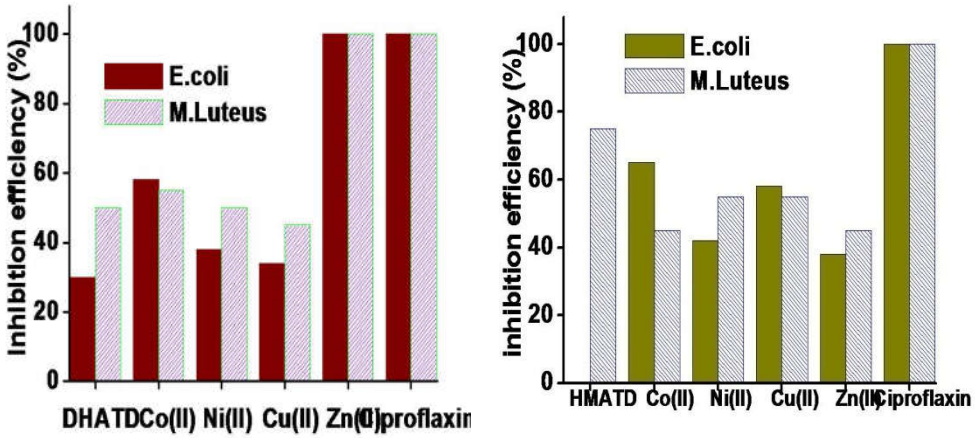

Fig 4.6: Antibacterial activity of ligand and complexes

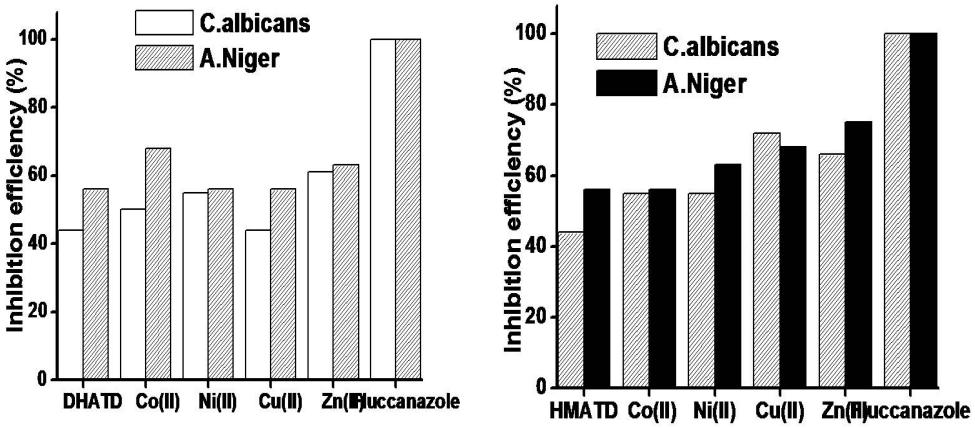

Fig 4.7: Antifungal activity of ligands and complexes

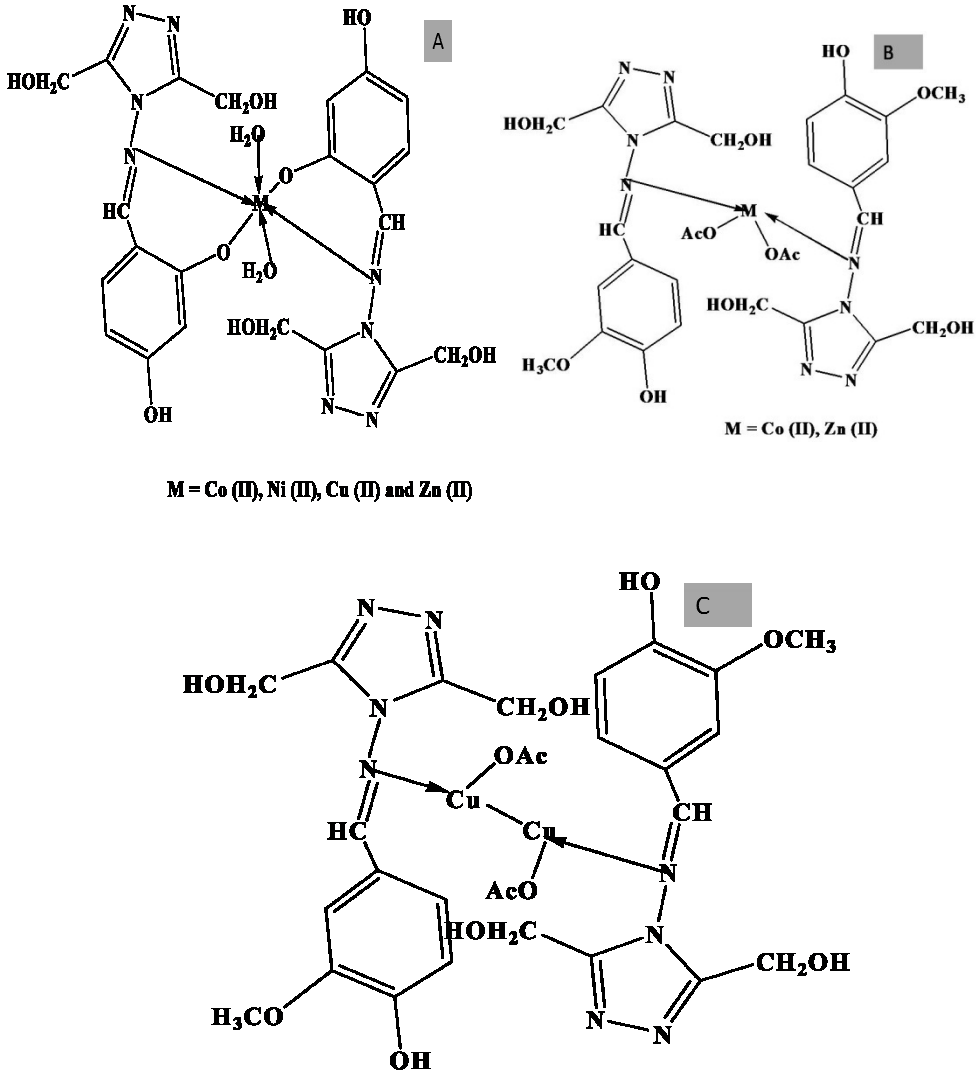

Fig 4.8: structure of complexes of (A) DHATD, (B) Co(II) and Zn(II) complexes of HMATD (C) Cu-HMATD

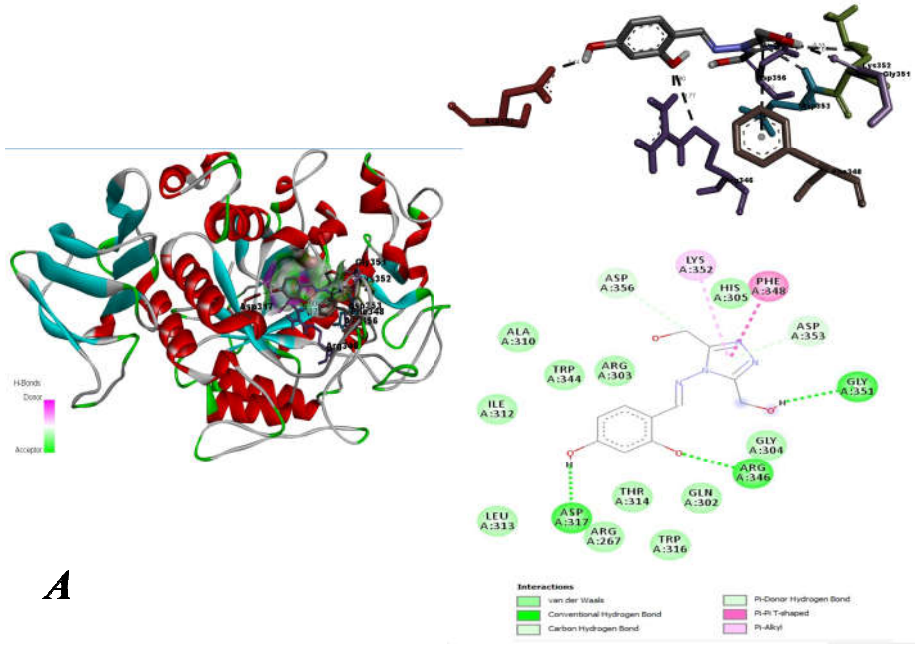
H-Bonds
Donor
Acceptor
LYS A:352
ASP A:356
HIS A:305
PHE A:348
ASP A:353
ALA A:310
TRP A:344
ARG A:303
GLY A:351
ILE A:312
GLY A:304
ARG A:346
THR A:314
GLN A:302
LEU A:313
ASP A:317
ARG A:267
TRP A:316
Interactions
van der Waals
Conventional Hydrogen Bond
Carbon Hydrogen Bond
Pi-Donor Hydrogen Bond
Pi-Pi T-shaped
Pi-Alkyl

A

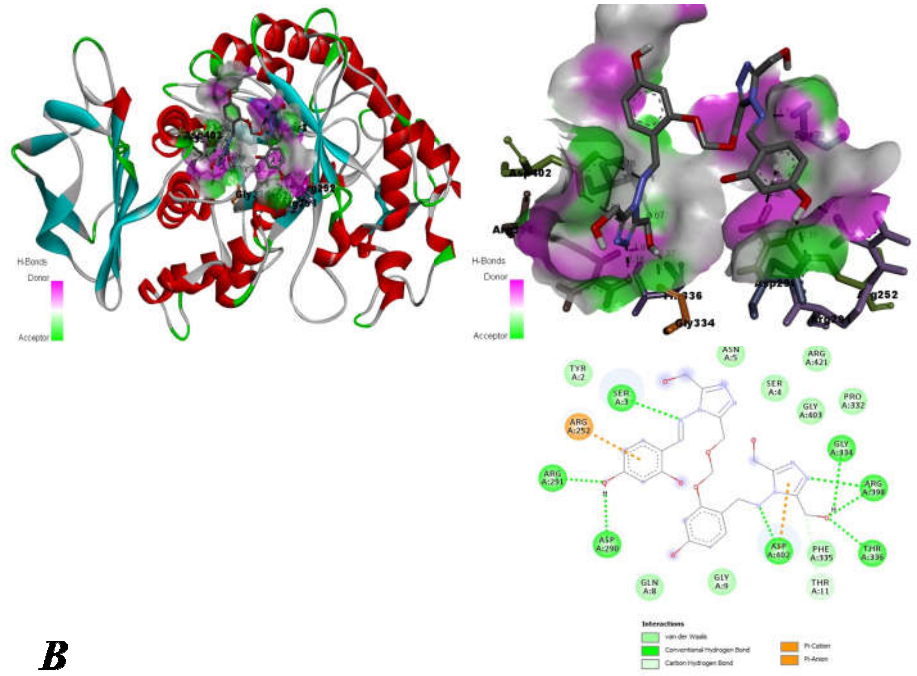
H-Bonds
Donor
Acceptor
Gly334
ASN A:5
ARG A:421
TYR A:7
SER A:4
SER A:3
GLY A:403
PRO A:332
ARG A:252
GLY A:334
ARG A:251
ARG A:398
ASP A:290
ASP A:802
PHE A:335
THR A:336
GLN A:8
GLY A:9
THR A:11
Interactions
van der Waals
Conventional Hydrogen Bond
Carbon Hydrogen Bond
Pi-Cation
Pi-Anion

B

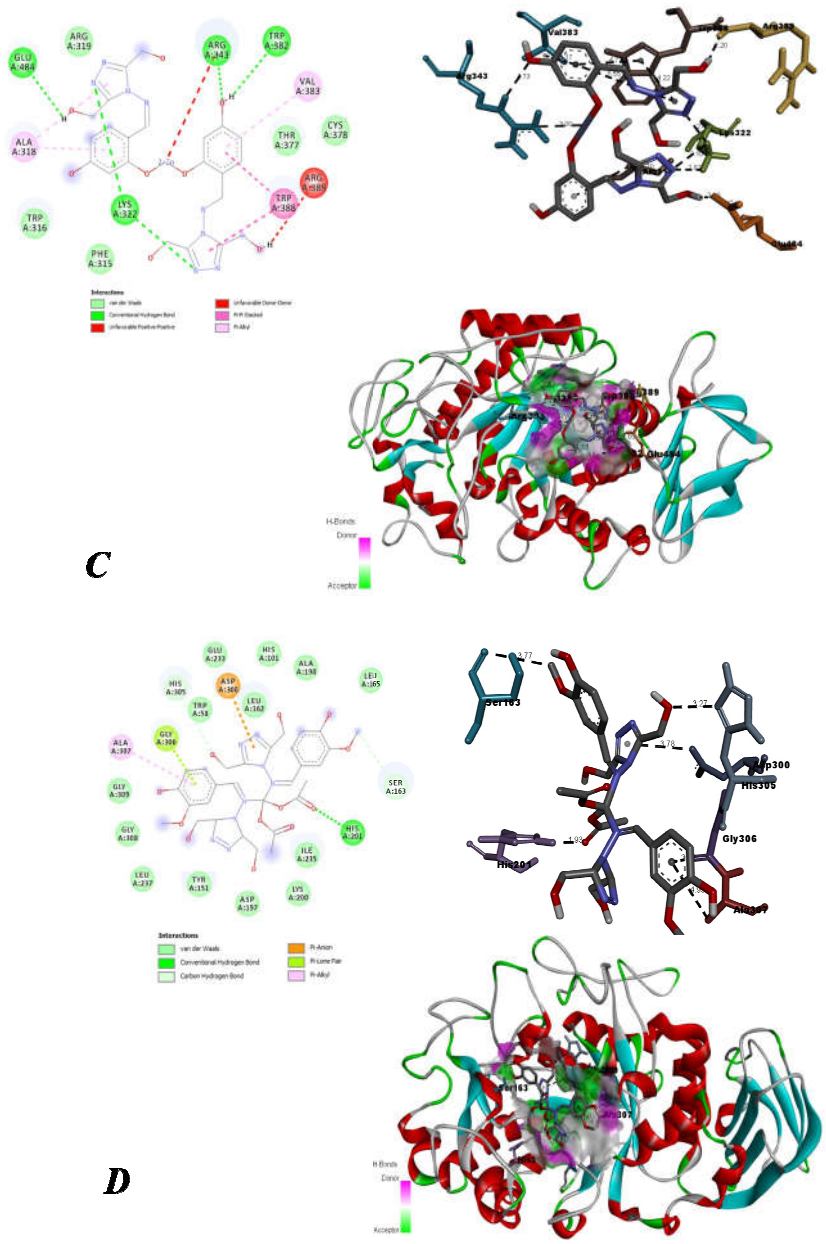

Fig 4.9 Snapshots of interactions between α-amylase and (A) DHATD (B) Co-DHATD (C) Zn-DHATD and (D) Co-HMATD

References

1. C A Hitchcock,. Biochem. Soc. Trans., 19 (1991) 782

2. A Almasirad, A Shafiee, M Abdollahi, R Khorasani,. Med. Chem. Res. 20 (4) (2010) 435

3. U V Kamble, S A Patil., P S Badami, J. Inc. Phenom.Macrocycl. Chem. 68 (2010) 347

4. Kiran Singh, Yogender Kumar, Parvesh Puri, Chetan Sharma K. R. Aneja, Med Chem Res., 21 (2012) 1708

5. Text book of Elements of Magnetochemistry, R.L.Dutta and Syamal, East West Press Pvt.Ltd., New Delhi

6. A B P Lever, Inorg.Chem.4 (1965) 763

7. C.Wang, et al J of Coord. Chem.., 61(24) (2008) 4033

8. Prateek Tyagi , Monika Tyagi , Swati Agrawal , Sulekh Chandra , Himanshu Ojha , Mallika Pathak , Spectrochimica Acta Part A: Molecular and Biomolecular Spectroscopy 171 (2017) 246

9. Khalil Abid, Sinann Al – Bayati, Anaam Rasheed, Am. J. of Chem., 6(1) (2016) 1

10. T D Thangadurai., K Natarajan Synth.React.Inorg. Met.Org.Chem., 31 (2001) 549

11. Kiran Singh Ritu Thakur, Vikas Kumar**,** Beni - suef University journal of basic and applied sciences, 5 (2 0 1 6) 21

12. Kazuo Nakamoto , Infrared and Raman Spectra of Inorganic and Coordination Compounds , , Wiley Interscience Publication, 1997

13. K Singh, S Raparia, P Surain, Med Chem Res., 24 (2015);2336

14. T. Ozen, M. Taş, , Journal of Enzyme Inhibition and Medicinal Chemistry 24 (2009) 1141–1147

15. C.A. Lipinski, F. Lombardo, B.W. Dominy, P.J. Feeney, Adv. Drug Deliv. Rev. 46 (2001) 3.

16. M. Zhu, X. Cui, S. Zhang, L. Liu, Z. Han, E. Gao,, J. Inorg. Biochem. 157 (2016) 34

17. T Khan, S Dixit, R Ahmad, S Raza, I Azad, S Joshi, A R Khan.J Chem Biol., 10(3) (2017) 91

18. A M Dar, M A Khan, M A Mir.S.Gatoo Pharm Anal Ata., 7 (2016) 464

19. A. Chaudhary, R.V. Singh, Phosphorus Sulfur Silicon Relat. Elem. 178 (2003) 603.

20. Y Anjaneyula, R P Rao., Synth React Inorg Met-Org Chem. 16 (1986) 257 21. B.G. Tweedy, , Phytopathology., 25 (1964) 910.

. .

5 CORROSION INHIBITION OF MILD STEEL IN HCl USING BENZIMIDAZOLE MOTIFS EMBAH EEBAH AND EPBAH

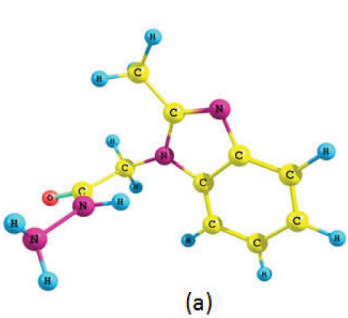

(a)

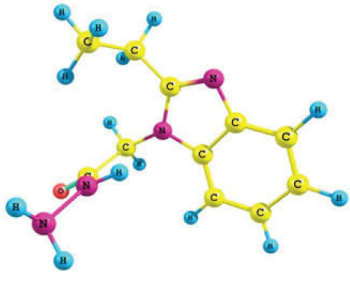

(b)

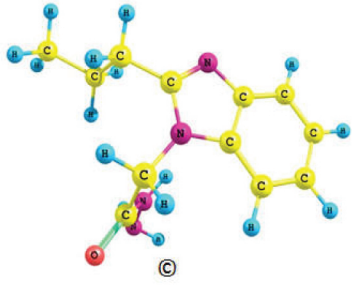

(c)

Chapter V *discusses the corrosion inhibition behaviour of three different benzimidazole motifs; 2-(2-methyl-1H-benzimidazol-1-yl)acetahydrazide (EMBAH), and 2-(2-ethyl-1H-benzimidazol-1-yl)acetahydrazide (EEBAH), and 2-(2-propyl-1H-benzimidazol-1-yl)acetahydrazide (EPBAH) for mild steel in HCl. The corrosion inhibition was investigated by weight loss measurements, electrochemical impedance spectroscopy (EIS) and potentiodynamic polarization studies (PDP). The temperature dependence of inhibition was explained by considering thermodynamic and kinetic parameters.*

V.1 Introduction

Mankind is very much grateful to metals, especially mild steel for its wide variety of thermal, mechanical and electrical properties and it became an inevitable material in many fields ranging from engineering to pharmaceutical industry. A cleaned smooth metal surface is required for the application of preventive measures for metals like painting, electroplating etc. and for this the metal surface is subjected to acid pickling in an acid bath to remove the mill scales. HCl is the most commonly used mineral acid for pickling and the strong reducing nature of HCl prevents the formation of passivation layer and made iron susceptible to corrosion. The use of organic compounds containing hetero atoms like N,S,O&P, π electron systems, and systems with multiple bonds as corrosion inhibitors was found to be one of the most favorable and effective methods to prevent corrosion. The excellent pharmacological properties like antibacterial, antifungal, anticancer etc. and a planar structure with two anchoring sites at sp^2 hybridized nitrogen with its lone pair electrons and aromatic rings make it a suitable scaffold for eco friendly corrosion inhibitor [1]. The derivatization of hydrogen in the ring NH yields a wide range of compounds with very good inhibition efficiency. Literature revealed the use of benzimidazole motif as a promising nitrogen heterocyclic scaffold for the development of corrosion inhibitors, which are effective only at higher inhibitor concentrations [2]. This chapter aims to explore three novel benzimidazole derivatives, which are easily synthesizable, non toxic, biologically important and best suited for the current scenario of development of non-toxic inhibitors, 2-(2-methyl-1H-benzimidazol-1-yl)acetahydrazide (EMBAH), and 2-(2-ethyl-1H-benzimidazol-1-yl)acetahydrazide (EEBAH), 2-(2-propyl-1H-benzimidazol-1-yl)acetahydrazide (EPBAH) (Section II.3.1), as corrosion inhibitors for mild steel in 0.5 M HCl at different temperatures varying from 303 K to 323 K.

V.2 Results and discussion

V.2.1 Effect of immersion time and inhibitor concentration

The effect of immersion time and inhibitor concentration on corrosion inhibition was studied by weight loss method. The corrosion rate (CR) and inhibition efficiency (IE) for mild steel corrosion in 0.5 M HCl are presented in Table 5.1 and Fig 5.1. The table points out a fall in corrosion rate and rise in inhibition efficiency with a rise in inhibitor concentration from 10 ppm to 50 ppm due to the formation of a protective layer. Maximum inhibition efficiency of 95% for EMBAH, 96% for EEBAH and 97% for EPBAH was obtained for an optimal concentration of 50 ppm. An increase in the immersion time, the inhibition efficiency of inhibitors and corrosion rate found to decrease due to various phenomenon like metal dissolution, slow desorption of adsorbed protective layer from the metal surface etc. The decrease in corrosion rate with time for a constant inhibitor concentration may be due to the extended life of the adsorbed inhibitor layer on the metal surface [4].

V.2.2 Effect of acid concentration

The variation in inhibition efficiencies of EMBAH, EEBAH and EPBAH with acid concentrations were studied by weight loss method at 303 K using three different acid concentrations 0.5 M, 1 M and 1.5 M HCl. The corrosion rate (CR) and inhibition efficiency (IE) were calculated using equations (1.13 and 2.2) and the results are listed in Table 5.1. It has been seen that an increase in acid concentration increases the corrosion rate with a decrease in the effectiveness of inhibitor. It can be attributed due to an increase in aggressiveness and dissolution rate for the adsorbed layer at higher acid concentration [3]. The pictorial representation of effect of acid concentration on corrosion inhibition efficiency is shown in Fig 5.2.

V.2.3 Potentiodynamic polarization studies

Potentiodynamic polarization studies gave insight into the effect of inhibitors on the anodic and/or cathodic reactions of metal-electrolyte corrosive system. The polarization curves for mild steel in 0.5 M HCl in the absence and presence of different concentrations of EMBAH, EEBAH and EPBAH at 303 K are given in Fig 5.3. Corrosion parameters like corrosion current density I_{corr}, corrosion rate CR, corrosion potential E_{corr} and inhibition efficiency calculated using the equation 2.4 are depicted in Table 5.2. It was evident from Table 5.2 that, I_{corr} values decreased considerably with increase in inhibitor concentration confirming the corrosion inhibition by them. The Tafel slopes of both anodic and cathodic curves get affected by inhibitors which support the mixed type behavior of inhibitors [5]. The Tafel plots for mild steel exposed in 0.5 M HCl for an optimal concentration of 50 ppm was shown in Fig 5.4 and the related parameters obtained are listed in Table 5.3. At higher temperatures, corrosion current density and corrosion rate increases while inhibition efficiency decreases due to desorption of inhibitor molecules from the mild steel surface. Variation of I_{corr} with temperature is represented in Fig 5.5. A moderately high efficiency was maintained by all the three inhibitors at higher temperature also.

V.2.4 Electrochemical impedance spectroscopy

The impedance study was done for mild steel samples in 0.5 M HCl at different temperatures. Fig 5.3 contains the Nyquist plots with different concentrations of EMBAH, EEBAH and EPBAH at 303 K and Fig.5.4 includes the Nyquist plot for mild steel in 0.5 M HCl containing optimal concentration (50 ppm) of these inhibitors at different temperatures. These plots are typical depressed semi circles with their centers located at the real impedance axis, resulting from the non-ideal behavior of the electrical double layer on metal/solution interface. The non-ideal behavior referred as

frequency dispersion is mainly observed in solid electrodes due to their surface heterogeneity caused by roughness, impurities or dislocation [6]. The various impedance parameters like charge transfer resistance R_{ct}, double layer capacitance C_{dl}, constant phase element CPE and inhibition efficiency IE were calculated using (eqn. 2.3) are enlisted in Table 5.4. It can be seen from Nyquist plots that with an increase in the concentration of the inhibitors, R_{ct} as well as the diameter of the Nyquist plot increases which can be related to the increasing rate of inhibition and an involvement of charge transfer process in corrosion [7]. A large value of R_{ct} of inhibited solutions compared to blank indicates the deficiency of an active surface necessary for the corrosion reaction i.e. a slow corroding system. The values of constant phase element remains almost same in the range 0.70-0.84 and its stability explains the charge transfer controlled dissolution mechanism of mild steel in 0.5 M HCl in the absence and presence of inhibitor [8]. The addition of inhibitors to the corrosive solution reduces the double layer capacitance $C_{dl,}$ which may be due to an increase in the thickness of electrical double layer or decrease in the local dielectric constant, due to the substitution of high dielectric water molecule by lower dielectric organic inhibitor molecules, leading to the formation of a protective film [9, 10]. A graphical representation of C_{dl} with inhibitor concentration is shown in Fig 5.6.

At 303 K, all the three inhibitors show maximum inhibition efficiency at 50 ppm. The order of inhibition efficiency is EMBAH<EEBAH<EPBAH. This may be due to an increase in the electron donating effect (+I) in the order methyl<ethyl<propyl. Increase in the electron density at the benzene nucleus, increases the corrosion inhibition through the formation of a stable surface film [7, 11]. As per Fig. 5.4, increase in temperature lead to a decrease in R_{ct} and hence decrease in inhibition efficiency (Table 5.3). The adsorbed inhibitor molecule will experience desorption on increasing the temperature.

V.2.5 *Temperature dependence of corrosion inhibition*

The influence of temperature on corrosion phenomenon is immense and the corrosion rate and temperature are directly proportional. The influence of temperature on the inhibited acid metal reaction is very convoluted due to the complicated changes like desorption, etching, and decomposition of inhibitor taking place on the metal surface. In order to explain the temperature dependence of corrosion inhibition, the two aspects-thermodynamic parameters of adsorption and kinetic considerations of metal corrosion are studied in detail.

V.2.5.1 Thermodynamic parameters of adsorption

It helps to determine the spontaneity of a reaction. Van't Hoff and Gibbs-Helmholtz equations are used for evaluating the thermodynamic parameters.

Van't Hoff equation combines a change in equilibrium constant K_{ads} and temperature as,

$$\ln K_{ads} = \frac{-\Delta H^0_{ads}}{RT} + \frac{\Delta S^0_{ads}}{R} \qquad (5.1)$$

Gibbs Helmholtz plot (Fig 5.7 A) of $\Delta G^0_{ads}/T$ Vs 1/T with a slope of ΔH^0_{ads} is also useful in evaluating ΔH^0_{ad} and Van't Hoff plot (Fig 5.7 B) of $\ln K_{ads}$ Vs 1/T will give a straight line with slope $-\Delta H^0_{ads}/R$ and intercept

$\frac{\Delta S^0_{ads}}{R} + ln\frac{1}{55.5}$. The various thermodynamic parameters like free energy of adsorption (ΔG^0_{ads}), equilibrium constant (K_{ads}), enthalpy of adsorption (ΔH^0_{ads}) are given in Table 5.5.

The perusal of Table 5.5 revealed a negative value of ΔH^0_{ads} for these inhibitors which supports the exothermic adsorption of inhibitors on the metal

surface. The physisorption involves weak forces of attraction with the evolution of less heat whereas chemisorption accompanies strong forces of attraction with more heat evolution. The value of ΔH^0_{ads} around 100 kJ/mol implies chemisorption and a value less than 40 kJ/mol suggest that the adsorption is a physisorption. In this case, it is in between 40 and 100 kJ/mol, so the adsorption will be mixed type i e. combined effect of physisorption and chemisorptions [12]. The ΔH^0_{ads} values from both the plots are in good agreement with each other.

The negative ΔS^0_{ads} values obtained from the intercept of Van't Hoff plots indicate exothermic nature of adsorption process which accompanies a decrease in entropy. The reduction in entropy can be due to the ordered arrangement of inhibitor molecules from aqueous solution to a solid metal surface [13].

V.2.5.2 Kinetic Parameters for corrosion inhibition process

The activation parameters of corrosion process can be studied from Arrhenius and Transition State equations. The Arrhenius equation can be written for corrosion rate as

$$CR = Ae^{-E_a/RT} \qquad (5.2)$$

where CR is the corrosion rate, A is the pre-exponential factor. Arrhenius plot of ln CR Vs 1/T gives a straight line with a slope of $-E_a/R$ (Fig 5.8 A).

The transition state equation is helpful for calculating ΔH^0_a and ΔS^0_a

$$CR = \frac{RT}{Nh} e^{\frac{\Delta S^*}{R}} . e^{\frac{-\Delta H^*}{RT}} \qquad (5.3)$$

Transition state plots of ln(CR/T) Vs 1/T (Fig 5.8 B) is a straight line with a slope of $\frac{-\Delta H^0_a}{R}$ and intercept $ln(\frac{R}{Nh}) + \frac{\Delta S^0_a}{R}$. With the help of these two plots

kinetic parameters of corrosion reaction like apparent activation energy (E_a), activation enthalpy (ΔH^0_a), activation entropy (ΔS^0_a) were determined and are tabulated in Table 5.6. The increase in E_a values in the inhibited solutions can be associated with an increase in the molecular adsorption of inhibitor which increased the energy barrier for the corrosion process. The E_a values greater than 20 kJ/mol pinpoint the role of surface reaction in the entire process [14]. The closeness of ΔH_a^0 and E_a values and an increase in the E_a values by the introduction of inhibitors indicated a hike in the energy barrier for the corrosion reaction without a change in the dissolution mechanism. The positive values of ΔH_a^0 suggest endothermic nature of metal dissolution process. The higher activation energy in the presence of inhibitors further supports the proposed physisorption mechanism [15]. The entropy of activation ΔS_a^0, is large and becomes positive in the inhibited solution compared to a negative value for blank supports the formation of activated complex in the rate determining step. The increase of ΔS_a^0 is generally interpreted by an increase in disorder taking place on converting from reactants to the activated complex.

V.2.6 *Adsorption studies and corrosion inhibition mechanism*

The primary concern for an organic compound to be considered as inhibitor is its capacity to get adsorbed on the metal surface by blocking active sites and substituting adsorbed water molecules to form a compact barrier film to decrease the corrosion rate. The inhibitors studied here follow Langmuir isotherm with a regression coefficient and slope almost equal to one (Fig5.9) and is given by the equation

$$\frac{C_{inh}}{\theta} = \frac{1}{K_{ads}} + C_{inh} \qquad (5.4)$$

where K_{ads} represents the equilibrium constant of adsorption process. This

isotherm suggests equal surface energy to all the sites on the substrate, so that only one adsorbate covers one substrate site with no interaction between adsorbates even at surface coverage very close to unity. The reciprocal of the intercept of isotherm gives K_{ads}, which is a reflection of the interaction between the inhibitor and mild steel surface [16]. The isotherm also provides a way for calculating the free energy of adsorption ΔG^0_{ads} using the equation

$$\Delta G^0_{ads} = -2.303RTlog(55.5K_{ads}) \qquad (5.5)$$

where 55.5 represents the molar concentration of water, R is the universal gas constant and T is the absolute temperature. The relatively high K_{ads} and negative ΔG^0_{ads} values, indicate a stronger and spontaneous adsorption of inhibitors on the mild steel surface [17]. The adsorption process is associated with the separation of a substance from one phase accompanied by its accumulation on the surface of the other. The adsorption of inhibitor molecules from the aqueous solution is supposed to be a quasi-substitution process between the organic inhibitor in the solution phase and the water molecules at the metal surface which controls the dissolution of iron since it is a part of iron dissolution mechanism [7].

Generally ΔG^0_{ads} values around −20 kJ/mol or less is expected for physisorption whereas that around −40 kJ/mol or higher for chemisorption. The ΔG^0_{ads} values for these inhibitors as shown in Table 5.5 was found to be in between −20 kJ/mol and −40 kJ/mol which in turn conform the mixed type behavior of adsorption, with a preferential physisorption [18].

V.2.7 Quantum chemical calculations

The quantum chemical studies have proven to be an excellent tool for elucidating the molecular and electronic structure as well as reactivity. To investigate the effect of substituent on inhibition mechanism and efficiency,

quantum chemical calculations were done. The energies of frontier molecular orbitals (E_{HOMO} and E_{LUMO}), HOMO-LUMO energy gap (ΔE) of EMBAH, EEBAH and EPBAH with their pictorial representation are given in Fig 2.7(A-C). E_{HOMO} is associated with electron donating ability of a molecule. Higher the E_{HOMO}, the higher will be the tendency of the molecule to donate electrons to an acceptor molecule. E_{LUMO} is associated with electron accepting ability of a molecule and lower values of E_{LUMO} facilitate increasing tendency to accept electrons [19]. Lower the ΔE values, higher will be the inhibition efficiency [20]. The order of ΔE values EMBAH>EEBAH>EPBAH is in good agreement with that of experimental inhibition efficiency EMBAH<EEBAH<EPBAH. The dipole moment of a molecule also influences the adsorption of a chemical entity to the metal surface. The higher values of dipole moment enhance the surface adsorption. The dipole moment of molecules is in the order EPBAH (2.1636) > EEBAH (2.1340)> EMBAH (2.0491) and the experimental efficiency is also following a similar trend. The number of transferred electrons between the inhibitor molecules and the metal is estimated according the equation

$$\Delta N = \frac{X_{Fe} - X_{inh}}{2(\eta_{Fe} + \eta_{inh})} \qquad (5.6)$$

The theoretical value of electronegativity of iron(X_{Fe}) and hardness of iron(η_{Fe}) are 7 and 0 eV/mol respectively as obtained from Pearson's electronegativity scale [21] and the assumption of equality between the ionization enthalpy and electron affinity for a metallic bulk [21]. The values of ΔN, EMBAH (0.6493), EEBAH (0.6570) and EPBAH (0.6596) suggest that inhibition is by electron donation. These inhibitors were found to have a ΔN<3.6, which point out the role of inhibitors as the donor of electrons and the mild steel surface as the acceptor [22].

Conclusions

The inhibitors EMBAH, EEBAH and EPBAH possess good protection efficiency for mild steel in HCl. The inhibition efficiency increases with increasing inhibitor concentration and gets saturated at 50 ppm. The increase in temperature as well as acid concentration causes a depression in efficiency. The potentiodynamic polarization studies revealed that these inhibitors act as mixed type affecting both cathodic and anodic reactions. The inhibition mechanism involves spontaneous adsorption preferentially physisorption of inhibitors on mild steel surface as evidenced by the negative values of ΔG^0_{ads} which follows Langmuir adsorption isotherm. The thermodynamic parameters indicate exothermic behavior of adsorption and kinetic parameters points out the endothermic nature of corrosion. The trend of efficiencies obtained by experimental and quantum chemical calculations are in good agreement.

Table 5.1: Variation of Corrosion rate (CR) in $mgcm^{-2}h^{-1}$ and inhibition efficiency (IE) % with immersion time and acid concentration for mild steel in HCl in presence of EMBAH, EEBAH and EPBAH

Imm. time (h) and acid conc.	Cinh ppm	EMBAH		EEBAH		EPBAH	
		CR	IE %	CR	IE %	CR	IE %
24 (0.5)	blank	9.2690	--	9.2690	--	9.2690	
	10	3.8738	49.85	2.9642	68.02	1.5387	83.40
	20	1.2590	83.70	1.5757	83.00	0.7508	91.90
	30	0.5625	93.73	0.6488	93.00	0.5747	93.80
	40	0.4479	94.20	0.5098	94.50	0.4820	94.80
	50	0.4352	95.30	0.3244	96.50	0.2688	97.10
48	blank	5.6018	--	5.6018	--	5.6018	--
	50	0.1823	95.10	0.2353	95.80	0.2128	96.20
72	blank	4.1138	--	4.1138	--	4.1138	--
	50	0.2139	94.80	0.2003	95.20	0.1945	95.34
96	blank	3.1099	--	3.1099	--	3.1099	--
	50	0.2144	93.10	0.1834	94.10	0.1890	93.92
24 (1)	blank	10.887	--	10.887	--	10.887	--
	50	0.8329	92.35	0.7720	94.10	0.7472	94.80
24 (1.5)	blank	11.291	--	11.291	--	11.291	--
	50	1.084	90.40	0.9985	91.20	0.8580	92.60

Table 5.2: Potentiodynamic polarization parameters for mild steel corrosion in 0.5 M HCl in the absence and presence of EMBAH, EEBAH and EPBAH at 303 K

Inhibitor	C_{inh} ppm	$-E_{corr}$ mV	β_a mV/ dec	$-\beta_c$ mV/ dec	I_{corr} mA/cm^2	CR mm/yr	IE %
Blank	0	459	152.92	244.3	1.0862	12.589	---
	10	464	100.97	186.69	0.5313	6.1581	51.08
	20	476	71.072	142.65	0.1699	1.9693	84.35
EMBAH	30	472	74.479	132.99	0.1149	1.3314	89.42
	40	487	73.868	149.58	0.0993	1.1515	90.86
	50	470	64.643	80.823	0.0460	0.5333	95.76
	10	464	92.502	144.92	0.3373	3.908	68.95
	20	478	79.005	83.312	0.1261	1.4618	88.39
EEBAH	30	501	90.63	77.406	0.0703	0.8148	93.53
	40	474	62.711	48428	0.0481	0.5569	95.57
	50	480	67.579	72.975	0.0429	0.4972	96.05
	10	469.	84.801	116.56	0.2110	2.4452	80.57
	20	469	66.705	145.44	0.1338	1.5504	87.68
EPBAH	30	479	74.344	137.24	0.1073	1.2439	90.12
	40	482	68.709	135.94	0.0798	0.9250	92.65
	50	506	43.196	44.074	0.0445	0.5152	95.90

Table 5.3: Electrochemical parameters of mild steel in 0.5 M HCl with optimum concentration (50 ppm) of inhibitors at various temperatures

Temp (K)	inhibitor	EIS			PDP	
		R_{ct} (Ωcm^2)	CR (mm/yr)	IE %	I_{corr}(mA/cm^2)	IE %
303 K	blank	12.46	24.27	--	1.0862	-
	EMBAH	288.4	1.046	95.68	0.0460	95.76
	EEBAH	434.6	0.82	97.13	0.0429	96.05
	EPBAH	1020.8	0.2947	98.77	0.0445	95.90
308 K	blank	8.371	36.12	--	1.8946	-
	EMBAH	180.3	1.677	95.35	0.1847	90.25
	EEBAH	200.0	1.505	95.81	0.0968	94.89
	EPBAH	218.9	1.381	96.18	0.1158	93.89
313 K	blank	7.135	42.38	--	2.6449	-
	EMBAH	105.6	2.852	93.24	0.2712	89.75
	EEBAH	136.3	2.218	94.76	0.1459	94.48
	EPBAH	153.8	1.966	95.36	0.1956	92.60
318 K	blank	5.561	54.37	--	4.5925	-
	EMBAH	57.44	5.264	90.31	0.4296	90.6
	EEBAH	88.80	3.403	93.74	0.4601	90.0
	EPBAH	50.58	5.978	89.00	0.4609	89.9
323 K	blank	6.764	46.93	--	3.4569	-
	EMBAH	41.37	7.308	83.65	0.4823	86.05
	EEBAH	36.10	8.375	81.27	0.5768	83.31
	EPBAH	28.26	10.70	76.07	0.5741	83.39

Table 5.4: Charge transfer resistance (R_{ct}), Corrosion rate in mm/yr (CR), double layer capacitance (C_{dl}) and % of inhibition efficiency of EMBAH,EEBAH and EPBAH in 0.5 M HCl at 303 K as obtained from Impedance studies

Inhibitor	Cinh ppm	R_{ct} Ωcm^2	C_{dl} $\mu F/cm^2$	CR mm/yr	CPE	IE %
None	Blank	12.46	491.0	24.27	0.80	--
	10	26.80	259.4	11.26	0.76	53.50
	20	81.31	197.1	3.718	0.73	84.67
EMBAH	30	163.1	119.6	1.854	0.80	92.36
	40	243.2	116.9	1.243	0.74	94.88
	50	288.4	116.6	1.046	0.78	95.68
	10	41.13	245.4	7.351	0.84	69.71
	20	76.06	188.6	3.975	0.75	83.62
EEBAH	30	145.4	108	2.079	0.79	91.43
	40	235.9	68.06	1.282	0.76	94.72
	50	434.6	83.72	0.6957	0.82	97.13
	10	79.85	285.8	3.786	0.70	84.40
	20	159	116.6	1.902	0.82	92.16
EPBAH	30	195.3	95.99	1.548	0.82	93.62
	40	249.9	71.65	1.197	0.80	95.01
	50	1020.8	41.29	0.2941	0.84	98.77

Table 5.5: Thermodynamic parameters of adsorption of EMBAH, EEBAH and EPBAH on mild steel in 0.5 M HCl

inhibitor	Thermodynamic parameters from				
	Langmuir adsorption isotherm		**Van't Hoff Plot**		**Gibbs-Helmholtz Plot**
	K_{ads} M^{-1}	$-\Delta G_{ads}$ kJ/mol	ΔH^0_{ads} kJ/mol	ΔS^0_{ads} J/mol.K	ΔH^0_{ads} kJ/mol
blank	--	--	--	--	--
EMBAH	24875	35.6	−58.66	−93.51	−58.88
EEBAH	38589	36.7	−72.86	−137.28	−72.77
EPBAH	87328	38.8	−117.7	−280.78	−115.45

Table 5.6: Kinetic parameters of corrosion of mild steel in 0.5 M HCl in presence of EMBAH, EEBAH and EPBAH

inhibitor	Activation Parameters from		
	Arrhenius Plot	**Transition state plot**	
	E_a kJ/mol	ΔH^0_a kJ/mol	ΔS^0_a J/mol.K
blank	28.38	25.86	−132.35
EMBAH	81.95	79.35	17.10
EEBAH	94.21	91.86	55.30
EPBAH	141.10	138.50	203.94

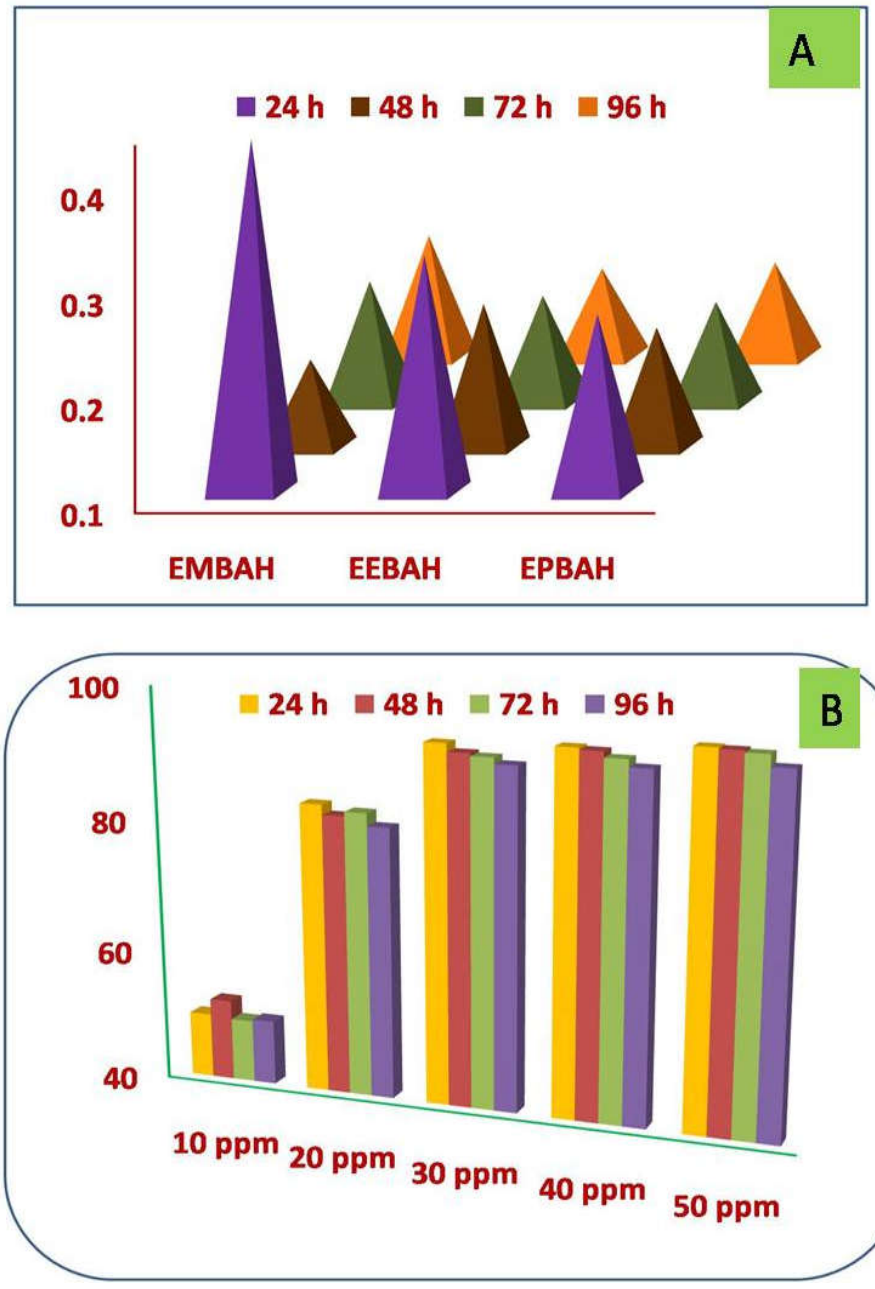

Fig 5.1 Pictorial representation of effect of immersion time on (A) corrosion rate and (B) inhibition efficiency of EMBAH

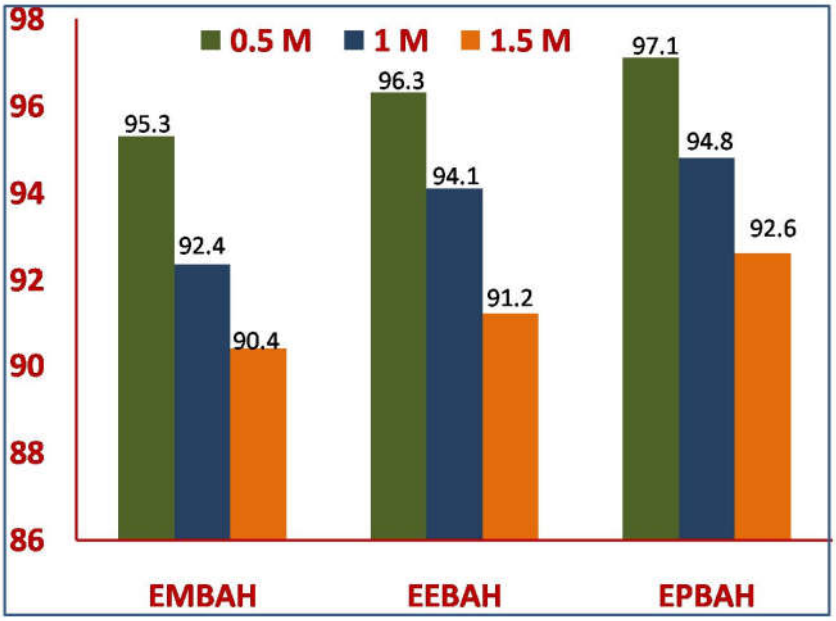

Fig 5.2 Graphical representation of effect of acid concentration on inhibition efficiency of 50 ppm of EMBAH, EEBAH and EPBAH for mild steel corrosion in different concentrations of HCl at 303 K

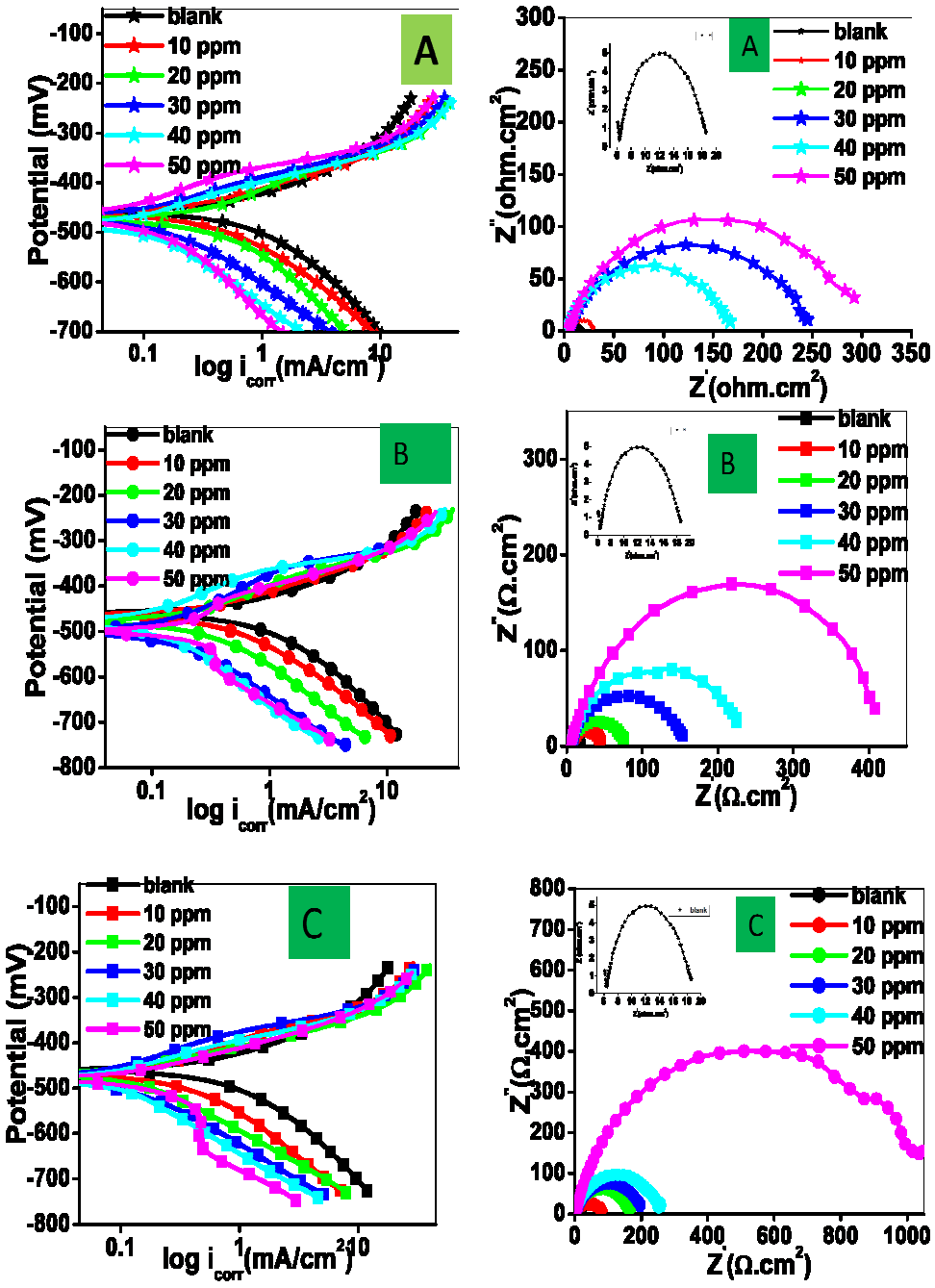

Fig 5.3 Tafel and Nyquist plots for mild steel corrosion in 0.5 M HCl containing (A) EMBAH (B) EEBAH and (C) EPBAH at 303 K

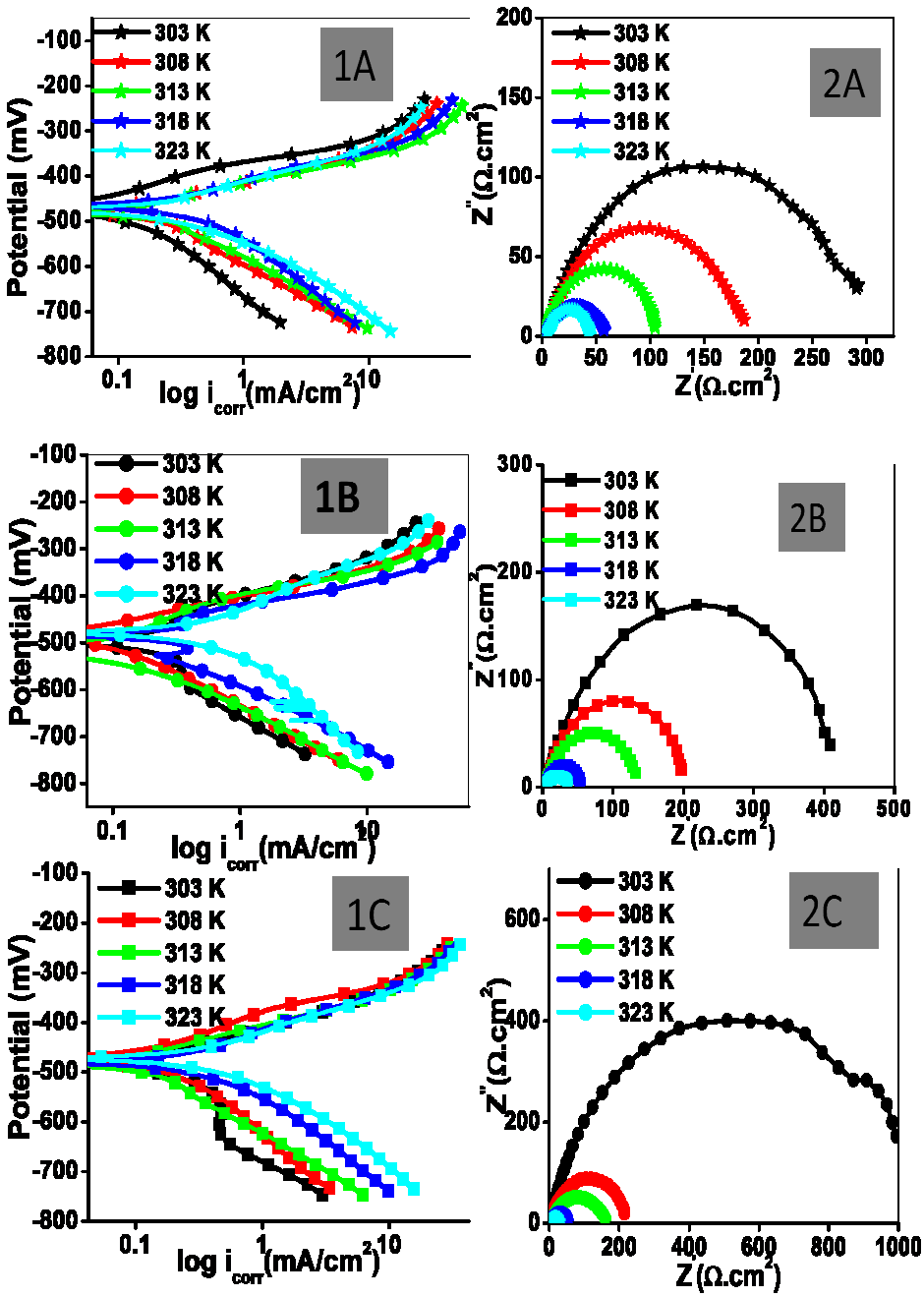

Fig 5.4 (1) Tafel and (2) Nyquist plots for mild steel corrosion in 0.5 M HCl containing optimal concentration 50 ppm of (A) EMBAH (B) EEBAH and (C) EPBAH at different temperatures

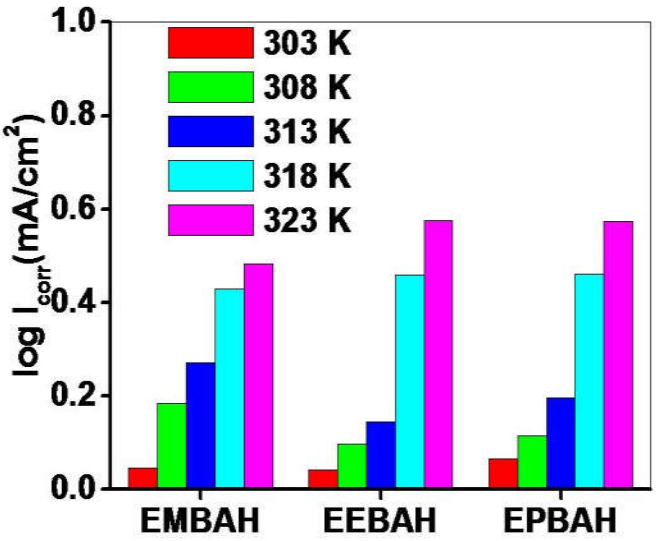

Fig 5.5 Graphical representation of variation of I_{corr} with temperature

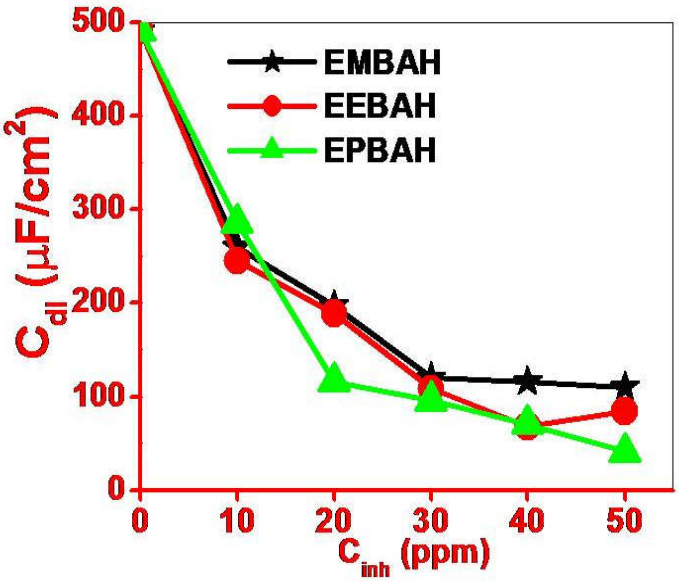

Fig 5.6 Graphical representation of effect of inhibitor concentration on double layer capacitance (C_{dl})

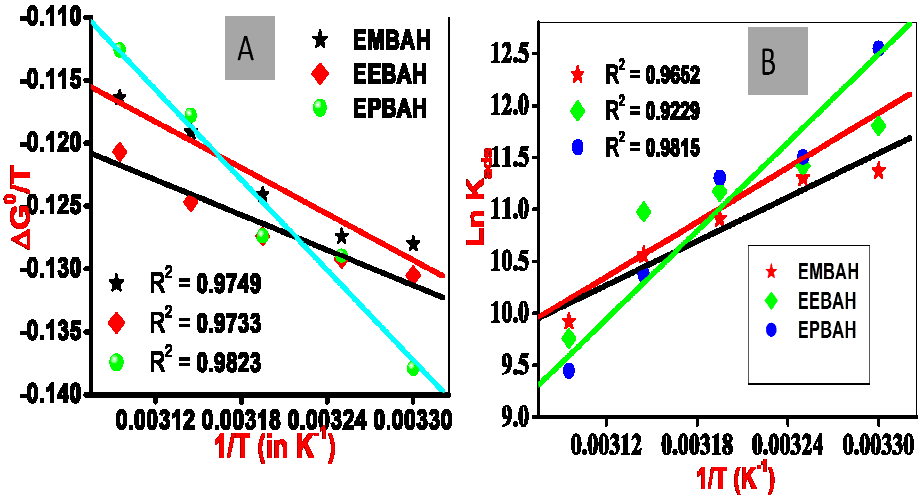

Fig 5.7 (A) Gibb's Helmholtz and (B) Van't Hoff plot of mild steel in 0.5 M HCl containing EMBAH, EEBAH and EPBAH

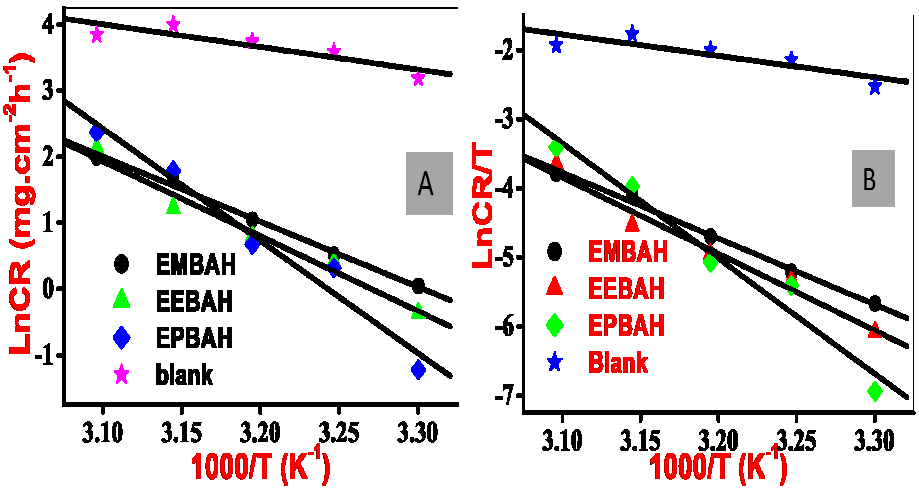

Fig 5.8 (A) Arrhenius and (B) Transition state plot of mild steel in 0.5 M HCl containing EMBAH, EEBAH and EPBAH.

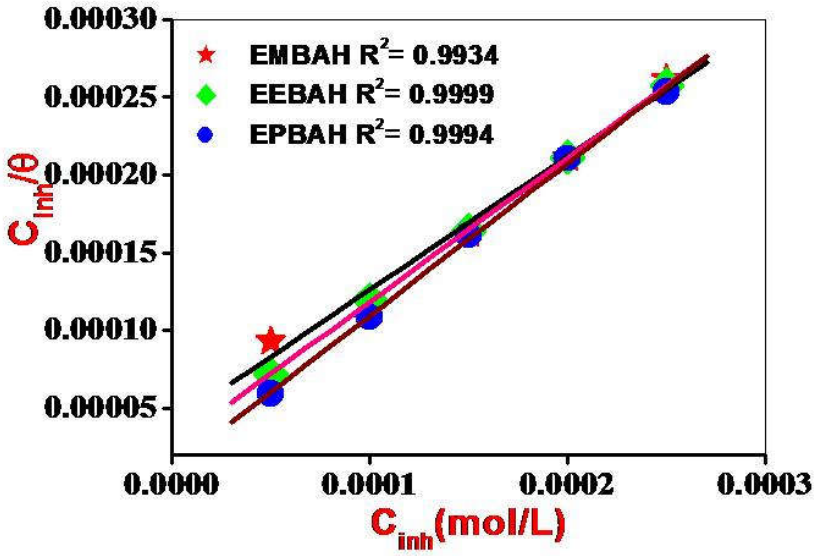

Fig 5.9: Langmuir Adsorption isotherm

References

1. Evelin Gutierrez, PandiyanThangarasu, Corros.Sci., 108 (2016) 23

2. Revathi Mohan, K. Ramya, K.K. Anupama, Abraham Joseph, , J.Mol,Liq, 220 (2016) 707

3. Monika Srivastava, Preeti Tiwari, Sanjay Kumar Srivastava, Rajiv Prakash, Gopal Ji, J. of Mol. Liq. 236 (2017) 184

4. Girma Biresaw, K.L. Mittal, Surfactants in Tribology volume 4 , CRC press (2014)

5. A Ahmed Al-Amiery, Abdul Amir, H.Kadhumetal., Materials7 (2014) 787

6. F.Zhang, Y.tang, Z.Cao, w.Jing, Z.Wu, Y.Chen, Corros. Sci., 61 (2012) 1

7. Hanane Hamani, Tahar Douadi, Mousa Al Noaimi, Saifi Issaadi, Djakel Daoud, Salah Chaffa, Corros. Sci, 88 (2014) 234

8. K.R.Ansari, M.A.Quaraishi, Ambrish Singh, Corros. Sci., 79 (2014) 5

9. B.Qian, J.Wang, M.Zheng, B.Hou, Corros. Sci, 75 (2013) 184

10. M.Moradi J.Duan, X.Du, Corros. Sci. 69 (2013) 338

11. S.Chithra, K.Parameswari, C.Sivakami, A.Selvaraj, Chemical Engineering Research Bulletin, 14 (2010) 1

12. E.A.Noor, A.H.Al-Moubaraki, Mater.Chem.Phys., 110 (2008) 145

13. A.S.Fouda, K.Shalabi, G.Y.Elewady, H.F.Merayyed, Int.J.Electrochem.Sci., 9 (2014) 7038

14. M. Tourabi,Sahibed-dine, Zarrouk,I. B. Obot, Hammouti, F. Bentissa and A.Nahlé, , Prot Met Phys Chem of surfaces 53(3) (2017) 548

15. Alpana Soni,Pratibha Sharma, Monika, Rekha Dashora and A.K.Goswami, ,Por.electrochim.acta. 35(2) (2017) 117

16. Sonia Benabid, Tahar Douadi, Saïfi Issaadi, Christophe Penverne, Salah Chafaa, Measurement 99 (2017) 53

17. A.Joseph, Revathi Mohan, Res.Chem.Intermed.41(2015) 4795

18. A.Doner, R.Solmaz, M.Ozcan, G.Kardas, Corros.Sci., 53 (2011) 2902

19. I.Lukovits, K.Palfi, E.Kalmann, Corrosion., 53 (1997) 9

20. K.F.Khaled,, Appl.Surf.Sci., 255 (2008) 1811

21. Sam John and Abraham Joseph, , RSC Adv., 2 (2012) 9944

22. I.Lukovits, Zucchi F, E.Kalmann, Corrosio*n., 57* (2001) 3

6 CORROSION INHIBITION OF MILD STEEL IN HCl AND H_2SO_4 USING BENZIMIDAZOLE BEARING 1,3,4 -OXADIAZOLE DERIVATIVES, MBIMOT, EBIMOT AND PBIMOT

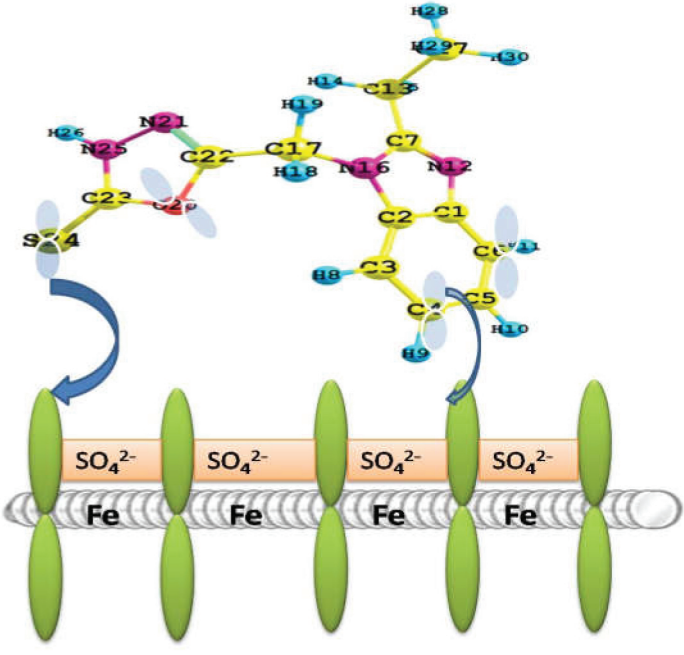

Chapter VI *encompasses inhibition effect of three 1,3,4-oxadiazole derivatives MBIMOT, EBIMOT, PBIMOT towards the corrosion of mild steel in HCl and H_2SO_4. Various techniques like gravimetric, EIS, PDP, and surface morphological studies were used for monitoring corrosion inhibition mechanism. The influence of immersion time, inhibitor concentration, temperature, and concentration of acid on inhibition was investigated. Adsorption and kinetic studies also were carried out.*

VI.1 Introduction

In metal industry, pickling treatment is the surface finishing process of removing oxide scales and other impurities from metal surface. Mineral acids like HCl and H_2SO_4 are the most widely used pickle liquors with a little preference for HCl due to its reducing nature, better solubility of chlorides and low operation temperature. The surface cleaning is accomplished by reducing the oxides which forms the scale. After the descaling, the base metals are prone to attack by these pickle liquors due to their aggressive nature and this can be prevented by corrosion inhibitors. The existence of planar aromatic ring, the hydrophobicity as well as the presence of hetero atoms made benzimidazole and its derivatives a very good candidate for corrosion inhibitors. In this chapter the synthesized benzimidazole bearing1,3,4-oxadiazoles,5-((2-methyl/ethyl/propyl)-1H-benzo[d]imidazol-1-yl)methyl)-1,3,4-oxadiazole-2-thiol(MBIMOT, EBIMOT, PBIMOT) (details given in Chapter II.3) are investigated for their corrosion inhibition in HCl and H_2SO_4 at different temperatures and different acid concentrations 0.5, 1 and 1.5 M HCl and 0.25, 0.5 and 0.75 M H_2SO_4 using weight loss and electrochemical methods. The choice of the compound is mainly due to their molecular structure considerations like presence of mercapto group, and hetero atoms in oxadiazole part and two anchoring sites of benzimidazole part: the nitrogen atom with its sp^2 electron pair and the aromatic rings which facilitates the adsorption of inhibitor on the metal surface [1]. The inhibition efficiency of organic compounds depend on various factors like nature of metal, nature of adsorption sites, interaction mode, molecular geometry, experimental conditions like pH, time of immersion, temperature, nature of aggressive medium, concentration of aggressive medium etc. In the present investigation we tried to correlate some of these factors with inhibition efficiency.

VI.2 Results and discussion

VI.2.1 Gravimetric Analysis

Effect of inhibitor concentration and acid concentration on corrosion rate were primarily studied using gravimetric analysis of mild steel coupons before and after 24 hours of immersion in acids with and without inhibitors at 303 K. The usual anodic reaction of metal dissolution, cathodic reaction of hydrogen evolution and the dissolution of corrosion products leads to weight loss during metal immersion process. The corrosion parameters like corrosion rate (CR) and inhibition efficiency (IE) were evaluated from weight loss data using eqn. (1.13) and (2.2) and are enlisted in Table 6.1(A,B). The perusal of the table affirmed the ability of all the three studied molecules as corrosion inhibitors towards mild steel corrosion in both the acids. It is clear that corrosion rate is diminished to a greater extent after the introduction of inhibitors into the aggressive medium. The inhibition efficiency gets increased with an increase in inhibitor concentration. It can be attributed to an increase in the adsorption of inhibitors on the mild steel surface forming a protective film [2]. On increasing acid concentration there occurred an increase in corrosion rate and a decrease in inhibition efficiency for these inhibitors in both the acids. These are primarily due to an increase in the concentration of active species (H^+ ion) which increases cathodic corrosion reaction of hydrogen evolution [3]. These salient behaviors are graphically represented in Fig 6.1. Fig. 6.2 is a representative plot of the trend of corrosion rate with time of immersion and it can be inferred that with an increase in the immersion time, the corrosion rate for a constant inhibitor concentration decreases due to the extended life time of the adsorbed inhibitor on the metal surface [4].

VI.2.2 Electroanalytical studies

VI.2.2.1 Potentiodynamic polarization studies (PDP)

The kinetics of anodic and cathodic reactions during corrosion process is probed by polarization studies. The effect of MBIMOT, EBIMOT, and PBIMOT on the polarization of mild steel in HCl and H_2SO_4 has been studied. Electrochemical corrosion kinetic parameters like corrosion potential (E_{corr}), corrosion current density (I_{corr}), inhibition efficiency (IE) etc. were obtained by Tafel extrapolation and are tabulated in Table 6.2(A-C) and 6.3 (A-C). As expected, corrosion current density decreases considerably on increasing the dosage of inhibitor suggesting a deceleration of anodic reaction of metal dissolution and cathodic reaction of hydrogen evolution. Considering the E_{corr} value, the maximum displacement between the E_{corr} of uninhibited and inhibited one was about 70 mV towards cathodic direction. These findings suggested mixed type behavior of the inhibitor with a pronounced cathodic type [5] which is also substantiated by the values of Tafel constants (β_a and β_c) both of which were affected by the introduction of inhibitors [6]. The Tafel plots of mild steel in 0.5 M HCl with the studied inhibitors depicted in Fig 6.3 (AB) and that in 0.25 M H_2SO_4 represented by Fig 6.4(A-B), clearly gave the evidence that the addition of inhibitors to the corrosive medium has significantly reduced the corrosion current density. The cathodic curves were shifted to more negative potentials and anodic curves to more positive potentials because of the adsorption of inhibitor over the metal surface [7].

VI.2.2.2 Electrochemical impedance measurements (EIS)

The results extracted from the gravimetric corrosion monitoring experiments can be improved by EIS methods. Electrochemical impedance spectroscopy has played a worthy role in quantifying and mitigating

corrosion effects. The impedance spectra for mild steel corrosion in 0.5 M HCl with and without inhibitors are given in Fig 6.5 (A-C) and that for 0.25 M H_2SO_4 in Fig 6.6 (A-C) respectively. The incremental addition of inhibitor up to 200 ppm caused an enlargement in the diameter of the Nyquist semicircle which was correlated with increase in the charge transfer resistance (R_{ct}) through metal-solution interface. The various useful impedance parameters obtained from non linear square fitting of impedance data to Randles circuit are tabulated in Table 6.2(A-C) and 6.3 (A-C). Observation of the table indicated the improvement of R_{ct} and decline of C_{dl} with inhibitor concentration. This supports the adsorption of more inhibitor molecules on the metal surface which provide better surface coverage and/or enhancement of the thickness of the protective layer at the metal solution interface as well as reduction in the local dielectric constant of the solution due to the replacement of polar water molecules adsorbed on the metal surface by non-polar organic molecules [8].

VI.2.2.3 Effect of acid concentration – Electroanalytical studies

The electro analytical data recorded in Table 6.4 implied a rise in I_{corr} as well as a depression in R_{ct} with increase in acid concentration. This can be attributed to the increase in the aggressive ion concentration which has promoted extensive cathodic corrosion. At higher concentrations of both the acids, these inhibitors showed lesser efficiency. The order of efficiency remains the same in both the acids as EBIMOT > PBIMOT > MBIMOT and this trend can be due to the combined effect of medium steric strain and inductive effect of ethyl group. A comparative Nyquist plot for mild steel in various acid concentrations with 200 ppm of inhibitors is presented in Fig 6.7-6.12(A). A schematic representation of effect of acid concentration on corrosion rate and I_{corr} are given as Fig 6.7-6.9 (B) and 6.10-6.12 (B) respectively.

VI.2.2.4. Effect of temperature – Electroanalytical studies:

It is evident from Table 6.2 and 6.3 (A-C) that increase in temperature has a pronounced effect on corrosion current density, corrosion rate and inhibition efficiency but a very little influence on corrosion potential and the order of efficiencies of these inhibitors also remained the same. The increase in temperature has caused an increase in CR, I_{corr} and C_{dl} and a decrease in R_{ct} which pointed towards increased corrosion at elevated temperatures due to the shifting of adsorption-desorption equilibrium to desorption at higher temperatures. Temperature found to have no effect on the shape of the Nyquist and Tafel plots.

VI.2.2.5: Bode plots:

The interpretation of impedance data along with frequency of AC waves can be obtained from Bode plots. Fig 6.5 (A-C) represent the Bode phase angle plots of phase angle (ϕ) Vs log(f) in HCl, which provide insight into the capacitive, inductive and resistive behavior of the system at different frequencies. The existence of a single peak in Bode phase angle plot manifested the role of charge transfer phenomenon in mild steel dissolution [9]. The maximum phase angles were shown at intermediate frequencies and it is the one deviated from that of the ideal capacitive value of 90^0 which again emphasizes the non-ideal behavior of mild steel in HCl system [10]. A quick investigation of Bode phase angle plots revealed the increase in phase angle with inhibitor concentration which hinted the retardation of corrosion rate with the introduction of inhibitors [11]. The increase of temperature to 308 and 313 K does not cause any change in the appearance of the plots but the phase angle shows deviation towards lower values.

Another mode of Bode curve, Bode magnitude plot of log (f)-log (Z) obtained for mild steel in 0.25 M H_2SO_4 is depicted in Fig 6.6 (A) - (C). The

Bode plots show the existence of only one time constant. The impedance at high frequency corresponds to sum of ohmic resistance and solution resistance and at low frequency it corresponds to the charge transfer resistance. The impedance value shows a positive trend with concentration.

VI.2.3 Adsorption studies

The contribution of adsorption of inhibitors on corrosion inhibition is enormous. The type of adsorption and various adsorption parameters can be excerpted from adsorption isotherms. The plots of C_{inh}/θ Vs.C_{inh} as given in Fig 6.13 and 6.14 are straight lines with an approximately unit correlation coefficient and slope, found to be the best fitted adsorption isotherm in the present study and this type of isotherms are known as Langmuir adsorption isotherms or ideal localized mono layer isotherm characterized by eqn. (1.9). These isotherms suggest a mono layer adsorption of MBIMOT, EBIMOT and PBIMOT on the metal surface. It also considers equivalent surface energies for all active sites on the surface with one adsorbate covering one site with no secondary interaction between the adsorbents even at unit surface coverage [12]. The slope and intercept of the isotherm provided us adsorption constant K_{ads} as 1/intercept and free energy of adsorption (ΔG^0_{ads}) using eqn. (5.5). The calculated adsorption parameters are listed in Table 6.5 (A & B). Careful examination of this table revealed a high value of K_{ads} indicating a stronger adsorption. The negative values of ΔG^0_{ads} which is in between −20 kJ/mol to −40 kJ/mol proposed the spontaneous nature of simultaneous physicochemical adsorption of inhibitors on mild steel surface immersed in these acids [13]. The inverse relation between efficiency and temperature also favors a mixed behavior of adsorption preferentially physisorption [14].

VI.2.4: Effect of activation energy and temperature on corrosion rate: Kinetics of metal corrosion

The electro analytical studies at different temperatures revealed that as in any other reaction, the rate of corrosion also increases with increase in temperature as shown in Fig 6.7-6.9 (B). The kinetic considerations of metal corrosion are studied in detail for explaining the effect of temperature on corrosion.

Arrhenius equation (5.2) and transition state eqn. (5.3) gave various activation parameters of corrosion like apparent activation energy (E_a), the apparent enthalpy of activation(ΔH_a^0), and apparent entropy of activation (ΔS_a^0) provides supplementary insight into corrosion inhibition mechanism. $-E_a/R$, the slope of Arrhenius plot of log CR Vs 1/T provides E_a at the same time, slope (ΔH_a^0/R) and intercept (log R/Nh + ΔS_a^0 /R) of transition state plot of log CR/T Vs 1/T (Fig 6.15 and 6.16) helps to determine ΔH_a^0 and ΔS_a^0. The various kinetic parameters are tabulated in Table 6.6. The perusal of the table inferred a rise in E_a values in presence of inhibitors suggesting a molecular adsorption of inhibitors, which increased the energy barrier for the corrosive molecules resulted in decreased corrosion rate [15]. In general, higher E_a values in the inhibited system compared to the blank, support physisorption mechanism whereas an unchanged or lower E_a values for inhibited systems indicate chemisorption mechanism [16]. In this study, higher E_a values of inhibited solutions signified a physisorption mechanism for corrosion inhibition. The lower values of E_a for uninhibited and inhibited solutions at higher concentration of acids supported the easier corrosion in higher acid concentration. A scrutiny of ΔH_a^0 values listed in the table evidenced positive enthalpy values with an enhancement in the presence of inhibitors compared to that in their absence suggesting an endothermic nature of metal dissolution process which is in need of more energy to attain

activated state or equilibrium in presence of inhibitors [17]. The average difference of E_a and ΔH_a^0 for each test in all the studied cases is around 2.5-2.6 kJ/mol which is approximately equal to RT (2.63 kJ/mol) proposed a unimolecular reaction for dissolution of metal [18]. The value of entropy, ΔS_a is negative in the blank solutions both in HCl and H_2SO_4 but tend to increase in presence of inhibitors. This is interpreted as a process of increase in disorder during the transition from reactants to activated complex [16].

VI.2.5 Surface morphological studies

SEM images were taken to evaluate the protection capacity of inhibitors towards mild steel in HCl and H_2SO_4. Fig 6.17 depicts the scanning electron micrographs of polished mild steel surface and that immersed in HCl in the absence and presence of inhibitors, which confirmed the efficacy of MBIMOT, EBIMOT and PBIMOT as corrosion inhibitors. The reduced corrosion rate of mild steel in HCl with inhibitors is clearly evidenced from the lesser amount of cracks and pits in Fig 6.17 (D and E) compared to that in Fig 6.17 (B and C).

VI.2.6 Corrosion and inhibition mechanism

The corrosion process of mild steel in any acidic environment consists of anodic metal dissolution and cathodic hydrogen evolution reactions as represented below [19]

Anodic metal dissolution:

$$Fe + X^{n-} \leftrightarrow \quad [FeX^{n-}]ads \tag{6.1}$$

$$[FeX^{n-}]ads \ \leftrightarrow (FeX)_{ads} \ + ne - \tag{6.2}$$

$$(FeX)ads \leftrightarrow \ FeX^{n+} + ne - \tag{6.3}$$

$$FeX^{n+} \leftrightarrow Fe^{2+} + X^{n-} \quad (6.4)$$

X = Cl^- in HCl and SO_4^{2-} in H_2SO_4

Cathodic Hydrogen evolution:

$$Fe + H^+ \leftrightarrow (FeH^+)ads \quad (6.5)$$

$$(FeH^+)ads + e^- \rightarrow (FeH)ads \quad (6.6)$$

$$(FeH)ads + H^+ + e^- \rightarrow Fe + H_2\uparrow \quad (6.7)$$

It has been proposed that the corrosion inhibition in a solution is by adsorption of the inhibitors to the metal surface. The nature of adsorption is determined by various factors like type of the aggressive media, nature and charge of metal, charge and dipole moment of inhibitor etc. The complex nature of corrosion as well as adsorption makes it difficult to foresee a single adsorption mechanism [20]. From the analysis of zero charge potential, it has been found that mild steel surface carries positive charges in acidic media [21]. So it has been recommended that Cl^- and SO_4^{2-} ions get adsorbed first and excess negative charges will be generated towards mild steel surface in acid solution [22, 23]. As proposed by several authors, an interaction between the protonated form of inhibitor and negatively charged metal/solution interface creates a protective film (FeX^- inhibitor-H^+)ads which prevents the oxidation of metal as shown by reactions 6.2-6.4 and this protective film prevents the metal from coming in contact with the aggressive medium (physisorption) [24, 25]. There is also a possibility of adsorption of inhibitors by the formation of a coordinate type bond between the d-orbital of Fe atoms and lone pair of sp^2 electrons of hetero atoms (N, S) and pi electrons of benzene ring (chemisorption). So both the models of adsorption can describe the behavior of MBIMOT, EBIMOT, and PBIMOT as efficient

corrosion inhibitors. A schematic representation of this corrosion inhibition mechanism is presented in Fig 6.18

VI.2.6 Theoretical studies

The experimental studies revealed the order of inhibition efficiencies of these inhibitors as EBIMOT>PBIMOT>MBIMOT for mild steel corrosion in both HCl and H_2SO_4. Theoretical study was carried in aqueous phase using self consistent reaction field (SCRF) theory and Tomasi's polarized continuum model (PCM), to explain order of inhibition efficiency and the optimized geometry of the inhibitors with their HOMO and LUMO obtained using Gaussian 09 package were also given in chapter 2 (Fig 2.7 D-F).

Recent literature on DFT calculations show that descriptors of inhibitors calculated using DFT can be correlated with their inhibition efficiencies [26]. Dipole moment which describes the global polarity of the molecule has positive as well as negative relationship with inhibition efficiency [27]. Tang et . al [28] proposed a dipole interaction between the charged centers of molecules and charged metal surface which resulted into a physical interaction of inhibitors and thus a positive relationship between the dipole moment and inhibition efficiency suggests a physisorption mechanism [29]. In this study also there is a positive correlation between the dipole moment and inhibition efficiency which can be a supporting factor for the physical adsorption of inhibitors on the metal surface as described earlier.

The observation of Fig 2.7 (D-F) revealed an inverse relationship between E_{LUMO} values and inhibition efficiencies which suggests that along with the dipole moment, the electron accepting capacity (back donation by Fe atoms) also contributes to higher efficiency of EBIMOT. E_{HOMO} is associated with the behavior of compounds as electron donors. Compounds with high

E_{HOMO} can act as potential anti corrosion agents. The HOMO-LUMO energy gap also can give some hint towards the reactivity of molecules towards metal surface. On the basis of E_{HOMO} and ΔE values the studied compounds can be ranked for efficiency as PBIMOT > EBIMOT > MBIMOT. But experimentally the efficiency of EBIMOT is found to be slightly more than that of PBIMOT. Although the difference in ΔE values and inhibition efficiency between EBIMOT and PBIMOT is small, the small difference can be attributed to steric hindrance of the propyl group [30,31]. The highest inhibition efficiency of EBIMOT can be correlated with its lowest E_{LUMO} value and highest dipole moment which suggested the contribution of back donation of electrons from iron atom in adsorption and corrosion inhibition. Theoretical studies can give a promising comparison between it and experimental results only if the selected parameters and the property studied are in good correlation. The discrepancy between theoretical and experimental results in corrosion inhibition can be due to some oversimplified assumptions regarding the corrosion system. It also confirms to the complex nature of interactions involved in the corrosion inhibition mechanisms. So a composite index of more than one parameter is required to explain the enhanced efficiency of an inhibitor [32].

Conclusions

The inhibitors 2-alkyl substituted benzimidazole bearing 1,3,4-oxadiazoles, MBIMOT, EBIMOT and PBIMOT are found to be efficient corrosion inhibitors for mild steel corrosion in HCl and H_2SO_4 following the order EBIMOT> PBIMOT> MBIMOT with a slight enhancement of efficiency in HCl. Gravimetric as well as electro analytical methods (both EIS and PDP) provided reasonably comparable values of inhibition efficiencies in both the acids. The increase in temperature as well as acid concentration reduces the inhibition efficiency to a small extent whereas

increase in inhibitor concentration increases the inhibition efficiency. The charge transfer mechanism of corrosion inhibition and mixed type behavior of inhibitors were suggested by EIS and PDP studies respectively. The Langmuir adsorption isotherms explained the spontaneous physico-chemical adsorption of inhibitors on mild steel surface in both the acids. The kinetic studies of the reaction show the endothermic nature of metal corrosion and supported the role of preferential physisorption of inhibitors on inhibition.

Table 6.1 (A): Variation of CR and IE with inhibitor concentration and acid concentration for mild steel immersed in HCl for 24 h

inhibitor	Cinh ppm	0.5 M HCl		1 M HCl		1.5 M HCl	
		CR $mg.cm^{-2}.h^{-1}$	IE %	CR $mg.cm^{-2}.h^{-1}$	IE %	CR $mg.cm^{-2}.h^{-1}$	IE %
blank	--	8.6320	--	16.6898	--	24.7234	--
MBIMOT	50	2.3032	73.30	5.9838	64.00	11.2325	54.56
	100	1.1215	87.00	4.7454	71.57	8.4325	65.89
	150	0.8623	90.00	2.8935	82.66	5.7234	76.85
	200	0.6963	91.93	2.0370	87.79	4.0652	83.53
EBIMOT	50	1.652	80.90	3.7269	77.67	6.5234	73,61
	100	0.9572	88.91	3.0092	81.97	4.9242	80.08
	150	0.5995	93.00	1.5625	90.60	2.8563	88.44
	200	0.4224	95.10	1.3773	91.75	2.3532	90.48
PBIMOT	50	1.8055	78.97	4.7685	71.25	7.5248	69.56
	100	0.9699	88.76	3.7731	77.39	6.4462	73.93
	150	0.6990	91.90	2.0949	87.45	3.9209	84.14
	200	0.6053	92.98	1.5046	90.98	3.0920	87.49

Table 6.1 (B): Variation of CR and IE with inhibitor concentration and acid concentration for mild steel immersed in H_2SO_4 for 24 h

inhibitor	Cinh ppm	0.25 M H_2SO_4		0.5 M H_2SO_4		0.75 M H_2SO_4	
		CR $mg.cm^2.h^{-1}$	IE %	CR $mg.cm^2.h^{-1}$	IE %	CR $mg.cm^2.h^{-1}$	IE %
blank	--	8.9375	--	10.5325	--	14.7362	--
MBIMOT	50	2.1550	75.8	8.0782	23.30	10.8600	26.30
	100	1.6921	81.06	4.5584	56.72	8.2652	43.91
	150	1.5880	82.23	3.0125	71.39	6.0362	59.04
	200	1.1620	86.9	2.3250	77.92	5.0350	65.83
EBIMOT	50	1.7639	80.26	6.8283	35.17	9.7187	34.05
	100	1.0995	87.70	3.8248	63.68	5.9286	59.77
	150	0.7894	91.17	1.4134	86.58	4.9728	66.25
	200	0.4178	95.33	0.8853	91.59	2.7001	81.68
PBIMOT	50	2.0324	77.20	6.9838	33.69	9.6182	34.73
	100	1.0162	88.60	4.1272	60.81	6.0780	58.75
	150	0.7269	91.87	1.8268	82.66	5.1475	65.07
	200	0.6481	92.75	0.9218	91.24	4.0729	72.36

Table 6.2(A): Electrochemical parameters for mild steel corrosion in 0.5 M HCl containing various concentrations of MBIMOT

Temp	Cinh ppm	EIS			PDP		
		R_{ct} Ωcm^2	C_{dl} x10^{-4} F	IE %	$-E_{corr}$ mV	I_{corr} mA/ cm^2	IE %
303 K	0	9.816	6.423	--	472	1.0895	--
	50	36.48	1.870	73.09	504	0.2619	75.96
	100	70.29	1.361	86.03	500	0.1738	84.01
	150	101.2	1.405	90.30	511	0.1087	90.02
	200	158.8	0.9354	93.82	509	0.0852	92.18
308 K	0	7.907	11.09	--	468	3.0613	--
	50	17.32	6.536	54.34	519	1.3641	55.44
	100	29.66	4.554	73.34	520	0.8110	73.50
	150	50.83	5.023	84.44	519	0.5001	83.66
	200	74.37	1.603	89.37	534	0.4532	85.19
313 K	0	5.801	6.870	--	465	4.0225	--
	50	13.68	2.138	57.59	521	1.6941	57.88
	100	21.98	3.552	73.60	514	1.0568	73.72
	150	35.89	1.618	83.83	523	0.6150	84.71
	200	51.48	2.388	88.73	527	0.4488	88.84

Table 6.2(B) Electrochemical parameters for mild steel corrosion in 0.5 M HCl containing various concentrations of EBIMOT

temp	Cinh ppm	EIS			PDP		
		R_{ct} Ωcm^2	$C_{dl}x10^{-4}$ F	IE %	$-E_{corr}$ mV	I_{corr} mA/ cm^2	IE %
303 K	0	9.816	6.423	--	472	1.0895	--
	50	32.05	2.695	69.37	501	0.3448	68.35
	100	90.97	1.117	89.21	507	0.1431	86.86
	150	144.5	0.6761	93.21	511	0.0907	91.67
	200	216.1	0.9137	95.46	502	0.0725	93.34
308 K	0	7.907	11.09	--	468	3.0613	--
	50	22.56	3.875	64.95	501	1.1767	61.50
	100	48.06	3.717	83.55	516	0.4847	84.17
	150	60.81	1.123	86.99	507	0.3161	89.67
	200	91.25	1.109	91.33	511	0.2497	91.85
313 K	0	5.801	6.870	--	465	4.0225	--
	50	15.36	4.084	62.23	511	1.617	59.80
	100	24.36	5.55	76.18	505	0.9265	76.93
	150	44.40	1.559	86.93	509	0.5747	85.71
	200	58.45	2.152	90.07	535	0.4832	87.99

Table 6.2(C) Electrochemical parameters for mild steel corrosion in 0.5 M HCl containing various concentrations of PBIMOT

temp	Cinh ppm	EIS			PDP		
		R_{ct} Ωcm^2	$C_{dl}x10^{-4}$ F	IE %	$-E_{corr}$ mV	I_{corr} mA/ cm^2	IE %
303 K	0	9.816	6.423	--	472	1.0895	--
	50	88.67	0.9425	88.84	492	0.1772	83.73
	100	100.6	0.8796	90.24	506	0.1518	86.16
	150	119.8	0.4199	91.81	509	0.1242	88.60
	200	179.9	1.023	94.54	503	0.1024	90.60
308 K	0	7.907	11.09	--	468	3.0613	--
	50	27.64	3.277	71.39	472	0.9706	68.29
	100	47.07	1.308	83.20	500	0.6862	77.58
	150	50.86	2.124	84.53	511	0.3770	87.68
	200	71.40	1.984	88.93	526	0.3020	90.13
313 K	0	5.801	6.870	--	465	4.0225	--
	50	19.91	4.206	70.86	508	1.1022	72.59
	100	23.39	2.308	75.28	500	1.0622	73.59
	150	34.74	1.265	83.30	533	0.5360	86.67
	200	49.54	1.270	88.29	526	0.3793	90.57

Table 6.3(A) Electrochemical parameters for mild steel corrosion in 0.25 M H_2SO_4 containing various concentrations of MBIMOT

temp	Cinh ppm	EIS R_{ct} Ωcm^2	EIS $C_{dl}x10^{-4}$ F	EIS IE %	PDP $-E_{corr}$ mV	PDP I_{corr} mA/ cm^2	PDP IE %
303 K	0	8.558	16.62	--	473	1.5710	--
	50	31.79	1.634	73.00	536	0.4146	73.61
	100	50.46	1.421	83.04	521	0.3349	78.68
	150	62.14	1.307	86.20	509	0.2946	81.24
	200	74.32	1.146	88.40	514	0.2615	83.35
308 K	0	7.799	18.86	--	479	2.9157	--
	50	20.31	2.954	61.59	523	0.8912	69.43
	100	25.07	2.785	68.90	525	0.7417	74.56
	150	29.18	4.048	73.30	532	0.7088	75.69
	200	42.72	1.509	81.74	516	0.6441	77.91
313 K	0	6.573	19.66	--	476	2.8268	--
	50	16.64	3.634	60.50	531	1.0649	62.30
	100	19.9	4.799	66.97	521	0.9068	67.92
	150	23.30	2.793	71.79	521	0.8081	71.41
	200	29.64	2.381	77.80	511	0.5563	80.30

Table 6.3(B) Electrochemical parameters for mild steel corrosion in 0.25 M H_2SO_4containing various concentrations of EBIMOT

temp	Cinh ppm	EIS R_{ct} Ωcm^2	EIS $C_{dl}x10^{-4}$ F	EIS IE %	PDP $-E_{corr}$ mV	PDP I_{corr} mA/ cm^2	PDP IE %
	0	8.558	16.62	--	473	1.5710	--
	50	34.55	1.347	75.2	527	0.4565	70.00
303	100	65.57	1.173	86.94	512	0.2249	85.68
K	150	91.32	1.071	90.62	507	0.2035	87.04
	200	143.6	0.7076	94.00	515	0.1272	91.90
	0	7.799	18.86	--	479	2.9157	---
	50	20.71	2.640	62.30	535	0.9867	66.16
308	100	39.50	1.791	80.20	514	0.4737	83.75
K	150	57.67	1.320	86.40	516	0.4218	85.53
	200	60.75	1.606	87.16	504	0.2810	90.36
	0	6.573	19.66	--	476	2.8268	---
	50	17.32	2.685	62.50	532	0.9621	65.96
313	100	24.25	1.820	72.80	503	0.7736	72.63
K	150	34.65	1.505	81.00	521	0.6236	77.94
	200	40.85	1.484	83.90	508	0.4226	85.05

Table 6.3(C) Electrochemical parameters for mild steel corrosion in 0.25 M H_2SO_4containing various concentrations of PBIMOT

temp	Cinh ppm	EIS R_{ct} Ωcm^2	EIS $C_{dl}x10^{-4}$ F	EIS IE %	PDP $-E_{corr}$ mV	PDP I_{corr} mA/ cm^2	PDP IE %
	0	8.558	16.62	--	473	1.5710	--
	50	29.28	2.136	70.70	497	0.4156	73.55
303	100	90.38	1.314	90.50	507	0.1898	87.92
K	150	107.6	0.8787	92.00	499	0.1751	88.85
	200	110.9	0.2190	92.30	519	0.1417	90.98
	0	7.799	18.86	--	479	2.9157	---
	50	24.22	2.110	67.79	522	0.7918	72.84
308	100	48.79	1.311	84.00	511	0.4041	86.14
K	150	49.43	1.193	84.20	509	0.3624	87.57
	200	60.60	1.327	87.13	504	0.2850	90.22
	0	6.573	19.66	--	476	2.8268	---
	50	20.78	1.890	68.30	528	0.7377	73.90
313	100	32.56	1.609	79.81	516	0.6329	77.61
K	150	42.71	0.7523	84.60	498	0.4707	83.35
	200	48.15	0.9845	86.30	508	0.3491	87.65

Table 6.4 (A) Effect of acid concentration on electrochemical parameters like R_{ct} and I_{corr} of mild steel corrosion in HCl containing 200 ppm of MBIMOT, EBIMOT and PBIMOT at various temperatures

inhibitor	Acid conc M	303 K R_{ct} Ωcm^2	I_{corr} mA/ cm^2	308 K R_{ct} Ωcm^2	I_{corr} mA/ cm^2	313 K R_{ct} Ωcm^2	I_{corr} mA/ cm^2
blank	0.5	9.816	1.090	7.907	3.0613	5.801	4.023
	1	6.491	3.193	5.352	2.6170	5.268	2.941
	1.5	5.254	3.099	5.723	3.3643	6.133	3.412
MBIMOT	0.5	158.8	0.085	74.37	0.4532	51.48	0.449
	1	55.51	0.453	26.83	0.6377	19.88	0.730
	1.5	34.45	0.512	18.22	0.9821	18.83	1.259
EBIMOT	0.5	216.1	0.073	91.25	0.2497	58.45	0.483
	1	96.06	0.249	45.45	0.3141	37.85	0.548
	1.5	52.29	0.303	30.14	0.662	22.92	0.851
PBIMOT	0.5	179.9	0.102	71.40	0.3020	49.54	0.379
	1	71.63	0.329	36.00	0.3494	23.50	0.628
	1.5	44.72	0.321	24.08	0.832	19.57	1.055

Table 6.4 (B) Effect of acid concentration on electrochemical parameters like R_{ct} and I_{corr} of mild steel corrosion in H_2SO_4 containing 200 ppm of MBIMOT, EBIMOT and PBIMOT at various temperatures

inhibitor	Acid conc M	303 K		308 K		313 K	
		R_{ct} Ωcm^2	I_{corr} mA/ cm^2	R_{ct} Ωcm^2	I_{corr} mA/ cm^2	R_{ct} Ωcm^2	I_{corr} mA/ cm^2
blank	0.25	8.558	1.571	7.7995	2.916	6.573	2.827
	0.5	8.366	2.344	7.919	2.653	7.290	3.489
	0.75	6.789	2.529	4.488	3.561	4.905	3.747
MBIMOT	0.25	74.32	0.262	42.72	0.644	29.64	0.556
	0.5	36.79	0.516	30.62	0.541	21.38	0.923
	0.75	24.25	0.928	14.94	0.984	13.80	1.315
EBIMOT	0.25	143.6	0.127	60.75	0.281	40.85	0.423
	0.5	92.69	0.263	40.13	0.427	31.87	0.573
	0.75	47.62	0.504	21.77	0.694	20.39	0.975
PBIMOT	0.25	110.9	0.142	60.60	0.285	48.15	0.349
	0.5	52.06	0.445	33.78	0.481	26.87	0.770
	0.75	31.90	0.616	16.76	0.974	15.19	1.116

Table 6.5 (A) Adsorption parameters for MBIMOT, EBIMOT and PBIMOT on mild steel in 0.5 M HCl

Temp (K)	MBIMOT		EBIMOT		PBIMOT	
	K_{ads} M^{-1}	ΔG^0_{ads} kJ/mol	K_{ads} M^{-1}	ΔG^0_{ads} kJ/mol	K_{ads} M^{-1}	ΔG^0_{ads} kJ/mol
303	13143	−34.01	11258	−33.63	44655	−37.10
308	5447	−32.32	9866	−32.30	15309	−34.97
313	6258	−33.21	7336	−33.62	11095	−34.70

Table 6.5 (B) Adsorption parameters for MBIMOT, EBIMOT and PBIMOT on mild steel in 0.25 M H_2SO_4

Temp (K)	MBIMOT		EBIMOT		PBIMOT	
	K_{ads} M^{-1}	ΔG^0_{ads} kJ/mol	K_{ads} M^{-1}	ΔG^0_{ads} kJ/mol	K_{ads} M^{-1}	ΔG^0_{ads} kJ/mol
303	16886	−34.6	14936	−34.3	14928	−34.3
308	8378	−33.1	9442	−33.7	14215	−34.8
313	9146	−34.2	8923	−34.1	13171	−35.1

Table 6.6 (A) Activation parameters of corrosion of mild steel in HCl in presence of MBIMOT, EBIMOT and PBIMOT

inhibitor	Conc of HCl M	C_{inh} ppm	E_a kJ/mol	ΔH^0_a kJ/mol	$\Delta S_a{}^0$ J/mol.K	$E_a - \Delta H^0_a$
blank		0	41.45	38.90	−38.35	2.55
MBIMOT		50	77.61	75.03	9.04	2.58
		100	91.98	89.44	27.35	2.54
	0.5	150	81.91	79.37	11.47	2.54
		200	89.04	86.48	20.07	2.56
	1	200	81.19	78.64	12.65	2.55
	1.5	200	57.61	55.05	−19.37	2.56
EBIMOT		50	57.98	55.42	−18.91	2.56
		100	103.90	101.34	43.11	2.56
	0.5	150	93.34	90.78	26.66	2.56
		200	103.34	100.78	39.46	2.56
	1	200	73.73	71.17	0.04	2.56
	1.5	200	65.19	62.63	−10.17	2.56
PBIMOT		50	118.23	115.67	64.25	2.56
		100	109.50	106.92	50.85	2.58
	0.5	150	98.34	95.63	34.24	2.71
		200	101.95	99.41	38.24	2.54
	1	200	88.07	85.51	21.47	2.56
	1.5	200	65.38	62.82	−10.17	2.56

Table 6.6 (B) Activation parameters of corrosion of mild steel in H_2SO_4 in presence of MBIMOT, EBIMOT and PBIMOT

inhibitor	Conc of H_2SO_4 M	C_{inh} ppm	E_a kJ/mol	ΔH_a^0 kJ/mol	ΔS_a^0 J/mol.K	$E_a - \Delta H_a^0$
blank		0	20.80	18.20	−155.5	2.60
MBIMOT	0.25	50	51.17	48.61	−65.57	2.56
		100	73.57	71.01	4.800	2.56
		150	77.63	75.06	16.54	2.57
		200	72.58	70.03	−2.030	2.55
	0.5	200	42.73	40.17	−95.21	2.56
	0.75	200	44.63	42.31	−83.88	2.32
EBIMOT	0.25	50	56.27	52.07	−54.72	4.20
		100	78.48	75.91	18.20	2.57
		150	76.41	73.85	8.54	2.56
		200	99.37	96.80	81.26	2.57
	0.5	200	84.48	81.91	41.57	2.57
	0.75	200	67.24	64.66	−15.30	2.57
PBIMOT	0.25	50	27.04	24.47	−144.8	2.57
		100	80.62	78.07	22.90	2.52
		150	73.20	70.59	−2.65	2.63
		200	64.12	61.58	−32.98	2.54
	0.5	200	52.23	49.68	−66.20	2.55
	0.75	200	58.74	56.19	−40.18	2.55

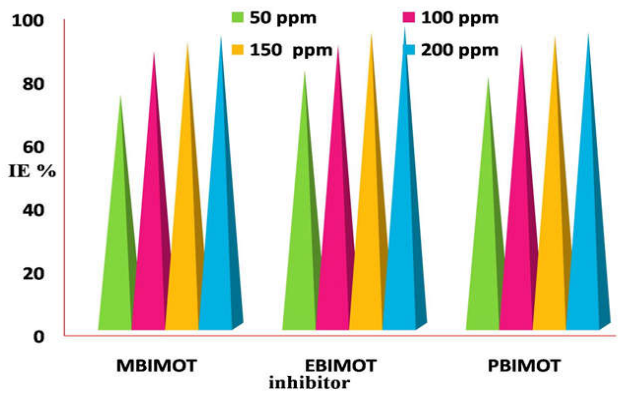

Fig 6.1 Pictorial representation of effect of inhibitor concentration on inhibition efficiency of MBIMOT, EBIMOT and PBIMOT for mild steel corrosion in HCl

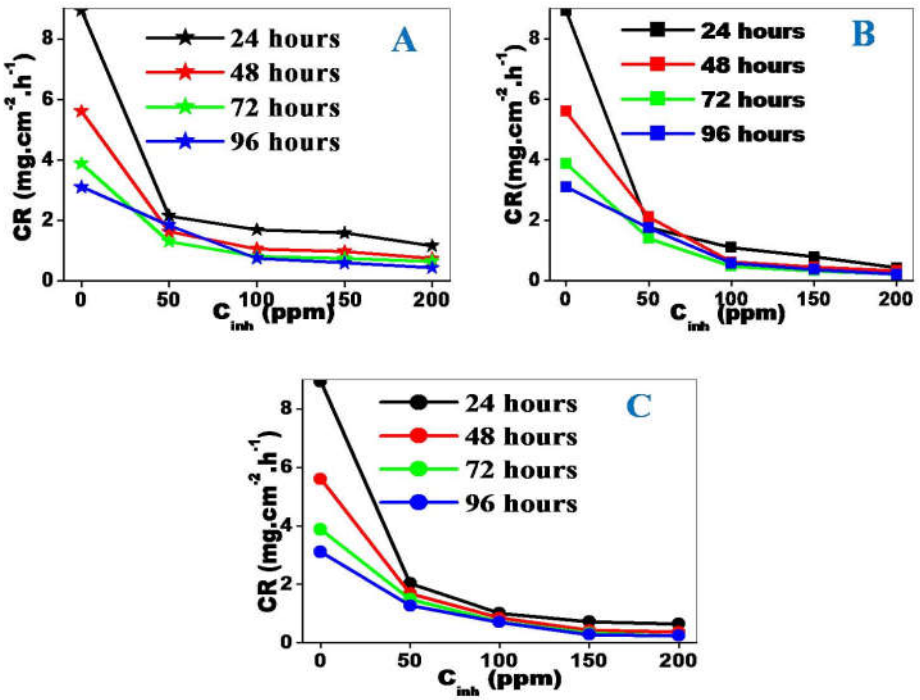

Fig 6.2: The variation in corrosion rate of mild steel in H_2SO_4 with concentration of inhibitors and immersion time for (A) MBIMOT (B) EBIMOT (C) PBIMOT

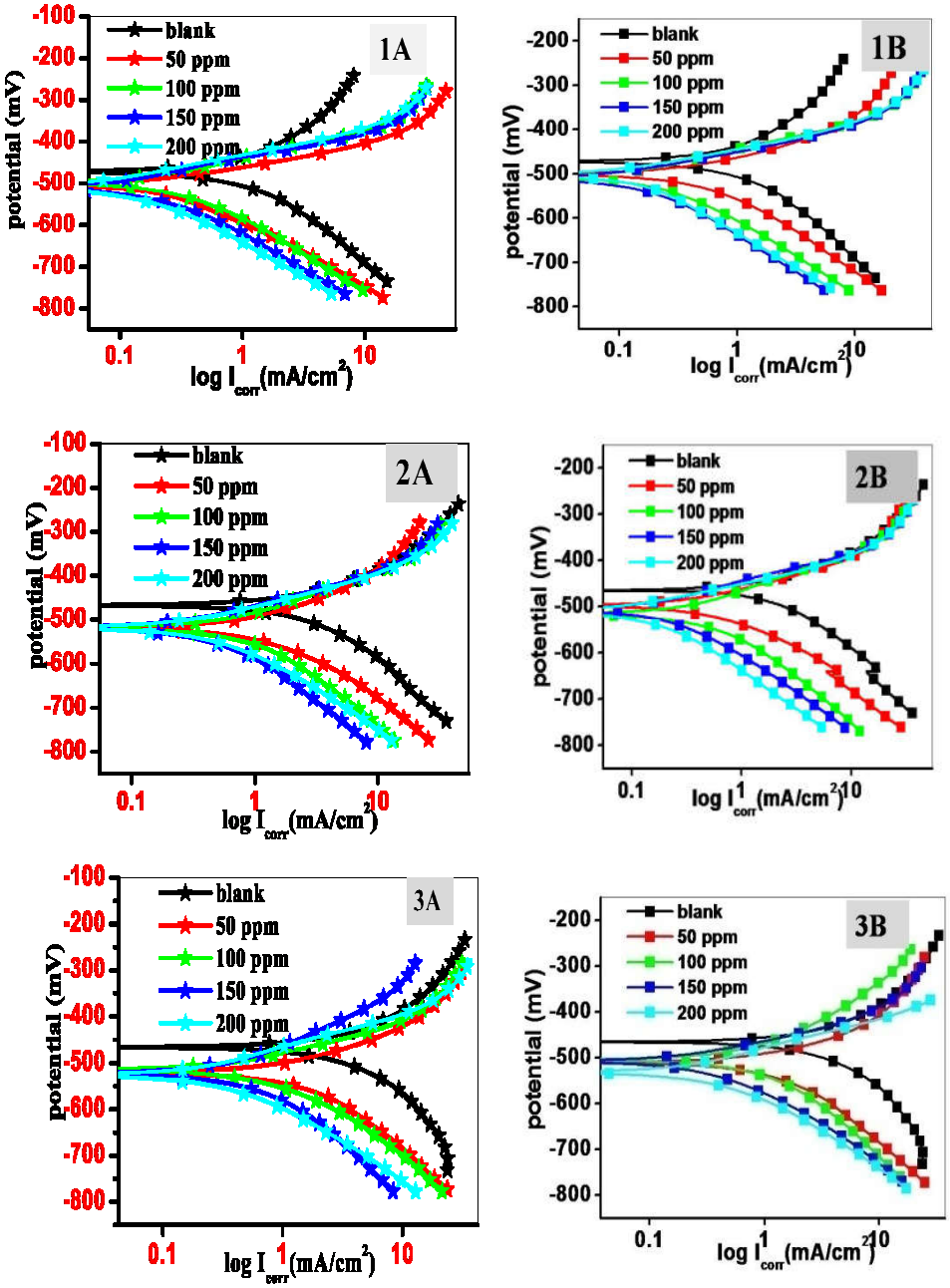

Fig 6.3(A): Tafel plots for mild steel in 0.5 M HCl containing (A) MBIMOT and (B) EBIMOT at (1) 303 K (2) 308 K and (c) 313 K

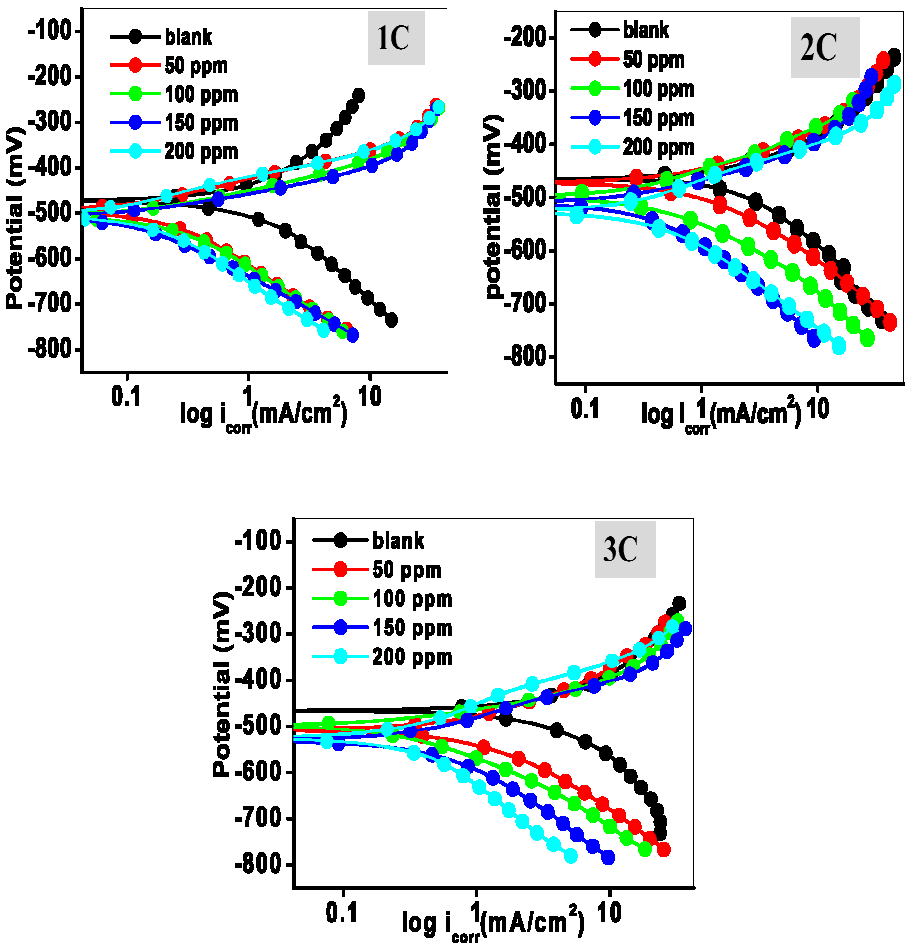

Fig 6.3(B) Tafel plots for mild steel in 0.5 M HCl containing PBIMOT at (1) 303 K (2) 308 K and (3) 313 K

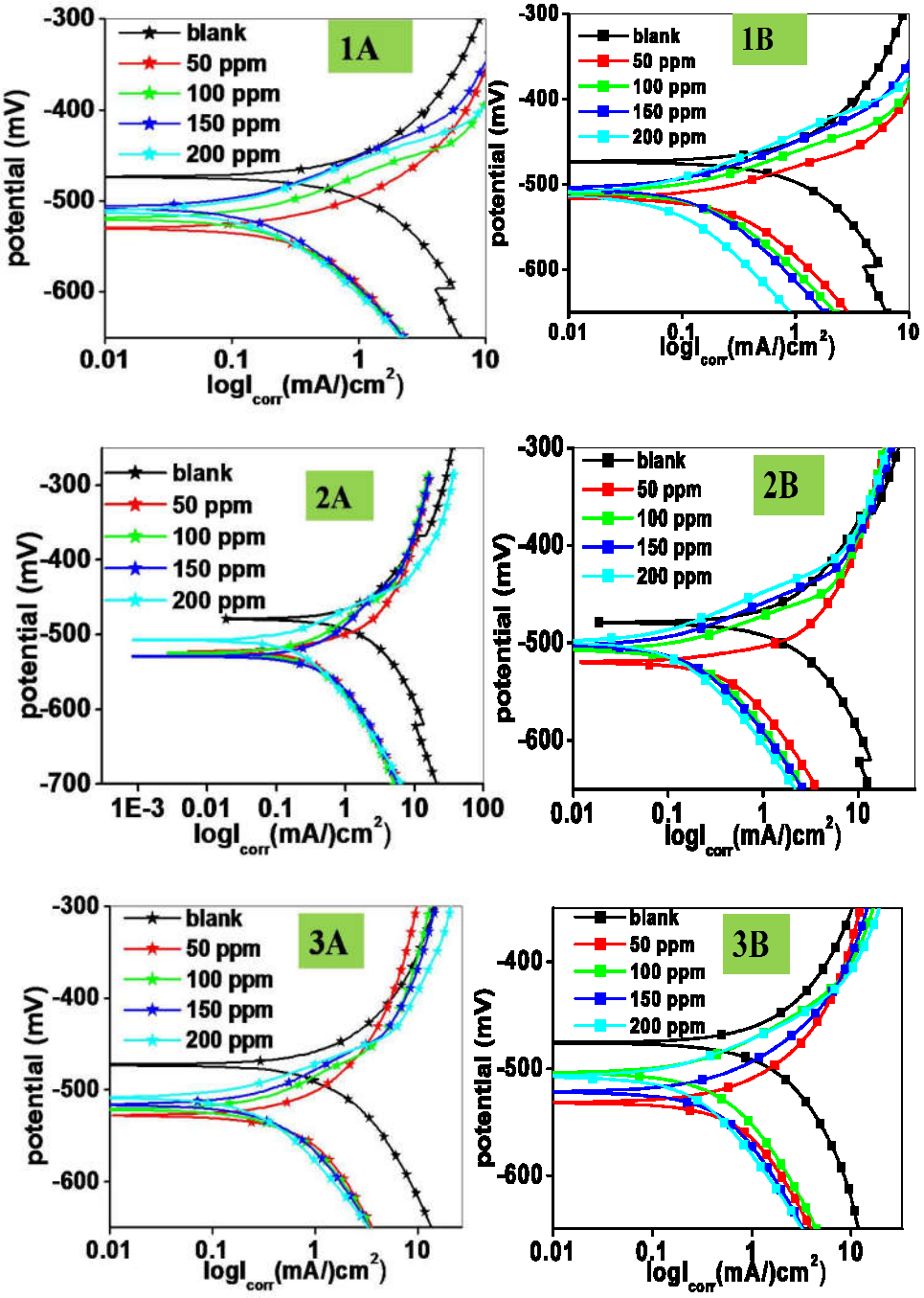

Fig 6.4 (A) Tafel plots for mild steel in 0.25 M H_2SO_4 containing (A) MBIMOT and (B) EBIMOT at (1) 303 K (2) 308 K and (c) 313 K

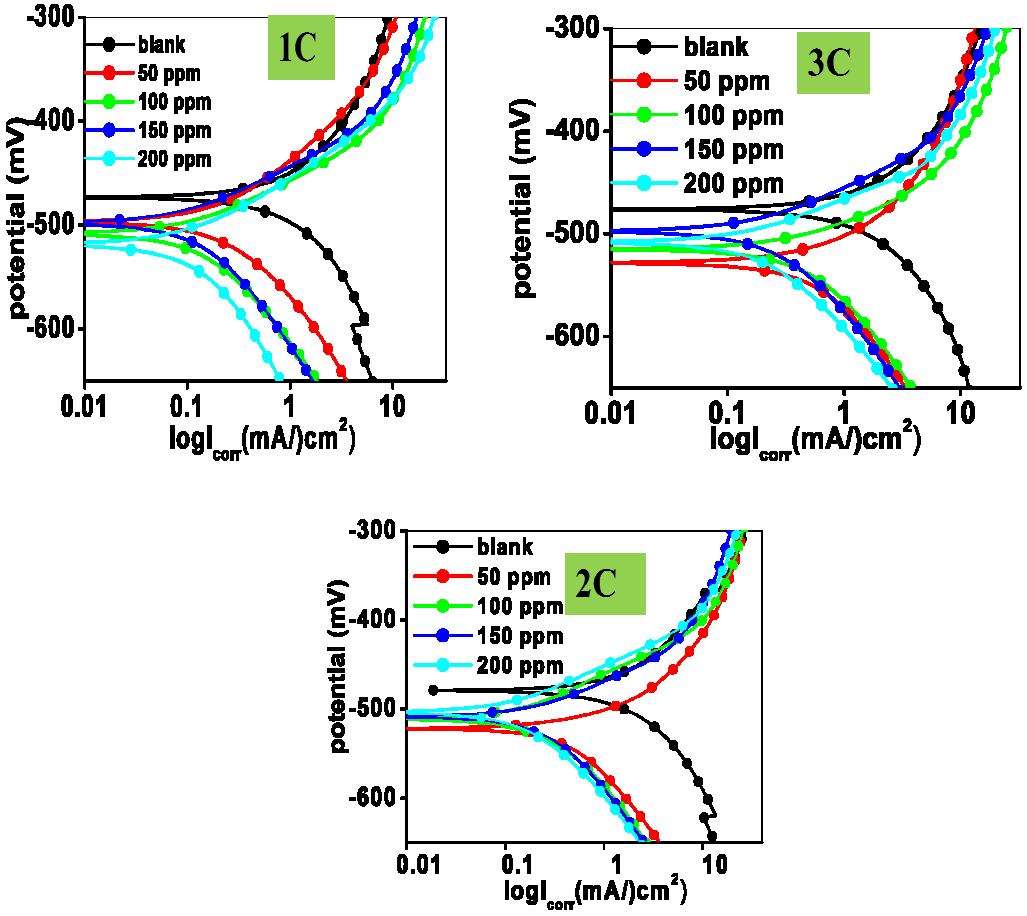

Fig 6.4(B) Tafel plots for mild steel in 0.25 M H_2SO_4 containing PBIMOT at (1) 303 K (2) 308 K and (3) 313 K

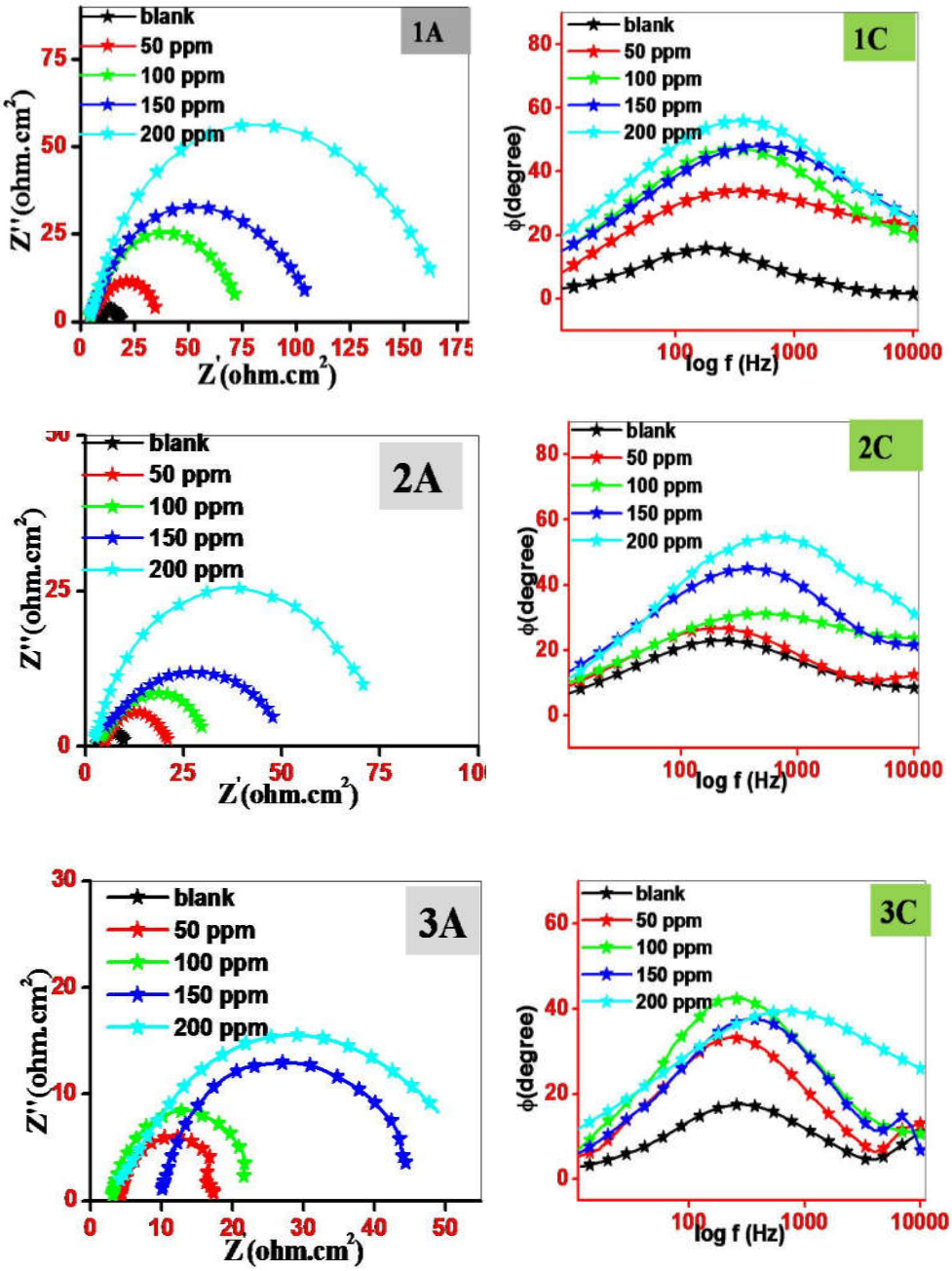

Fig 6.5(A) Nyquist (A) and Bode (C) plots of mild steel in 0.5 M HCl with MBIMOT at (1) 303 K (2) 308 K (3) 313 K

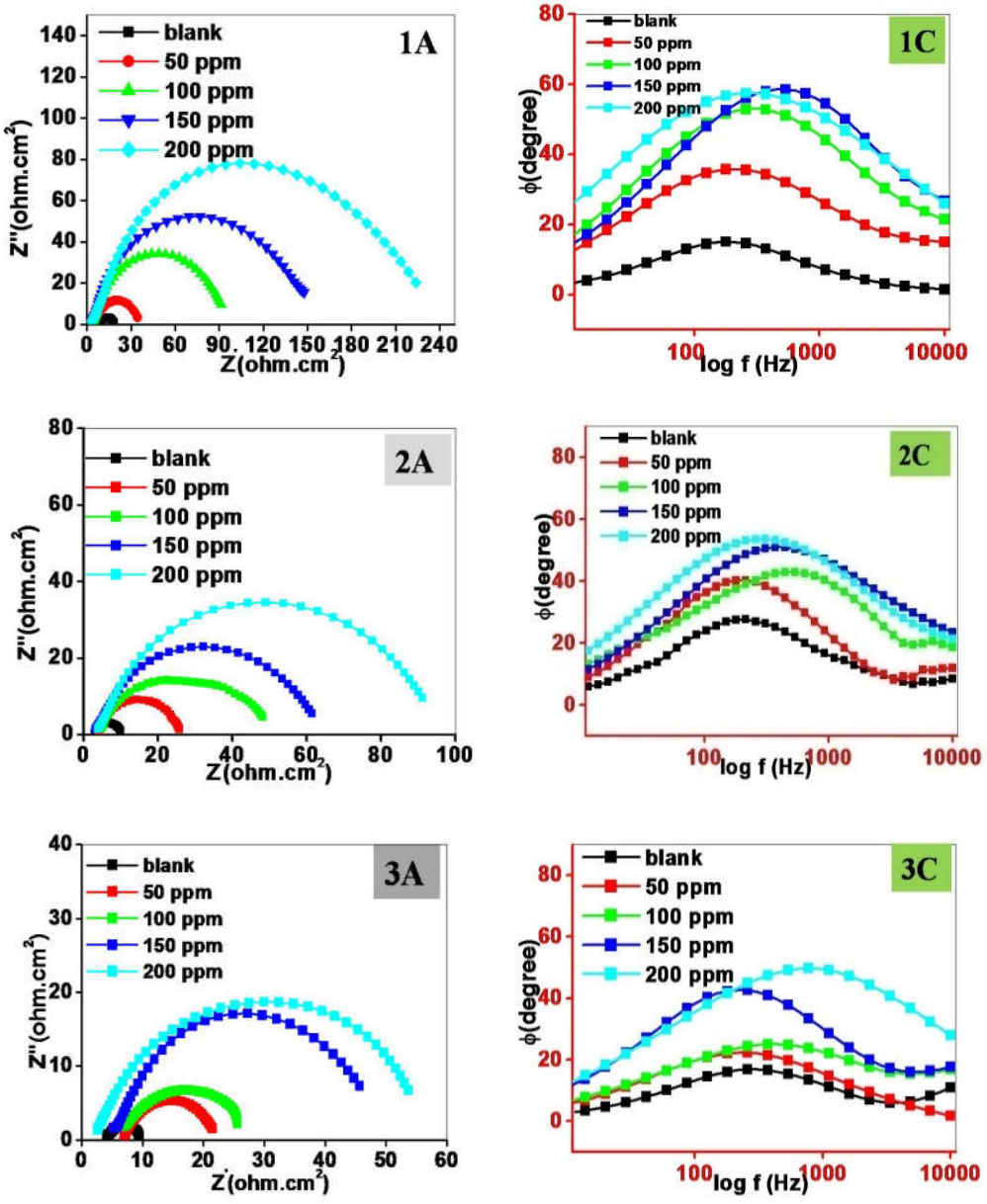

Fig 6.5(B): Nyquist (A) and Bode (C) plots of mild steel in 0.5 M HCl with EBIMOT at (1) 303 K (2) 308 K (3) 313 K

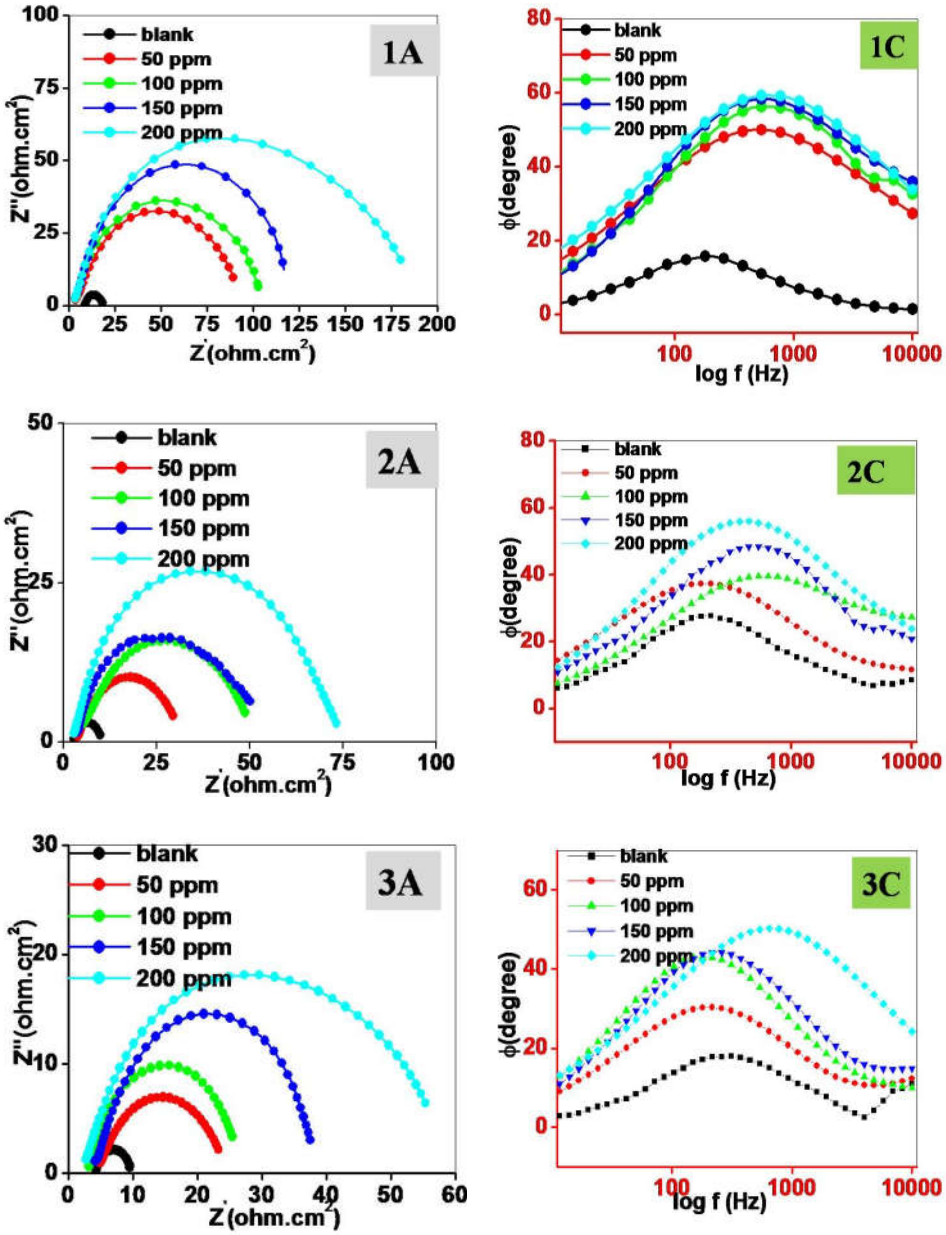

Fig 6.5(C): Nyquist (A) and Bode (C) plots of mild steel in 0.5 M HCl with PBIMOT at (1) 303 K (2) 308 K (3) 313 K

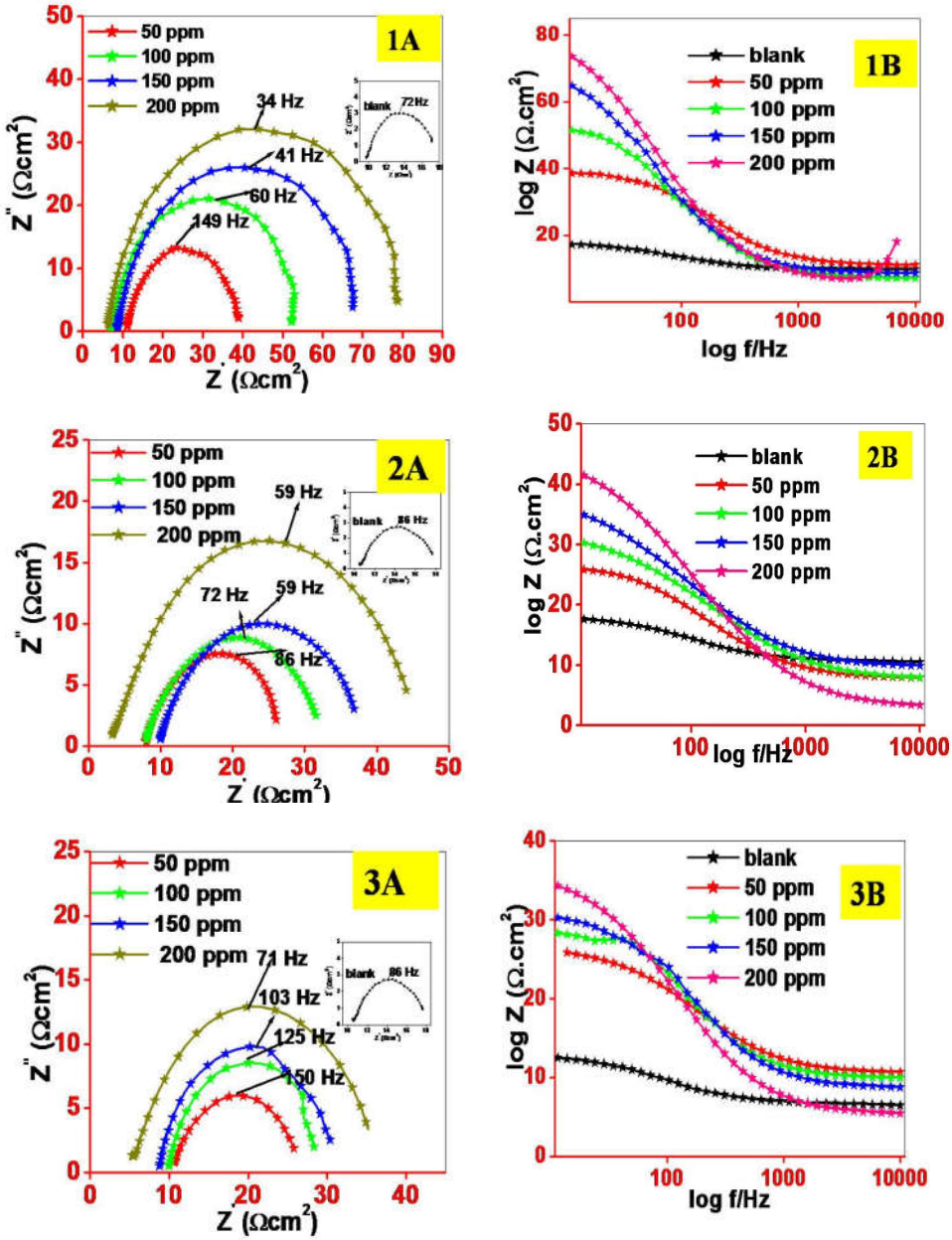

Fig 6.6(A): (A) Nyquist and (B) Bode plots for mild steel corrosion in 0.25 M H_2SO_4 containing MBIMOT at (1) 303 K (2) 308 K and (3)313K

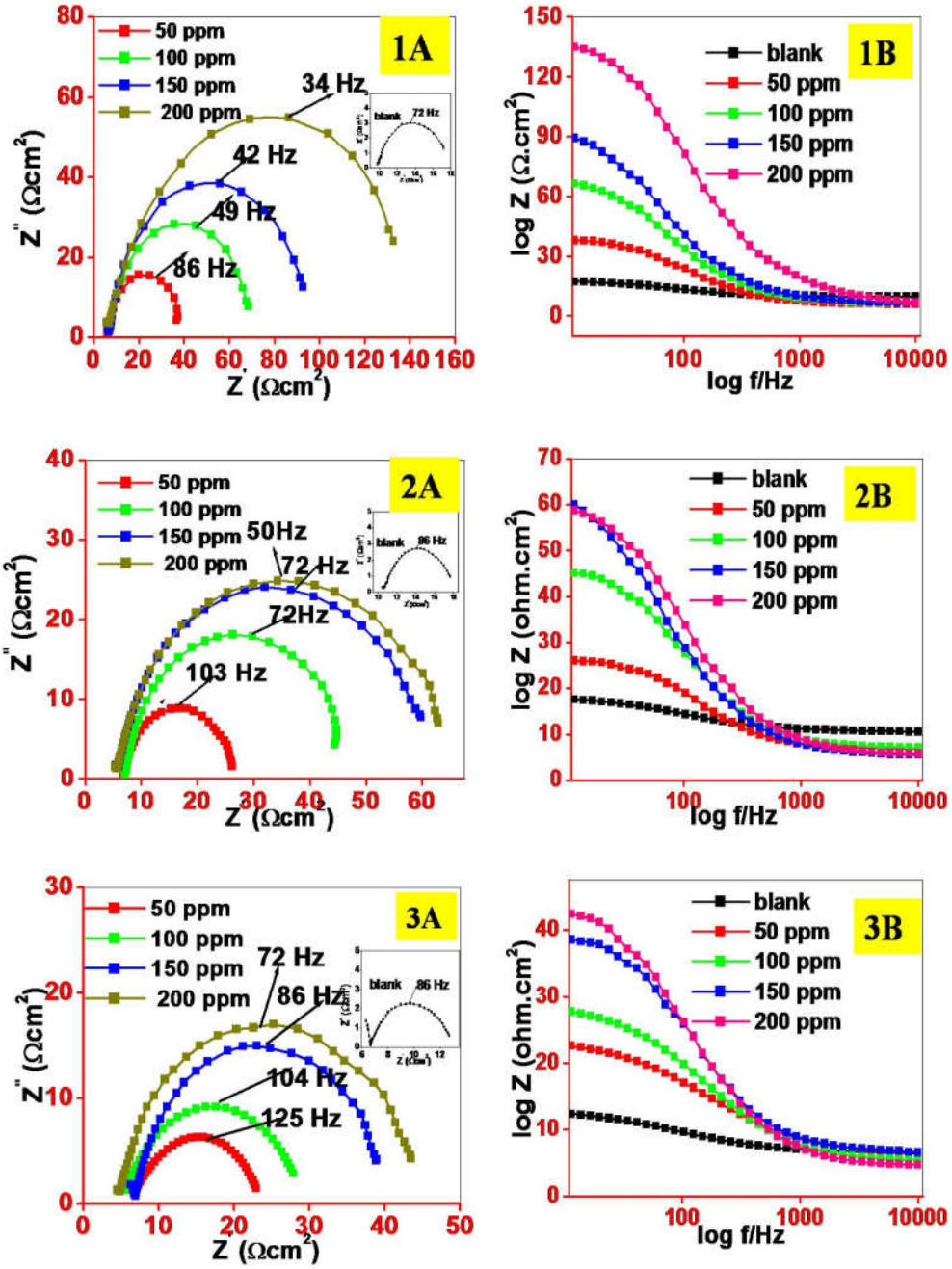

Fig 6.6 B: (A) Nyquist and (B) Bode plots for mild steel corrosion in 0.25 M H_2SO_4 containing EBIMOT at (1) 303 K (2) 308 K and (3) 313 K

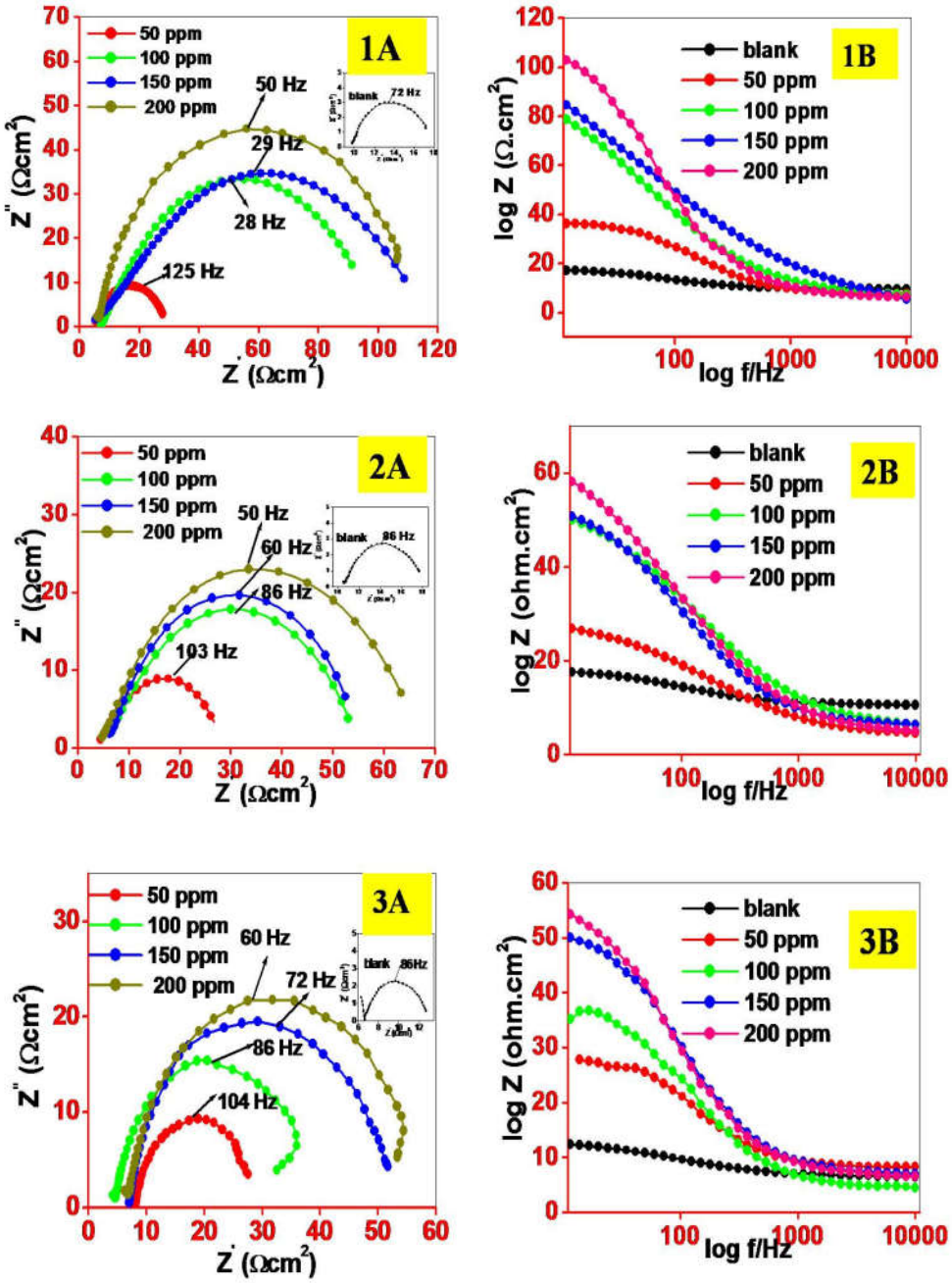

Fig 6.6 (C): (A) Nyquist and (B) Bode plots for mild steel corrosion in 0.25 M H_2SO_4 containing PBIMOT at (1) 303 K (2) 308 K (c) 313 K

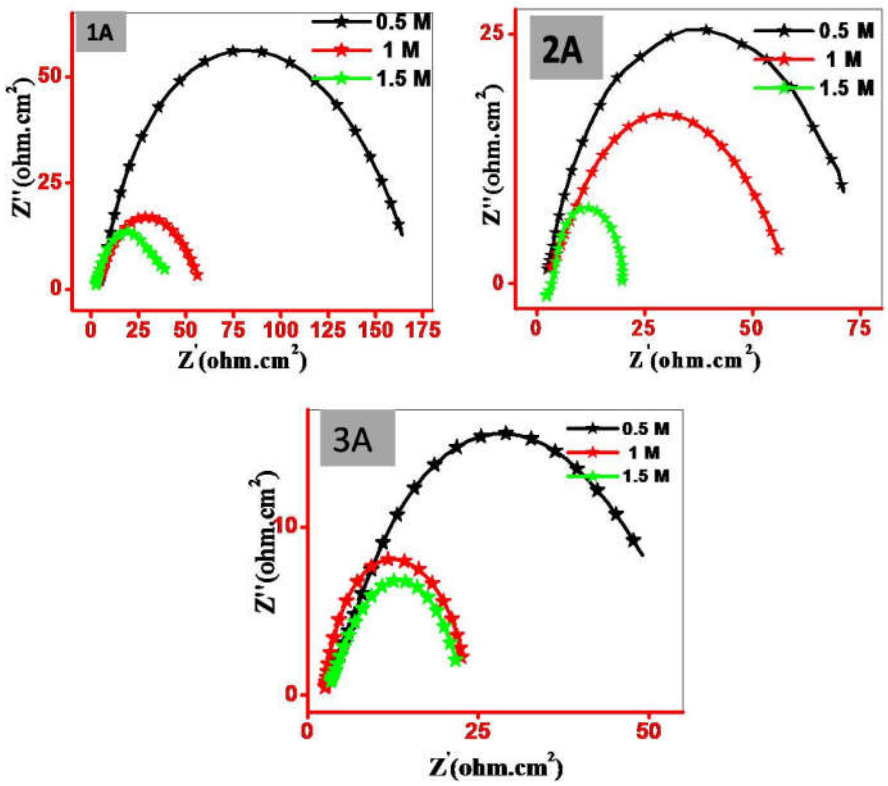

Fig 6.7 (A) Nyquist plot for mild steel corrosion in various concentrations of HCl containing 200 ppm of MBIMOT at (1) 303 K (2) 308 K (3) 313 K

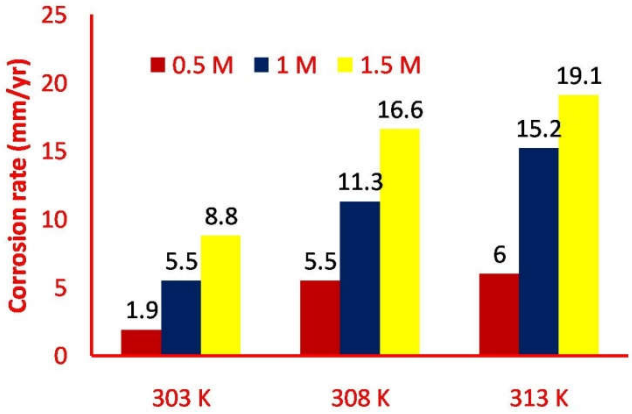

Fig 6.7 (B): Effect of acid concentration and temp. on corrosion rate of mild steel in HCl containing 200 ppm of MBIMOT

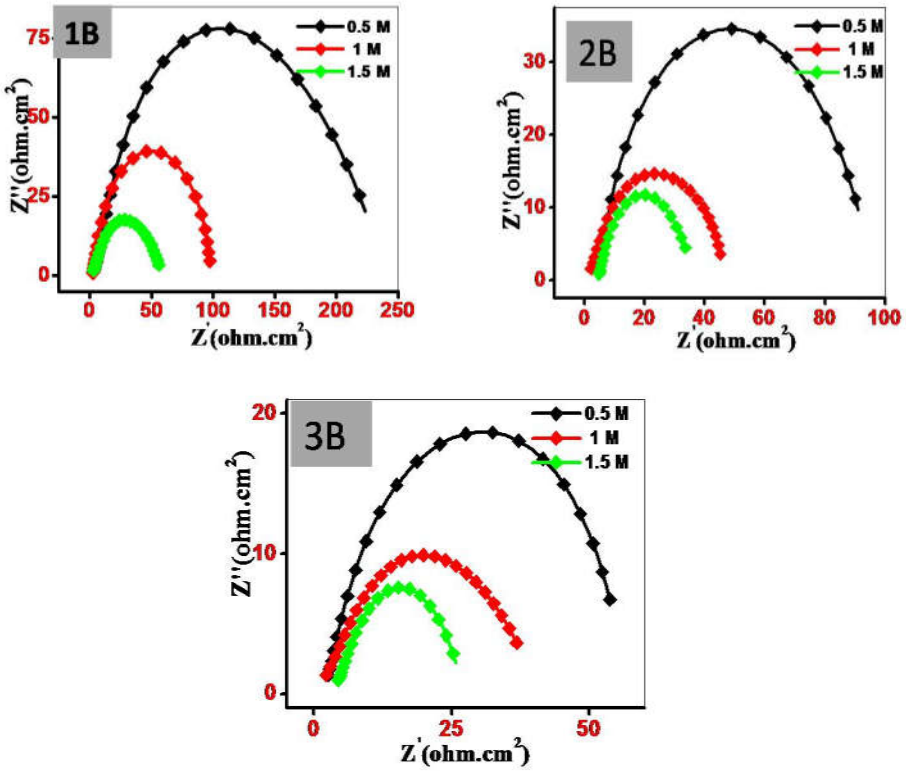

Fig 6.8 (A) Nyquist plot for mild steel corrosion in various concentrations of HCl containing 200 ppm of EBIMOT at (1) 303 K (2) 308 K (3) 313 K

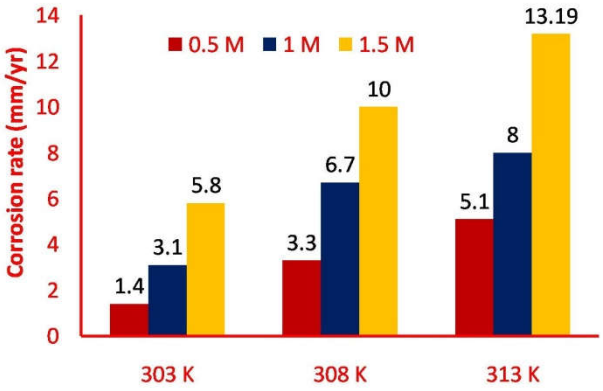

Fig 6.8 (B): Effect of acid concentration and temp. on corrosion rate of mild steel in HCl containing 200 ppm of EBIMOT

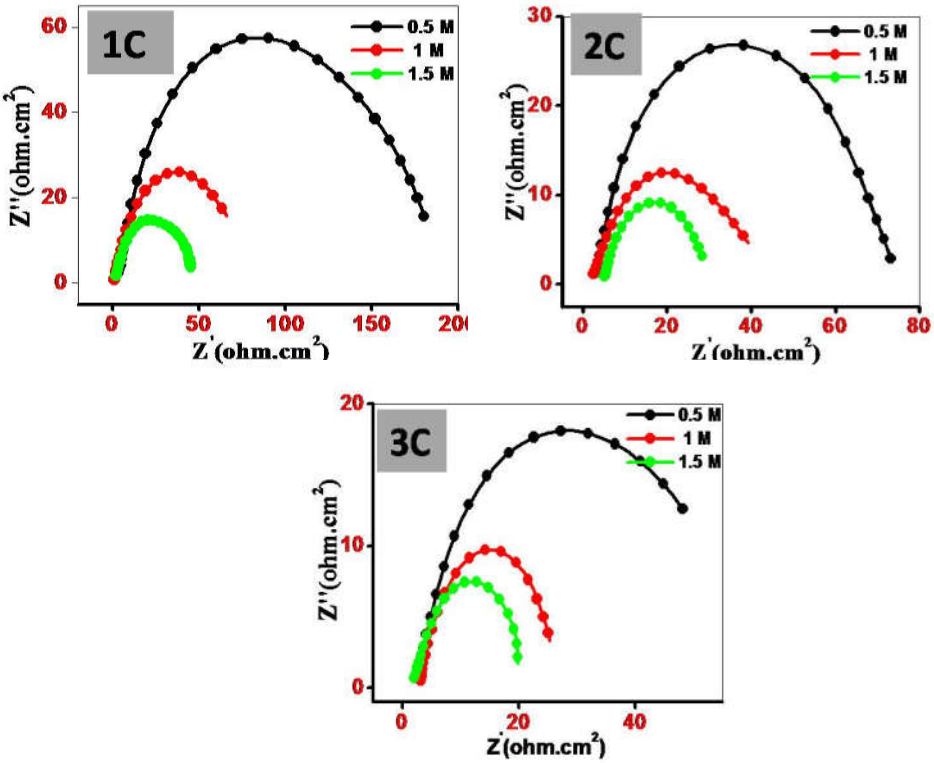

Fig 6.9 (A) Nyquist plot for mild steel corrosion in various concentrations of HCl containing 200 ppm of PBIMOT at (1) 303 K (2) 308 K (3) 313 K

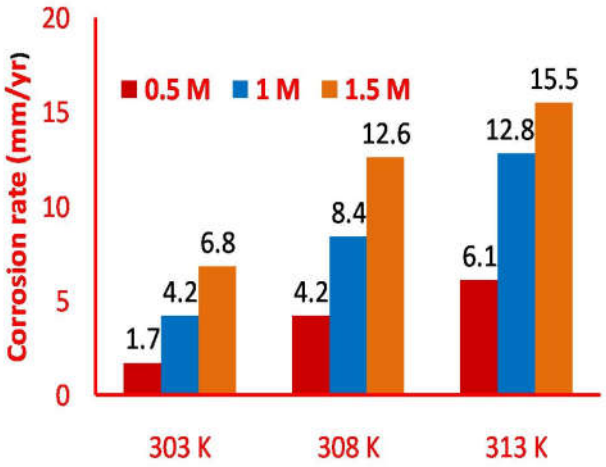

Fig 6.9 (B): Effect of acid concentration and temp. on corrosion rate of mild steel in HCl containing 200 ppm of PBIMOT

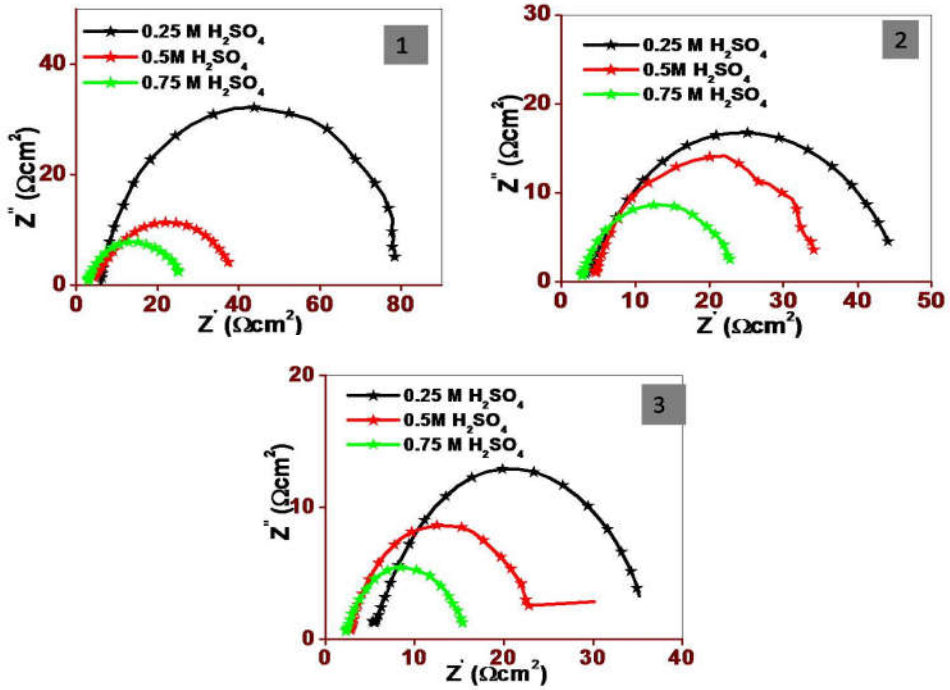

Fig 6.10 (A) Nyquist plot for mild steel corrosion in various concentrations of H_2SO_4 containing 200 ppm of MBIMOT at (1) 303 K(2) 308 K (3) 313 K

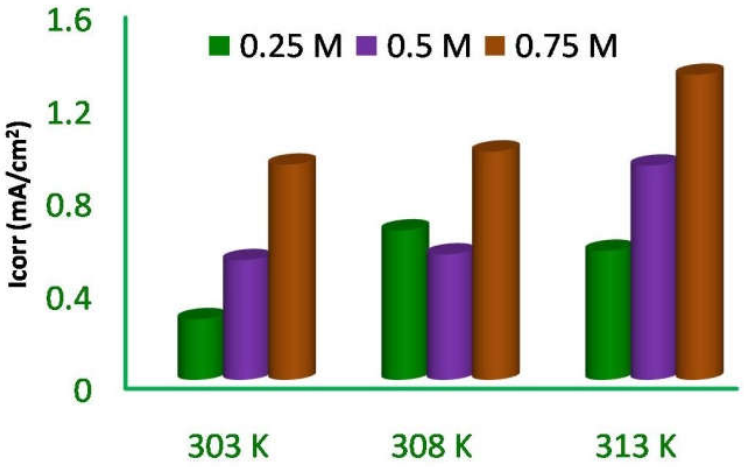

Fig 6.10(B): Effect of acid concentration on I_{corr} of mild steel in H_2SO_4 containing 200 ppm of MBIMOT

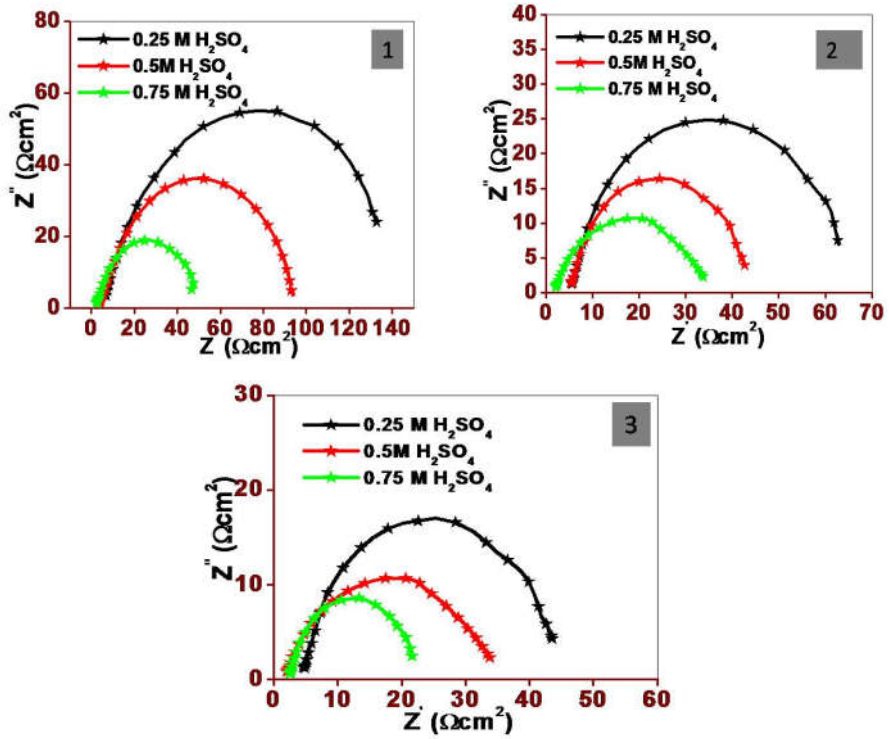

Fig 6.11 (A): Nyquist plot for mild steel corrosion in various concentrations of H_2SO_4 containing 200 ppm of EBIMOT at (1) 303 K (2) 308 K (3) 313 K

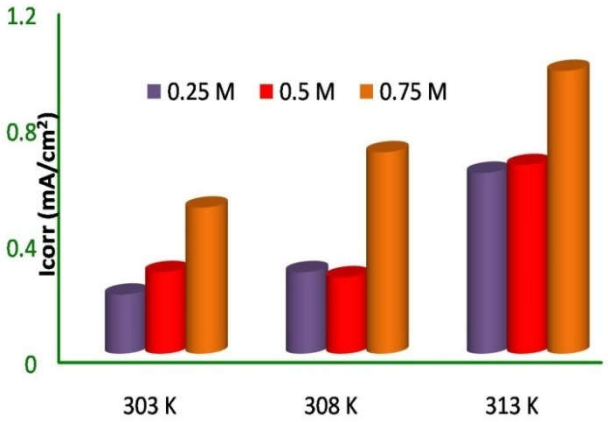

Fig 6.11 (B): Effect of acid concentration on I_{corr} of mild steel in H_2SO_4 containing 200 ppm of EBIMOT

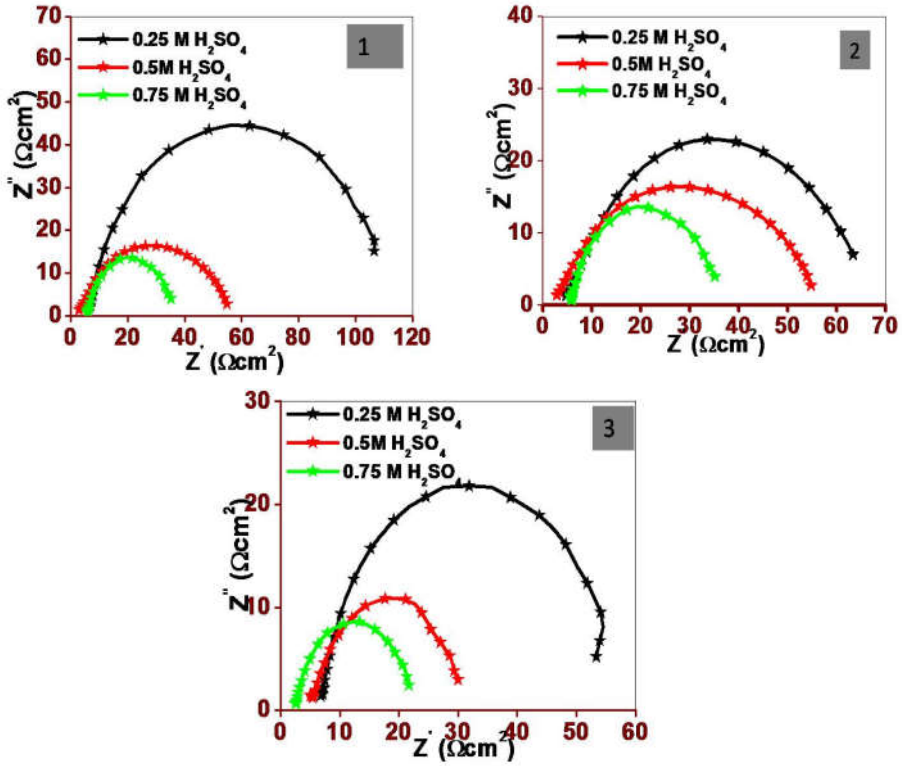

Fig 6.12 (A) Nyquist plot for mild steel corrosion in various concentrations of H_2SO_4 containing 200 ppm of PBIMOT at (1) 303 (2) 308 K (3) 313 K

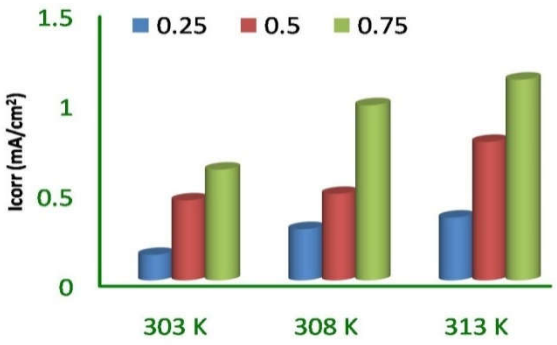

Fig 6.12 (B): Effect of acid concentration on I_{corr} of mild steel in H_2SO_4 containing 200 ppm of PBIMOT

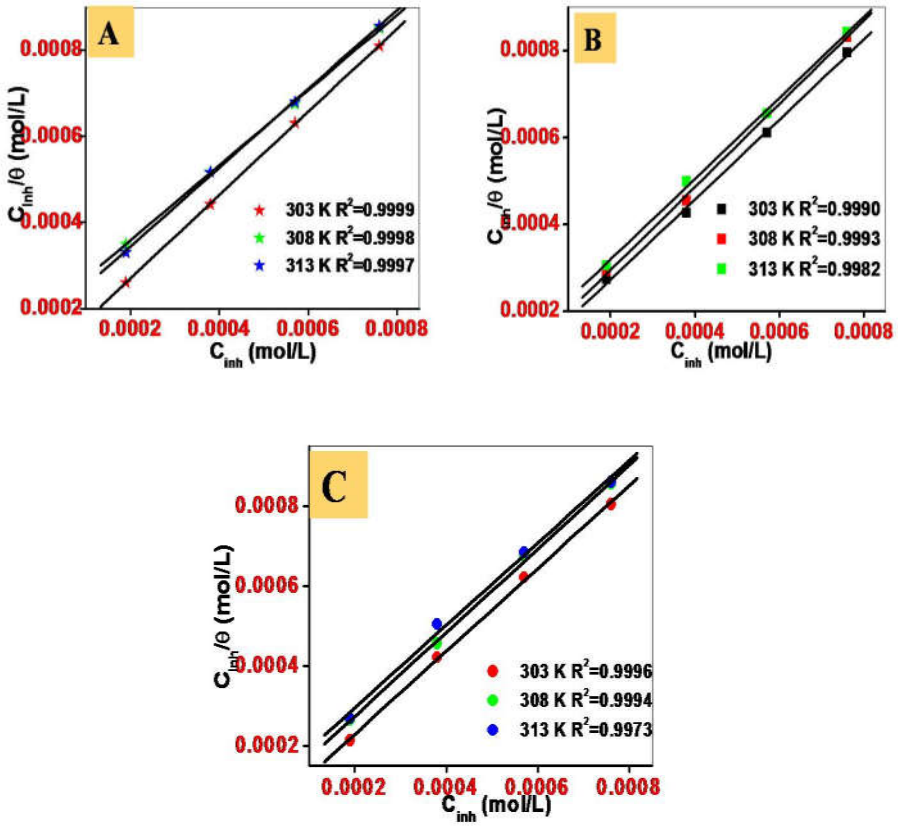

Fig 6.13 Langmuir adsorption isotherms of (A) MBIMOT (B) EBIMOT and (C) PBIMOT adsorption on mild steel in 0.5 M HCl at different temperatures

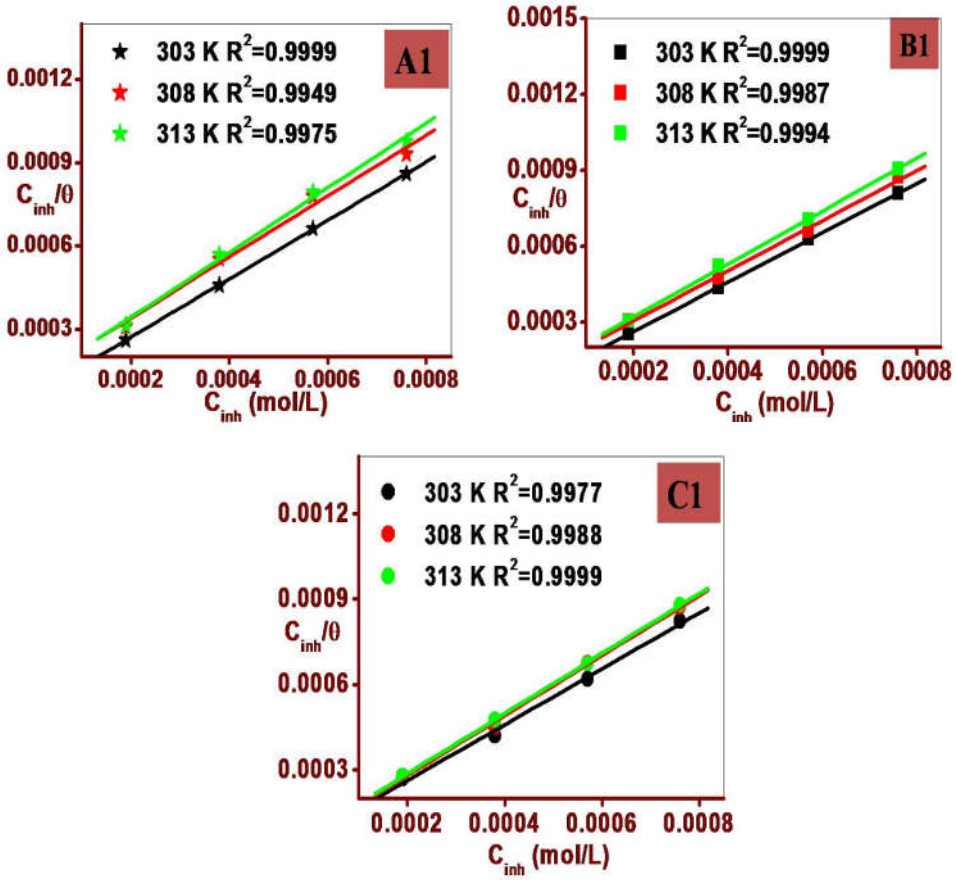

Fig 6.14 Langmuir adsorption isotherms for (A) MBIMOT (B) EBIMOT (C) PBIMOT adsorption on mild steel in 0.25 M H_2SO_4

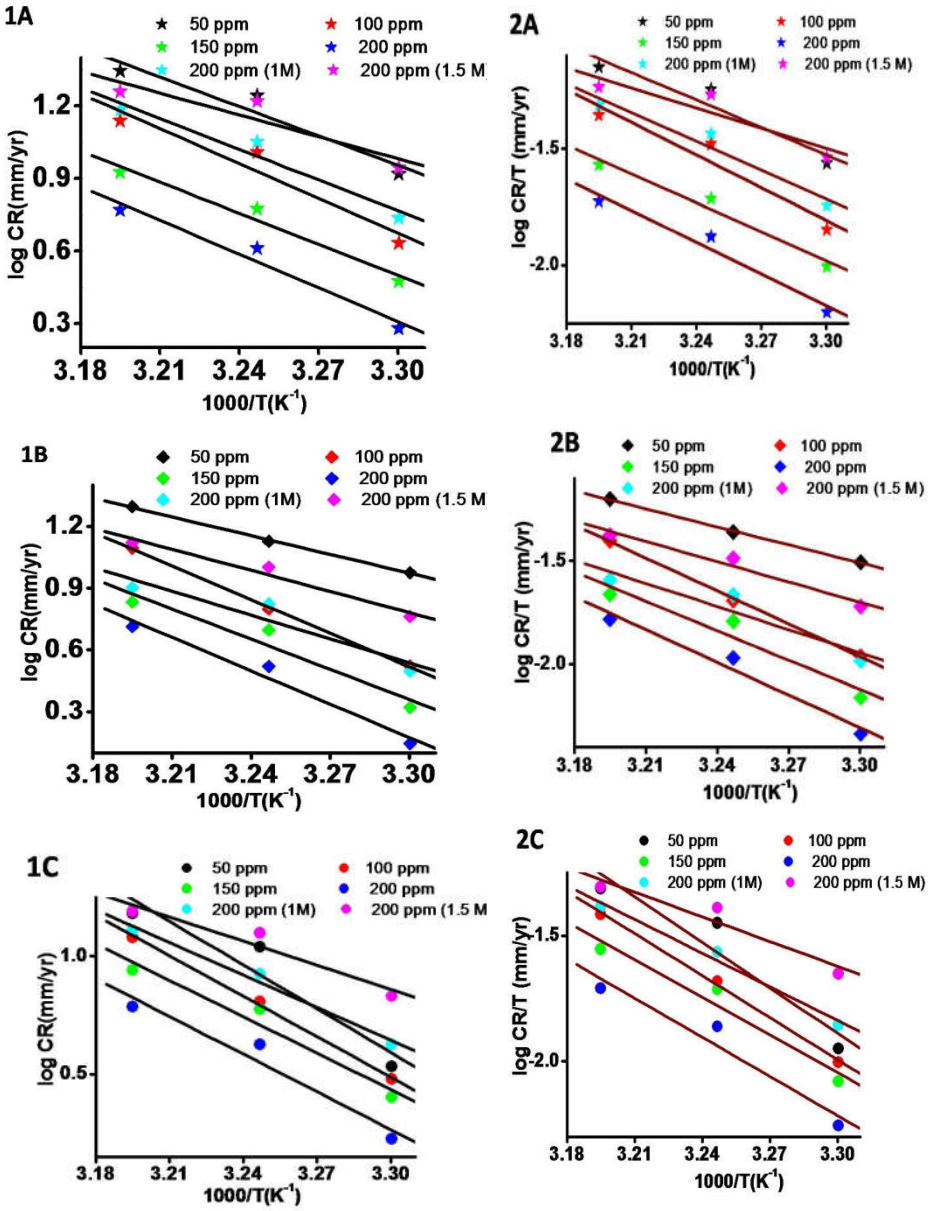

Fig 6.15 (1) Arrhenius plot of log (CR) Vs 1/T and (2) Transition state plot of log CR/T Vs 1/T for mild steel in HCl in the presence of (A) MBIMOT (B) EBIMOT and (C) PBIMOT

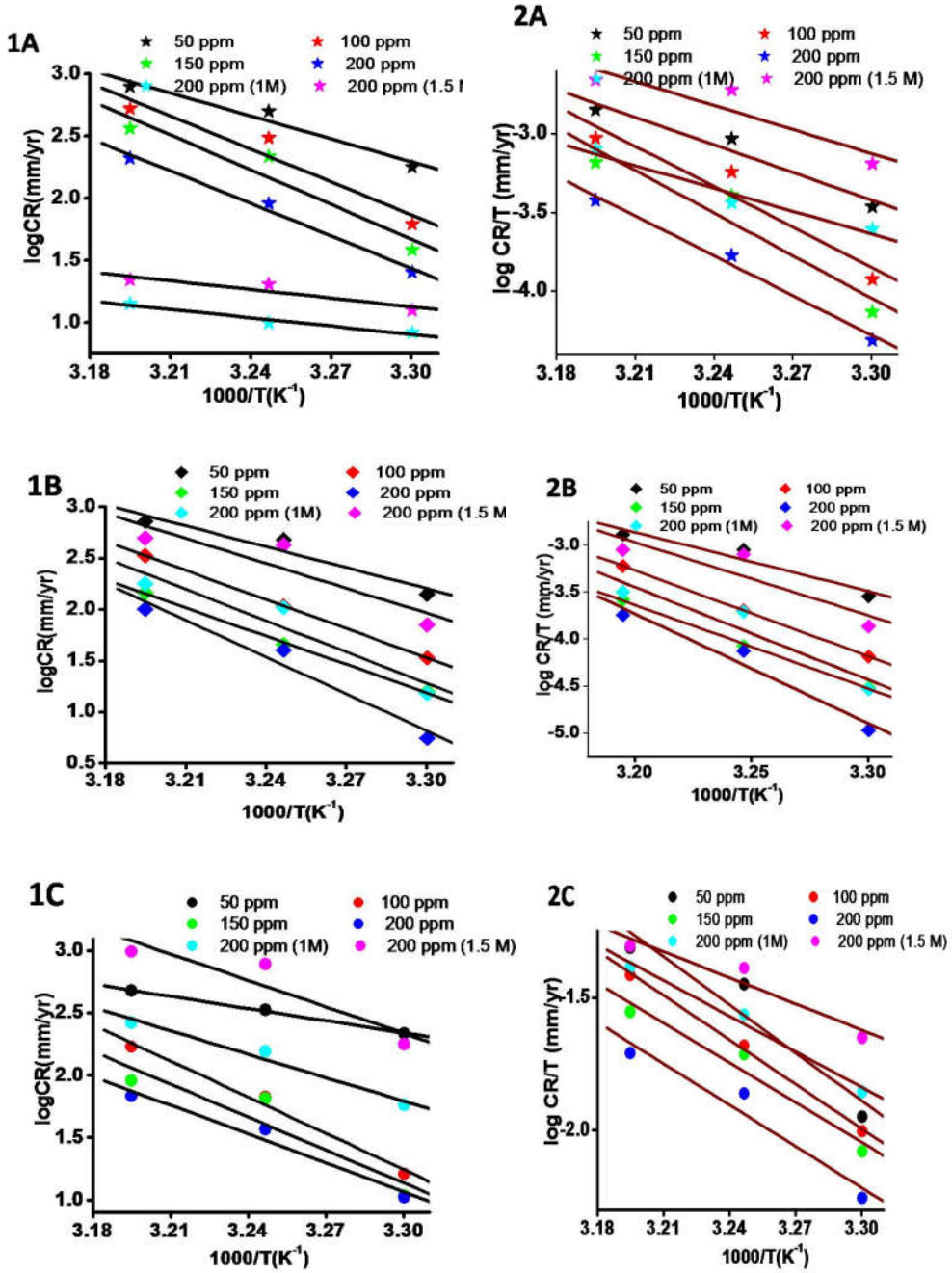

Fig.6.16 (1) Arrhenius plot of log (CR) Vs 1/T and (2) Transition state plot of log CR/T Vs 1/T for mild steel corrosion in H_2SO_4 in the presence of (A) MBIMOT (B) EBIMOT and (C) PBIMOT

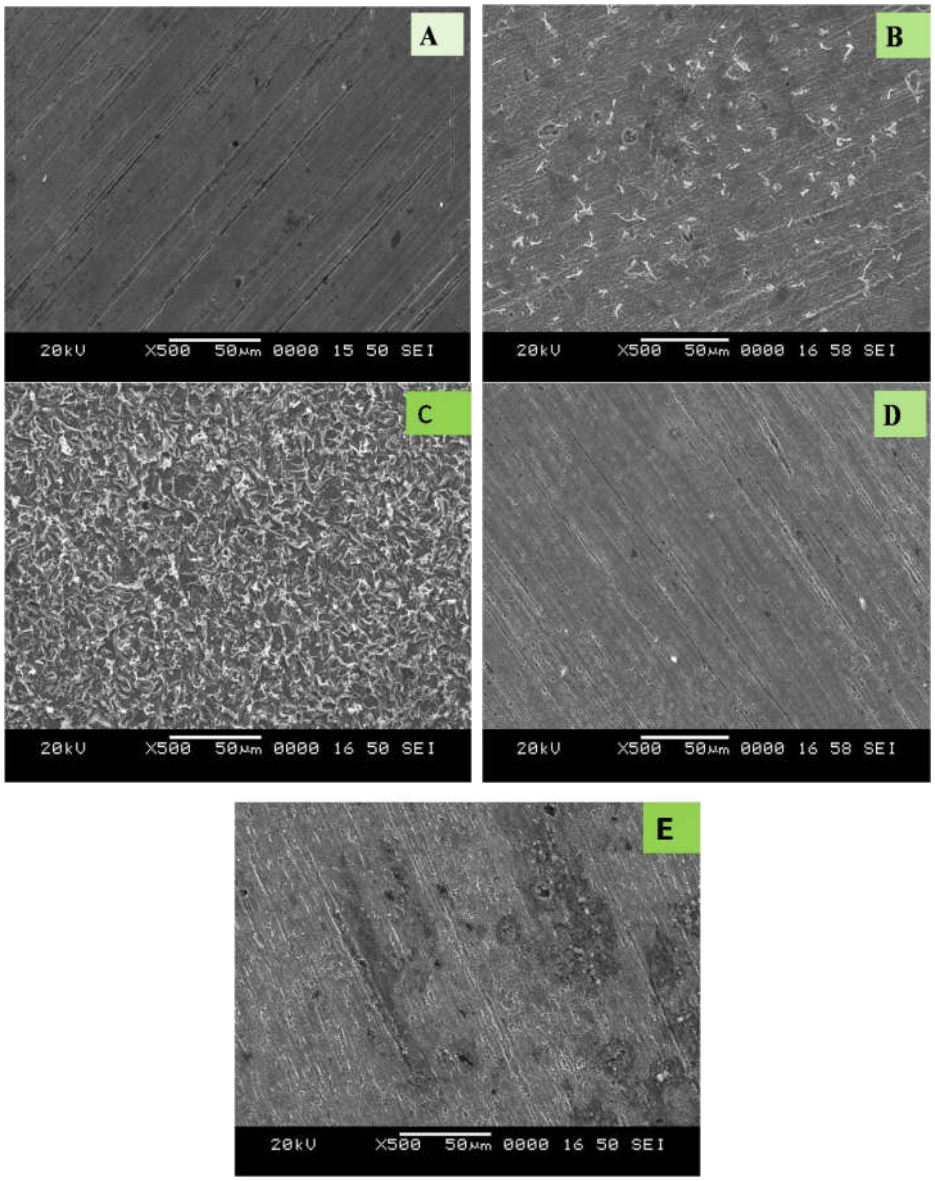

Fig 6.17 SEM micrographs of (A) bare mild steel (B) mild steel immersed in 0.5 M HCl (C) mild steel in 0.25 M H_2SO_4 (D) mild steel in HCl + EBIMOT (E) mild steel in H_2SO_4 + PBIMOT

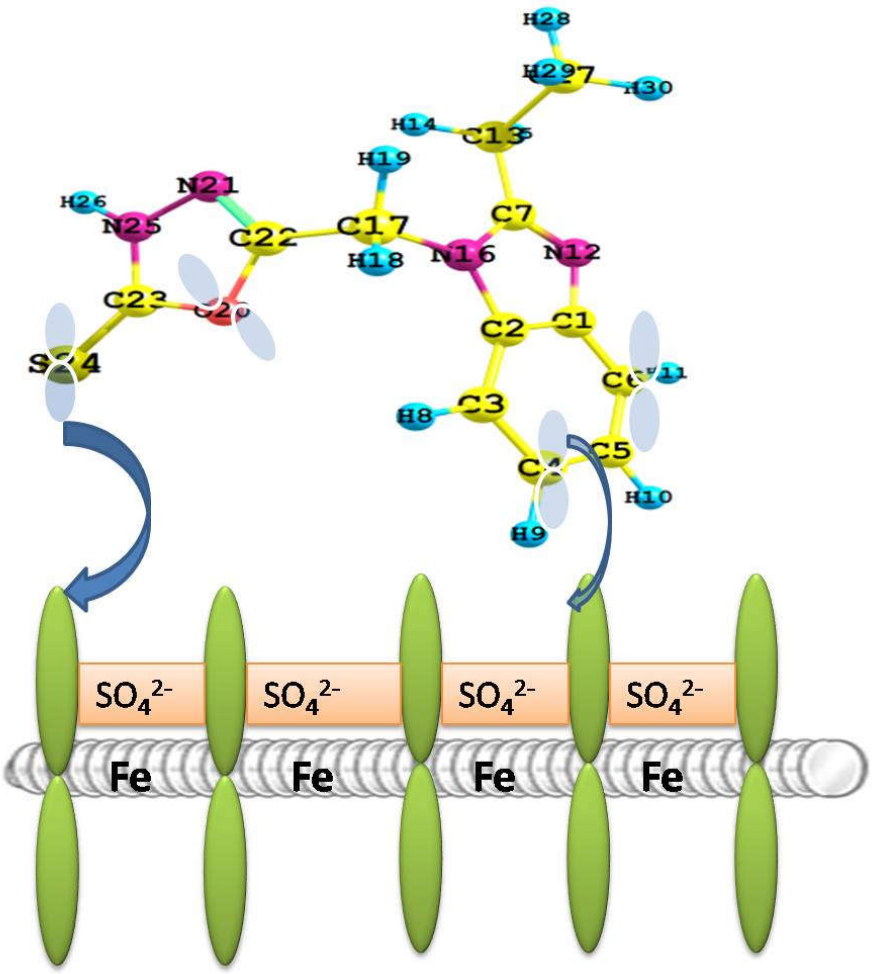

Fig 6.18: Mechanism of corrosion inhibition of mild steel in acidic solutions by MBIMOT

References

1. K.F. Khaled, *Electrochim.Acta*, 48 (**2003**) 2493

2. V.M. Abbasov , M Hany. Abd El-Lateef, L.I. Aliyeva, E.E. Qasimov, I.T. Ismayilov Mai, M. Khalaf, Egyp. J. of Pet., 22 (2013) 451

3. V B Singh, Ray Monali , Int. J. Electrochem. Sci., 2 (2007) 329

4. Surfactants in Tribology volume 4 text book

5. J. Saranya, P. Sounthari, K. Parameswari, S. Chitra, Measurement, 77 **(**2016) 186

6. K.Babic Samardzija, K.F.Khaled, N.Hackerman, Anti corros Method., *M*, 52 (2005) 11

7. H.M. Abd El-Lateef, A.H. Tantawy, RSC Ad**v: 6** (2016) 8681

8. A.Pourghasemi, Hanza, R.Naderi, E.Kowsari, M.Sayebani, Corros.Sci., 107 (2016) 96

9. D Daoud, T Douadi, S Issaadi, S Chafaa, Corros. Sci. 79 (2014) 58

10. P. Singh, E.E. Ebenso, L.O. Olasunkanmi, I.B. Obot, M.A. Quraishi, J. Phys. Chem. C 120 (2016) 3408

11. Monika Srivastava, Preeti Tiwari, Sanjay Kumar, Srivastava Rajiv Prakash Gopal , J.Mol.Liq., 236 (2017) 184

12. Evelin Gutierrez, Jose A.Ratriguez, Julian Cruz Borbolla, Pandiyan Thangarasu, Corros.Sci., 108 (2016) 23

13. Revathi Mohan, Abraham Joseph, Res.Chem.Intermediate., 41 (2015) 4795

14. E E Ebenso., E E Oguzie,. Mater. Lett. , 59 (17) (2005) 2163

15. A. Zarrouk , B. Hammouti , H. Zarrok , S.S. Al-Deyab , M. Messali Int. J. Electrochem. Sci., 6 (2011) 6261

16. M.R. Laamari , J. Benzakour , F. Berrekhis , A. Derja , D. Villemin, Arab. J. Chem., 9 (2016) S245

17. D Wahyuningrum, S Achmad, Y M Syah, B Buchari, B, Bundjali, Ariwahjoedi, Int. J. Electrochem. Sci. 3 (2008) 154

18. K.J. Laidler, Reaction Kinetics, Pergamon Press, New York, 1963

19. B M Mistry, N S Patyl, S Sahoo, S Junhari, Bull. Mater. Sci.35 (2012) 459

20. H. Ma, S. Chen, B. Yin, S. Zhao, X. Liu, Corros. Sci. 45 (2003) 867

21. G. Banerjee, S.N. Malhotra, Corrosion., 48 (1992) 10

22. M. Lebrini, M. Lagrenee, H. Vezin, L. Gengembre, F. Bentiss, Corros. Sci. 47 (2005) 485.

23. Deng, X. Li Corros. Sci. 64 (2012) 253

24. M Karthik, Sundara vadivelu , P. Rajkumar, Res.Chem. Intermed., 41 (2015) 1543

25. M. Farsak, H. Keles and M. Keles, Corros. Sci., 98 (2015) 223

26. N.O. Obi-Egbedi, I.B. Obot, M.I. El-Khaiary, J. Mol. Struct. 1002 (2001) 86

27. I.B. Obot, N.O. Obi-Egbedi, S.A. Umoren, Corros. Sci. 51 (2009) 1868

28. Y.M. Tang, Y. Chen, W.Z. Yang, W. Liu, Z.S. Yin, J.T. Wang, Mater.Chem. Phys. 116 (2009) 479.

29. M. Bouklah, N. Benchat, A. Aouniti, B. Hammouti, M. Benkaddour, M.Lagrenee, H. Vezin, F. Bentiss, Prog. Org. Coat. 51 (2004), 118

30. Gokhan Gece, Corros. Sci. 50 (2008) 2981

31. N. Soltani, M. Behpour, E.E. Oguzie, M.Mahlugi, M.A Ghasemzadeh, *RSC Adv.,* RA-ART-10-2014-011642.R2 (2014)

32. K.F. Khaled et al. *Electrochimica Acta*, 50 (2005) 2515

7 CORROSION INHIBITION OF MILD STEEL IN HNO_3 USING BENZIMIDAZOLE BEARING 1,3,4-OXADIAZOLE DERIVATIVES, MBIMOT, EBIMOT AND PBIMOT

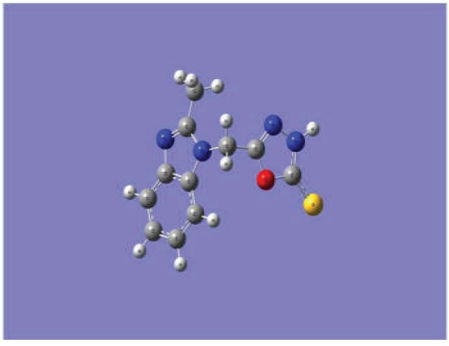

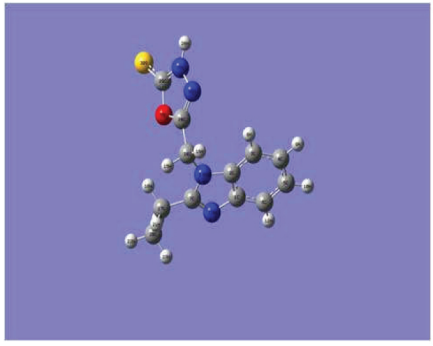

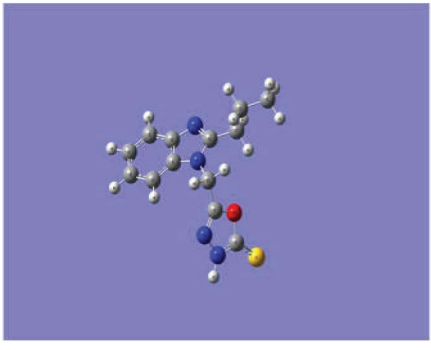

The effect of MBIMOT, EBIMOT and PBIMOT on the corrosion of mild steel in 0.25 M HNO_3 is illustrated in Chapter VII. The investigation was done using electro analytical techniques like EIS and PDP. The effect of temperature on corrosion inhibition was analysed for five different temperatures. The inhibitive mechanism, kinetics and adsorption properties of mild steel in 0.25 M HNO_3 have also been discussed.

VII.1 Introduction

Human community is trying to understand and control the corrosion process as long as they have been using metal objects. During the metal cleaning process like acid pickling, acid descaling etc. the metals like mild steel are very much prone to corrosion. The practice of using corrosion inhibitors is one of the most cost effective ways to mitigate corrosion [1]. A detailed review of literature has shown that a very little work has been reported on mild steel corrosion in HNO_3 medium. It has been reported that HNO_3 at low concentrations is more corrosive than other mineral acids of comparable concentration and its peculiar nature as strong oxidizing agent makes its corrosion behavior more significant [2,3]. Iron and steel found to become passive at concentrated HNO_3 but at lower concentrations they get dissolved [4]. The use of organic compounds as corrosion inhibitors for mild steel in HNO_3 was scarcely tried because of the presumption of its low stability and poor inhibition capacity in this medium [5]. However, some successful corrosion inhibitors of mild steel corrosion in HNO_3 was also reported [6, 7, 8]. In continuation of our quest for developing corrosion inhibitors with high efficiency for mild steel in HNO_3, the inhibition studies of the three 5-((2-alkyl-1H-benzo[d]imidazol-1-yl)methyl)-1,3,4 oxadiazole-2-thiol derivatives (MBIMOT, EBIMOT and PBIMOT) were presented in this chapter. The inhibitors were synthesized and characterized as described in chapter II (Section II.3.2). Various electroanalytical, thermodynamic and kinetic studies were done to examine the effect of inhibitor concentration and temperature on corrosion inhibition.

VII.2 Results and discussion

VII.2.1 Electrochemical measurements:

VII.2.1.1 Electrochemical impedance spectroscopy (EIS)

EIS measurements are performed to study the metal/electrolyte solution interface characteristics. The Nyquist plots at various temperatures (303 K – 323 K) are represented in Fig 7.1 A-C. The Nyquist plots are depressed semi circles with their centers lying below the real impedance axis. It is clear from these plots that the impedance response has appreciably changed after the introduction of inhibitor into the corrosive medium and the impedance as well as the radius of Nyquist plots has increased with increase in concentrations of inhibitor which indicate the involvement of charge transfer phenomenon in corrosion process [9]. The depressed nature is characteristic of solid electrodes which often subjected to frequency dispersion due to roughness and other inhomogeneities of metal surface [10-12]. Various electrochemical parameters like charge transfer resistance (R_{ct}), double layer capacitance (C_{dl}) etc., are extracted by fitting the experimental data to Randles circuit (Fig 1.3) and inhibition efficiency (IE) was calculated using the eqn.(2.3) and are tabulated in Tables 7.1 A-C. The perusal of tables revealed that in the case of these inhibitors, an increase in IE as well as R_{ct} and a decrease in C_{dl} were occurred with an increase in concentration of inhibitors at these temperatures. The increase in R_{ct} is attributed to the formation of a protective film on the metal/solution interface. The decrease in the C_{dl} values can be due to the replacement of high dielectric water molecules by low dielectric organic inhibitor molecules [13-15]. R_{ct} as well as IE show a decrease and CR shows an increase with temperature indicated the role of adsorption of inhibitors on corrosion inhibition which becomes difficult at higher temperatures due to a tendency for desorption [16, 17]. The EIS measurements revealed that EBIMOT is best among these inhibitors

with an efficiency of 97% for 200 ppm at 303 K and inhibition efficiency follows the order EBIMOT > PBIMOT > MBIMOT.

VII.2.1.2 Potentiodynamic polarization studies (Tafel extrapolation)

The effect of the addition of varying concentrations of inhibitors on anodic and cathodic Tafel curves at temperatures 303 K to 323 K are shown in Fig 7.2A-C. The electrochemical parameters like corrosion potential (E_{corr}), corrosion current density (i_{corr}), anodic and cathodic Tafel slopes (β_a and β_c) were determined using the extrapolation of anodic and cathodic Tafel curves to E_{corr} and IE was calculated using (eqn. 2.4) and the parameters obtained are given in Table 7.2A-C. The addition of inhibitors has little effect on the general shape of anodic and cathodic Tafel curves, but the corrosion current density showed a remarkable decrease in its value. Table 7.2A-C exemplifies the effectiveness of these inhibitors against mild steel in 0.25 M HNO_3. There is a considerable increase in i_{corr} with temperature due to increased corrosion rate which is schematically represented by the Fig7.3. The difference of E_{corr} before and after the addition of inhibitors was found to be within 85 mV suggested mixed type behavior of inhibitors [18, 19]. The mixed type behaviors of the inhibitors are by getting adsorbed on the metal surface and blocking the active sites of corrosion and reduce the anodic metal dissolution and retard the cathodic reduction of HNO_3 to liberate oxides of nitrogen [20]. The inhibition efficiency values of these inhibitors obtained by PDP method are in good agreement with EIS measurements.

VII.2.2 Effect of temperature on corrosion

The interdependence of temperature and corrosion rate is studied from kinetic parameters which are extracted from Arrhenius and Transition state equations (eqn. 5.2 and 5.3) [22]. Activation parameters like apparent activation energy (E_a), apparent enthalpy of activation (ΔH_a^0), and apparent

entropy of activation (ΔS_a^0) for the dissolution of iron into 0.25 M HNO_3 were determined by incorporating the corrosion rate in mm/year as obtained from EIS measurements into Arrhenius plot and transition state plots (Fig 7.4). The slope and intercept of these plots helped to calculate the activation parameters and are presented in Table 7.3. The addition of inhibitors into the aggressive medium has remarkably increased the activation energy for iron dissolution and this increase in activation energy in the presence of inhibitors supported a predominant physisorption mechanism [23]. The positive values of ΔH_a^0 suggested an endothermic nature for metal dissolution and an increase in ΔH_a^0 in presence of inhibitors reflected the formation of activated complex in the rate determining step [24]. The larger values of Ea compared to the analogues ΔH_a^0 values suggested the involvement of gaseous reactions in corrosion process, the evolution of hydrogen and NO_2 associated with a decrease in total reaction volume. The difference between Ea and ΔH_a^0 is 2.6 kJ/mol approximately equal to the average value of RT indicated the unimolecular mechanism of corrosion process [25]. The negative values of ΔS_a^0 indicated the activated complex formation in the rate determining step as association rather than dissociation and an ordering takes place on going from reactants to activated complex. The increase in ΔS_a^0 in the presence of inhibitors compared to that in blank suggest the replacement of water molecules on the metal surface by inhibitor molecules which helps in retarding the metal dissolution and hydrogen evolution [26].

VII.2.3 Adsorption studies

The foremost and essential step of corrosion inhibition is assumed to be the adsorption of inhibitor molecules at the metal/solution interface by a quasi-substitution process between the organic compound in the aqueous phase and adsorbed water molecules as per the eqn. (1.7). The fitting of surface coverage (θ) obtained from impedance measurements to various

isotherms, the Langmuir adsorption isotherm was found to be the best fitted one with approximately unit regression coefficient and slope. The isotherms for the adsorption of inhibitors on mild steel in 0.25 M HNO_3 at 303 K to 323 K was represented in Fig 7.5. They indicated a monolayer adsorption at all studied temperatures. At higher temperatures the slope showed deviations from unity, which means a non ideal simulation due to interactions between the adsorbed species on metal surface [21]. The reciprocal of the intercept of the isotherms represent equilibrium constant K_{ads}, from which the free energy of adsorption was calculated using the eqn. (5.5). The adsorption parameters listed in Table 7.4 revealed a strong adsorption of inhibitors as evident from high K_{ads} values. The negative values of free energy change which lies in between −20 kJ/mol and −40 kJ/mol implied a comprehensive mixed physicochemical adsorption.

VII.2.4 Corrosion and inhibition mechanism in nitric acid

It has been reported that the corrosion of mild steel in nitric acid was not a simple homogeneous process, but consists of various intermediate steps [2]. The cathodic corrosion reaction in nitric acid involves the following steps [6]

$$H^+ + e^- \rightarrow H \tag{7.1}$$

$$HNO_3 + H^+ + e^- \rightarrow NO_2 + H_2O \tag{7.2}$$

$$NO_2 + e^- \rightarrow NO_2^- \tag{7.3}$$

$$H^+ + NO_2^- \rightarrow HNO_2 \tag{7.4}$$

$$HNO_2 + H \rightarrow H_2O + NO \tag{7.5}$$

The HNO_2 formed in eqn. (7.4) regenerates NO_2 by an interaction with nitric acid by the reaction and the reaction is auto catalytic.

$$HNO_2 + HNO_3 \rightarrow 2NO_2 + H_2O \quad (7.6)$$

Ammonium salts are also formed during the cathodic reaction which decomposes to form N_2 and NO_x compounds. So the cathodic reaction is not the evolution of H_2 gas as in the case of other acids, but a mixture of gases like NO_2, N_2, NO etc. are evolved.

The anodic reaction is the oxidation of iron to its +2 oxidation state.

$$Fe \rightarrow Fe^{2+} + 2\,e^- \quad (7.7)$$

The oxidizing nature of HNO_3 may promote oxide formation on mild steel and at higher concentration a passivation can result.

The corrosion inhibition of mild steel in nitric acid can be explained as follows: The organic corrosion inhibitors have a tendency to protonate in acidic solutions and there will be equilibrium between the neutral and cationic form of inhibitor molecules [27]. If the metal surface is positive, the negative ions of the acid solution NO_3^- will first get adsorbed on the metal surface as $(FeNO_3^-)ads$ which in turn attract the cationic form of inhibitors in addition to protonated water molecules forming an electrostatic bond (physisorption). So a protective triple layer will be formed on the metal surface and inhibit iron from coming into contact with the corrosive medium. Also the neutral inhibitor molecules get adsorbed on the metal surface by removing adsorbed water molecules through its active centres. This confirms the role of a physicochemical adsorption in corrosion inhibition.

VII.2.5 Surface morphological studies

Surface morphologies were analysed using SEM techniques. Fig 7.6 represents the SEM images of polished mild steel surface and the same immersed in 0.25 M HNO_3 without and with inhibitors at 303 K. From SEM

images it is clear that the mild steel surface immersed in 0.25 M HNO_3 without inhibitor is damaged severely by acid attack and is full of pits and cracks, but the one in the presence of inhibitors Fig7.6 C – E is more smooth with visible picture of adsorbed layer of inhibitor molecules.

Conclusions

1, 3, 4-oxadiazole derivatives act as powerful corrosion inhibitors for mild steel in 0.25 M $HNO_3$and reduce the corrosion rate to a large extent at lower and higher temperatures following the order of inhibition efficacy as EBIMOT > PBIMOT > MBIMOT. The highest inhibition efficiency of EBIMOT can be correlated with its lowest E_{LUMO} value and highest dipole moment which suggested the contribution of back donation of electrons from iron atom in adsorption and corrosion inhibition. The electro analytical measurements along with adsorption studies suggested the formation of protective mono layer of inhibitors on the metal surface which prevents both anodic and cathodic corrosion reaction and is further confirmed by surface morphological studies. The kinetic, thermodynamic and adsorption studies revealed the prominent role of physisorption in corrosion inhibition.

Table 7.1A: AC impedance parameters for mild steel corrosion in 0.25 M HNO_3 in presence of various concentrations of MBIMOT at different temperatures

Temp. K	Cinh ppm	R_{ct} Ωcm^2	C_{dl} x10^{-4} F	CR mm/yr	IE %
303	0	4.539	12.06	66.61	--
	50	19.84	6.976	15.24	77.12
	100	42.53	4.836	7.109	89.30
	150	48.94	9.445	6.178	90.70
	200	66.17	2.157	4.569	93.10
308	0	3.290	17.03	78.19	--
	50	9.659	9.929	31.30	65.93
	100	26.87	4.231	11.25	87.70
	150	30.12	4.022	10.04	89.00
	200	37.27	3.265	8.112	91.17
313	0	3.638	10.67	83.11	--
	50	7.269	10.40	41.59	49.95
	100	25.64	2.860	11.79	85.81
	150	28.27	2.596	10.70	87.13
	200	33.56	2.588	9.009	89.16
318	0	3.905	30.30	87.43	--
	50	7.100	7.146	49.66	45.00
	100	15.33	7.097	19.72	74.53
	150	21.71	4.248	13.93	82.01
	200	33.78	2.402	9.950	88.44
323	0	3.243	15.99	93.23	--
	50	5.820	17.07	79.15	44.27
	100	10.66	5.830	28.36	69.58
	150	17.06	3.689	17.72	80.99
	200	21.35	2.906	14.16	84.81

Table 7.1B: AC impedance parameters for mild steel corrosion in 0.25 M HNO_3 in presence of various concentrations of EBIMOT at different temperatures

Temp K	Cinh ppm	R_{ct} Ωcm^2	C_{dl} $x10^{-4}$ F	CR mm/yr	IE %
	0	4.539	12.06	66.61	--
	50	31.33	3.023	9.650	85.51
303	100	47.42	2.080	6.410	90.40
	150	68.39	2.646	4.431	93.36
	200	161.9	1.392	1.867	97.19
	0	3.290	17.03	78.19	--
	50	29.33	2.532	10.29	88.80
308	100	35.50	1.969	8.517	90.70
	150	45.89	1.532	6.589	92.80
	200	63.41	1.569	4.768	94.80
	0	3.638	10.67	83.11	--
	50	12.43	12.85	24.32	70.73
313	100	30.126	1.847	9.992	87.97
	150	41.00	1.623	7.382	91.12
	200	58.77	1.611	5.145	93.80
	0	3.905	30.30	87.43	--
	50	7.681	9.772	39.36	49.16
318	100	25.97	3.713	11.64	84.90
	150	28.26	1.823	10.70	86.18
	200	34.27	2.916	8.823	88.60
	0	3.243	15.99	93.23	--
	50	5.668	11.18	53.34	42.70
323	100	11.97	6.40	25.36	72.91
	150	22.17	3.317	13.64	85.30
	200	31.78	2.40	9.514	89.80

Table 7.1C: AC impedance parameters for mild steel corrosion in 0.25 M HNO_3 in presence of various concentrations of PBIMOT at different temperatures

Temp K	Cinh ppm	R_{ct} Ωcm^2	C_{dl} $x10^{-4}$ F	CR mm/yr	IE %
303	0	4.539	12.06	66.61	--
	50	25.06	6.928	12.06	81.88
	100	62.41	2.128	4.845	92.70
	150	68.66	2.088	4.404	93.30
	200	78.05	1.823	3.874	94.10
308	0	3.290	17.03	78.19	--
	50	19.17	5.701	15.77	82.80
	100	32.30	3.961	9.361	89.80
	150	35.36	2.041	8.351	90.60
	200	40.56	2.694	7.454	91.80
313	0	3.638	10.67	83.11	--
	50	12.08	5.452	25.03	69.88
	100	24.86	1.967	12.16	85.30
	150	35.98	1.853	8.403	89.88
	200	41.81	1.727	7.231	91.29
318	0	3.905	30.30	87.43	--
	50	6.842	9.112	44.19	42.92
	100	23.12	4.439	13.08	83.10
	150	26.32	2.237	11.49	85.16
	200	33.52	1.533	9.020	88.30
323	0	3.243	15.99	93.23	--
	50	5.014	25.91	60.30	35.3
	100	12.52	6.104	24.15	74.10
	150	21.40	3.858	14.13	84.80
	200	26.75	2.004	11.30	87.80

Table 7.2A: Electrochemical parameters for mild steel determined from polarization measurements in 0.25 M HNO_3 solution without and with various concentrations of MBIMOT

Temp. K	Cinh ppm	$-E_{corr}$ mV	I_{corr} mA/cm^2	β_a mV/ dec	$-\beta_c$ mV/ dec	IE %
	0	508	3.157	267	273	--
	50	513	0.8912	96	199	71.77
303	100	500	0.4708	87	193	85.10
	150	513	0.4042	139	195	87.20
	200	502	0.2722	86	162	91.40
	0	505	3.212	309	317	--
	50	542	1.2452	114	150	61.20
308	100	516	0.5122	104	146	84.00
	150	518	0.4606	84	138	85.70
	200	507	0.3629	82	137	88.70
	0	522	3.3744	236	239	--
	50	521	1.2906	190	225	40.00
313	100	526	0.6528	114	163	80.65
	150	515	0.5959	91	180	82.34
	200	515	0.5257	91	163	84.42
	0	516	4.3211	245	313	--
	50	536	2.7991	205	245	35.20
318	100	538	1.1587	135	212	73.18
	150	520	0.9540	138	211	77.90
	200	517	0.6867	113	193	84.10
	0	521	4.3495	214	318	--
	50	527	3.7779	228	232	13.14
323	100	537	1.1838	87	144	72.78
	150	515	0.7330	87	157	83.10
	200	520	0.7196	112	169	83.40

Table 7.2B: Electrochemical parameters for mild steel determined from polarization measurements in 0.25M HNO_3 solution without and with various concentrations of EBIMOT

Temp. K	Cinh ppm	$-E_{corr}$ mV	I_{corr} mA/cm^2	β_a mV/ dec	$-\beta_c$ mV/ dec	IE %
	0	508	3.157	267	273	--
	50	509	0.6193	98	207	80.38
303	100	506	0.4068	88	182	87.11
	150	496	0.3644	107	200	88.40
	200	494	0.1506	83	160	95.22
	0	505	3.212	309	317	--
	50	536	0.5809	79	108	81.91
308	100	543	0.4067	111	103	87.34
	150	536	0.3167	108	127	90.10
	200	502	0.2317	87	133	92.70
	0	522	3.3744	236	239	--
	50	536	1.1966	135	189	64.53
313	100	517	0.5353	115	182	84.14
	150	515	0.3976	124	171	88.22
	200	502	0.3429	100	172	89.83
	0	516	4.3211	245	313	--
	50	518	2.1466	202	225	50.32
318	100	521	0.7231	88	166	83.26
	150	516	0.6359	99	169	85.30
	200	523	0.5496	115	153	87.30
	0	521	4.3495	214	318	--
	50	533	2.6409	173	207	39.28
323	100	535	1.1742	140	202	73.00
	150	516	0.6666	96	190	84.67
	200	562	0.5745	79	172	86.79

Table 7.2C: Electrochemical parameters for mild steel determined from polarization measurements in 0.25M HNO_3 solution without and with various concentrations of PBIMOT

Temp. K	Cinh ppm	$-E_{corr}$ mV	I_{corr} mA/cm^2	β_a mV/ dec	$-\beta_c$ mV/ dec	IE %
	0	508	3.157	267	273	--
	50	506	0.6783	124	180	78.50
	100	506	0.3350	87	168	87.30
303	150	508	0.2734	82	160	91.30
	200	500	0.2151	86	141	93.19
	0	505	3.212	309	317	--
	50	514	0.9147	100	188	71.50
	100	518	0.5066	96	154	84.20
308	150	509	0.4149	83	163	87.00
	200	466	0.2004	74	180	93.70
	0	522	3.3744	236	239	--
	50	513	1.2906	110	217	61.75
	100	513	0.8117	87	172	75.94
313	150	519	0.5405	97	163	83.98
	200	509	0.4375	99	168	87.00
	0	516	4.3211	245	313	--
	50	519	2.4521	231	250	43.20
	100	520	0.8802	158	195	79.60
318	150	509	0.8362	108	198	80.65
	200	506	0.6000	116	190	86.10
	0	521	4.3495	214	318	--
	50	522	2.5394	389	313	41.60
	100	508	0.9231	113	194	78.77
323	150	509	0.8713	110	189	79.96
	200	511	0.7636	122	188	82.44

Table 7.3: Corrosion kinetic parameters for mild steel corrosion in 0.25 M HNO_3 in the absence and presence of MBIMOT, EBIMOT and PBIMOT

	Cinh (ppm)	Ea (kJ/mol)	ΔS_a^0 (kJ/mol)	ΔH_a^0 (kJ/mol)	Ea−ΔH_a^0
blank	--	12.82	−76.48	10.22	2.60
MBIMOT	50	61.30	−11.93	58.70	2.60
	100	54.11	−25.53	51.50	2.62
	150	39.71	−46.35	37.11	2.60
	200	40.31	−46.48	37.67	2.64
EBIMOT	50	77.47	8.53	74.87	2.60
	100	49.60	−32.64	47.00	2.60
	150	44.51	−40.89	41.90	2.61
	200	63.37	−16.23	60.77	2.60
PBIMOT	50	69.12	−2.31	66.58	2.54
	100	57.81	−21.19	55.20	2.60
	150	43.30	−42.23	40.70	2,60
	200	38.68	−49.25	36.07	2.61

Table 7.4: Adsorption parameters MBIMOT, EBIMOT and PBIMOT on mild steel in 0.25 M HNO_3

inhibitor	Temp.	slope	K_{ads} M^{-1}	$-\Delta G^0_{ads}$ kJ/mol
	303 K	1.0067	19608	35.02
	308 K	0.9702	11363	34.20
MBIMOT	313 K	0.9784	5695	32.96
	318 K	0.788	4044	32.58
	323 K	0.8270	4001	33.07
	303 K	0.9838	24125	35.44
	308 K	1.0307	44179	37.68
EBIMOT	313 K	0.9571	10537	34.56
	318 K	0.8691	5896	33.58
	323 K	0.7111	3541	32.74
	303 K	1.0025	27000	35.80
	308 K	1.0533	36900	37.20
PBIMOT	313 K	0.9845	12800	35.10
	318 K	0.7716	4160	32.70
	323 K	0.6008	2763	32.10

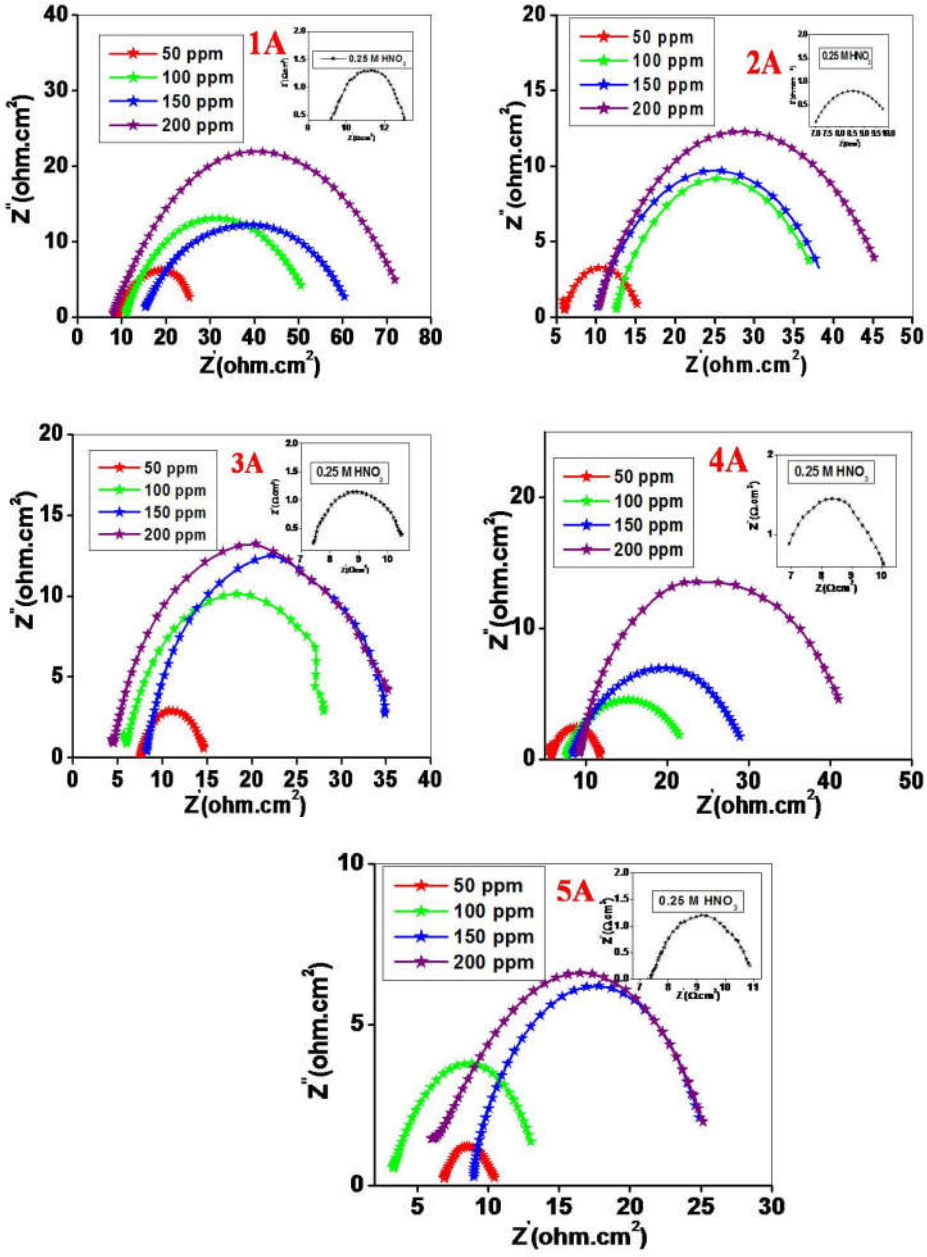

Fig 7.1 (A): Nyquist plots for mild steel in 0.25 M HNO_3 without and with MBIMOT at (1) 303 K (2) 308 K (3) 313 K (4) 318 K (5) 323 K

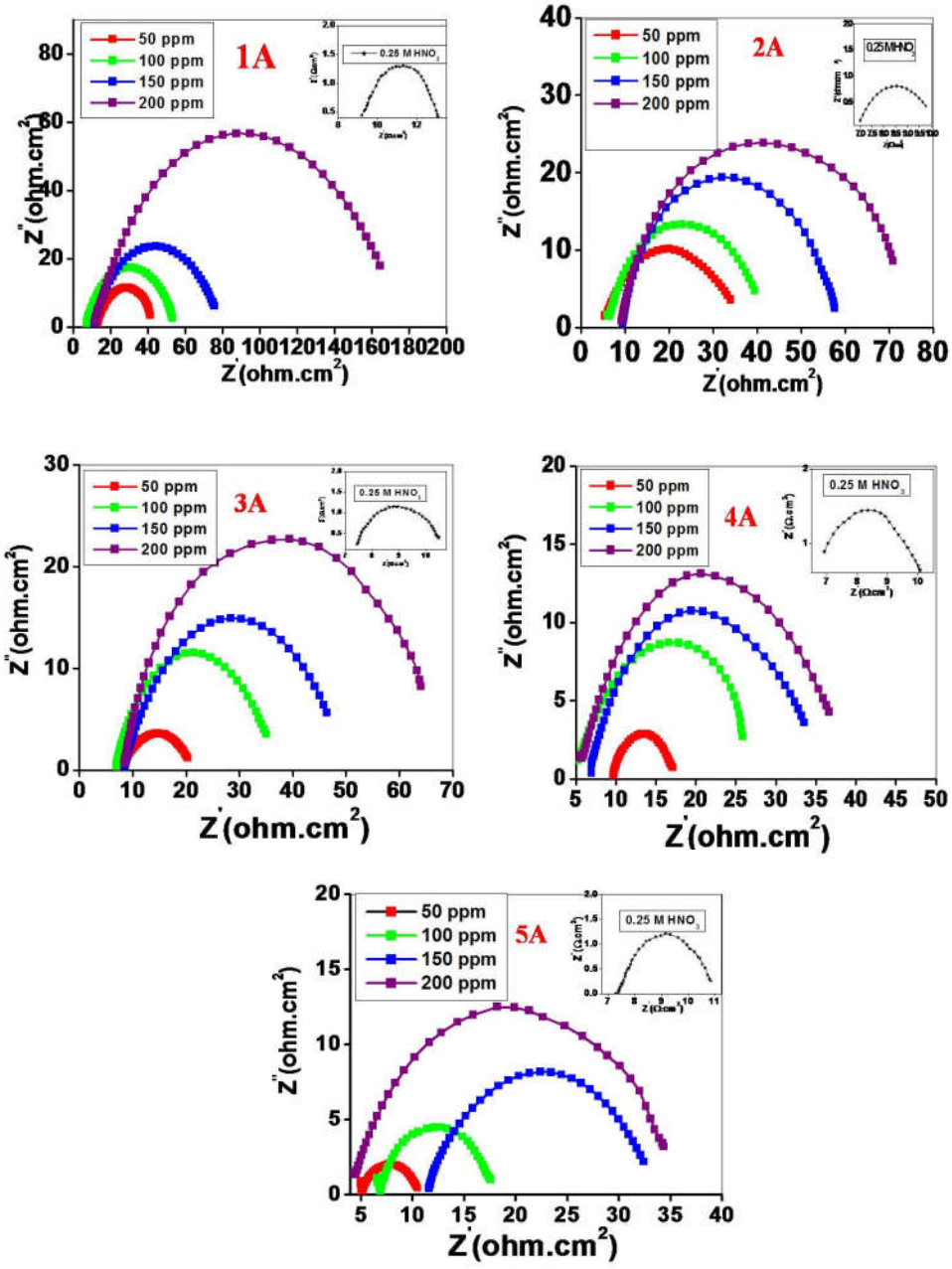

Fig 7.1 (B): Nyquist plots for mild steel in 0.25 M HNO_3 without and with EBIMOT at (1) 303 K (2) 308 K (3) 313 K (4) 318 K (5) 323 K

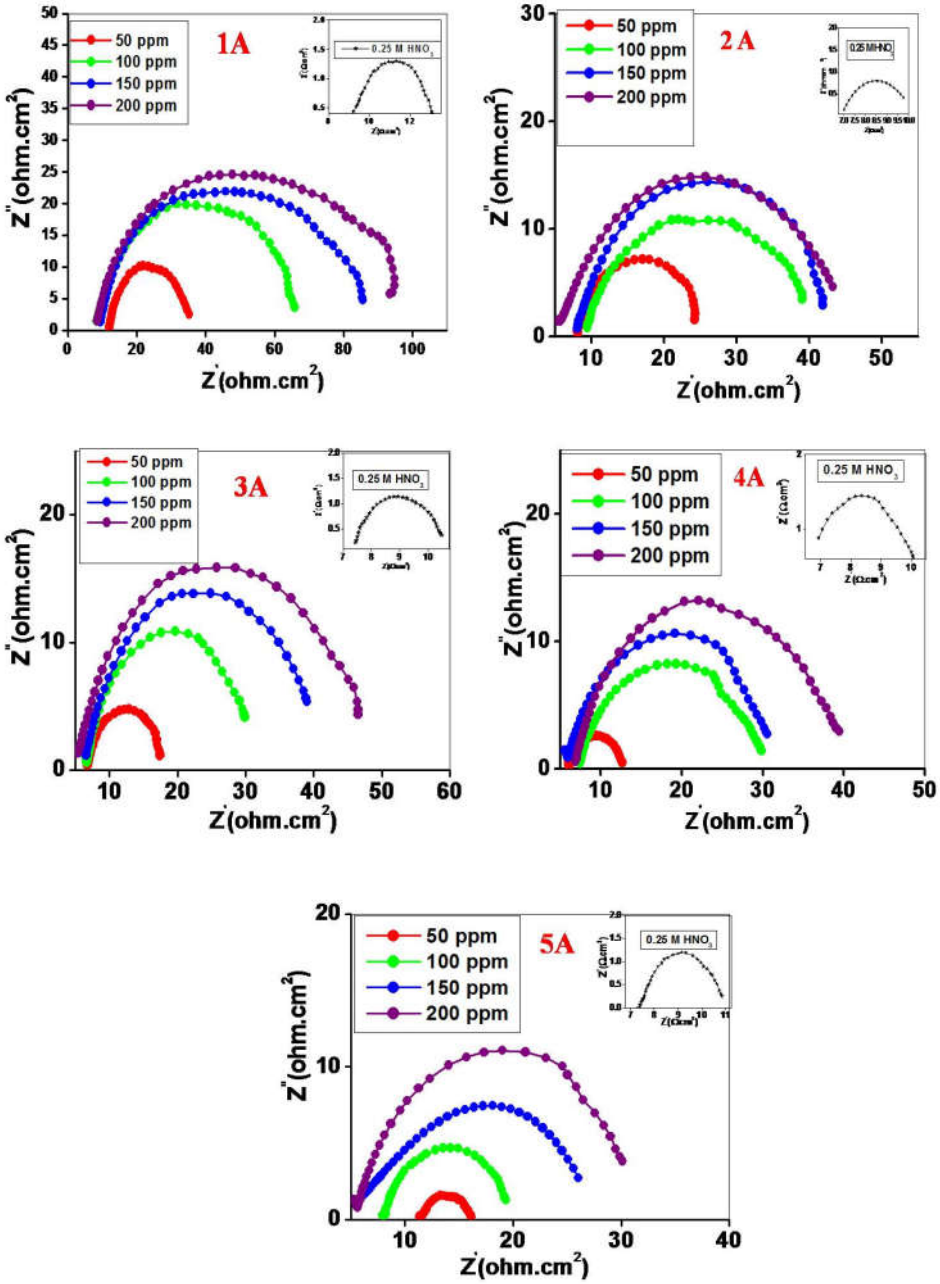

Fig 7.1 (C): Nyquist plots for mild steel in 0.25 M HNO_3 without and with PBIMOT at (1) 303 K (2) 308 K (3) 313 K (4) 318 K (5) 323 K

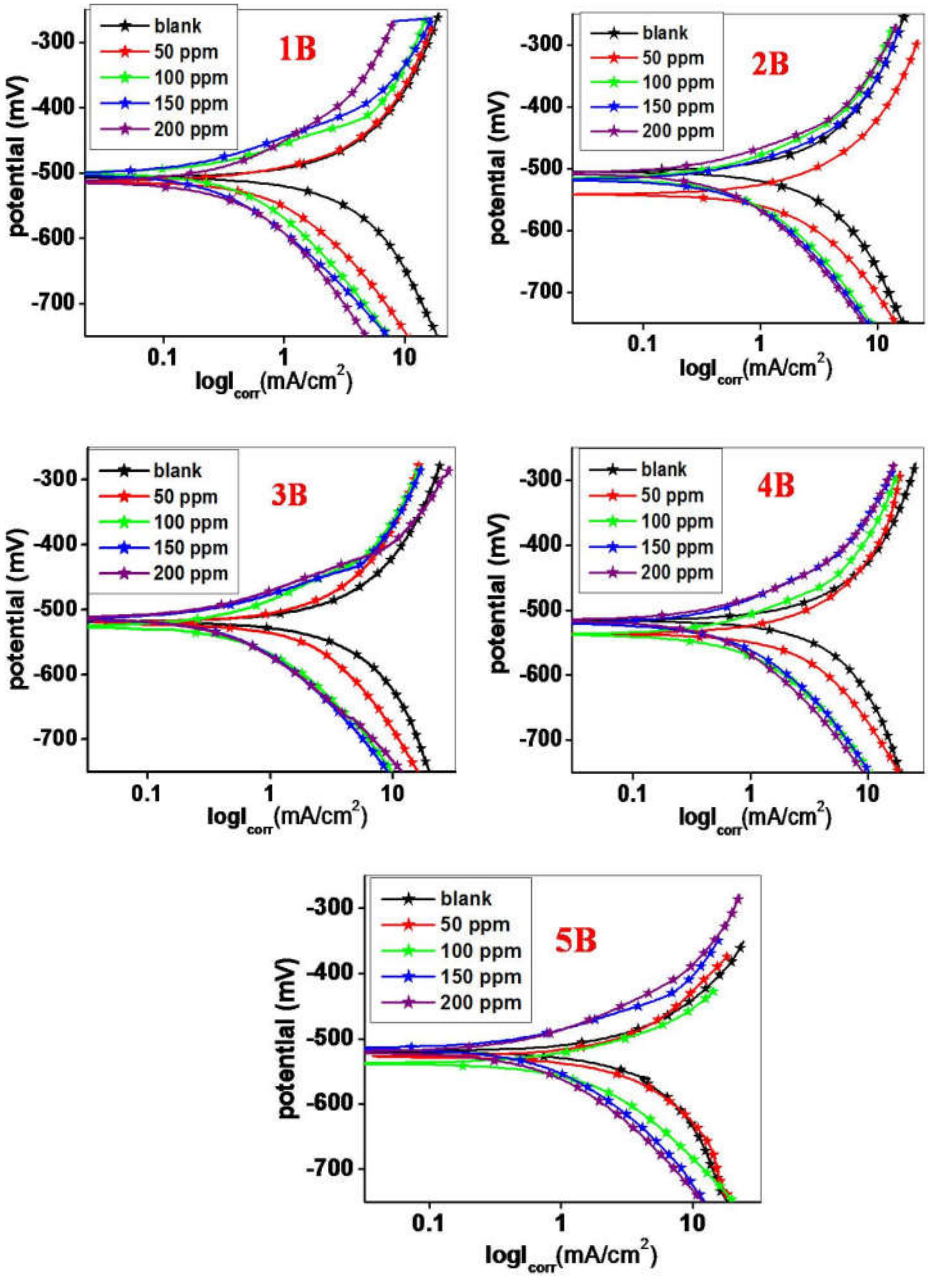

Fig 7.2(A): Tafel plots of mild steel in 0.25 M HNO_3 with different concentrations of MBIMOT at (1) 303 K (2) 308 K (3) 313 K (4) 318 K (5) 323 K

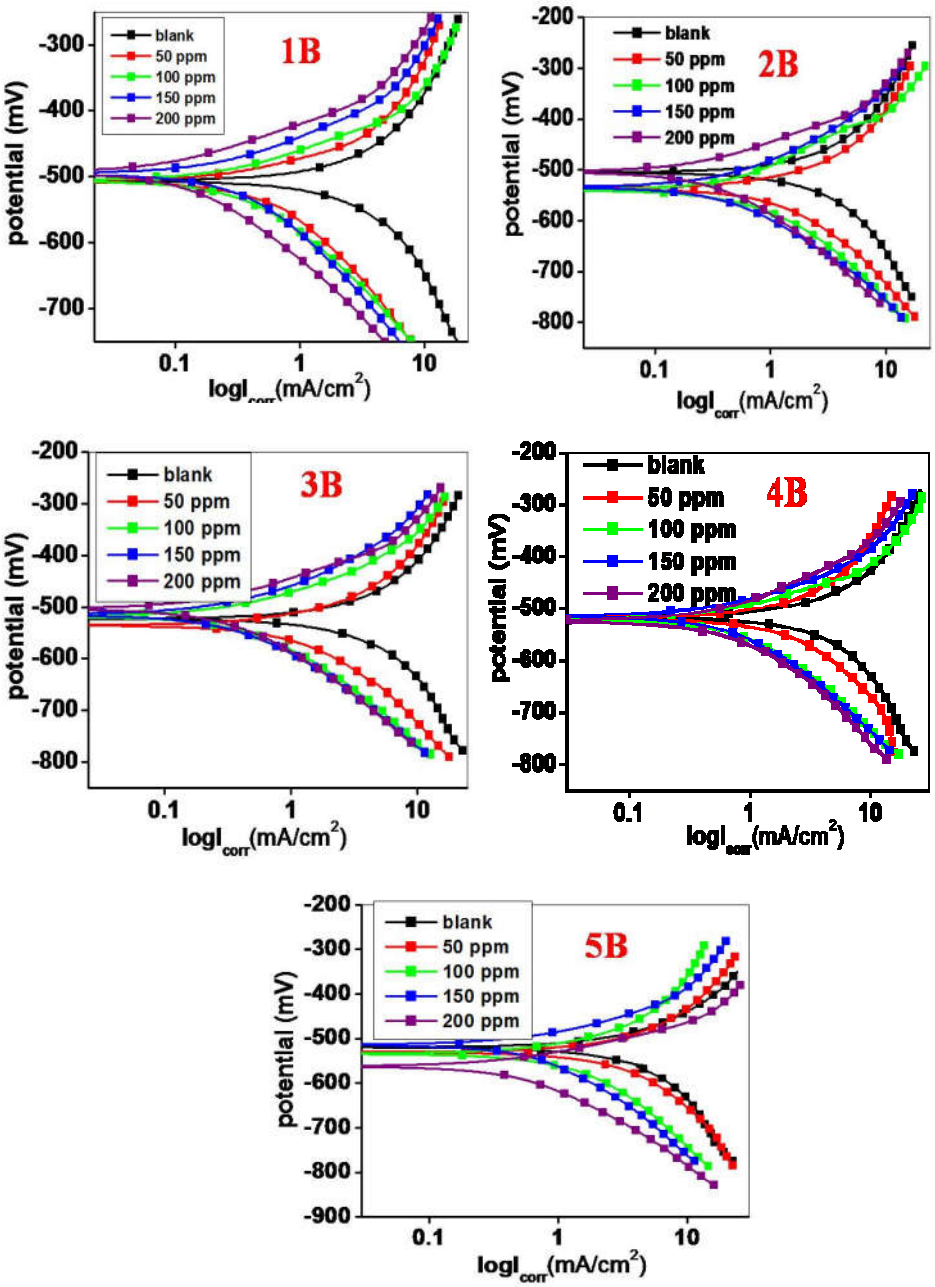

Fig 7.2(B): Tafel plots of mild steel in 0.25 M HNO_3 with different concentrations of EBIMOT at (1) 303 K (2) 308 K (3) 313 K (4) 318 K (5) 323 K

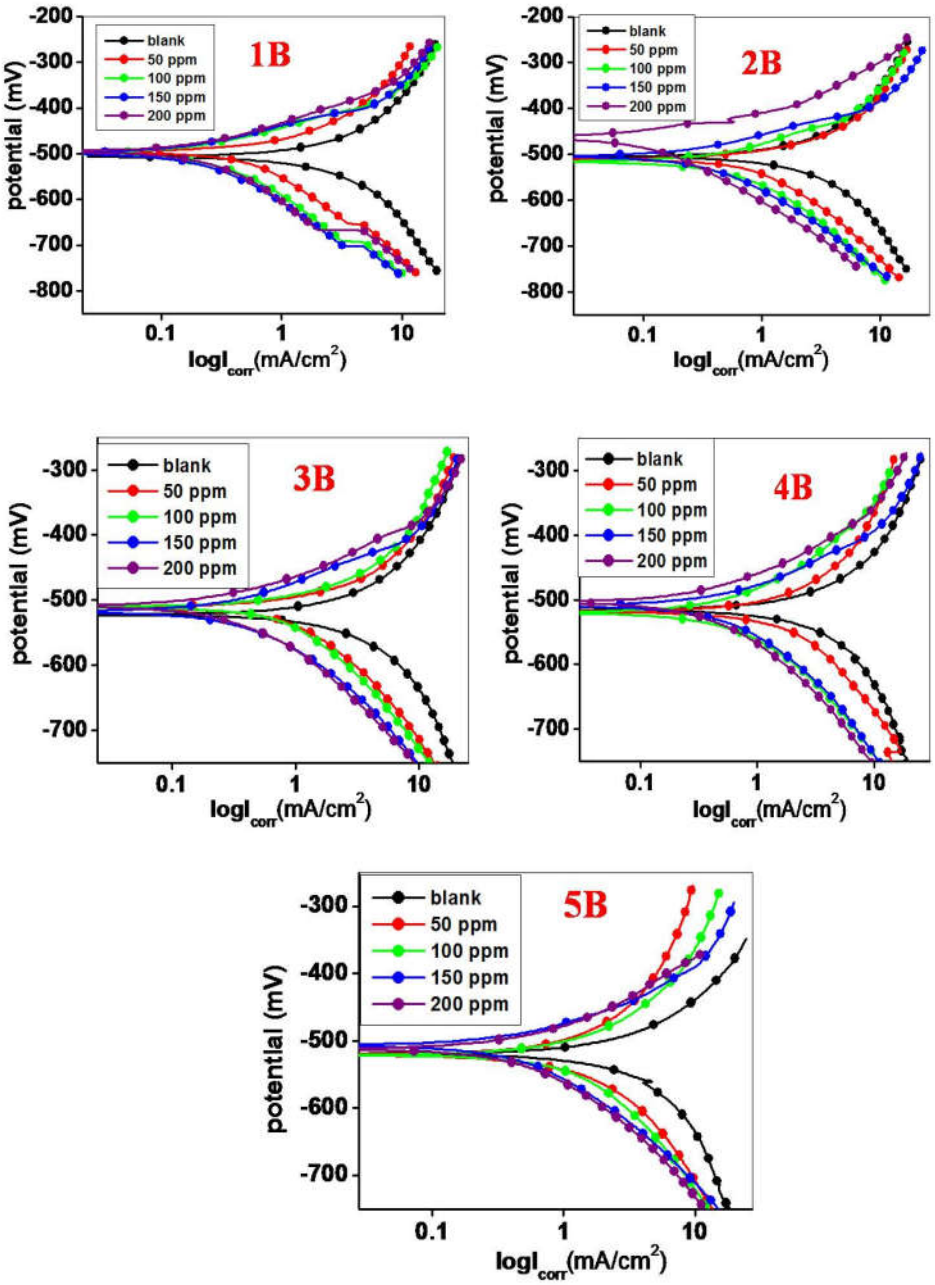

Fig 7.2(C): Tafel plots of mild steel in 0.25 M HNO_3 with different concentrations of PBIMOT at (1) 303 K (2) 308 K (3) 313 K (4) 318 K (5) 323 K

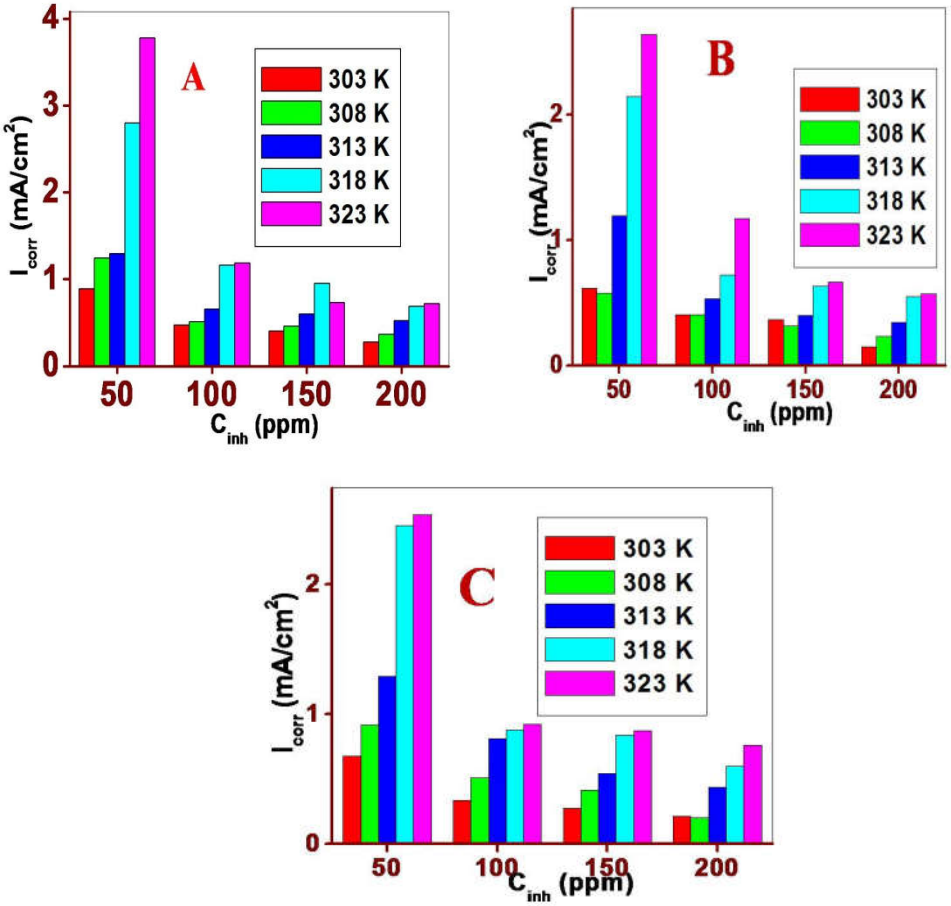

Fig 7.3: Schematic representation of variation of I_{corr} with temperature for mild steel in HNO_3 in presence of (A) MBIMOT (B) EBIMOT and (C) PBIMOT

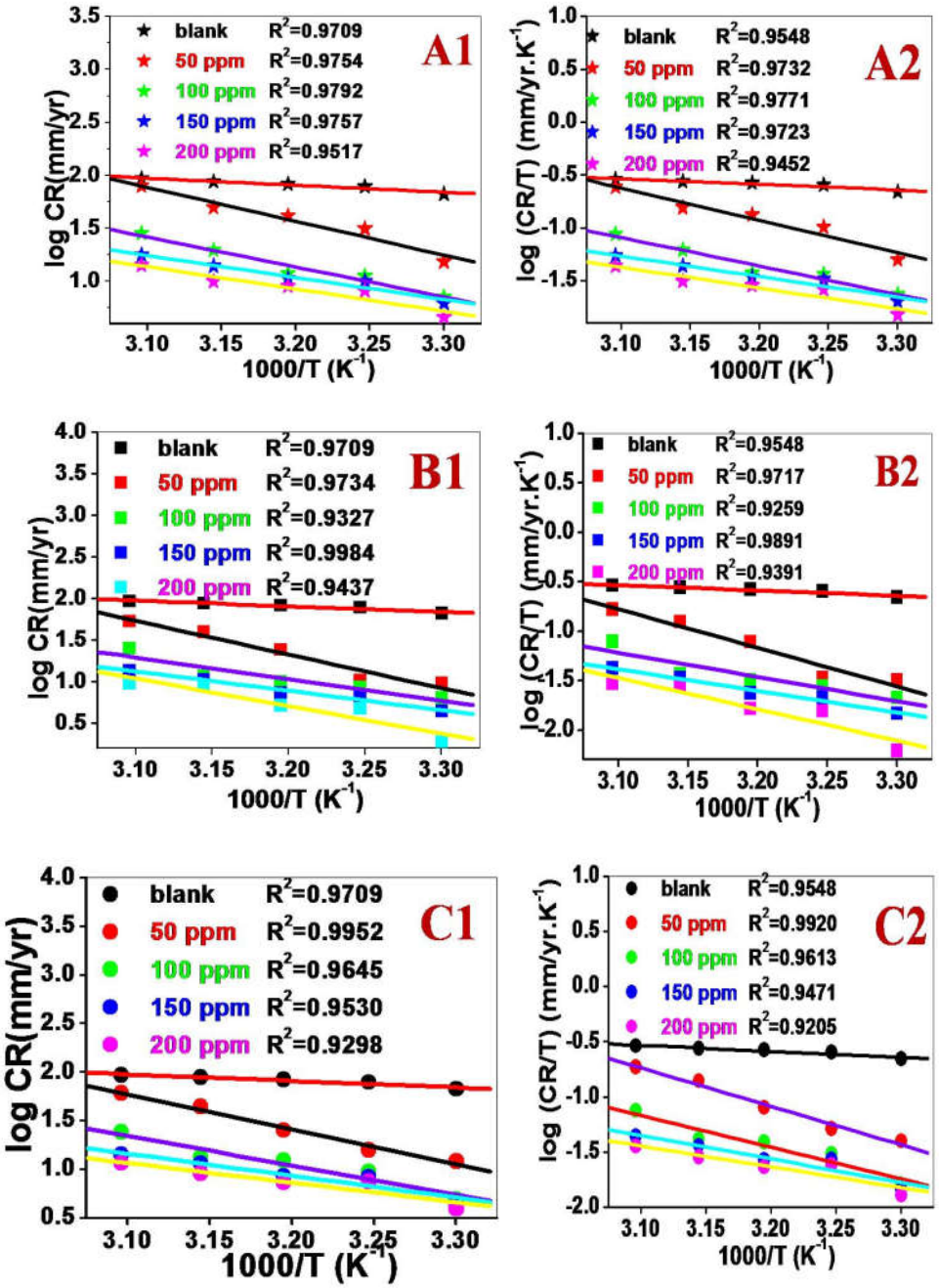

Fig 7.4: (1) Arrhenius and (2) transition state plot of mild steel in HNO_3 in presence of (A) MBIMOT (B) EBIMOT and (C) PBIMOT

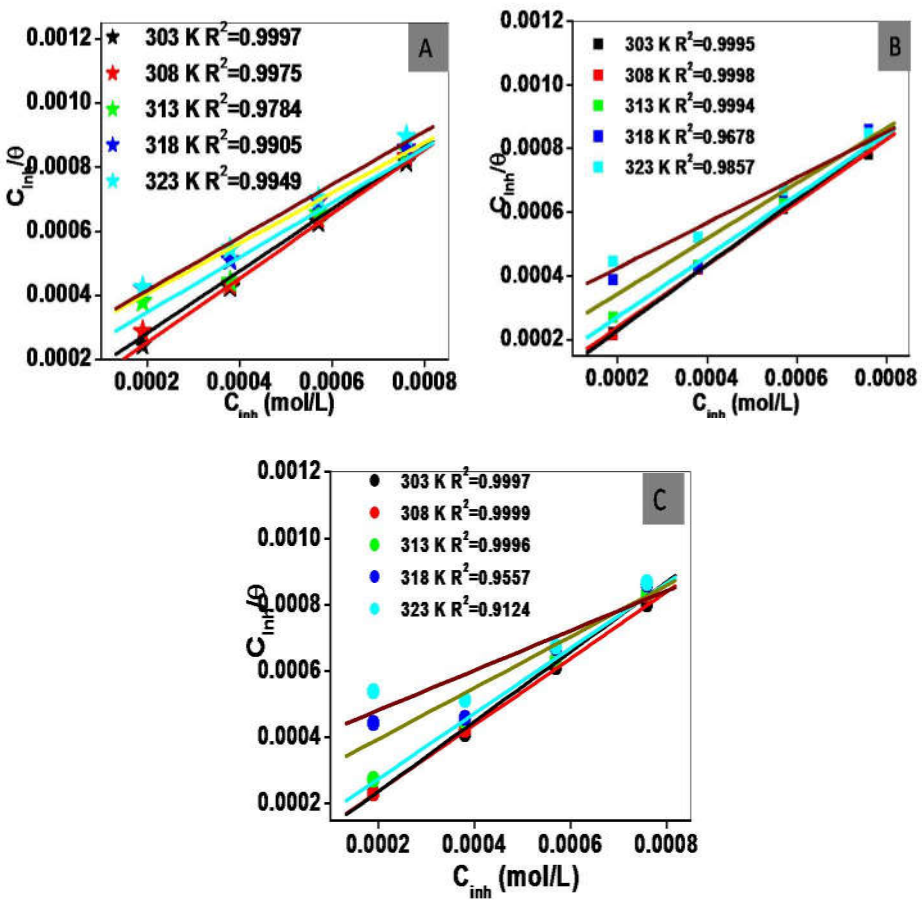

Fig 7.5 Langmuir adsorption isotherm for the adsorption of (A) MBIMOT (B) EBIMOT and (C) PBIMOT on mild steel in 0.25 M HNO_3

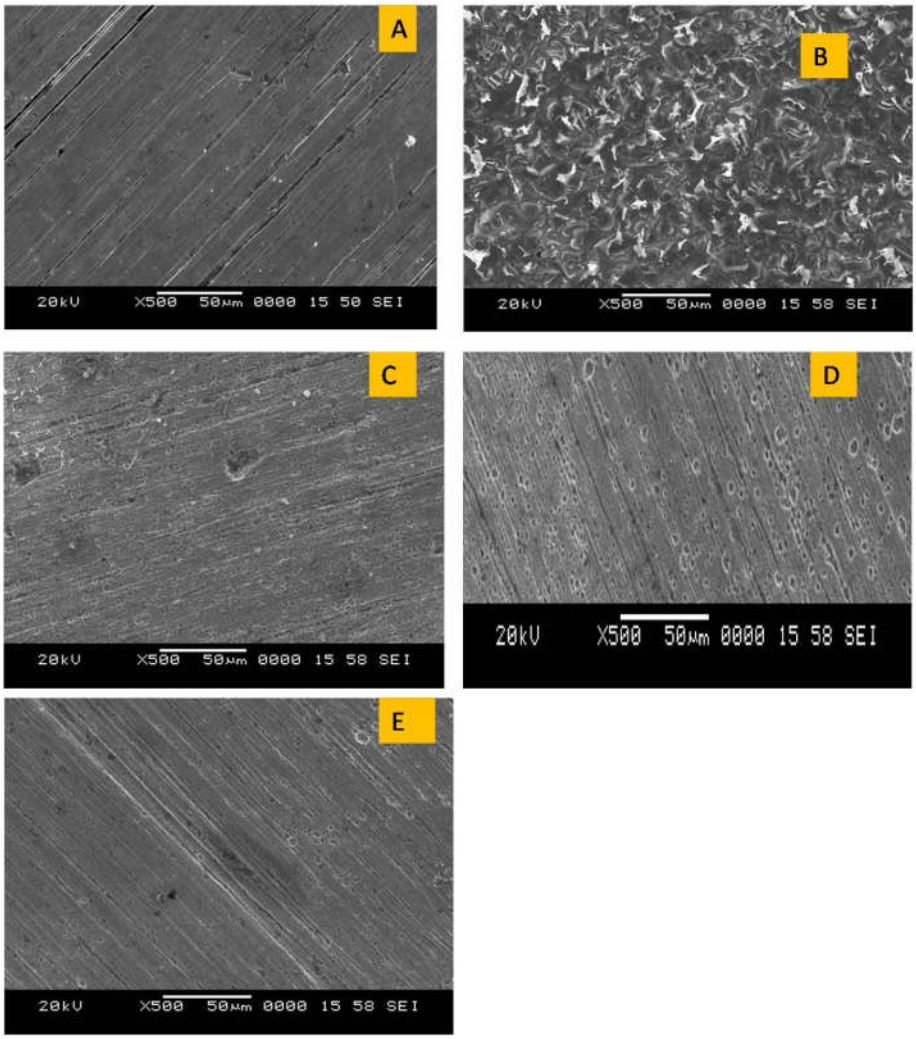

Fig 7.6: SEM images of polished mild steel (A) and mild steel specimen in 0.25 M HNO_3 (B) and mild steel specimens in 0.25 M HNO_3 in the presence of (C) MBIMOT (D) EBIMOT and (E) PBIMOT

References

1. R Yildiz R . Corros Sci., 90 (2015) 544

2. E Osarolube, I O Owate, N C Oforka, Scientific Research and Essay 3 (6) (2008) 224

3. K.F. Khaled, Electrochim. Acta 55 (2010) 6523

4. Sastri, V. S. Green Corrosion Inhibitors-Theory and Practice, John Wiley & Sons, Inc.

5. A.H. Roebuch, T.R. Pritchett, Mater. Prot. 5 (1966) 16

6. Makanjuola Oki, A L Paul Anawe and John Fasakin, Asian J. of Appl. Sci., 3 (1) (2015) 110

7. Sourav Kr. Saha, Pritam Ghosh, Additi Roy Chowdhury, Pranab Samanta, N. C. Murmu, Aditya Kr. Lohar and Priyabrata Banerjee, Can Chem.Trans., 2 (4) (2014) 381

8. Nutan Kumpawat, Alok Chaturvedi and R.K. Upadhyay, Research Journal of Chemical Sciences 2(5) (2012) 51

9. Farhad Mohsenifar Hojat Jafari Koray Sayin, J Bio Tribo Corros ,(2016) 2:1

10. K. Ramya, Revathi Mohan & Abraham Joseph, JMEPEG 23 (2014) 4089

11. Sam John, Abraham Joseph, Mathew Kuruvilla, T Sajini, J Bio Tribo Corros., (2017) 3:3

12. K. Ramya, Revathi Mohan, K.K. Anupama, Abraham Joseph, Mat. Chem. and Phy. 149-150 (2015) 632

13. Hejazi , Sh. Mohajernia , M.H. Moayed , A. Davoodi M. Rahimizadeh , M. Momeni A. Eslami, A. Shiri A. Kosari J. . Ind. and Eng. Chem. 25 (2015), 112

14. J. J. Fu, S. N. Li, Y. Wang, L. H. Cao, L. D. Lu., *J. Mater. Sci.* 45: (2010) 6255

15. E.Mc Cafferty, N.Hackermann, J.Electrochem.Soc. 119(9) (1972) 146

16. K Sudhish Shukla, E Eno Ebenso, Int. J. Electrochem. Sci., 6 (2011) 3277

17. A.K. Maayta, N.A.F. Al-Rawashdeh, Corros.Sci. 46 (2004) 1129

18. E.S. Ferreira, C. Giacomelli, F.C. Giacomelli, A. Spinelli Mater Chem Phys.,83 (2004) 129

19. H Loutfy Madkour , S Sava Kaya , Cemal Kaya , Lei Guo

JTICE., 68 (2016) 461

20. G. Karthik , M. Sundaravadivelu, Egypt. J. Pet, 25 (2016) 183

21. Ashish Kumar Singh, M.A. Quraishi, Corros.Sci. 51 (2009) 2752

22. R Omyma Khalifa , M Shadia Abdallah, Port. Electrochimica Acta 29(1) (2011) 47

23. H.Zarrok, H.Oudda, A.Zarrouk, R.Salghi, B.Hmmouti, M.Bouachrine, Der Pharma chemical, 3(6) (2011) 576

24. G Cristofari., M Znini, L Majidi, A Bouyanzer, S S Al-Deyab, J Paolini., B Hammouti , and J Costa, Int. J. Electrochem.Sci., 6 (2011).6699.

25. A. Hamdy, Nour Sh. El-Gendy, Egy. J. of Pet. 22 (2013) 17

26. D Ben Hmamou, R Salghi, H Zarrok, A Zarrouk, B Hammouti, M El Hezzat, and M Bouachrine, Adv. Mater. Corros., 1 (2013) 36

27. I Ahamad, R Prasad, E E Ebenso, and M A Quraishi, Int. J. Electrochem. Sci., 7 (2012) 3436

8 CORROSION INHIBITION OF MILD STEEL IN HCl USING 1,2,4-TRIAZOLE SCHIFF BASE, HMATD

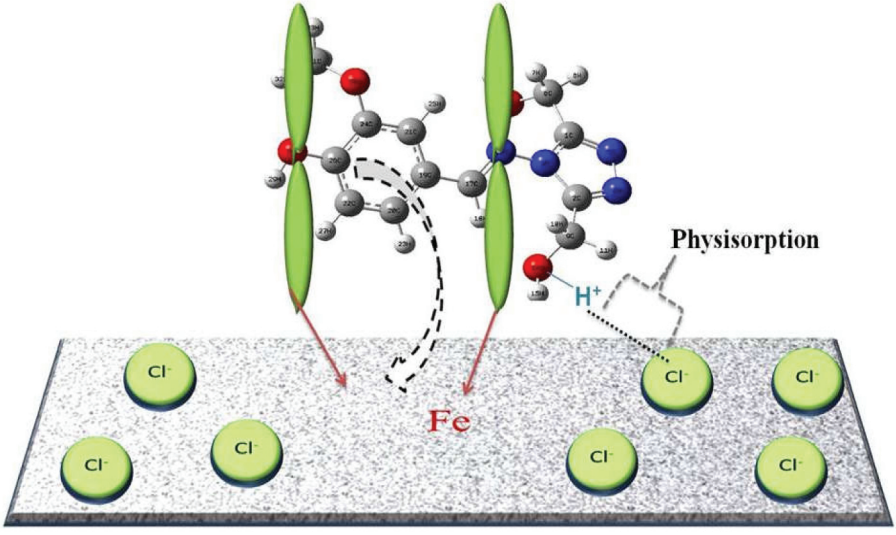

Chapter VIII presents the anti-corrosion behaviour of 1,2,4-triazole based Schiff base, HMATD, towards mild steel in HCl. Various techniques like weight loss measurements, EIS, PDP, Scanning electron microscopy (SEM) were used for elucidating the variation of inhibition efficiency with temperature and acid concentration. The inhibition mechanism was ascertained using adsorption and kinetic studies.

VIII.1 Introduction

Corrosion of metals in mineral acids is a terrible waste both of money and resources [1]. Out of the various methods practised for combating aqueous and process industry, the use of corrosion inhibitors has attained an interesting concern among the researchers. Among various classes of N-containing heterocyclics, Schiff bases were tested to offer very good corrosion inhibition efficiency for mild steel [2], aluminium [3], copper [4] etc. as they possess the structural features required for corrosion inhibition. The process of synthesis of Schiff base is relatively simple and we can introduce groups with hetero atoms to tune the molecules for desired properties. Some of the researchers reported the enhanced corrosion inhibition of Schiff bases compared to their parent amine and/or aldehyde due to the introduction of azomethine group (-C=N-) in the molecule [5].The present work intends to investigate the function of 1,2,4-triazole based Schiff base 4-(4-hydroxy-3-methoxy benzyledene amino)-4-H-1, 2, 4-triazole-3, 5-dimethanol, HMATD, as an inhibitor to mitigate mild steel corrosion in HCl by weight loss and electrochemical methods. The synthesis and characterization of the inhibitor molecule is given in chapter II (Section II.2.1)

VIII.2 Results and discussion

VIII.2.1 Weight loss method

The weight loss method of corrosion monitoring being simple, accurate and reliable is considered as "gold standard" in corrosion testing. The mild steel corrosion in 0.5 and 1 M HCl using HMATD was subjected to gravimetric technique for different immersion times 24 h, 48 h and 72 h. The corrosion rate (CR) in $mgcm^{-2}h^{-1}$ and inhibition efficiencies (IE) were calculated using the equations (1.13) and (2.2) [6] respectively and are

tabulated in Table 8.1. The values of the table pinpointed the inverse relationship of inhibitor concentration with corrosion rate and direct relationship with inhibition efficiency. But considering acid concentration, there is an inverse relation with inhibition efficiency and a direct relation with corrosion rate. These suggested the role of adsorption and surface coverage which increases with increase in inhibitor concentration. The increase in inhibition efficiency with inhibitor concentration is due to an increase in the number of molecules adsorbed on the metal surface at optimum concentration and reactive sites of the metal are protected by the inhibitor molecules [7]. Schematic representations of these trends are given in Fig 8.1 and 8.2.

VIII.2.2 Electrochemical measurements

VIII.2.2.1 Electrochemical impedance spectroscopy

EIS studies with HMATD were performed at open circuit potential and the resulted Nyquist plots are depicted in Fig 8.3 (with blank on insite). The impedance spectra displayed imperfect semi circles with one capacitive loop whose radius increases with the addition of inhibitors. This is an indication of the adsorption of inhibitor molecules on the mild steel surface which reduces the reactive sites and enhances the corrosion resistance. The similarity in the appearance of Nyquist plot throughout the experiment points out that the addition of inhibitor does not cause any change in the corrosion mechanism [8]. Various electrochemical parameters like charge transfer resistance (R_{ct}), double layer capacitance (C_{dl}), corrosion rate (CR) etc. were calculated by interpreting the EIS data with an equivalent electrical circuit. At metal/solution interface, the charge is controlled by electrons on metal side and ions on solution side. Since ions are larger than electrons, in order to neutralize equivalent charge, the ions should occupy more volume on solution side of double layer so instead of ideal capacitance, a differential

capacitance will be formed at the interface. Randle's circuit, the best model for describing processes at the electrochemical interface, shown in Fig 1.3 was used to fit the EIS data [9]. The inhomogenities, porous layer, dislocation, adsorption of inhibitors, grain boundaries etc. of the metal surface suggested the replacement of imperfect double layer capacitance of Randle's circuit by a constant phase element (CPE) whose impedance (Z_{CPE}) was represented by the equation given below [9]

$$Z_{CPE} = \left(\frac{1}{Y_0}\right)[(j\omega)_n]^{-1} \tag{8.1}$$

where Y_0 denotes the admittance which measures how easily a circuit or device will allow the current to flow, ω is the angular frequency, j the imaginary number, n is the phase shift constant which measures the degree of inhomogeneity on the metal surface formed by porous layer, dislocation grain boundaries etc. whose value lies between 0 and 1. n equals 1 describes an ideal capacitor and n equals 0 describes a pure resistor [10]. The double layer capacitance (C_{dl}) and admittance Y_0 are related by the equation

$$C_{dl} = Y_0(\omega_{max})^{n-1} \tag{8.2}$$

where ω_{max} represents the frequency at which imaginary part of impedance has the maximum value. Various electrochemical parameters like inhibition efficiency extracted from R_{ct} using the equations (2.3), corrosion rate etc. are tabulated in Table 8.2. It is clear from the table that inhibitor concentration has inverse relation with double layer capacitance and direct relation with charge transfer resistance. These trends support the formation of protective adsorption layer on the surface which isolates the metal from aggressive solution [11]. The decrease in double layer capacitance with HMATD supports the possibility of adsorption of less dielectric HMATD on metal surface by the replacement of high dielectric water molecule [12]. Maximum

inhibition efficiency of 95.5% was recorded for an optimum concentration of 300 ppm at 303 K.

Table 8.2 also revealed the decrease in R_{ct} and inhibition efficiency with increasing temperature which is graphically represented in Fig 8.5. The enhancement of temperature causes a disturbance to adsorption-desorption equilibrium shifting more towards desorption until equilibrium is again established at a different value of equilibrium constant [13].

VIII.2.2.2 Potentiodynamic polarization measurements

It is a method of monitoring the current produced as a function of time or voltage by altering the potential of working electrode to gather information regarding the kinetics of anodic and cathodic reactions [14]. Fig 8.3 represents the Tafel curves at various temperatures from 303 K to 318 K. Parameters like corrosion potential E_{corr}, corrosion current density I_{corr}, corrosion rate CR, anodic and cathodic Tafel slopes β_a and β_c were determined by the extrapolation of Tafel curves to E_{corr} and inhibition efficiency (using Eqn. 2.4) are listed in Table 8.3. The table disclosed the reduction in the I_{corr} of inhibited solutions compared to inhibitor free solution [16]. The shift of corrosion potential between the inhibited and inhibitor free solution was not found to be much more pronounced and is less than 85 mV which recognized HMATD as a mixed type inhibitor retarding the anodic reaction of metal dissolution and cathodic reaction of hydrogen evolution [17]. The efficiency values obtained from weight loss, EIS and polarization methods were found to be in good agreement with each other.

VIII.2.3 Effect of acid concentration – electrochemical study

In order to confirm the effect of acid concentration on corrosion inhibition, electrochemical measurements were conducted in 1 M HCl with

and without the optimum concentration (300 ppm) of HMATD at different temperatures and comparative Nyquist and Tafel plots in 1 M and 0.5 M HCl with 300 were shown as Fig 8.4 and corresponding electrochemical parameters are listed in Table 8.2 and 8.3. It was noticed that a reduction in charge transfer resistance and inhibition efficiency and an increase in corrosion rate and corrosion current density occurs at higher acid concentration due to various reasons like increase in concentration of Cl^- ions and H^+ ions which enhance both anodic and cathodic corrosion, dissolution of the adsorbed inhibitor, solubility of corrosion product etc. [14]. In both cases, the changes in R_{ct}, I_{corr} and IE % with temperature follows the same trend. A rise in temperature as well as acid concentration led to an increase in I_{corr} and a decrease in R_{ct} both in inhibited and inhibitor free solutions indicating more corrosion at higher temperatures and acid concentration.

VIII.2.4 Adsorption studies

In this study the best fitted adsorption isotherm was found to be Langmuir (eqn 1.9) at different temperatures. Langmuir plot (Fig 8.6) gave unit regression coefficient (R^2) and slope at these temperatures. The adsorption-desorption equilibrium constant (K_{ads}) and free energy of adsorption ΔG^0_{ads} determined according to eqn 5.5 [17] are listed in Table 8.4. The high value of adsorption constant indicated the stronger adsorption which gets decreased to some extent with increase of temperature. The negative value of ΔG^0_{ads} reflected the spontaneous and stable adsorption of HMATD on mild steel [18]. The calculated ΔG^0_{ads} values for HMATD were found as −36.2, −32.3, −32.6 and −31.9 kJ/mol at 303, 308, 313, 318 K respectively which are between the threshold values for physisorption and chemisorption, indicated mixed type behaviour of HMATD [19].

VIII.2.5 Kinetic and thermodynamic studies

Temperature is an important factor which influences the corrosion process and modifies the adsorption of inhibitor on metal surface. Various complex changes like rapid etching, desorption of inhibitor, decomposition of inhibitor etc. occur on the metal surface during temperature enhancement. The Arrhenius and Transition state equations (eqn. 5.2 and 5.3) were used for studying activation parameters like apparent activation energy (E_a), apparent enthalpy of activation(ΔH_a^0), apparent entropy of activation (ΔS_a^0) etc. whereas Van't Hoff equation (eqn.5.1) gave insight into the HMATD adsorption parameters on mild steel surface. Fig 8.7 represents the Arrhenius plots of log CR against 1/T. The E_a values of the inhibited and inhibitor free solutions were obtained from the slopes of the Arrhenius plot. A plot of log (CR/T) Vs 1/T produces a straight line (Fig 8.8) with a slope of $\frac{\Delta H_a^0}{R}$ and an intercept of $log(\frac{R}{Nh}) + \frac{\Delta S_a^0}{R}$ from which the activation parameters ΔH_a^0 and ΔS_a^0 were calculated. Various activation parameters are presented in Table 8.5. It could be seen from the table that E_a values increases by the introduction of inhibitor into the corrosive solution. It can be inferred that in the presence of inhibitor the acid molecules must cross higher threshold energy to interact with metal surface and to cause corrosion compared to that in an inhibitor free solution [20]. The condition of E_a(inh) > E_a(inhibitor free) is consistent for the process of adsorption of inhibitor on most active adsorption sites having lowest energy and the corrosion takes place chiefly on the higher energy active sites [21]. The increase in activation energy is in consistent with the reported trends in literature and this type of behaviour is associated with preferable physical adsorption [22]. It can be inferred from the trend of activation energy that corrosion rate of mild steel is mainly controlled by activation parameters. The positive values of enthalpy of activation point towards the endothermic nature of metal dissolution process.

The increase in ΔH_a^0 in the presence of inhibitors than that in their absence may be attributed to the deceleration of metal dissolution by the influence of inhibitors [23]. The value of entropy of activation is found to be higher and positive in the inhibited solution compared to the negative value in the inhibitor free solution. This reflects the decrease in randomness on converting from reactants to activated complex due to the adsorption of organic inhibitors from the acid solution which could be regarded as a quasi substitution process between the organic inhibitor in the aqueous phase and water molecules at the electrode surface. The values of E_a and ΔH_a^0 found to decrease with increase in acid concentration suggesting a low energy barrier for corrosive molecules to cross resulting in enhanced corrosion.

The thermodynamic parameters of adsorption like enthalpy of adsorption, ΔH_{ads}^0 and entropy of adsorption, ΔS_{ads}^0 were calculated using Van't Hoff plot (Fig 8.9) of $\ln K_{ads}$ against 1/T with a slope of $\frac{-\Delta H_{ads}^0}{R}$ and intercept $\frac{\Delta S_{ads}^0}{R} + ln\frac{1}{55.5}$. The values of adsorption parameters obtained are enthalpy of adsorption as −110 kJ/mol and entropy of adsorption as −249 kJ/mol. The negative value of enthalpy of adsorption indicated the exothermic nature of adsorption process. Generally, an exothermic process signifies either physisorption or chemisorption while endothermic process is attributable unequivocally to chemisorptions [24]. The large and negative value of entropy of adsorption also suggested adsorption as an exothermic process with decrease in entropy due to the loss of certain degrees of freedom due to the confinement of adsorbed molecule into a thin surface layer [21].

VIII. 2.6 Quantum chemical studies

The pictorial representation of optimized geometry, HOMO and LUMO of HMATD with various quantum chemical parameters are given in Fig 2.7(G) [4]. The high value of E_{HOMO} of HMATD explains the adsorption

of it on mild steel surface via lone pair of electrons on hetero atoms and delocalized π electrons. Along with these properties, solubility of inhibitor also has a considerable role in corrosion inhibition. The high value of dipole moment leads to a quasi substitution state between the inhibitor in aqueous phase and water molecule on the metal surface which enhances adsorption and thus inhibits corrosion.

VIII.2.7 Surface morphological studies

The SEM images of the mild steel specimens were taken in order to understand the influence of HMATD on metal surface. Fig 8.10 gives the surface images of polished mild steel surface and mild steel surface after immersion in 0.5 M HCl without and with inhibitor. It is clear from the images that the surface is strongly damaged in acid solution (B) in the absence of the inhibitor but damage is significantly reduced by the introduction of HMATD (C).

VIII.2.8 Mechanism of inhibition

The corrosion inhibition of organic inhibitors can be explained by the process of molecular adsorption on mild steel surface. It can be either physisorption or chemisorption. In the present study, the adsorption parameters suggested the mixed adsorption. The activation and thermodynamic parameters led into the conclusion of mixed adsorption with preferential physisorption. Because of the basic character of Schiff bases, neutral HMATD molecules exist in equilibrium with its protonated form through the nitrogen atoms of azomethine group or oxygen atoms of OH or OCH_3 groups in HCl solution as HMATD-H^+. It is well known that the mild steel surface is positively charged in HCl solution due to which the chloride ions get adsorbed first. This creates excess negative charge on solution side of metal and favours the adsorption of protonated Schiff base molecule by

electrostatic interaction (physisorption) and forms a metal-Cl-HMATDH$^+$ protective layer thus reducing the oxidation of metal. Later HMATD-H$^+$ and H$^+$ compete each other for cathodic sites of metal. After the evolution of H_2 gas, the HMATD-H$^+$ returns to its neutral form and undergo chemical adsorption with metal atoms via electrons on hetero atoms (HOMO). To relieve off extra negative charge on metal, the back donation of electrons takes place from metal to the LUMO of HMATD molecule. This back donation strengthens the adsorption process. Thus it can be pointed out that the corrosion inhibition by Schiff base, HMATD is a comprehensive adsorption involving both physisorption and chemisorption (Fig 8.11) [5].

Conclusions

The Schiff base, HMATD, with hetero atoms N, O, multiple bonds and aromatic rings, is an efficient inhibitor for the corrosion of mild steel in HCl. The potentiodynamic polarization studies revealed the mixed type behaviour of HMATD. The inhibition mechanism is attributed to adsorption process which follows Langmuir adsorption isotherm. The free energy of adsorption obtained from isotherm suggested mixed adsorption comprehensive of physisorption and chemisorption. The major contribution of physisorption was confirmed by the higher values of E_a in presence of inhibitor.

Table 8.1: Corrosion parameters for mild steel corrosion in HCl in the absence and presence of HMATD as obtained from weight loss experiments

		Immersion time (hours)					
		24 h		48 h		72 h	
Acid conc.	Cinh ppm	CR $mgcm^{-2}h^{-1}$	IE	CR $mgcm^{-2}h^{-1}$	IE	CR $mgcm^{-2}h^{-1}$	IE %
0.5 M	0	7.3264	--	5.2708	--	3.6069	--
	50	2.1759	70.30	2.2986	56.30	1.1504	68.10
	100	1.1458	84.36	1.1886	77.40	0.9838	72.70
	200	0.7049	90.30	0.8698	83.40	0.7677	78.70
	300	0.5752	92.00	0.4520	91.40	0.3870	89.27
1 M	0	10.943	--	9.2882	--	7.0417	--
	50	4.0509	62.75	8.8151	57.82	3.4298	51.29
	100	2.5266	76.89	2.6620	71.40	2.0833	70.40
	200	1.4918	86.36	1.5046	83.80	1.1736	83.33
	300	1.0069	90.79	0.9837	89.41	0.7870	88.82

Table 8.2: Electrochemical impedance parameters for the corrosion of mild steel in HCl in the presence of various concentrations of HMATD at different temperatures

Temp.	Acid Conc.	Cinh ppm	R_{ct} Ωcm^2	C_{dl} x10^{-4} F	CR mm/yr	IE %
		0	13.65	5.575	22.15	--
		50	81.09	2.568	3.732	83.10
	0.5 M	100	157.9	1.837	1.915	91.30
303 K		200	185.4	1.425	1.631	92.60
		300	301.0	1.374	1.004	95.50
		0	13.27	15.65	22.78	--
	1 M	300	149.2	2.714	2.026	91.11
		0	9.899	7.396	30.54	--
		50	21.83	3.853	13.85	54.60
	0.5 M	100	29.48	2.525	10.26	66.40
308 K		200	110.0	1.852	2.749	91.00
		300	153.4	1.623	1.971	93.50
		0	9.345	5.697	32.35	--
	1 M	300	100.7	1.715	3.002	90.72
		0	6.824	11.28	44.31	--
		50	14.04	4.283	21.53	51.30
	0.5 M	100	19.69	1.755	15.36	65.30
313 K		200	37.33	1.224	8.099	81.70
		300	77.40	1.248	3.906	91.10
		0	8.475	3.186	35.68	--
	1 M	300	47.12	1.907	6.417	82.01
		0	5.671	14.00	53.31	--
		50	8.151	11.46	37.09	30.40
318 K	0.5 M	100	12.52	3.697	24.15	54.70
		200	13.69	3.089	22.58	58.50
		300	22.17	2.017	13.64	74.40
		0	4.715	26.21	64.12	--
	1 M	300	18.08	4.657	16.72	73.92

Table 8.3: Electrochemical parameters for mild steel corrosion in HCl in the presence of various concentrations of HMATD at different temperatures as obtained from potentiodynamic polarization studies

Temp	Acid conc	Cinh ppm	$-E_{corr}$ mV	I_{corr} mA/cm^2	β_a mV/ dec	$-\beta_c$ mV/ dec)	IE %
		0	468	0.9628	195	203	--
		50	504	0.1564	80	133	83.80
303 K	0.5 M	100	487	0.1161	81	151	88.00
		200	495	0.0777	73	137	91.90
		300	492	0.0434	65	112	95.40
		0	441	1.8533	208	160	--
	1 M	300	397	0.2264	96	150	87.78
		0	468	2.1125	210	256	--
		50	482	0.6823	93	210	67.70
	0.5 M	100	479	0.6582	89	178	68.10
308 K		200	493	0.2133	74	168	89.90
		300	498	0.1334	64	144	93.6
		0	459	2.5045	127	175	--
	1 M	300	527	0.2611	79	127	89.57
		0	473	2.7009	215	234	--
		50	476	1.3935	112	225	48.40
	0.5 M	100	483	0.8467	105	195	68.60
313 K		200	499	0.3464	70	162	87.10
		300	498	0.2697	64	151	90.00
		0	459	2.6127	175	215	--
	1 M	300	529	0.4616	88	159	82.30
		0	461	3.5522	165	214	--
		50	481	2.5003	171	251	29.60
	0.5 M	100	480	1.4013	131	234	60.50
318 K		200	478	1.2692	122	232	64.20
		300	503	1.0958	129	175	69.10
		0	450	4.3292	143	196	--
	1 M	300	504	1.0709	155	222	75.26

Table 8.4: Adsorption parameters - K_{ads} and ΔG^0_{ads} values for HMATD on mild steel in 0.5 M HCl at various temperatures as obtained from Langmuir adsorption isotherm

Temp. K	R^2	Intercept X 10^{-4}	K_{ads} x 10^4 M^{-1}	ΔG^0_{ads} kJ/mol
303	0.9999	0.3205	3.1206	−36.2
308	0.9963	1.8793	0.5321	−32.3
313	0.9988	2.0387	0.4905	−32.6
318	0.9826	3.2099	0.3115	-31.9

Table 8.5: Activation parameters for mild steel corrosion in HCl

C_{inh} ppm	E_a kJ/mol	ΔH^0_a kJ/mol	ΔS^0_a J/mol.K
blank(0.5 M HCl)	48.30	45.7	−68.5
50	117.9	115.2	148.1
100	129.0	126.3	180.2
200	143.4	140.8	222.1
300	136.1	133.0	192.7
300 (1 M HCl)	113.4	110.7	236.7

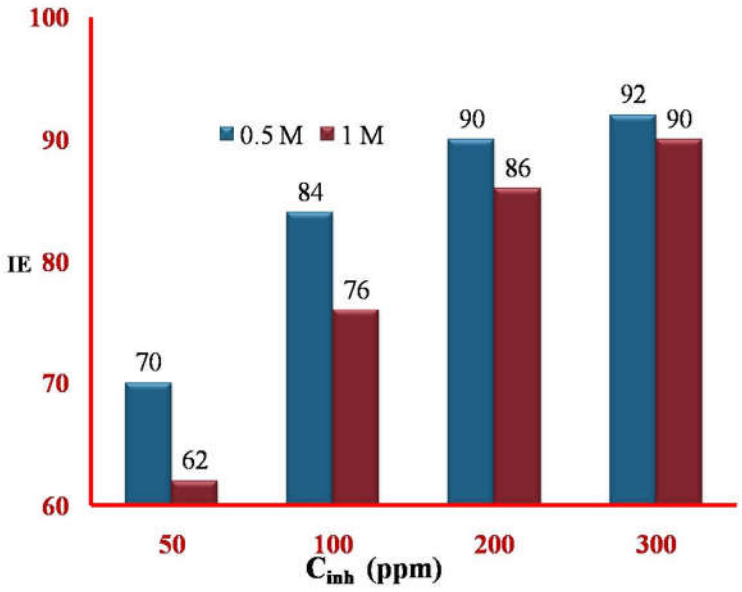

Fig 8.1 Pictorial representation of effect of acid concentration on inhibition efficiency of HMATD

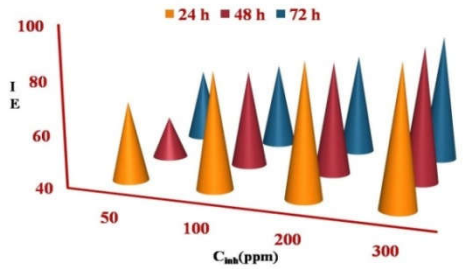

Fig 8.2: Schematic representation of effect of HMATD concentration on inhibition efficiency

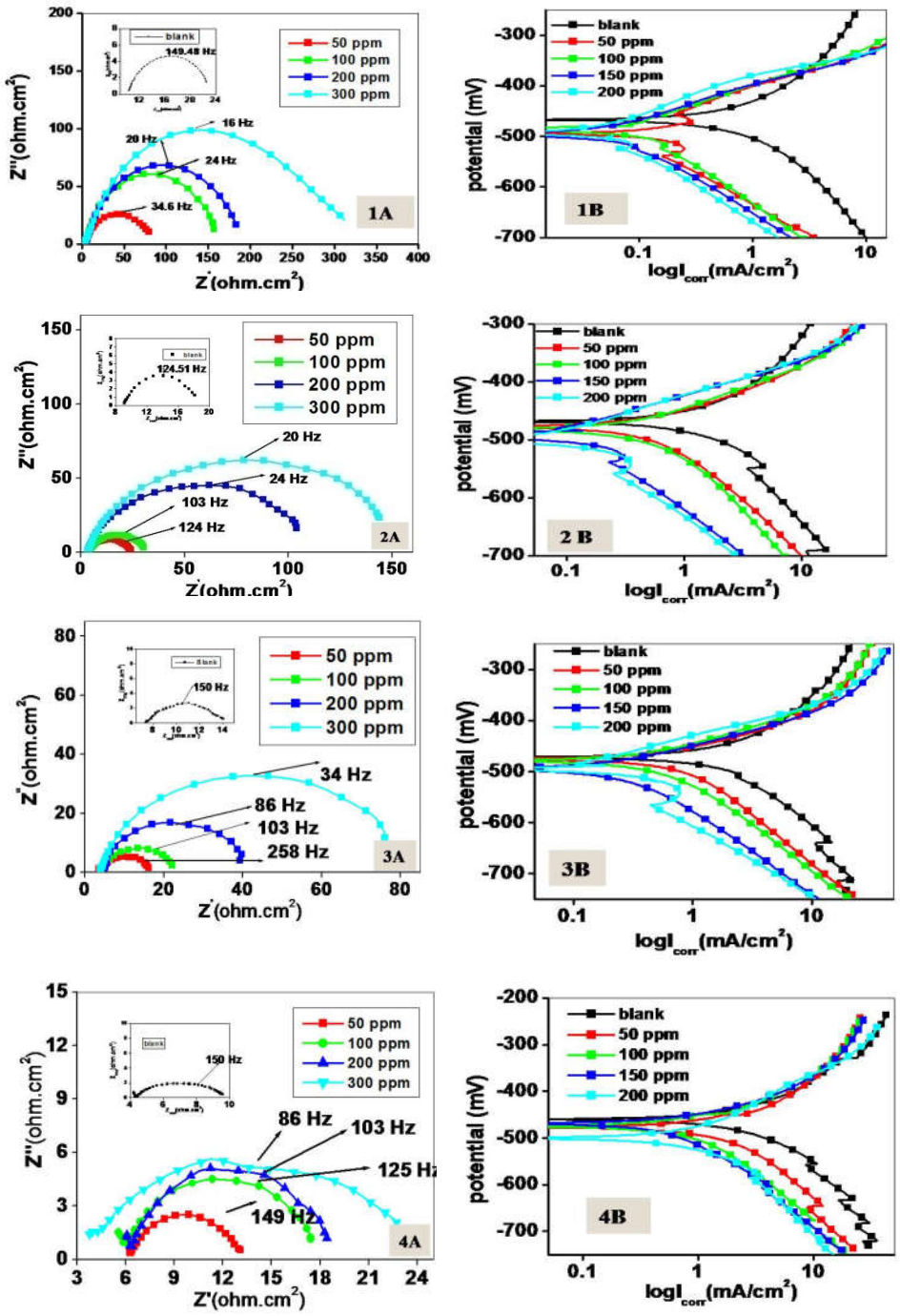

Fig 8.3 Nyquist (A) and Tafel (B) plots of mild steel in 0.5 M HCl at (1) 303 K (2) 308 K (3) 313 K and (4) 318 K

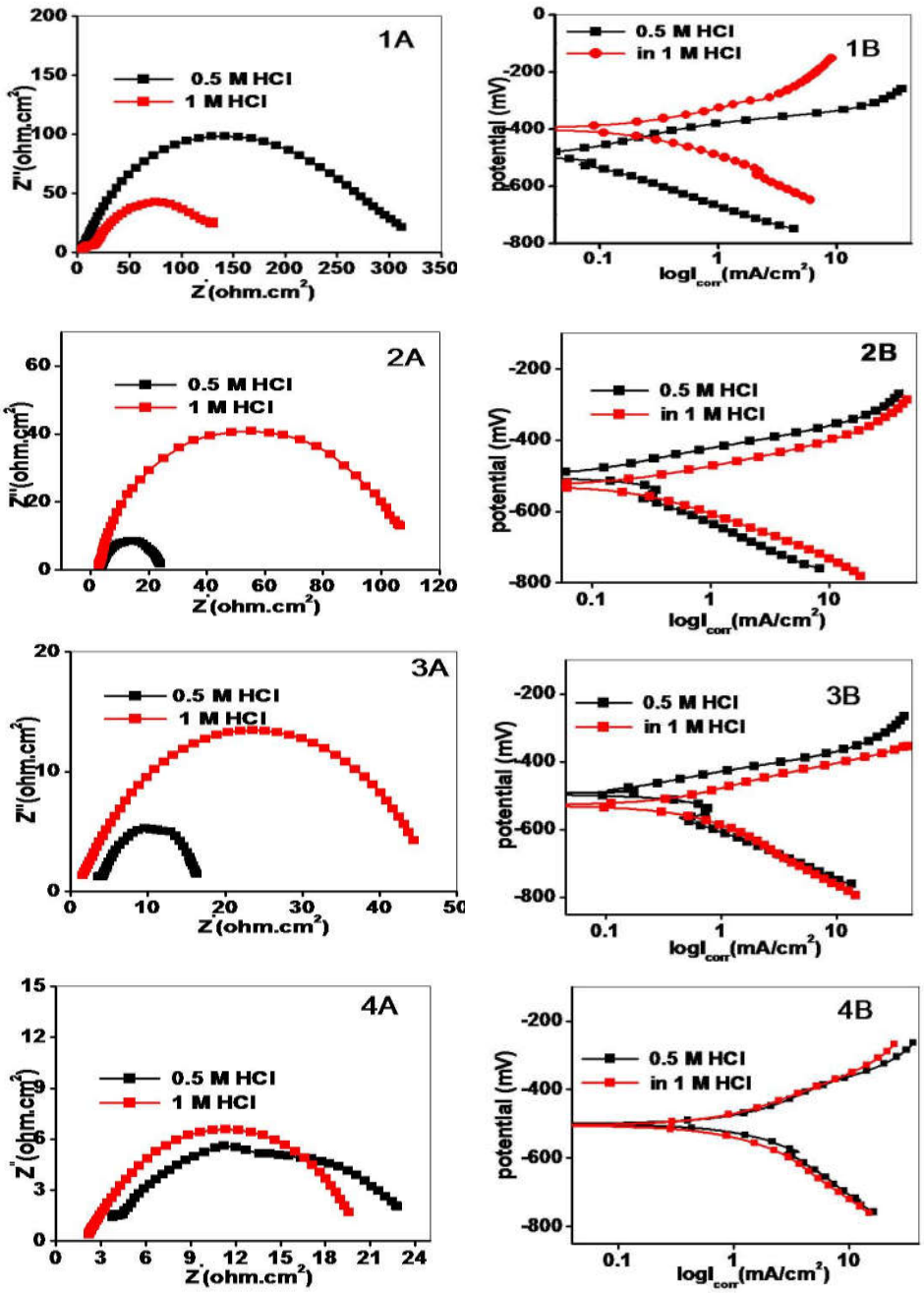

Fig 8.4 Nyquist (A) and Tafel (B) plots of mild steel in 0.5 M and 1 M HCl with 300 ppm of HMATD at (1) 303 K (2) 308 K (3) 313 K (4) 318 K

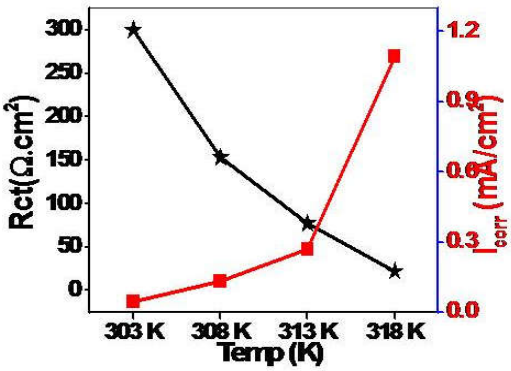

Fig8.5:Graphical representation of variation of R_{ct} and I_{corr} of 300 ppm inhibited solution with temperature

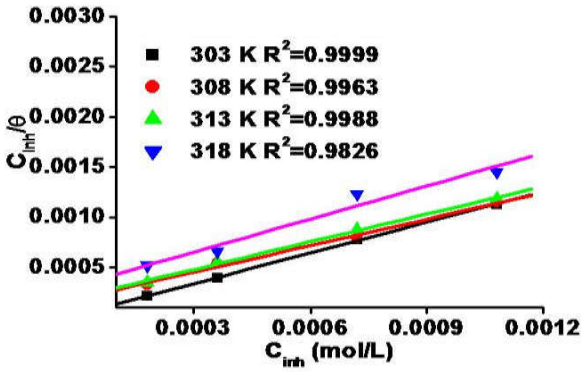

Fig8.6: Langmuir adsorption isotherms for HMATD

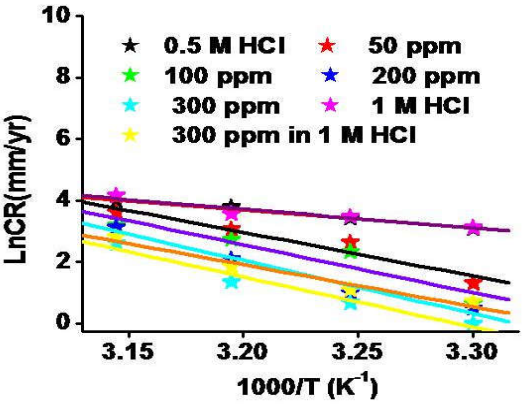

Fig8.7: Arrhenius plot for mild steel corrosion in HCl with and without HMATD

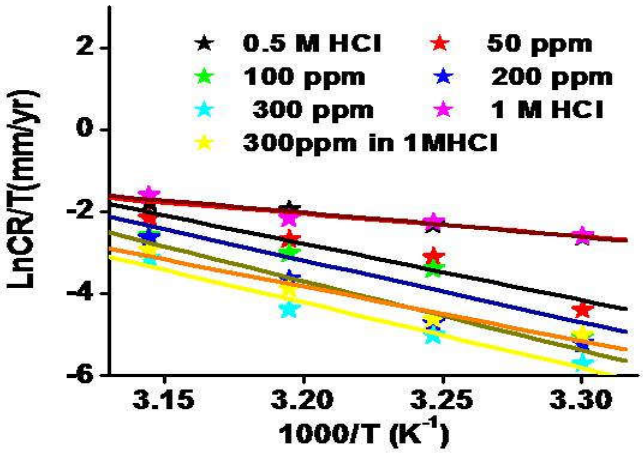

Fig 8.8 Transition state plot

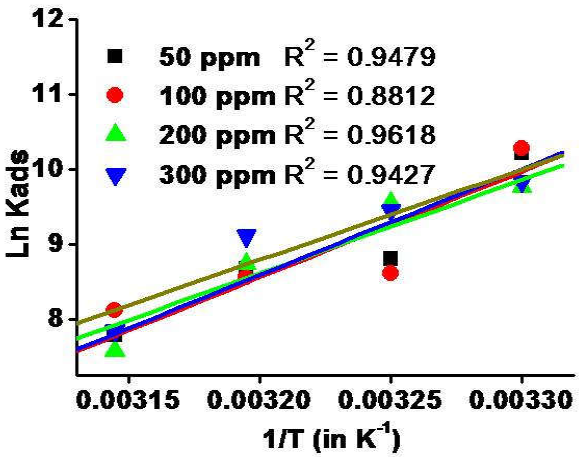

Fig 8.9 Van't Hoff plot

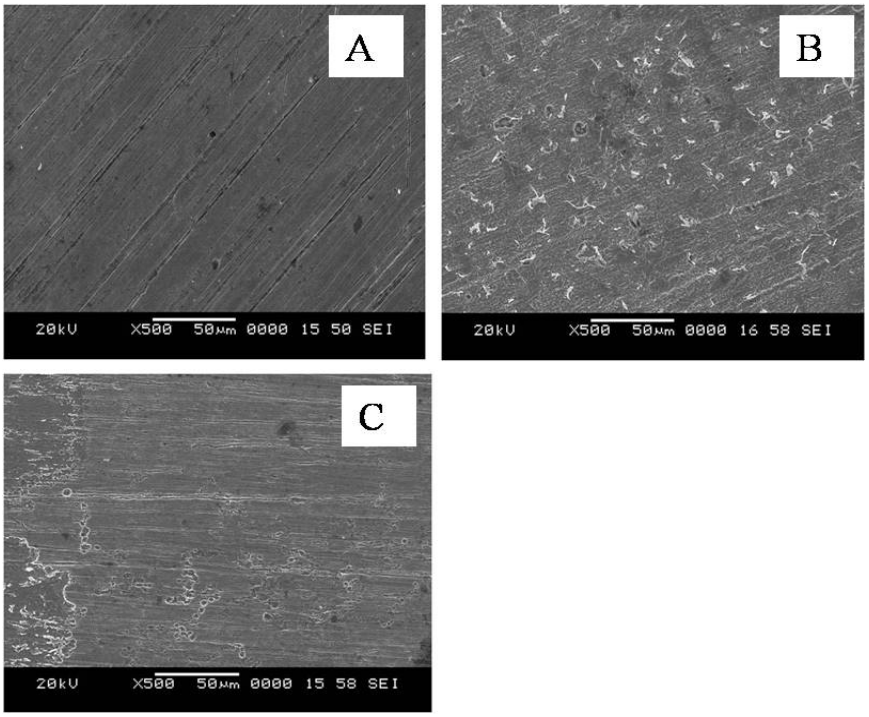

Fig 8.10 SEM micrographs of (a) polished mild steel (b) mild steel immersed in 0.5 M HCl and (c) mild steel immersed in 0.5 M HCl with HMATD

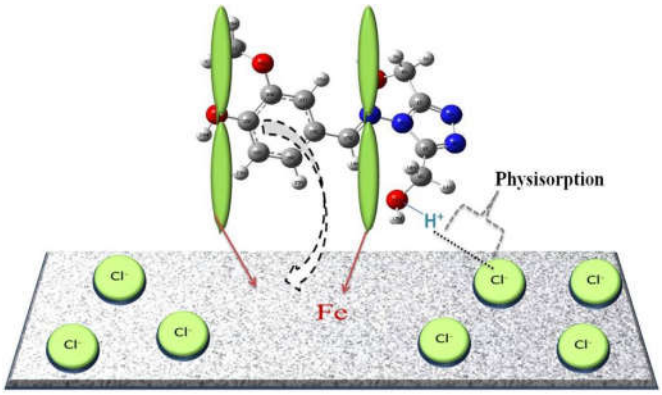

Fig 8.11 Interactions between active sites of HMATD and mild steel surface

References

1. M. Lagrene, B. Mernari, M. Bouanis, M. Traisnel, F. Bentiss, Corros. Sci.44 (2002) 573

2. N. Soltani, H. Salavati, N. Rasouli, M. Paziresh, and A. Moghadasi, Chem. Eng. Commun . 203 (6) (2016) 840

3. Serpil Şafak, Berrin Duran, Aysel Yurt , Gülşen Türkoğlu, Corros.Sci. 54(2012) 251

4. K. Ramya, Abraham Joseph, Res. on Chem. Intermed.*, 4*1 (2*) (*2015) 1053

5. Ramazan Solmaza, Ece Altunbas, Gulfeza Kardas, Mater.Chem Phy 125 (2011) 796

6. I.B. Obot1, E.E. Ebenso, Zuhair M. Gasem, Int. J. Electrochem. Sci.,7 (2012) 1997

7. C. Kamal, M.G. Sethuraman , Arab. J. Chem, 5 (2012) 155

8. A R Hoseinzadeh,., I Danaee, M H Maddahy, . Z. Phys. Chem. *227* (2013) 403

9. İ. Dehri, M. Özcan, Mater.Chem.Phy. 98 (2006) 316

10. K. Anupama, K. Ramya, K.M. Shainy, Abraham Joseph Mater.Chem.Phy 167 (2015) 28

11. Chandrabhan Verma, O Lukman, O Olasunkanmi, I. B. Obot, Eno E. Ebensob and M. A. Quraishi, RSC Adv., 6 (2016) 53933

12. Gopi, El-Sayed M. Sherif, M. Surendiran, P. Jothi, L. Kumaradhas, Kavitha, Mater. Chem. Phys. 147 (2014) 572.

13. S. Ramesh Kumar, I. Danaee, M. Rashvand Avei, M. Vijayan, J. Mol. Liq. 212 (2015) 168

14. B.N.Oza and P.B. Tandel, J. Electrochem. Soc. India, 45(2) (1996) 77

15. Sam John and Abraham Joseph, RSC Advances, 2 (2012) 9944

16. Ayse Ongun Yuce, Basak Dogru Mert, Gulfeza Kardas, Birgul Yazıcı, Corros. Sci.83 (2014) 310.

17. K Ramya et al Mater.Chem.Phy 149-150 (2015), 632

18. K Ahmed Abdel Nazeer Shalabi, A. S. Fouda, Res Chem Intermed 41 (2015) 4833

19. A.Doner, R.Solmaz, M.Ozcan, G.Kardas, Corros. Sci.,53 (2011) 2902

20. Ekemini Ituen, Abosede Jamesc and Onyewuchi Akaranta Portugaliae Electrochimica Acta 34(6) (*2016)* 417

21. A. Khadiri, A.Ousslim, K.Bekkouche, A.Aounit A.Elidrissi, B.Hammout Portugaliae Electrochimica Acta *32(1), (2014), 35*

22. A. Bousskri, R. Salghi, Anejjar, M. Messali, S. Jodeh, O. BenaliM. Larouj,I.Warad O. Hamed*c* and B. Hammouti *Portugaliae Electrochimica Acta 34(1) (2016) 1*

23. R. Geethanjali*,* S. Subhashini*, Portugaliae Electrochimica Acta 33(1), (2015), 35*

24. I.B. Obot1, E.E. Ebenso, I. A. Akpan, Z. M. Gasem, Ayo S. Afolabi *Int. J. Electrochem. Sci.,* 7 (2012**)** 1978

SUMMARY

In this concluding section, the summary of the results obtained from this work is summarized. Two types of N,S,O-donor heterocycles were explored in this work , derivatives of 1,2,4-triazine and 1,2,4-triazole for studying the complex formation ability and biological screening studies and 2-alkylbenzimidazole derivatives and benzimidazole bearing 1,3,4-oxadiazoles for corrosion inhibition studies.

The complex formation capacity and biological screening studies were done using ligands namely: MHMMT, DMSTT, HMATD, and DHATD. MHMMT and DMSTT was found to be bidentate coordinating through N of azomethine group and S atom of thiol group after deprotonation. DHATD was found to be bidentate whereas HMATD has a monodentate nature. In vitro antimicrobial studies revealed that MHMMT and DMSTT exhibit a higher activity compared to their complexes against the microbial strains used in this study. MHMMT was found to be highly active against the fungal strain *C.albicans* and DMSTT was found to be as active as the standard against *A.Niger*. But in the case of anti-bacterial studies Zn complex of DHATD was found to be the most active with activity similar to that of standard. The antidiabetic activities of metal complexes were found to be more than that of ligands. The Cu(II) and Zn(II) complexes of MHMMT were found to show significantly high antidiabetic activity. Fe-MHMMT complex showed a comparatively good anticancer activity with an IC_{50} value of 24 μM against breast cancer cells MCF7.

The corrosion inhibition studies were carried out for compounds of benzimidazole motifs viz: EMBAH, EEBAH, EPBAH, MBIMOT, EBIMOT, PBIMOT, and 1,2,4-triazole based Schiff base HMATD for mild steel in HCl, H_2SO_4 and HNO_3. Both electrochemical and classical gravimetric methods were used for monitoring the anti-corrosion behaviour. The results obtained from both the methods are in good agreement. The influence of

various factors like inhibitor concentration, acid concentration, immersion time, and temperature on corrosion prevention behaviour of inhibitors was observed. All the systems showed significantly good efficiencies at ppm level concentration. In all the cases, with an increase in temperature and acid concentration, there results a decrease in efficiency. But the increase in inhibitor concentration causes an increase in efficiency up to a certain limit.

The inhibition efficiencies of various inhibitors used for mild steel in HCl are graphically represented in Fig S.1. All the synthesized inhibitors showed a comparatively high efficiency of greater than 90% with EPBAH with an efficiency of 98.77 as the best one.

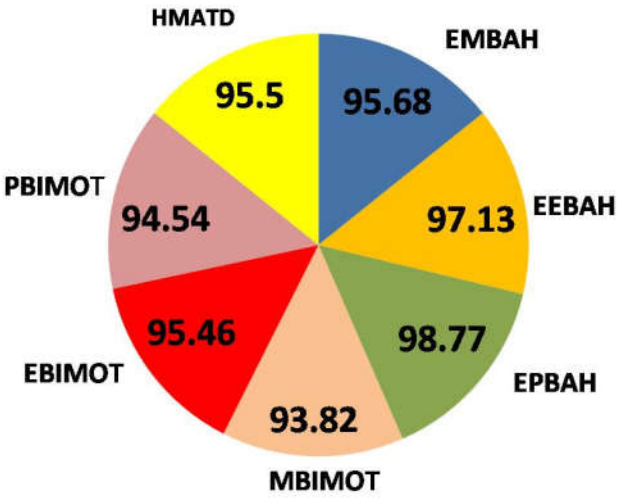

Fig S.1 Summary of inhibition efficiency of various inhibitors for mild steel in 0.5 M HCl at 303 K

The inhibition efficiencies of MBIMOT, EBIMOT, and PBIMOT for mild steel in H_2SO_4 and HNO_3 at 303 K are graphically represented in Fig S.2and S.3 respectively. Among the three inhibitors MBIMOT, EBIMOT and PBIMOT, EBIMOT was found to be the best one. This may be due to the combined influence of inductive and steric effect.

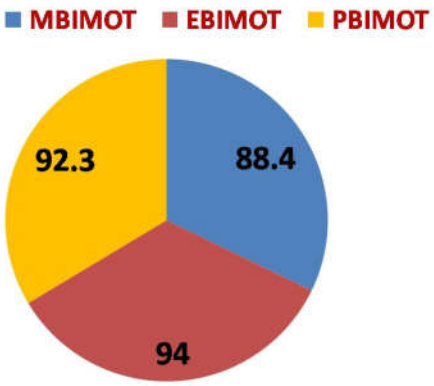

Fig S.2: Summary of inhibition efficiency of various inhibitors for mild steel in 0.25 M H_2SO_4 at 303 K

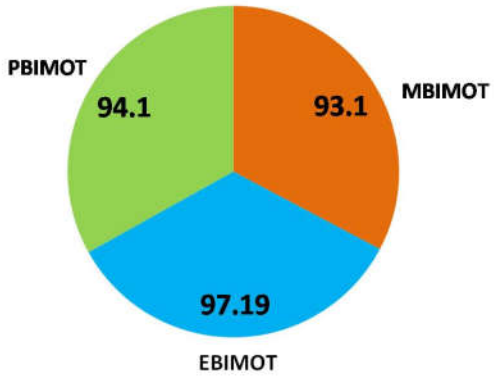

Fig S.3: Summary of inhibition efficiency of various inhibitors for mild steel in 0.25 M HNO_3 at 303 K